DEPARTMENT OF BIOCHEMICAL ENGINEERING

Microscale Tissue Engineering: A Modular Approach For Vascularized Bone Regeneration

Carlotta Peticone

Department of Biochemical Engineering

University College London

A thesis submitted for the degree of

Doctor of Philosophy

-2017-

Declaration

I, Carlotta Peticone confirm that the work presented in this thesis is my own. Where information has been derived from other sources, I confirm that this has been indicated in the thesis.

Acknowledgements

First of all, I would like to express my sincere gratitude to my principal supervisor Dr Ivan Wall for his continuous support and guidance throughout this four years' journey. I will always be grateful for all the opportunities and challenges he gave me the chance to undertake, for his trust and constant encouragements during the course of this project.

I am very thankful to Prof. Jonathan Knowles at the Eastman Dental Institute at UCL for his valuable suggestions and fruitful discussions on the biomaterial side of the project.

A special "grazie" to Dr Martina Micheletti for all the guidance in planning all the flow dynamic experiments and for her constant professional and human mentorship since my early days at UCL.

I am sincerely grateful to Prof. Justin Cooper-White at the University of Queensland for his supervision and constant help during my time at the Australian Institute for Bioengineering and Nanotechnology (AIBN) and for all the bright contributions and ideas to the development of this project. Spending nine months in his lab was a great learning experience and I will always be grateful to him for this opportunity.

I would like to acknowledge Dr Nilay Lakhkar (Eastman Dental Institute) for introducing me to the field of phosphate glass and for training me on manufacturing and characterization during the early days of my PhD, and Dr Gareth Owens (Eastman Dental Institute) for all the help with the degradation and ion release studies.

I would like to acknowledge Dr Nick Glass at AIBN for training me in microfluidics manufacturing and for all his help and advices in the development of the microfluidic device.

I am grateful to Prof. Nicholas Szita and all members of the Microfluidic Group at UCL for all their advices and technical support in device fabrication.

I would also like to acknowledge Prof Alan Burns at the Institute of Child Health for his kind and generous collaboration on planning and setting up the CAM assay experiments and in particular Ben Jevans for all his help in performing the experiments.

I am very grateful to EPSCR who funded this project, to the UCL Graduate School for supporting my research project at AIBN and to UCL Advances for awarding me with the UCL Advances PhD Enterprise Scholarship.

I would like to thank all the students, postdocs and technicians in the Regenerative Medicine and Tissue Engineering Lab at UCL for all their help and for having made the lab a great place to work in. In particular special thanks to Ludmila for all the tissue culture training and technical advices, to the "early days" students Giulia, Owen, Shahz, Nathalie, Vishal, Ben, Rui, Zi and the "new generation" Mel, Ana, Gerry, Rachel, Rana, Reema, Joana, Ivano and Ganaa and "my past, present and future" friend Fatumina.

This project wouldn't have been possible without the constant support of my "partner in crime", David. Thank you for all your help as a colleague, but most importantly as a friend, these four years wouldn't have been the same without having you constantly on my side.

I also would like to thank the entire Department of Biochemical Engineering that has been like a family for the past eight years of my life. Thank you to all the people that, in different ways, have contributed to my professional and personal growth. In particular thank you to my friends Asma, Damiano, Nehal, Nelson, Yiannis for all the laughs and good time together and to Prof Suzanne Farid for being a great life and professional mentor.

Also, a special thanks to my friends and colleagues "down under" and in particular to Jane, Nick, Jess, Clem, Taryn, Li, Owen and the entire TEaM lab at AIBN as well as the Australial National Fabrication Facility (ANFF) staff. And of course, a special thank you to the Italians Ilaria, Milena and Paola for sharing with me all the good (and the bad) moments of this Australian adventure.

My deepest gratitude goes to my family for their love and for constantly being there to support me, always pushing me to reach higher. Grazie per aver sempre creduto e supportato le aspirazioni di questa figlia "girovaga" e per essere sempre stati una fonte di ispirazione per me.

Finally, "un grazie di cuore" to Massi who shared with me every single joy, frustration, triumph and pressure of this project. Thank you for your understanding, love and patience, especially in the last months of thesis writing and also for teaching me how to approach difficulties with a smile. Thank you for being a great friend, a caring partner and also an inspiring scientist. I probably wouldn't have made all the way to the end without you.

Abstract

Four million surgeries involving bone grafting or bone substitutes for the treatment of bone defects are performed yearly worldwide. However, limited donor tissue availability, pain and the risk of infection and immune rejection, have led to the development of alternative strategies for bone repair. Tissue engineering represents an alternative to current treatments as it consists of using a biomaterial scaffold alone or in combination with proteins, genes or cells, as a bioactive implant to stimulate bone repair. Microspherical scaffolds have been proposed as a potential modular unit for bone tissue engineering applications as their shape could facilitate filling of irregular shaped defects. Furthermore, microspheres could be used as a support for *ex vivo* expansion of adherent cells as well as a carrier to directly deliver cells to the defect site.

In this study, the use of phosphate glass microcarriers for bone tissue engineering applications was investigated. As this material is completely soluble and non-toxic, it can be implanted in the patient together with cells. Furthermore, the tuneable glass composition can be easily engineered to induce specific structural and biological properties. Here, the effect of culturing MG-63 and hBM-MSCs on titanium-doped phosphate glass microspheres containing increasing concentration of cobalt (0, 2 and 5%) was investigated, as these ions have been shown to induce osteogenesis and angiogenesis, respectively. Furthermore, as part of this study a novel perfusion microfluidic bioreactor was fabricated to culture cells on microspheres under perfusion and to enable parallel screening of multiple culture variables.

Cells proliferation on the microspheres as well as secretion of ECM proteins in response to the substrate was observed over time, thus confirming the biocompatibility of all compositions tested. Upregulation of osteogenic markers by MSCs also occurred in response to the microspheres in the absence of exogenous supplements. However, this effect was suppressed when cobalt was added to the glass composition. On the other hand, while cobalt-doping was found to induce key angiogenic responses (i.e. VEGF secretion), this did not translate into improved functional vascularization in comparison to the cobalt-free microspheres. Successful MSCs culture on the microspheres within the microfluidic reactor was achieved and it was possible to efficiently quantify functional outputs, such as the expression of ECM proteins as a function of microspheres substrates and nutrient feeds under perfusion.

In conclusion, titanium-doped phosphate glass microspheres were identified as a potential substrate for bone tissue engineering applications in terms of MSCs expansion and differentiation, as well as to support endothelial cells migration towards the scaffold and vessel formation, while additional doping with cobalt was not found to improve the functionality of the microspheres. Furthermore, the microfluidic bioreactor enabled to identify optimal parameters for perfused cell culture on microspheres that could be potentially translated to a scaled-up system for tissue-engineered bone manufacturing.

List of contents

List of figures

List of tables

List of abbreviations

2D: two dimensional

3D: three dimensional

BG: bioglass

BM-MSCs: bone marrow mesenchymal stromal cells

BSA: bovine serum albumin

BTE: bone tissue engineering

CAM: chorioallantoic membrane

CaP: calcium phosphate

CB: cord blood

Cbfa1: core-binding factor subunit alpha-1

CFU: colony forming unit

DLX-5: distal-less homeobox 5

DMEM: Dulbecco modified Eagle's medium

DTA: differential thermal analysis

EBM: endothelial basal medium

ECM: extracellular matrix

ECs: endothelial cells

ESCs: embryonic stem cells

FBS: fetal bovine serum

FDA: Food and Drug Administration

FTIR: Fourier transform infrared spectroscopy

GAPDH: glyceraldehyde-3-phosphate dehydrogenase

HA: hydroxyapatite

HIF-1α: hypoxia inducible factor 1-alpha

hOB: human osteoblast

HSCs: hemapoietic stem cells

HUVECs: human umbilical vein endothelial cells

ISCT: International Society of Cellular Therapy

LDH: lactate dehydrogenase activity

MDA: malonyldialdehyde

MSCs: mesenchymal stem cells

OPN: osteopontin

PBS: phosphate buffered solution

PFA: paraformaldehyde

PG: phosphate glass

PGLA: poly(lactide-co-glycolide)

PLA: poly(lactic acid)

PDMS: polydimethylsiloxane

pNPP: *p*-nitrophenyl phosphate

qPCR: quantitative polymerase chain reaction

rhBMP-2 recombinant human bone morphogenetic protein-2

RUNX2: runt-related transcription factor 2

UC: umbilical cord

VEGF: vascular endothelial growth factor

XRD: X-ray diffraction

β-TCP: beta tricalcium phosphate

Chapter 1: Introduction and literature review

1.1 Introduction

Replacing damaged or diseased body parts using living artificial tissues has been the focus of the field of tissue engineering in the last thirty years. According to the classic definition of Langer & Vacanti (1993), Tissue Engineering is ‘‘an interdisciplinary field of research that applies the principles of engineering and the life sciences towards the development of biological substitutes that restore, maintain, or improve tissue function’’. In contrast to traditional clinical approaches that have been simply focusing on using implants or prostheses to replace mechanical functions, the goal of tissue engineering is that of inducing the formation of new functional living tissue that, like its native counterpart, is biologically active and continuously evolve in response to the physiological environment.

Being the second most transplanted tissue in the world and with an increasing need for bone grafts and substitutes (Liu et al. 2013), bone regeneration has been one of the first target of tissue engineering.

Currently, autologous bone grafting is the clinical standard in bone repair and regeneration (Amini et al. 2012). The strengths of this procedure are that grafts are biocompatible, non-immunogenic and present the same properties of the original bone. However, these procedures are very expensive and may cause injury and morbidity at the harvesting site, together with significant surgical risks (Amini et al. 2012). Furthermore, this technique is not feasible when large quantities of bone are required. Allografts, using graft from other donors or cadavers, are also a common treatment. However, they present the risks of immunoreactions and infection transmission. Freeze-drying or irradiation are performed to minimize these reactions, however these techniques cause alterations of the structural and physiological properties of the material (Delloye et al. 2007).

Key elements of the bone tissue engineering approach are extracellular matrix secreting cells, a biocompatible three dimensional (3D) scaffold to accommodate cells in a correct spatial geometry, biochemical stimuli to attract cells to the implant site and drive their differentiation and a vascular supply (Amini et al. 2012). Finding an optimal combination between these components has been the area of focus of several research groups worldwide. Despite the advances, approaches involving the combined use of scaffolds, cells and growth factors have not yet been successfully translated to the clinic.

Several examples exist of commercially available acellular inorganic (beta tricalcium phosphate (β-TCP), hydroxyapatite (HA) and bioactive glasses) and organic (natural and synthetic polymers) biomaterials used as bone filler for skeletal tissue regeneration (Shrivats et al. 2014). Although promising results have been obtained, these approaches are still less effective than the clinical standards, especially in the treatment of critical sized bone defects (Shrivats et al. 2014).

Similarly, many clinical trials involving the use of cellular suspensions (i.e. bone marrow cells) for small non-union defects or cellular seeded scaffolds for the treatment of larger defects have been reported, showing promising preliminary data (Salter et al. 2012). However, none of these approaches have been commercially approved, with the only exception of Osteocel (NuVasive, USA), which consists of human allogeneic mesenchymal stromal cells (MSCs), mixed with spongy bone material obtained from donors or cadavers and used for the treatment of spinal defects or fractures (Grayson et al. 2015).

InFuse™ from Medtronic is an example of a Food and Drug Administration (FDA)-approved combined product for the delivery of recombinant human bone morphogenetic protein-2 (rhBMP-2) through a purified collagen matrix scaffold for single-level anterior lumbar interbody fusions (Epstein 2011). However, several significant complications have been linked to the use of rhBMP-2, including dysphagia, airway compression in cervical spine fusion and heterotopic bone formation to name a few. Currently, bone grafting still represents the gold standard for the treatment of spine fusions (Hollister & Murphy 2011).

The examples above suggest that for an impactful translation of Bone Tissue Engineering (BTE) to the clinic, a combinatorial product presenting a scaffold integrated with cells and biochemical stimuli is required to obtain effective bone repair and regeneration and to overcome clinical standards.

In the following paragraphs, a literature review is provided which analyses some of the key advances and challenges of BTE. In particular, after a short description of bone structure and physiology, a detailed state of the art review of scaffolds, biomaterials (with a particular emphasis on bioactive glasses), cells and bioreactors, which have been investigated for BTE applications, is given. This is followed by a brief overview of the current challenges that are limiting BTE translation to the clinics. Finally, the hypothesis and objectives of the present research are listed.

1.2 Literature review

1.2.1 Bone

1.2.1.1 Biology and physiology

"The skeleton, out of site and often out of mind, is a formidable mass of tissue occupying about 9% of the body by bulk and no less than 17% by weight. The stability and immutability of dry bones and their persistence for centuries and even millions of years after the soft tissues have turned to dust give us a false impression of bone during life. Its fixity after death is in sharp contrast to its ceaseless activity during life".

This famous quote from Cooke (1955) synthesizes the dual nature of the skeletal system: although often seen as a static support structure, bone is a dynamic, metabolically active organ that undergoes remodeling throughout life in order to maintain bone shape, size and quality.

The skeleton provides both a structural and a metabolic function. It not only gives support and protection to vital organs and the bone marrow, favors respiration and serves as muscle attachment for locomotion, but also acts as a reserve of calcium and phosphate to maintain serum homeostasis and acid-base balance (Hadjidakis & Androulakis 2006; Clarke 2008)

Bone is a highly vascularized and innervated, mineralized connective tissue, whose main components consist of an extracellular matrix, collagen and cells. In humans, 206 bones constitute the skeleton and two main types of bone are present: cancellous and cortical (Brydone et al., 2010). Cancellous bone (trabecular bone) constitutes the internal porous structure of bone. It is less dense, more elastic and presents a higher turnover rate than cortical bone. It provides mechanical support, particularly in the vertebrae, and actively participates in metabolic responses, providing mineral supply in the early stages of acute deficiency (Hadjidakis et al., 2006). Cortical bone (compact bone) forms an outer shell surrounding cancellous bone. It is dense and compact, presents slow turnover rate and it is mainly calcified. It does provide mechanical support and protection, contributing to metabolic response only in case of severe or prolonger mineral deficit (Hadjidakis et al., 2006).

The bone matrix mainly consists of type I collagen fibers mineralized with hydroxyapatite crystals and it constitutes 90% of the organic composition of the whole bone tissue (Hadjidakis et al., 2006). Three main types of cells are found in the bone: osteoblasts, osteoclasts and osteocytes. Osteoblasts are the cells responsible for secreting the bone matrix. They are found in clusters on the bone surface, lining on the newly deposited layer of bone matrix and they are derived from MSCs. Towards the end of the bone matrix secretion process,

15% of osteoblasts are entrapped within the matrix, thus differentiating into osteocytes; other cells remain on the bone surface, becoming flat lining cells (Hadjidakis et al., 2006).

Osteocytes are terminally differentiated osteoblasts that are not capable of cell division. They are responsible for the synthesis and mineralization of bone matrix wherein they are localized (Hench, 2006).

Osteoclasts are giant multinucleated cells of hematopoietic derivation and they are the cells responsible for bone resorption. Osteoclasts attachment to bone surface occurs through special dynamic structures called podosomes. Bone resorption occurs through acidification and dissolution of the bone matrix and of the hydroxyapatite crystals (Hadjidakis et al., 2006). The combined action of osteoblasts and osteoclasts give rise to the process of bone remodeling, through which microfractures are repaired and the structure is remodelled according to mechanical and biochemical stimulation, thus maintaining bone strength and mineral homeostasis (Clarke, 2008).

Bone formation occurs via two distinct processes, intramembranous and endochondral ossification. In intramembranous ossification, mesenchymal progenitor cells are first recruited to the site of ossification and differentiate directly into osteoblasts, while in osteochondral bone formation, they first differentiate into chondrocytes, thus forming a cartilaginous template that is then mineralized and replaced by bone (Amini et al. 2012). Intramembranous ossification occurs in the development of most cranial bones, the clavicle and the mandible, while all long bones and vertebrae formation occurs through the endochondral process (Amini et al. 2012).

Fracture repair occurs through the combined action of both intramembranous and endochondral ossification. It starts with an inflammatory response that leads to recruitment of MSCs that differentiate into both chondrocytes and osteoblasts (Fazzalari 2011) and signalling molecules involved in bone formation (Amini et al. 2012). Following resorption of the calcified cartilage through chondroclasts and bone formation through the osteoblasts, remodelling occurs through resorption to restore the functional load-bearing anatomical structure.

1.2.1.2 Pathologies and current therapies

Despite its intrinsic regeneration capacity, bone defects, due to traumatic events or to pathological or physiological conditions, remain a key challenge in global health, with muscoskeletal conditions representing the main cause of pain and disability worldwide (Guldberg 2009).

Main causes that lead to large bone defects are trauma, tumor resection and degenerative diseases (i.e. osteoporosis, degenerative disc disease) that are increasingly common in aged patients. Furthermore, the increasing ageing world population requires advanced techniques to replace, restore or regenerate bone in the field of orthopedic, spinal, dental, maxillofacial and cranial surgery (Brydone et al., 2010).

Autologous bone grafting is the clinical standard for osseous reconstruction as it consists of transplanting a bone from one part of the body (donor site) to the defect site, thus being histocompatible, non-immunogenic and presenting all key properties of native bone (Amini et al. 2012). Although clinically effective, autologous graft is an expensive procedure, limited by donor tissue availability and that can result in significant morbidity and pain at the site of harvest (Banwart et al. 1995; Ebraheim et al. 2001; Dimitriou et al. 2011).

Alternatively, decellularized allografts from cadavers or other patients can be used. However, the risk of infections, immune reaction and disease transmission associated with this type of grafts is significant (Brydone et al., 2010, Amini et al. 2012). Furthermore, the risk of re-fracture after one or two years from implantation is very high, as these implants are acellular and present reduced bioactivity, remodeling and vascularization capacity (Berrey et al. 1990).

In the US alone, approximately half a million operations involving bone grafting or bone substitutes are performed on a yearly basis (Amini et al. 2012), and this number is expected to double by 2020 due to increased life expectancy (Salter et al. 2012). This is due to the fact that 5% of all fractures and 20% of high-impact fractures present delayed healing or non-union, thus requiring a surgical intervention (Brydone et al. 2010). Spinal surgery alone represents a big market, with spinal fusions being 50% of the total autologous bone graft operations performed in USA (Brydone et al., 2010). Joint replacements represent another widely performed surgery, with currently 10% undergoing revision and this figure is likely to increase as the population ages and life expectancy increases (Brydone et al., 2010).

Bone is also often replaced by metal implants. Commonly used materials are titanium, stainless steel 316L, cobalt chromium (CoCr) alloy, titanium and titanium alloy (Brydone et al., 2010). These bioinert implants, now referred to as first generation biomaterials, have been widely used for load-bearing prosthesis or fracture fixation devices and they have been developed to provide minimal response in the host. However, there are large differences between the elastic moduli of bone and that of a metal implant. As most of the load is carried by the high modulus implant, the load on the bone decreases (stress shielding). This leads to biological changes causing bone resorption and weakening, thus increasing the likelihood of re-fracture (Brydone et al., 2010). Other techniques adopted in bone repair consists of distraction osteogenesis, bone cement fillers, and bone morphogenic proteins (Amini et al. 2012). Although some positive results have been obtained using these approaches, they still lack most of the key properties required in bone repair such as osteoinductive and angiogenic potentials, biological safety, reasonable cost and low patient morbidity (Amini et al. 2012).

1.2.2 Bone Tissue Engineering

1.2.2.1 Tissue engineered construct: key features

The limitations of current strategies have led to development of new approaches to stimulate bone repair. Tissue engineering represents a possible solution to the standard issues associated with current treatments, such as poor implant integration and long-term mechanical stability (El Haj & Cartmell 2010). This strategy consists of using a biomaterial scaffold alone or in combination with proteins, genes or cells, as a bioactive implant to stimulate bone repair.

Different strategies have been proposed due to the diversity of clinical problems requiring bone regeneration. For example, in craniofacial reconstruction complex shapes are required, thus a filling material that can be shaped to fit the defect, would be ideal (Guldberg et al. 2007). In spinal fusion, where osteogenic formation has to be induced in area where no bone existed previously, a locally delivered osteinductive solution would be particularly effective (Guldberg et al., 2007). When proposing a tissue engineering solution for large segmental bone defects, mechanical considerations become of critical importance and dictate the design of the scaffold (Guldberg et al., 2007). Finally, the age, physiology and life-style of the patient also have a crucial impact on the design of the construct (Guldberg et al., 2007).

Despite the diversity of factors that need to be taken into considerations under each pathological condition, the following key elements are necessary for successful bone regeneration (Amini et al. 2012):

1. a biocompatible scaffold made of an osteoinductive biomaterials and presenting similar characteristics of bone extracellular matrix;
2. osteogenic cells secreting bone tissue matrix;
3. a vascular supply to provide the new tissue with nutrients and waste removal;
4. morphogenic signals, to promote cells differentiation into the desired phenotype and vessels ingrowth.

In the last three decades, several classes of biomaterials and scaffold assembly, cell types and engineering strategies for successful bone tissue replacement have been investigated. A review of some of the key approaches reported in the literature is provided in the following paragraphs.

1.2.2.2 Top-down versus bottom-up modular tissue engineering

Traditional tissue engineering is based on the so called top-down approach, in which cells are first isolated and expanded, and then seeded on a degradable scaffold of predefined size and shape (Mei, Luo, Tang, Ye, Zhou & W. S. Tan 2010). This is followed by cells spreading homogenously within the scaffold, secreting the tissue-specific extracellular matrix and reassembling into the appropriate tissue structure. Despite the advances in surface patterning

and material development to closely mimic tissue, this type of approach often fails in recreating native tissue microstructures (Nichol & Khademhosseini 2010).

An alternative is represented by modular tissue engineering in which small building blocks of tissue are formed and then assembled into large-scale constructs (Mei, Luo, Tang, Ye, Zhou & W. S. Tan 2010). Working at the micron scale enables engineers to recreate tissue functional units, and unit modules can be created through different methods such as controlled cell aggregation, cell sheet assembly, cell-laden hydrogels or tissue printing (Nichol & Khademhosseini 2010; Liu & Gartner 2012). A further advantage of the "bottom-up approach" is that during tissue assembly, an interconnected macrostructure is formed that could potentially facilitate in vivo vascularization (Mei, Luo, Tang, Ye, Zhou & W. S. Tan 2010). Furthermore, in regards to bone tissue engineering, a patient tailored approach could be used, where building blocks are assembled to repair bone defects of specific size and shape.

Microspherical scaffolds have been proposed as a potential modular unit for bone tissue engineering applications (Hong et al. 2009; Chan et al. 2010; Mei et al., 2010, Lakhkar et al. 2012, Chen et. al 2013), as their sphericity could facilitate filling of irregular shaped defects (Perez et al. 2014). Microspheres have been used both as a tool to expand adherent cells ex vivo and also to directly deliver cells to repair or regenerate tissues (Martin et al., 2011).

While for cell expansion, inert, plastic microcarriers are usually used, microspheres for tissue engineering applications need to be made of a suitable implantable biomaterial that support cell growth and ideally could direct differentiation towards a specific tissue and promote biological responses in vivo (Park et al. 2013). In bone tissue engineering, three main types of microspheres have been investigated: solid-filled with cells growing on their surface, porous with cells growing within the microcarriers or alternatively, cell encapsulation within the particle hollow inner space (Park et al., 2013).

Similar to other types of scaffold, several materials including bioactive ceramics, polymers and their composites have been synthesized in the form of spherical particles and they have been found to support cell attachment to the curved surface, together with growth and differentiation towards an osteogenic phenotype under specific culture conditions (Park et al., 2013). Furthermore, being suitable for integration within a bioreactor system, they are particularly attractive from a bioprocessing prospective as they are easily scalable compared to other type of scaffolds.

1.2.2.3 Scaffold properties

Independently of the type of approach adopted, scaffolds for skeletal tissue engineering need to meet several requirements in order to be efficiently used at the clinical level. Firstly, the scaffold needs to be biocompatible, thus being non-immunogenic and non-toxic upon degradation (David et al. 2007). Resorbability is another key property. The scaffold should

degrade at the same rate at which bone regeneration occurs, thus transferring mechanical load from the scaffold to the new formed bone (Bose, Roy, et al. 2013). The degradation rate should vary according to the application, with spinal fusion requiring at least 9 months or more, while 3 to 6 months being sufficient for scaffold in cranio-maxillofacial applications (Bose, Roy, et al. 2013).

Whether the scaffold should have good mechanical properties, matching those of the original bone, is a controversial question. Some authors state that the scaffold should be designed to have sufficient mechanical strength to withstand hydrostatic pressure and maintain adequate spacing for cell growth and matrix deposition, when cultured in vitro (Salgado et al. 2004). Furthermore, the mechanical properties should match those of living bone, thus facilitating early mobilization of the injured site (Salgado et al., 2004). However, other authors believe that physiological mechanical properties are not a key requirement and that the scaffold should be mainly designed to support bone ingrowth, rather than mechanical loading (David et al., 2007). Appropriate orthopedic devices such as internal plates or external fixators could be used if required to provide mechanical stability during the regeneration phase (David et al., 2007).

Porosity, on the other hand, is universally accepted as a key characteristic. Porous interconnected structures and large surface-to-volume ratio are required to maximize cell ingrowth and homogenous distribution through the scaffold. Furthermore they favor transport of nutrients, oxygen and signaling factors across the scaffold. Pore size in the 200-900μm have been found to be ideal not only for the attachment of osteoprogenitor cells, but also for the integration of endothelial cells and the formation of a vascular network (Salgado et al., 2004; David et al., 2007).

Vascularization is a key issue in tissue engineering. *In vivo*, the distance between cells and the nearest capillary is between 100-200μm, thus enabling effective diffusion of oxygen, nutrients and waste products (Lovett et al. 2009). This limits the size of any tissue constructs produced *in vitro*. Furthermore, tissue engineering constructs are usually implanted in poorly vascularized, fibrotic areas, thus compromising *in vivo* survival. Thus, the scaffold should present a structure that support *in vitro* and *in vivo* vascularization.

As cells are sensitive to the surface chemistry and topography of the material substrates to which they adhere to, these properties should also be taken into consideration. In particular, cells adhesion, proliferation and phenotypic expression are affected by the size, shape and roughness of the scaffold (David et al., 2007). For example, it was shown that a rough titanium (Ti) surface was able to induce an osteogenic phenotype and to upregulate osteogenic genes expression in hMSCs and to limit their proliferation, compared to cells grown on a Ti-smooth surface (Wall et al. 2009). Rough surfaces have also be proven to facilitate osteogenic cells

adhesion to the implant, thus improving osteoconduction that is the growth of bone at the material surface (Davies 1996).

From a processing point of view, the material should be easy to manufacture and sterilize, easy to handle in the operating theater (David et al., 2007), and should be suitable for being pressed or injected into the bone defect (Jones 2015).

Materials presenting osteoinductivity properties, that is the capacity to recruit stem and progenitor cells to the bone healing site and to stimulate their differentiation, are the ideal candidate. A material is considered osteoinductive when it is able to induce bone formation heterotopically, so that the newly formed bone can be only attributed to the capacity of the material to recruit progenitor cells (Barradas et al. 2011). On the other hand, in orthotopic implantation, bone forming on the implant surface could be induced by existing bone forming cells rather than osteoprogenitors, a property known as osteoconductivity (Barradas et al. 2011).

Biodegradable ceramics and polymers are the classes of materials more widely investigated for bone tissue engineering. Calcium phosphate (CaP) based ceramics have been widely used for bone substitution/regeneration, as CaP is a main component of bone (Bose, Fielding, et al. 2013). They can be derived from natural source such as coralline hydroxylapatite or can be synthesized, such as synthetic HA, β-TCP or biphasic calcium phosphate, a mixture of HA and β-TCP or bioactive glass. These materials have been found to be osteoinductive and osteoconductive (Salgado et al., 2004), to promote the absorption of bioactive proteins and to enhance vascular ingrowth. 45S5 Bioglass® is an example of a ceramic material that has been successfully used at the clinical level as a bone filler material for periodontal disease and to replace damaged middle ear bones.

Main limitations of this class of material are their brittleness and low mechanical stability. Furthermore, their degradation rate must be controlled, in order to prevent a too rapid dissolution of the scaffold when implanted in vivo (Guldberg et al., 2007, Smith & Grande 2015). Doping CaP scaffolds with metal oxides has been proposed as a successful strategy to control their degradation rate, mechanical strength and biocompatibility (Bose, Roy, et al. 2013).

From a structural point of view, polymers represent a better option as their architecture can be more easily controlled (Smith & Grande 2015). Examples are chitosan (a natural occurring polymer derived from the shells of crustaceans), collagen and fibrinogen for the naturally derived polymers and poly(a-hydroxyacids), poly(e-caprolactone) and poly(carbonates), for those artificially synthesized. However, they present limited capacity for cells attachment and high hydrophobicity if not properly modified (Guldberg et al., 2007). Furthermore, some polymers present fast degradation rate and the formation of an acidic environment upon dissolution that can have detrimental effects on the surrounding tissues (Bose, Roy, et al. 2013).

Composite scaffolds, combining ceramics and polymers, represent an attractive alternative. For example, ceramic particles can be embedded in a polymer matrix, thus combining bioactivity and optimal structural properties in one single scaffold (Bose, Roy, et al. 2013). Promising results have been shown *in vitro* an *in vivo*, combining polymers poly(lactic acid) (PLA), poly(lactide-co-glycolide) PLGA, chitosan and collagen in combination with HA crystals, with generally observed enhanced osteoconductivity properties compared to pure polymers (Amini et al. 2012).

1.2.2.4 Bioactive glass in bone tissue engineering

1.2.2.4.1 Silicate bioglass (BG)

As previously stated, bioceramics are among the materials most commonly used for bone repair and they include glasses, glass–ceramics and ceramics used as implant materials (Jones, 2015). In particular, bioactive glass has been used in the last forty years as material for bone implants and has been reported to stimulate bone regeneration more efficiently than other ceramics (Jones, 2015). They were first discovered by Larry Hench in 1969 at the University of Florida (Jones, 2015). Professor Hench was looking for an implant material that could integrate and create a stable bond with bone tissue, rather than promoting fibrous encapsulation, as most of the bioinert implant material available at the time (Jones, 2015). He developed a degradable glass, containing Na_2O,P_2O_5, CaO and SiO_2, that was able to form a stable and permanent bond with bone. The glass was named Bioglass 45S5®, and it is currently found in several products available in the market for bone repair (Jones, 2015). It was first implanted in 1984 in a patient deaf from an infection that caused the loss of two of the three bones in the middle ear. The 45S5 Bioglass® implant formed a bond with the native bone and hearing was fully restored. In the first clinical trial, each implant was custom shaped to fit individual bone defects, however, as this option was not commercially feasible, they were later produced in conical shapes of three different sizes (Jones, 2015).

Bioactive glasses such as 45S5 are referred to as second generation biomaterials (Hench et al. 2004). They differ from inert first generation biomaterial used in transplant that were developed to provide minimal response in the host. In particular, first generation biomaterials had to present the following characteristics: (i) suitable mechanical properties, (ii) corrosion resistance, and (iii) biocompability, thus showing no carcinogenicity, toxicity, allergy and inflammation effects (Narayan 2010). The limited life span of those materials and high risk of implant failure, led to the development of a second generation of biomaterials, whose aim was that of interacting, in a controlled fashion, with the physiological host environment.

Hench identified the controlled released rate of ionic dissolution products from bioactive glass as the critical phenomenon leading to bone regeneration, by inducing mitosis in bone osteoprogenitor cells (Hench 2006). A study performed by Xynos et al. (2000)

investigated the effect of 45S5 Bioglass® versus a bioinert control (Thermanox® plastic) on the cell cycle of human osteoblasts (hOBs) derived from patients aged 50-70 years.

Normally, formation of new bone *in vivo* is obtained when osteoprogenitor cells undergo mitosis. However, in elderly patients, the percentage of cells capable of dividing is very limited, as the capacity of cells to divide diminishes with age. As shown by Kassem et al. (1997), similarly to other somatic cells, human osteoblasts cultured in vitro present a limited division potential (Hayflick limit) and an increase of the population doubling time. Furthermore, a decrease of number of cells in S-phase and a decrease in their differentiation potential are observed as a result of long term culture.

During the S phase, all chromosomes are duplicated; the cell then eventually enters phase G2 of the cell cycle, during which it prepares for division and checks DNA replication accuracy (Hench 2006). The cell is then ready to enter the mitotic phase, where cell division occurs. If the cell is not in the correct local environment, and full completion of phase G1 or G2 is not achieved, the cell proceeds to programmed cell death (Hench 2006).

Xynos et al. (2000) showed that the number of osteoblasts in the S-phase or G2-M phase was 100% higher on the bioactive glass substrate than in the bioinert control after two days of culture. The apoptotic population at 48hrs was also found to be five times higher on the glass than in the control. Then, in the first 48 hours of culture, a selection process occurs in which cells that are able to differentiate into mature osteoblasts survive, and those that are not able to divide enter the apoptotic fate. In the bioinert control, cells were found to attach and divide rapidly, forming a confluent layer of cells, with a lower percentage of apoptotic cells. However, a smaller population of cells grown on the control substrate was able to differentiate and produce bone matrix, compared to the bioactive glass. Despite the slower initial growth, by 48 hours the number of mitotically active cells in bioactive glass significantly increased.

Xynos et al., (2000) also observed the formation of three dimensional structures of cells and mineralized cellular matrix after six days of culture on bioactive substrate, in the absence of osteogenic supplements such as ascorbate and/or b-glycerophosphate, while no bone nodules were formed in the bioinert control.

After the first clinical trial, 45S5 Bioglass® and other types of third generation bioactive glass have been used in several clinical applications (Hench 2011). In particular 45S5 Bioglass® is found in two products available in the market: NovaBone® (NovaBone Products LLC) and NovaMin® (GlaxoSmithKline, UK) (Jones, 2015). These products are synthesized in the form of particulates, to address the request of surgeons and dentists of a bone substitute that could easily be pressed within a bone defect (Jones, 2015). The first is a synthetic bone graft for orthopedic and periodontal applications, usually mixed by surgeons with blood to create a putty-like consistency (Jones, 2015). In particular, the glass is used to fill bone cavities due to trauma

or tumor/cyst removal or in jaw bone defects around the tooth root or as a bone grafting for not load-bearing sites (http://www.novabone.in/pdf/0603.pdf).

NovaMin® is a 45S5 Bioglass® fine powder that is used as the active repair agent in toothpastes (i.e. Sensodyne) produced by GlaxoSmithKline, for reducing teeth sensitivity caused by exposed dentine. The NovaMin® particles when in contact with fluid (i.e. water or saliva) reacts by releasing calcium (Ca) and phosphate (PO_4) ions, thus facilitating the dentin remineralization process. This leads to the formation and crystallization of a layer of hydroxycarbonate apatite, that results in a physical occlusion of exposed dentinal tubules and blocking of nerve endings, thus leading to a reduction in tooth sensitivity (Hench 2006; Joshi et al. 2013). Clinical trials have shown reduction in dentine hypersensitivity even after a single application of Novamin® containing pastes (Neuhaus et al. 2013).

1.2.2.4.2 Phosphate glasses

As the dissolution rate of silica glasses ranges between 1 to 2 years and due to concerns regarding the long term effect of silica accumulation within the body (E A Abou Neel et al. 2009), other types of glass have been investigated for bone engineering purposes. Phosphate glass, for example, present a tunable dissolution rate that can be adjusted to be within hours to several weeks, by modifying the glass composition. Phosphate glass consists of phosphate (rather than silicate or borosilicate) as the glass former, thus presenting chemical similarity to the inorganic phase of bone (Hoppe et al. 2011). They can fully dissolve in aqueous media, giving ionic species commonly found in the human body, and this property makes them particularly relevant for biomedical applications. The basic composition of phosphate glasses is the following: $CaO\text{-}Na_2O\text{-}P_2O_5$. This, however, can be modified by including metal dopants to enhance biocompatibility, durability or to induce specific functions.

Their capacity to be tailored to express specific biological functions, together with their full dissolution, make them fall in the category of third generation biomaterials (Abou Neel et al., 2009). Furthermore, phosphate glasses can be produced in several forms (fibre, melt-quenched or sol-gel bulk, microspheres), thus offering a great potential for both soft and hard tissue engineering (Abou Neel et al., 2009; Lakhkar et al., 2012).

Both silica and phosphate glasses consist of a basic tetrahedral unit (Brauer 2012).

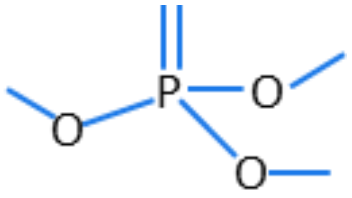

Figure 1.1: The basic tetrahedal unit in phosphate glass structures.

However, while the SiO_4 tetrahedron can share all its oxygen atoms to form a network, PO_4 can only share three out of the four oxygen atoms, with one of the oxygen linked by a double bond to the P^{5+} ion. Bridges between distinct phosphate tetrahedral can be obtained by covalent POP bonds, thus forming chains, rings or branching networks (Brauer, 2012). A phosphate glass purely made of a phosphate network can be obtained; however, the POP bonds are not chemically stable and hydrolysis occurs at atmospheric moisture (Brauer, 2012). Network modifiers such as CaO and Na_2O can be added to increase durability. The modifiers cause the cleavage of POP bonds and the formation of ionic cross-linkages between units. An opposite trend is observed in silica glasses, where less stable glasses are obtained upon modifying oxides addition (Abou Neel et al., 2009).

As previously mentioned, the capacity of phosphate glasses to completely dissolve in aqueous solution into non-toxic products, makes them a very attractive material for biomedical applications. Metal oxides can be used as dopant to control phosphate glasses degradation rate. This can be achieved by stabilizing the glass network by doping with several oxides such as TiO_2, Al_2O_3, B_2O_3, ZnO, MgO, SrO, CuO and Fe_2O_3 (Hoppe et al. 2011). Furthermore, these ions have been found to induce biological responses on human cells, such as promoting activation of osteogenic and angiogenic pathways. From an osteogenesis point of view, some inorganic ions (i.e. Si, Ca, P, Zn, Mg, Sr, Cu, B, Ti) have been found to overstimulate the expression of osteogenic markers, to increase osteoblasts proliferation and/or to induce early osteoblasts towards an osteogenic differentiation pathway (Hoppe et al. 2011; Lakhkar et al. 2013). On the other hand, enhanced endothelial cells proliferation, the formation of cell tubules networks or the stimulated secretion of angiogenic growth factors (i.e. VEGF) are some of the angiogenic responses that have been observed on cells exposed to trace elements such as copper (Cu) and cobalt (Co) (Hoppe et al. 2011).

In the following paragraphs, the capacity of titanium and cobalt ions doping to induce osteogenic and angiogenic responses respectively, will be reviewed.

1.2.2.4.3 Inducing osteogenic responses – titanium doping

Titanium (Ti) is widely used in clinical applications in dental and orthopedic implants. Abou Neel and Knowles (2008) were the first to introduce titanium oxide in phosphate glasses and to test their biocompatibility. They used a glass with composition $50P_5O_2$-30 CaO -20 Na_2O (mol%) and they substituted Na_2O with progressively increasing amount of Ti (0,1,3 and 5 mol% TiO_2). Osteosarcoma cells attachment and viability up to 7 days of culture was tested. The fast degradation rate of the compositions without or with minimum Ti concentration caused a rapid decrease in pH that resulted in lower attachment and viability compared to other compositions. However, results obtained with the 3 and 5% compositions were comparable to

tissue culture treated flasks, thus suggesting the suitability of this substrate for bone engineering applications.

Dissolution of phosphate glasses containing Ti in simulated physiological conditions was found to be one order of magnitude lower than in TiO_2-free glasses (Novajra et al. 2011).It was also found that the decrease in pH observable in simulated body fluid, was not seen in experiments where cells were present. In the same study, cytotoxicity levels were tested in terms of lactate dehydrogenase activity (LDH) in culture media and cell lysate, and intracellular malonyldialdehyde (MDA) that is a product of the peroxidation of cell membrane lipids. It was found that cytotoxicity level of the osteosarcoma cell line MG-63 grown with phosphate glass powders (with up to 5% mol Ti) were comparable to that of cells grown in contact with Hench's Bioglass 45S5®, used as a control.

Upregulation of osteogenic markers such as type-1 collagen, alkaline phosphatase, osteonectin and core-binding factor subunit alpha-1 (Cbfa-1) was observed on osteosarcoma cells grown on 5% mol TiO_2 phosphate glasses (Abou Neel et al. 2007). Higher gene expression was statistically significant after 14 days of culture when compared to that of cells grown on phosphate glasses with a lower TiO_2 %mol content or the plastic control.

Even in animal models, TiO_2 doped phosphate glasses implanted in bone defect *in vivo* were found to be fully surrounded by new bone tissues, while in Ti-free glasses the presence of some voids and/or soft tissue formation was observed (Kiani et al. 2012).

Sanzana et al. (2008) compared two calcium phosphate cements and two phosphate glass particles (with or without 5% TiO) in an *in vivo* rabbit femoral model. The glass microparticles (size range 150-300μm) were mixed with blood and implanted as a putty. The macroporous structure of the putty enabled newly formed bone to grow between the particles as the glass was resorbed and to support colonization and vascularization towards the center of the defect. Interestingly, in terms of degradation rate *in vivo*, both glass particles performed similarly, despite the higher solubility of the Ti-free composition observed *in vitro* in both water and simulated body fluid. At 4 weeks, both cements presented more resorption and new bone formation compared to the glass particles, probably due to their higher specific surface; however, no differences were observed after 12 weeks from implantation and all materials showed good level of biocompatibility and osteoconductive properties and similar level of bone formation of the control group, consisting of autologous bone.

1.2.2.4.4 Inducing angiogenesis – cobalt doping

As previously stated, one of the main issue associated with the use of scaffold in tissue engineering is nutrient supply and cells viability at the center of the scaffold. The diffusion of oxygen and nutrients is limited to 150-200μm for cell survival (Lovett et al., 2009).

Hypoxia (low oxygen pressure) has a key role in coupling angiogenesis with osteogenesis, by progenitors recruitment and differentiation and vessel formation (Wu et al., 2012). Hypoxic conditions activates a series of pathways that induces angiogenesis, mediated by the hypoxia inducing factor-1α (HIF-1α). This transcription factor is able to activate the expression of several angiogenic factors, such as the vascular endothelial growth factor (VEGF) (Zhang et al. 2012).

The effect of VEGF on bone regeneration has been tested in vivo, by implanting VEGF coated scaffold in calvarian defects in rats (Kaigler et al. 2006). VEGF coated scaffold not only presented higher level of vascularization, but also enhanced bone formation when compared to the control scaffold. Furthermore, in another study, mice lacking HIF-1α in osteoblasts, presented thinner, less vascularized bone than the wild type control (Wang et al. 2007). HIF-1α pathway was also found to enhance fracture repair and to induce MSCs differentiation, by regulating both osteogenesis and osteoclastogenesis (Azevedo et al. 2010).

Following these results, scaffold coating with recombinant angiogenic growth factors has been investigated as a possible vascularization strategy. However, the limited stability of growth factors *in vivo*, their potential to cause undesirable effects and their prohibitive manufacturing cost, have led to the development of alternative solutions (Boccaccini et al. 2012).

Interestingly, HIF-1α expression can be artificially induced by metallic ions such as cobalt (Co^{2+}) and copper (Cu^{2+}). In particular, cobalt was found to have a stabilizing effect on HIF-1α, inhibiting degradation that usually occurs under normoxic conditions (Yuan et al. 2003). Cobalt is an essential element in human physiology and it is a component of B12, a vitamin that the human body is not able to produce (Wu et al., 2012). Furthermore, cobalt chromium metal alloys have been extensively used for orthopedic and dentistry applications, due to their lower wear rate and stability compared to other materials (Chen & Thouas 2015). However, *in vitro* and *in vivo* cobalt-induced toxicity has been observed, if administered extensively or at high concentrations (Azevedo et al., 2010) and from ion leaching from CoCr implants (Bose, Fielding, et al. 2013). In particular, Co^{2+} ions can promote osteolysis, by increasing osteoclastic bone resorption and suppressing osteoblast activity, leading to implant loosening (Patntirapong et al. 2009; Andrews et al. 2011). Concentrations of cobalt ions in patients presenting CoCr implants was found to be up to 4.6 μM and 30 μM in whole blood and in local hip synovial fluid, respectively (Andrews et al. 2011). In an *in vitro* study, osteoblasts proliferation over 13 days was not affected by Co^{2+} concentration up to 5μM (Andrews et al. 2011). Fleury et al. (2006) reported a decrease in MG-63 cell number when exposed to 2.5-10 ppm Co^{2+} ions in a dose dependent manner.

On the other side, controlled Co^{2+} ions release from tissue engineering scaffold (at lower concentration than its cytotoxic threshold) has been proposed has a strategy to induce angiogenesis in skeletal regeneration (Bose, Fielding, et al. 2013).

For example, the effect of tricalcium phosphate ceramic powders and discs, with different cobalt contents (2-5% mol), on proliferation and VEGF expression of human bone marrow MSCs have been tested (Zhang et al., 2012). Cytocompatibility and enhanced angiogenesis was observed when cobalt was present. A similar trend was observed using mesoporous bioactive glass scaffold containing cobalt (Wu et al., 2012). A limiting 5% CoO content was found to support BM-MSCs differentiation without evidence of cytotoxicity.
Common results observed in several *in vitro* studies are upregulation of HIF-1α and VEGF expression in response to cobalt ions (Zhang et al. 2012; Wu et al. 2012; Azevedo et al. 2015). Furthermore, functional responses such as enhanced vessel formation in the presence of cobalt releasing bioactive glass scaffold have also been shown (Zhang et al., 2010; Quinlan et al. 2015).

In an *in vivo* study, BM-MSCs pre-treated with 100μM $CoCl_2$ showed higher degree of vascularization and osteogenesis when seeded on collagen scaffold either subcutaneously and in a critical size cranial defect model in SCID mice (Fan et al. 2010).
Birgani et al. (2016) reported that incorporation of Co^{2+} into a CaP coating resulted in the formation of more and larger blood vessels upon intramuscular implantation in goats, as well as resulting in a wider distribution blood vessels size distribution.

More controversial is the role of Co^{2+} ions on osteogenesis both *in vitro* and *in vivo*.
Wu et al. (2012) tested alkaline phosphatase (ALP) activity on bone marrow MSCs grown on mesoporous cobalt free and cobalt releasing BG scaffold and reported no differences in expression between the two groups. However, when looking at osteocalcin secretion in the supernatant, they found it to be enhanced in cobalt releasing scaffold.

Another study by Quinlan et al. (2015) tested the effect of cobalt loaded bioactive glass/collagen glycosaminoglycan composite scaffold on the pre-osteoblastic cell line MC3T3-E1. Interestingly, they observed enhanced ALP expression induced by cobalt-releasing scaffold. However, they reported reduced calcium deposition in the presence of cobalt.

In another study (Osathanon et al. 2015), testing the effect of 50 and 100 μM CoCl2 on human periodontal ligament cells, a decrease in ALP activity and expression of osteogenic genes including ALP, OC and RUNX2 as well as a significant reduction in mineralization was observed. Interestingly, stem cells markers like Oct4 and Rex 1 were upregulated in the presence of cobalt, suggesting the capacity of cobalt of maintaining a stem-cell state.

Similarly, Birgani et al. (2016) showed reduced ALP activity, BSP gene expression and mineralization by hMSCs exposed to Co^{2+} ions either dissolved in the cell medium or incorporated to CaP coatings.

Ignjatović et al. (2013) investigated the effect of cobalt-substituted hydroxyapatite nanoparticles on the regeneration of mandibular osteoporotic bone. Although cobalt had a detrimental effect on osteoblastic cell viability and caused alteration of the cytoskeleton *in vitro*, best results *in vivo* in terms of osteoporotic bone tissue regeneration were observed for hydroxyapatite nanoparticles with the largest content of cobalt ions. In a second study, they reported enhanced bone matrix formation and deposition of calcium, magnesium and phosphate when the defect was reconstructed using hydroxyapatite nanoparticles with the highest cobalt concentration (Ignjatović et al. 2015).

Thus, while scaffold release of Co^{2+} ions has been reported to induce angiogenic responses both *in vitro* and *in vivo*, the effect of cobalt on osteogenesis is controversial and more studies are required to prove its efficacy in bone regeneration.

1.2.3 Cells in bone tissue engineering

For large bone defects or compromised patients, the integration of cells within the scaffold would be necessary in order to ensure an effective intervention. Cell numbers in the range of 40-100 x 10^6/patient have been estimated for the treatment of non-union bone defects (Chen et al. 2013) but these numbers are likely very low given that defect sizes can be considerable and large cell numbers are required initially even if a mature remodeled tissue would see a reduced cell number. An ideal cell source would be easily expandable, non-immunogenic and presenting protein expression similar to the tissue to be generated (Salgado et al., 2004). In the following paragraphs, potential cell types for BTE applications are reviewed.

1.2.3.1 Osteoblasts

Osteoblasts would represent the most obvious choice, since they can be autologously derived, thus not presenting any risk of immunogenicity (Salgado et al., 2004). However, only a small number of cells can be dissociated from the biopsy and their relative low expansion rate, make the scaffold seeding laborious and time-consuming (Salgado et al., 2004). Furthermore, in patients presenting bone related diseases, their osteoblastic phenotype would not be ideal for transplantations (Salgado et al., 2004). Also, as previously stated, the division and differentiation capacity of osteoblasts *in vitro* is donor-age dependent (Kassem et al. 1997). Thus, similarly to other fields in tissue engineering, the use of stem cells seems particularly appropriate.

1.2.3.2 Stem cells

Stem cells are undifferentiated cells that have the unique capacity to proliferate indefinitely through self-renewal and the potential to differentiate into different types of mature cells (Li & Xie 2005). Despite somatic cells (fully differentiated cells) they can undergo symmetrical division, in which two identical daughter cells are generated, or asymmetric division, in which one identical daughter stem cells and a differentiated cells are formed. There are two main types of stem cells: embryonic and adult.

Embryonic stem (ES) cells are derived from the inner cell mass of the blastocyst stage of the embryo and they are pluripotent, that is, they can give rise to each of the three germ layers − ectoderm, mesoderm and endoderm (Li & Xie 2005). As the embryo develops, cells of each germ layer undergo further proliferation and their differentiation potential decreases and they become progenitor cells that will eventually form fully differentiated cells. These cells are referred to as adult stem cells, to distinguish them from the pluripotent embryonic stem cell population.

Adult stem cells can be unipotent or multipotent with respect to the number of specific tissue lineages that can be achieved (Young & Black Jr. 2004). After birth, adult stem cell

populations are present in approximately each tissue in the body in special microenvironments, called “niches”, and they contribute to tissue homeostasis, replacing cells lost by apoptosis or injury during the life span of an individual. Adult stem cells still present self-renewal capacity and differentiation potential, but they have a limited proliferation potential in vitro and they conform to Hayflick’s limit of 50-70 population doublings, before reaching senescence and entering apoptosis (Young & Black Jr. 2004). Since a very small number of adult stem cells is present in each tissue, and due to their limited proliferation capacity *in vitro*, these cells are difficult to expand *ex vivo* in clinically relevant quantities.

1.2.3.3 Embryonic Stem Cells (ESCs)

ESCs present two unique properties: they have a nearly unlimited self-renewal capacity and they can give rise to every differentiated cell lineages (Salgado et al., 2004). When these cells have been implanted in early stage murine embryos, they were found to be able to give rise to all somatic cell types. They can be kept undifferentiated *in vitro* in the presence of specific factors, thus exploiting their proliferation potential to expand them in clinical relevant quantities, before starting the differentiation process.

When these factors are removed from culture, ESCs spontaneously differentiate and aggregate in structures known as embryoid bodies that comprise derivatives of all three germ layers (Keller and Snodgrass, 1999). Protocols have been established to differentiate ES cells into different lineages. For bone applications, the differentiation of ES cells into osteoblasts have been shown in the presence of dexamethasone (Salgado et al., 2004).

ES cells’ unlimited self-renewal capacity make them ideal candidates for therapies requiring a significant number of cells. However, ethical concerns regarding the use of tissue derived from embryos and the potential formation of teratomas often restrict their usage for clinical applications. Furthermore, immunological incompatibility might represent a further barrier to their application at a clinical level (Salgado et al. 2004; Lee et al. 2009).

1.2.3.4 Mesenchymal Stromal Cells (MSCs)

Currently, there are two main types of adult stem cells used at a clinical level, hematopoietic stem cells (HSCs) and mesenchymal stromal cells (MSCs) (Lee et al., 2009). Both types of cells can be isolated from the bone marrow.

HSCs can differentiate into all blood cell types from the myeloid and lymphoid lineages. MSCs are non-hemapoietic stem cells in the bone marrow and they can differentiate into bone, cartilage, muscle, tendon, ligament and adipose tissue (Chamberlain et al. 2007).
They are alternatively referred to as mesenchymal stromal cells or marrow stromal cells, as they are thought to reside in the stroma that is the supportive tissue in the bone marrow.

Apart from the bone marrow, MSCs have been isolated from several adult sources including peripheral blood (Kuznetsov et al. 2001), adipose tissue (Zuk et al. 2002) and dental pulp (Shi & Gronthos 2003). Furthermore, MSCs can be isolated from extra-embryonic tissue including placenta, amniotic fluid, umbilical cord (UC) and cord blood (CB) (Hass et al. 2011). The latter present the advantage of being easily and non-invasively derived from tissues normally discarded at birth, thus being exempt from ethical concerns (Pipino & Pandolfi 2015). Furthermore, several studies have shown that extra-embryonic tissue derived MSCs present improved proliferation capacity, life span and differentiation capacity than adult-tissue derived MSCs (Hass et al. 2011).

MSCs were firstly isolated from the bone marrow by Friedenstein at the beginning of 1970 by removing non-adherent cells (HSCs) after a few days of culture. A non-homogeneous population of adherent cells appeared, that were able to form fibroblast colonies and they were firstly referred to as colony forming unit fibroblasts (CFU-F) (Friedenstein et al. 1970; Friedenstein et al. 1976). The multipotent nature of these cells was later described (Prockop et al., 1997), since these cells were found to be able to give rise to osteoblasts, chondrocytes and adipocytes.

According to the International Society of Cellular Therapy (ISCT) (Dominici et al. 2006), the three criteria used to characterize MSCs are:

1) They must show adherence to plastic under standard tissue culture conditions;
2) They must express certain surface markers such as CD73, CD90 e CD105 and should be negative for CD45, CD34, CD14, or CD11b, CD79α or CD19 and HLA-DR surface molecules;
3) They must be able to differentiate in vitro into osteoblasts, adipocytes and chondrocytes.

These cells were first referred to as mesenchymal stem cells by Caplan in 1991 (Caplan 1991) to describe their stem-cell like nature. The term mesenchyme identifies the embryonic connective tissue derived from the mesoderm, from which hematopoietic and connective tissue derive.

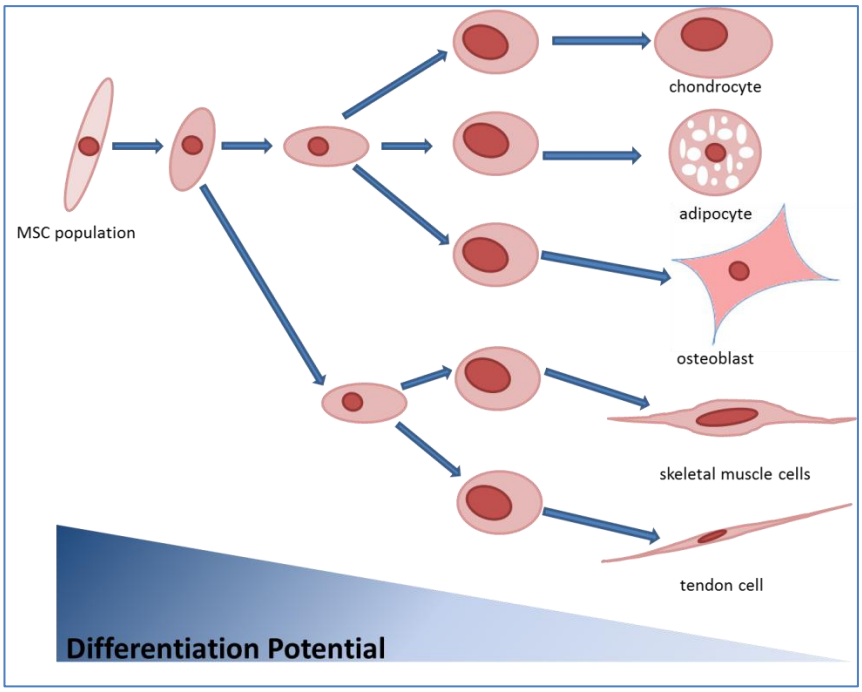

Figure 1.2: The multilineage differentiation potential of MSCs.

However, the term “mesenchymal stem cells" has been criticized, since the definition of a stem cell includes the two key properties of self-renewal and multi-lineage differentiation potential (Lindner et al. 2010). However, differently that for HSCs and ESCs, these two characteristics have never been confirmed by *in vivo* testing for MSCs (Lindner et al, 2010). This is mainly due to the fact that, these cells are present at very low frequency in most tissues, thus making their in vivo tracking very challenging; in human bone marrow their frequency is between $1:10^4$ to $1:10^6$ depending on age (Sarugaser et al., 2009).

As MSCs derived from different tissues express different immunophenotypes (Lindner et al., 2010) and considering that there are not any specific surface markers or gene products to distinguish MSCs from other mesenchymal cells (Yagi et al. 2010), there is a need to identify a distinctive immunophenotypic profile. Up to now, the term mesenchymal stromal cells seems more appropriate to identify the general population of MSCs and the term mesenchymal stem cells should not be used until self-renewal and differentiation capacity can be documented and linked to a precise identity profile (Keating 2012). Furthermore, this is the recommended terminology suggested by the ISCT (Dominici et al., 2006).

Despite the controversies in their definition, there are some interesting functional properties associated with these cells that have been widely documented in the literature.
For example, a key characteristic of these cells is their capacity to be rapidly expanded in vitro without losing their progenitor characteristics. Human bone marrow derived MSCs were found to be able to undergo up to 38 doublings, while retaining their undifferentiated phenotype (Bruder et al. 1997). However, other studies showed that heterogeneity between MSCs derived even from the same donor exists, and while some cells retained their multipotentiality through a

number of passages, some either committed to a specific cell lineage or begin to senesce (Digirolamo et al. 1999).

Another key property of MSCs is that they can modulate immunological responses via T-cell suppression (Yagi et al., 2010). For this reason, they have been widely investigated as a potential strategy for T-cell mediated diseases such as Crohn's disease, graft-versus-host-disease and to prevent organ transplantation rejection (Yagi et al., 2010). Furthermore, MSC migration towards injured sites in lungs, heart, kidney and liver, have been observed after systemic administration (Yagi et al., 2010).

The successful application of MSCs in combination with scaffold for the treatment of bone defects has been demonstrated in several pre-clinical studies using animal models (Kadiyala et al. 1997; Kon et al. 2000; Boyde et al. 1999; Shang et al. 2001; Schliephake et al. 2001).

In human, the first clinical study involving the use of MSCs for the treatment of large bone defect was reported in 2001 in three patients (Quarto et al. 2001). Autologous bone marrow MSCs were expanded *ex vivo* and loaded to a custom-shaped macroporous hydroxyapatite scaffold and implanted at the defect size. External fixation was provided for mechanical stability. Recovered limb function and integration with native bone was observed in all patients, without long-term side effects associated with the implant in the 6-7 years follow-up post implantation. Angiographic evaluation in one of the patient showed vascularization of the grafted zone, which confirmed the presence of vital bone in the grafted area (Marcacci et al. 2007).

Morishita et al. (2006) showed healing in three patients treated with MSCs expanded and differentiated into osteoblasts ex vivo on an HA scaffold for the treatment of bone defects following tumour curettage.

On the other hand, some clinical studies have reported limited regeneration. For example, Meijer et al. (2008) showed bone regeneration in only 3 out of the 6 patients treated with BM-MSC seeded hydroxyapatite particles to reconstruct jaw defects. However, in only one of the patients treated bone regeneration was induced by the tissue-engineered scaffold, while in the other two it was attributed to migration of osteoblasts from the surrounding bone tissue. Interestingly, parallel subcutaneous implantations of the constructs in nude mice resulted in successful ectopic bone formation, thus showing a clear discrepancy between preclinical studies and clinical outcomes. This is common to several studies and can partially be explained by the lack of standardization in the cell isolation protocol and culture conditions that leads to heterogeneous cell populations, thus making comparison between studies difficult to perform (Ma et al. 2014).

Other studies have followed, however they have been limited in the number of patients treated and only few of them were able to demonstrate the actual efficacy of cell-based

strategies for BTE (Ma et al. 2014). In particular, key limitations are represented by the lack of effective examination methods performed (e.g. biopsy) to quantify regeneration and of appropriate control groups (i.e. bare scaffolds) to distinguish between the contribution of MSCs and that of osteoinductive scaffolds (Ma et al. 2014).

Currently, no commercially available MSCs product exist in the field of bone regeneration (Grayson et al. 2015). The only exception is represented by Osteocel by Osiris Therapeutics Inc., which consists of allogeneic MSCs, mixed with spongy bone material obtained from donors or cadavers and used for the treatment of spinal defects or fractures. However, as the cells are not manipulated, but simply harvested and stored, Osteocel is not classified as a drug or medical device, but as a tissue transplant, thus considerably facilitating the approval process (Grayson et al. 2015).

Regulatory approval for bone tissue engineering product consisting of cells and bioactive material will most likely be more complex, with higher manufacturing cost, due to the patient specific nature of these products. The establishment of robust and safe protocol for the isolation and expansion of MSCs, scaffold seeding and culture is then required to accelerate the translation of these therapies to the clinics (Amini et al. 2012).

1.2.4 Bioreactors for bone tissue engineering

The development of new therapies involving the use of living cells needs to be accompanied by parallel progress in the establishment of suitable manufacturing platforms. There is a need to translate individualized culture protocols developed by research laboratories, into reproducible, scalable, standardized, robust and safe industrial bioprocesses (Hambor 2012).

At lab scale, adherent cells (i.e. MSCs) are usually cultured on flat 2-D surfaces (e.g. t-flasks) under static conditions. Limitations in gas transfer and the formation of concentration gradients are typical of these systems. Furthermore, scale-up represents a key limiting factor due to the low surface area/volume ratio of this type of system and the limited amount of cells they can accommodate (Hambor, 2012).

Most of the FDA-approved cell therapies currently used do not involve highly manipulated cellular products, but often rely on autologous or allogeneic transplants of harvested cells (Hambor, 2012). These cells are not usually expanded ex-vivo, and the same amount of cells harvested from the patient (or the donor) is usually injected back into the patient. However, the development of new cell therapies whose efficacy is based on dose, and the unlikelihood of obtaining the required number of cells from the donor, make the development of efficient expansion systems a necessity. This is of particular relevance, since early stage clinical trials have demonstrated the positive effect of increasing the number of cells and the frequency of injection, and the effect of *ex vivo* expansion and differentiation on the regeneration capacity of cellular based approaches (Hernigou et al. 2005; Kitoh et al. 2009)

For example, for bone tissue engineering applications, the low frequency of MSC in the bone marrow ($1:10^4$ to $1:10^6$ depending on age (Sarugaser et al., 2009), makes the establishment of a robust platform for cell expansion crucial for their clinical applications (Rodrigues et al. 2011). Culture in tissue flasks, apart from being laborious and time-consuming, limit the number of cells achievable per dose. However, it has been estimated that a minimum of 40-100 x 10^6 MSCs/patient are required for the treatment of non-union bone defect (Chen et al. 2013).

Furthermore, the need of a more robust and standardized manufacturing platform is also dictated by the requisite to comply with strict quality and safety regulations. Several physicochemical and biochemical parameters need to be fully controlled, since they play a key role in cells expansion and differentiation. For example pH, temperature, osmolarity, dissolved oxygen tension and shear stress, together with nutrient and cytokine concentration and waster products accumulation are all critical factors affecting cell culture that need to be carefully monitored (Rodrigues et al., 2011).

Growing cells within a bioreactor offers a controlled environment where cells can be consistently expanded and differentiated into a desired lineage. As cells in bioreactors are

cultured under dynamic conditions, this enables some of the limitations found in static systems to be overcome. For example, from a tissue engineering perspective, improved seeding efficiency of cells on the scaffold, increased mechanical stimulation to improve matrix deposition and enhanced nutrient and oxygen exchange and waste removal can be obtained compared to standard 2-D, static systems (Amini et al. 2012).

Several designs have been investigated for bone tissue engineering applications, including stirred flasks, rotary vessels and perfusion bioreactors. Adherent cells can be attached to a support such as a microcarrier or a scaffold, or can be encapsulated within porous particles, in order to be integrated within a bioreactor system.

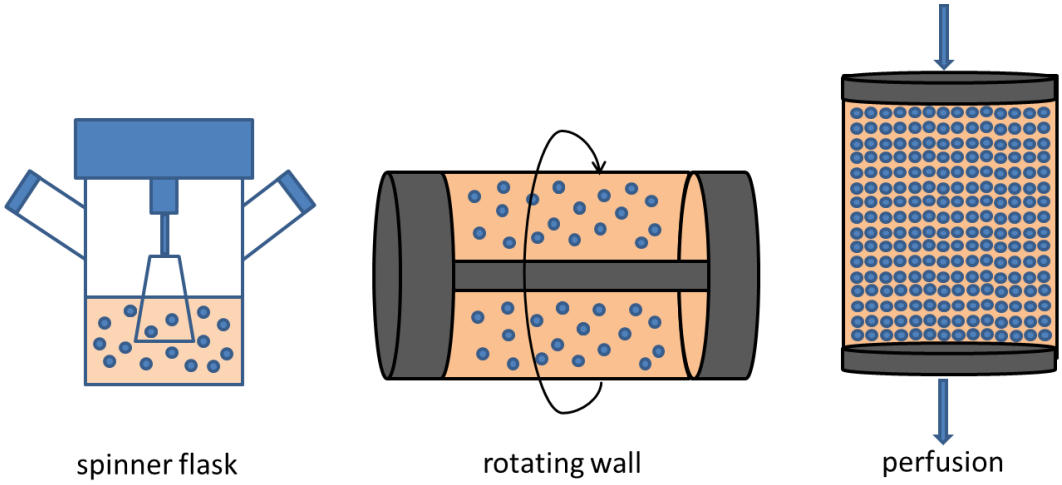

Figure 1.3: Bioreactors for cell culture on microcarriers.

1.2.4.1 Spinner flasks and rotating wall bioreactors

One of the simplest designs proposed is the spinner flask bioreactor. Scaffolds can be inserted into needles attached to the lid of the flask or can be grown in suspension. A magnetic stirrer enables mixing of the media surrounding the scaffold at selected rotation.

Improved cell viability, proliferation and distribution in the construct have been achieved in this type of system, compared to static culture (El Haj and Cartmell, 2010). However, large constructs cannot be produced in this type of reactor, since the mixing required to obtain an effective mass transfer, will create excessive shear rates at the periphery of the tissue, leading to cells necrosis.

Microcarriers are also often used within spinner flasks. From a processing point of view, microcarriers are more cost –effective than standard tissue culture flasks, as they have been estimated to have 20 cm^2/ml surface area to volume ratio compared to the 4 cm^2/ml of plastic monolayers (Frauenschuh et al. 2007). Hewitt et al. (2011) were able to grow human MSCs derived from placental tissue in attachment to Cytodex 3 microcarriers in 250ml spinner flasks, obtaining a 20-fold expansion of cells per microcarrier.

Yang et al. (2007) have shown the feasibility of growing BM-MSCs on resorbable gelatin beads in spinner flasks culture. Better expansion and a significant higher fold increase in osteoblast markers expression was obtained in the 3-D dynamic culture. One of the key advantages of this system was that MSCs did not need to be harvested from microcarriers and so direct implantation of cells coated beads was possible, thus reducing cells apoptosis and improving survival upon implantation. In the same study, beads seeded with cells were implanted in rat femur defects and improved formation of trabecular bone was observed compared to cell-free microcarriers. A similar result was obtained in a rat calvarium defect that was filled with MSCs seeded on evacuated calcium phosphate microspheres (Jin et al. 2012). Also in this case, a higher level of bone formation was observed than in cell-free scaffold (Jin et al., 2012). In another study, porcine BM-MSCs were cultured on Cytodex carriers in spinner flasks (Frauenschuh et al., 2007) for 14 days, after which new carriers were added to the culture in a 1:1 ratio. Recolonization of freshly added beads was obtained through bead-to-bead transfer of cells.

Another common design adopted in bone tissue engineering is the rotating-wall vessel (RWV) reactor that consist of a vessel rotating horizontally, filled with medium, and a central silicone membrane for oxygen diffusion. This system was developed to minimize shear stresses and turbulence found in stirred tank reactors, as the rotation of the vessel simulates microgravity and cells are suspended in low shear within the reactor.

In a study by Kasper et al. (2007), a rotating bed bioreactor was fitted with ceramic carrier discs (Sponceram®). Sponceram® is a ceramic material doped with zirconium oxide. It present a porous structure that enhance cell adherence and stimulates cells deposition of extracellular matrix. The discs are fixed to a central shaft in the center of the vessel and rotate during culture, thus improving mass and oxygen transfer to the cells. Improved proliferation and enhanced osteogenic differentiation of preosteoblastic cells was observed compared to static conditions (Kasper et al., 2007).

In another study, silk porous scaffold were seeded with hMSC derived from the bone marrow and grown in rotating bioreactors (Marolt et al. 2006). Cells were grown under chondrogenic and osteogenic differentiation media and constructs obtained were analyzed. Under osteogenic conditions, bone tissue constructs, presenting calcium content and volume fraction of mineralized tissue similar to that of trabecular bone, were obtained. Chondrogenesis, on the other hand, was not as effective as osteogenesis. The authors identified the improved mixing conditions of the rotating bioreactor as opposed to static conditions, in combination to the osteogenic media, as the key factors for the positive results in bone formation.

Polymeric microcarriers were also used to culture osteosarcoma cells in a rotating bioreactor (Botchwey et al. 2001). Cells grown in this system maintained their osteoblastic phenotype and expressed more alkaline phosphatase than when cultured in static conditions. A

model to predict microcarriers trajectories within the reactor was also developed and no damaging wall collisions emerged from the study.

In a previous study, rat MSCs grown in a rotating wall bioreactor formed 3-D aggregates by bridging together Cytodex beads (Qiu et al. 2007). Beads were embedded under a single layer of cells. The stronger alkaline phosphatase expression was found among the cells growing in the region between beads, together with enhanced matrix mineralization, thus indicating that bone-like tissue formation and differentiation are more advanced in these regions between beads.

From a vascularization perspectivey, in a co-culture of retinal and endothelial cells on Cytodex microcarriers in a rotating wall reactor, the assembly of endothelial cells into capillary like structures connecting adjacent microcarriers was observed (Dutt et al. 2003). This study provided a unique neovascularization model that could be used for the formation of vascularized tissue constructs in a bioreactor system.

1.2.4.2 Perfusion reactors

For the production of tissue-engineered constructs, spinner flasks and rotating vessels are not particularly suitable, since they improve mass transfer on the surface of the construct only, but there is not perfusion of media throughout the scaffold. Furthermore, scaffolds presenting density similar to water and specific dimensions are required in order to be kept in suspension within a stirred system (Amini et al. 2012). Possible collision of scaffolds with the bio-reactor wall can also occur in rotating wall reactor, thus damaging the tissue-engineered construct (Amini et al. 2012).

Perfusion reactors can be used to actively induce the flow of media through the construct. Perfusion systems usually consists of a pump, a media reservoir and a growth chamber filled with either a scaffold or matrix. Both degradable and non-degradable scaffolds have been used as packing materials for perfusion reactors.

The role of flow perfusion on MSCs proliferation is controversial (Brindley et al. 2011)Conflicting results have shown enhanced proliferation, reduced proliferation and cell death or no difference of MSCs cultured under different shear stress conditions (Brindley et al., 2011).

More consistent results were found when investigating the effect of shear stress on MSCs osteogenic differentiation (Bancroft et al. 2002; Yourek et al. 2010). Yourek et al. (2010) described the effect of shear stress on hMSCs using a 2-D parallel chambers apparatus. They measured alkaline phosphatase activity and expression of osteogenic genes in hMSCs cultured with or without osteogenic differentiation media and in static controls. They found that mechanical stimulation alone was able to upregulate the expression of osteogenic factors. Thus, interestingly, when exposed to shear stress, hMSCs tend to differentiate towards osteoblasts,

rather than other mesenchymal lineages. However, in cells exposed to both osteogenic and mechanical stimulation, ALP levels and osteogenic marker expression were less evident.
Thus, undifferentiated hMSCs were found to be more sensitive to mechanical stimulation than pre-committed cells and in 2-D cultures, shear stress seemed to be able to direct MSCs osteogenic differentiation, by preventing their proliferation and selecting a pool of cells presenting osteogenic potential (Yourek al., 2010).

The effect of increasing flow rate on osteodifferentiated rat marrow stromal cells, seeded on a titanium fiber mesh in a perfusion flow reactor, has been investigated (Bancroft et al., 2002). Three flow rates were tested, 0.3, 1 and 3ml/min over an extended time period. In all conditions, matrix deposition was significantly higher than in static constructs and total calcium content increased with increasing flow rate. Flow perfusion enhanced cell distribution throughout the scaffold and induced osteoblast differentiation in vitro.

A similar study performed by Sikavitsas et al. (2003) demonstrated the relationship between fluid shear stresses and the osteoblastic differentiation of MSCs. Rat BM-MSCs were cultured on a 3-D porous titanium fiber scaffold in a perfusion reactor using culture media of different viscosities pumped at the same flow rate. Cells were then exposed to increasing levels of shear stress, while maintaining chemotransport conditions constant. Increasing level of shear stress resulted in increased mineral deposition and better spatially distributed matrix inside the scaffold. Thus, the relevance of mechanosensing on the expression of an osteoblastic phenotype was confirmed.

Grayson et al. (2008) investigated the effect of increasing flow rate and initial cell density on hMSCs seeded on a decellularized bovine trabecular bone scaffold cultured in a perfusion bioreactor. While a higher initial cell number did not result in improved bone formation, higher flow rates had an impact on the quality of the tissue construct. Higher perfusion enabled better nutrients transfer, more uniform tissue development and supported higher cell densities within the constructs.

In another study, a porous calcium phosphate ceramic scaffold in a flow perfusion bioreactor was used to culture MSCs (Holtorf et al. 2005). Even in this case, better cells growth and distribution throughout the scaffold and more mineralized matrix production was observed in the perfusion mode, compared to the static control. The suitability of this type of reactor and the calcium phosphate scaffold to support MSCs growth and enhance osteoblastic differentiation was shown.

While perfusion bioreactor packed with different porous scaffold configurations have been extensively investigated, their use with microcarriers for MSCs expansion and osteoblastic differentiation is not well documented in the literature, with few exceptions.

The model cell line MSC-TERT was grown on a fixed bed bioreactor, packed with non-porous borosilicate glass beads. MSC-TERT is a modified cell line, transfected with a

telomerase reverse transcriptase (TERT) that counteracts telomerase shortening at each division, thus increasing the number of achievable populations doubling (Weber et al. 2010). Inoculation, expansion and harvesting of cells was achieved within the reactor. However, this system was only used for MSCs expansion and not for the formation of bone tissue engineered constructs.

hMSCs were also embedded in alginate beads and grown in a perfusion bioreactor (Yeatts & Fisher 2011). The authors showed an increase in oxygen and nutrients supply to the cells in the scaffold, thus overcoming one of the main issue associated with static culture of bone tissue engineered constructs. Expression of late osteogenic genes was significantly higher in the dynamic culture and it was shown to increase with media flow rate. However, early osteoblastic markers such as ALP were not overexpressed. The authors suggested that this might be caused by the level of shear stress sensed by cells in the reactor. Since in this system cells are encapsulated within alginate beads, they are not all exposed to shear stresses, as they would be if seeded on the surface of a porous scaffold. After 28 days of culture, alginate beads were removed from the reactor, the scaffold was dissolved and matrix deposition of approximately the same size of the original scaffold were observed in the bioreactor group. In the static control, matrix deposition was not as large and intact as in the bioreactor. They also observed that although higher flow rates led to the overexpression of osteogenic markers, they were not able to support growth of macroscopic tissue that broke apart before the final culture point. Thus, an optimum flow rate, that can induce osteogenic marker expression without being detrimental for the construct needs to be identified.

Kou et al. (2016), recently described a potential bottom approach, in which rat BM-MSCs were first expanded in spinner flasks on gelatin microspheres and then transferred to a perfusion bioreactor for osteogenic differentiation. The MSC –gelatin microspheres were then mixed with collagen microfibers, presenting controlled release of BMP-2, to drive their osteogenic differentiation. BMSC –gelatin microspheres cultured in the absence of the BMP-2 releasing collagen microfibers were used as a control. After two weeks of perfusion, osteogenic genes such as ALP, bone sialoprotein, osteocalcin and collagen I were upregulated in the experimental group, together with increased ALP activitity and mineral deposition. Similarly, higher in vivo bone nodule formation, upregulation of osteogenic markers and the formation of tissue presenting a compression module in the range of that of original bone tissue, was observed when the mixture of BMSC –gelatin microspheres and BMP-2 releasing collagen microfibers were implanted into subcutaneous pockets of rats, compared to the collagen microfibers-free control.

1.2.4.3 Microfluidic bioreactors

Despite being a precious tool to culture cells in a three-dimensional, dynamic environment, most current bench scale bioreactors present limitations in not being suitable for

high throughput investigations, as they usually involve the use of large quantities of cell and reagents. Furthermore, often these technologies fail to accurately control process variables and to provide continuous monitoring of the cellular product.

Recently, the development of microfluidic bioreactors has given the potential to overcome some of these challenges. These technologies are a scaled down version of conventional bioreactors and operate at a time and length scale comparable to that of cellular phenomena (Pasirayi et al. 2011). As microfluidic device dimensions generally fall in the micrometer scale, this significantly reduces the quantity of cells and reagents required, thus reducing experimental costs and being particularly advantageous for high-throughput screening. Microfluidic bioreactors can be designed to control process parameters such as temperature, pH, dissolved gas concentration, shear stress, and medium exchange rates (Titmarsh et al. 2014). This is of particular relevance in tissue engineering, as complex 3-D microenvironment mimicking physiological conditions can be obtained, thus providing a powerful tool to investigate cell behaviour *ex-vivo.* Furthermore, at these scales, fluid flow within the microdevices is laminar, thus enabling to expose cells to controlled spatial and temporal gradients of environmental factors and to test their biochemical and morphological responses *in vitro* (Pasirayi et al. 2011).

Microfluidic bioreactor are usually fabricated using low-cost polymers through soft-lithography techniques. By combining components like chambers, channels, membranes and valves, their design can be easily customized to address specific research questions.

Due to the importance of mechanotransduction in bone homeostasis, microfluidic technologies offer great potential to investigate skeletal regenerative medicine and bone cell physiology , under relevant conditions (Riehl & Lim 2012). Several studies have focused, for example, on the effect of shear stresses on osteodifferentiation using microfluidic platforms (Riehl & Lim 2012). For example, Kou et al. (2011) have developed a microfluidic device to study calcium dynamics in osteoblastic cells under controlled shear stress conditions. The device consisting of four chambers for cell culture, each presenting increasing flow shear stress, enabled to establish a linear relationship between cytosolic calcium concentration and shear stress intensity. Similarly, increased ALP activity (Leclerc et al. 2006) and enhanced osteogenic genes expression (Jang et al. 2008) was observed in osteoblastic cells grown in 3-D microchannel, under flow conditions, compared to the static control. Other studies have focused on using microfluidic platforms as screening tool for biomaterials for skeletal regeneration. For example, a microfluidic bioreactor was developed to find optimal substrate combinations for preventing bacterial infection while promoting osteoblastic differentiation and calcium deposition (Lee et al. 2012). In another study, Jusoh et al. (2015) developed a platform to investigate bone angiogenesis by co-culturing endothelial and stromal cells. The device was

designed to simulate *in vivo*-like microenvironments for bone vessel sprouting, by integrating ECM components and HA nanocrystals, for drug screening applications.

Compared to their full-scale counterparts, microfluidic bioreactors provide ideal platforms for studying bone cells in controlled 3-D microenvironments, under dynamic flow conditions and for performing high throughput screening of biomaterials and optimal processing conditions for skeletal tissue engineering applications.

1.2.5 Bone Tissue Engineering: current limitations to clinical translation

Despite many bone tissue engineering strategies have been investigated, only a limited number have been successfully translated to the clinics (Hollister & Murphy 2011). Among the bone grafts that obtained clinical approval there are mainly scaffold, powder, pastes and putty for bone anchoring/fixation systems, bone void filler, dental bone void filler and spinal fusion applications (Hollister & Murphy 2011; Liu et al. 2013). Most of these products, classified as medical devices, obtains FDA approval through the 510k pathway, meaning that no human clinical trials are required and the material only needs testing for biocompatibility and mechanical properties *in vitro*. *In vivo* animal tests are also performed to compare their efficacy to existing clinical device (Hollister & Murphy 2011). However, these products are usually approved for the treatment of small bone defects and for minimally or non-bearing load applications, due to limited mechanical stability (Hollister & Murphy 2011; Canadas et al. 2015). Pre-market approval (PMA) requiring human clinical trials, on the other hand, is required for scaffolds used in combination with drugs or other biologics, such as cells and growth factors. Despite several clinical studies currently ongoing, no tissue engineering products containing cells have been yet approved (Canadas et al. 2015) and scaffolds coupled with growth factors, such as rhBMP-2, represent the most common approved products involving multiple components.

In order to become clinically relevant, bone tissue engineering strategies need to outperform current gold standard (i.e. autologous bone graft) in terms of improved bone regeneration, reduced morbidity, number of invasive surgeries and cost of the procedure (Hollister & Murphy 2011).

However, there are several challenges that still need to be faced in order for bone tissue engineering to become a clinical reality. Together with identifying the optimal combination of scaffold type, biomaterial, cell source and combination of growth factors among the multiple options available, proper vascularization and integration with host tissue remain two main fundamental challenges (Amini et al. 2012). Furthermore, other challenges include minimizing infections associated with scaffold implantation, identifying suitable degree of degradation that ideally would match bone formation and increasing mechanical properties, in order to treat larger defects (Liu et al. 2013). Moreover, following complications observed for example with the use of rhBMP-2, there is a need to perform complete studies to assess possible complications in the use or growth factors or other bioactive substances, thus requiring better predictive animal models (Amini et al. 2012).

Producing clinical grade bone at reasonable cost is also a critical manufacturing challenge. It has been estimated that the cost of a bioreactor-based bone graft would be in the $10,000-15,000 range (Salter et al. 2012). While this cost falls in a similar range of that of other

cellular therapies, it is still more expensive than current treatments, thus making the high cost justifiable only when clear benefits compared to standard grafts are observed.

Cellular and tissue-engineered products need to comply with a complex network of regulations established by healthcare regulatory authorities. Detailed information on biosafety (in terms of sterility, absence of mycoplasma, adventitious viral agent and endotoxins), purity (i.e. lack of contaminants, animal-derived components) and final product characterization of the tissue-engineered construct need to be provided at the end of the manufacturing process (Logeart-Avramoglou et al. 2005). Acceptance criteria for product release are also currently hindered by the lack of well-defined protocols for MSCs isolation and characterization, and that of a unique set of markers to predict clinically efficiency of bioengineered bone (Logeart-Avramoglou et al. 2005). Finally, while long-term product storage would facilitate clinical translation, as it would provide enough time to perform all required release testing and would offer higher flexibility, cryopreservation of tissue constructs still presents several technical limitations (Logeart-Avramoglou et al. 2005).

As from a clinical perspective, bioengineered bone has shown promising results and presents the potential to become the treatment of choice when supply of autologous bone is not sufficient, for a successful translation of BTE therapies to the clinics, new generation products need to be designed and developed by taking into considerations regulatory constraints and manufacturing challenges since early stage conceptual research.

1.3 Aims and objectives

The overall aim of work in this thesis is to determine the suitability of phosphate glass microspheres doped with titanium and cobalt oxides as a modular tissue engineering approach for vascularized bone tissue engineering applications.
The research objectives include:

1. To determine the physical characteristics of titanium/cobalt doped phosphate glass microspheres;
2. To identify an optimal glass composition that elicit favourable responses from BM-MSCs and that could be proposed as a scaffold for bone tissue engineering applications;
3. To evaluate the role of cobalt doping of phosphate glass microspheres in terms of:
   i) Osteoblastic cells and BM-MSCs attachment and proliferation;
   ii) BM-MSC osteodifferentiation;
   iii) BM-MSC mediated angiogenic responses and endothelial cells vascularization;
4. To develop a microfluidic bioreactor to optimize cell culture on microspheres under perfusion and to enable parallel screening of multiple culture variables.

1.4 Outline of results chapters

Chapter 2, provides a comparison of three compositions of phosphate glass microcarriers in regards to their physical and cyto-compatibility properties. The three compositions analysed present an equivalent concentration of titanium oxide and increasing concentrations of cobalt oxide (0, 2 and 5% CoO). In terms of physical characterization, the following analysis were performed: FTIR, XRD, DTA, dissolution and cobalt ion release. In this chapter, the osteosarcoma cell line MG-63 was used for initial biocompatibility studies. The effect of dynamic conditions on cells attachment and proliferation on the microspheres substrate was also investigated, by introducing agitation through an orbital shaker. Furthermore, the capacity of cobalt of inducing VEGF secretion was also tested. A threshold in cobalt concentration was identified as part of this initial characterization and only two of the three original compositions were further analysed in the consecutive chapters.

Chapter 3 focuses on the effect of cobalt and titanium doping on hBM-MSCS, in terms of osteo-differentiation and promoting functional vascularization. Several studies were performed looking at extracellular matrix compositions, expression of osteogenic genes (i.e. type I Collagen, ALP, RunxII) and angiogenic responses (i.e. VEGF secretion, matrigel tubule formation assay, CAM assay). Furthermore, the effect of soluble species released by the microspheres on hMSCs cultured in monolayers was tested. As part of this study, cobalt doping was found to inhibit expression of osteogenic markers and despite activating the HIF-1a pathway and inducing enhanced VEGF secretion, did not improve functional vascularization by endothelial cells. On the other hand, doping with titanium only was found to induce osteogenic differentiation and to still support endothelial cells recruitment.

Chapter 4 describes the design and development of a microfluidic bioreactor for cell culture on microspheres, to test the effect of multiple variables on bone tissue formation within a well defined microenvironment and using minimum quantities of reagents. In particular, the device was designed to enable 3-D cell culture under perfusion conditions and to screen the effect of multiple parameters (i.e. microspheres composition, media feeds) on micro-tissue assembly. hBM-MSCs were cultured in the microbioreactor for up to one week and it was possible to measure functional outputs (cell number, ECM protein expression) within the device.

Appendix 1 elaborates on a commercial evaluation of the microfluidic bioreactor. Novel potential applications of the device, in addition to those described in Chapter 4, are presented, together with a review of competitor technologies and potential strategies to overcome current technical limitations. This chapter was written as part of a UCL Advances Enterprise Scholarship which was awarded to this project.

Chapter 2. Ti-Co doped phosphate glass microspheres: material characterization and preliminary cytocompatibility studies

2.1 Introduction

Bone tissue engineering consists of the combined use of cells, biomaterial scaffolds and signaling molecules for the regeneration of bone defects. Key requisites for a successful therapy are the capacity to expand cells to therapeutic quantities and to be able to drive their differentiation into the appropriate cell type. Despite several studies have been performed in the field, the production of bone tissue *ex vivo* is still an unmet clinical challenge. A bottom-up approach, in which modular micro-units of tissue are used as building blocks to produce larger tissue, could be used as a valid alternative to a more traditional "top-down" approach, involving the use of scaffold of predefined size. For example, microcarrier-based tissue engineering has been proposed as a potential strategy to address osseous defects of different sizes and shapes. In particular, microcarriers made of implantable biomaterials can be used as a substrate for cell expansion *in vitro* as well as a delivery system to the defect size (Malda & Frondoza 2006; Park et al. 2013).

In this contest, titanium doped phosphate glass microspheres have been reported as potential substrates for osteoblastic cell expansion (Lakhkar et al. 2012; Guedes et al. 2013). As this material is completely soluble in aqueous media (Knowles 2003), it can be implanted *in vivo* together with cells. Furthermore, the tuneable glass composition can be easily engineered to induce specific structural and biological properties through incorporation of therapeutic ions (Lakhkar et al. 2013).

In this study, the effect of doping the glass microspheres with titanium and cobalt was investigated, as these ions have been shown to induce osteogenesis (Wall et al., 2009, Lakhkar et al. 2012; Lakhkar et al. 2013, Abou Neel et al. 2014) and angiogenesis (I.-H. Lee et al. 2013; Wu et al. 2012; Azevedo et al. 2015), respectively. Three glass compositions containing 5% mol TiO_2 and different concentrations of CoO (0, 2 and 5% mol) were studied. The molar concentration of titanium was chosen based on previous studies, showing cytocompatibility and osteogenic potential of 5% mol TiO_2 doped phosphate glass microspheres (Lakhkar et al. 2012; Guedes et al. 2013). As cobalt-induced cytotoxicity has been reported (Catelas et al. 2001; Fleury et al. 2006; Simonsen et al. 2012), two molar concentrations previously tested in cobalt-releasing bioactive glass scaffold that proved to be safe from a cytotoxic perspective and to promote *in vitro* angiogenesis, were selected (Wu et al. 2012; I.-H. Lee et al. 2013).
Characteristics of the glass structure and glass transition temperatures were obtained through X-Ray diffraction, Fourier transform infrared spectroscopy and differential thermal analysis. Glass microsphere degradation and cobalt release over time were also determined for all three compositions.

The human osteosarcoma cell line MG-63 was used for initial biocompatibility studies. Despite presenting some characteristics typical of a pre-osteoblast phenotype, these cells differ

from normal bone cells in their functional activities, proliferation and mineralization capacity (Clover & Gowen 1994; Czekanska et al. 2012). However, the use of osteosarcoma or other cell lines for *in vitro* biocompatibility testing for preliminary screening of biomaterials is widely accepted and has been reported in several studies (Declercq et al. 2004; E. A. Abou Neel & Knowles 2008; Martin et al. 1995; Price et al. 1997).

As part of this work, the effect of mixing conditions on cell proliferation on the microsphere substrate was investigated. A microwell plate format was used for cell attachment and proliferation experiments where agitation is achieved by orbital shaking. Mixing and flow characteristics in shaken systems have been studied by Zhang et al. (2005 and 2008), Zhang et al. (2010), Discacciati et al. (2013) and Klöckner & Büchs (2012) among others. Recent work by Weheliye et al. (2013) has demonstrated the presence of two areas, a diffusion-limited area at the bottom of the well and a convection dominated region at the top, the extent of which depends on geometrical ratios and other operating parameters. A flow transition was also reported, corresponding to a critical Froude number at which the transition occurs, and the analysis has been extended to two-phase flows in the presence of microcarriers (Pieralisi et al, 2015). While their study has been carried out using a well internal diameter d_i = 10 cm (larger than the one employed in this work), the equations can be applied in first approximation to smaller systems to be able to calculate the critical speed at which transition occurs and predict the flow pattern inside the well. A schematic diagram of the flow present in each well at different shaking speeds is presented in Figure 2.1. Two shaking speeds of 150 and 300RPM were selected in this work as they were lower than the critical speed (N_c = 350RPM) and offering two different mixing patterns to investigate the effect of these on cell proliferation and metabolism.

Finally, as cobalt was added to the glass composition due to its pro-angiogenic properties, the effect of increasing concentration of Co^{2+} ions on VEGF secretion by MG-63 cells was investigated.

2.2 Materials and methods

2.2.1 Glass preparation and microspheres fabrication

Glasses were prepared from the precursors: sodium dihydrogen orthophosphate (NaH_2PO_4), calcium carbonate ($CaCO_3$), phosphorus pentoxide (P_2O_5), titanium dioxide (TiO_2) and cobalt oxide (CoO). All the precursors were obtained from VWR-BDH (Poole, UK).
Three different compositions CoO 0%, CoO 2% and CoO 5% were manufactured as shown in table 2.1.

Glass Code	Glass composition (mol%)				
	P_2O_5	CaO	Na_2O	Ti_2O	CoO
CoO %	45	30	20	5	0
CoO 2%	45	28	20	5	2
CoO 5%	45	25	20	5	5

Table 2.1: Summary of glass compositions, showing molar concentration of precursors.

The precursors were weighed and mixed in a Pt/10% Rh crucible (Type 71040, Johnson Matthey, Royston, UK) which was introduced into a preheated furnace (Carbolite, RHF 1500, Sheffield, UK) at 700°C to remove H_2O and CO_2 for 30min. The mixture was then melted at 1300°C for 3 hours. Upon removal from the furnace, the melted glass was quenched onto a steel plate.

The glasses were first broken into fragments and then ball-milled at 10Hz using a Retsch MM301 milling machine (Haan, Germany). The microparticles obtained were then sieved down to 63-106μm (Endecotts Ltd., London, UK) on a Fritsch Spartan sieve shaker (Fritsch GmbH, Idar-Oberstein, Germany). The microparticles were spheroidized by passing them through a flame spheroidization apparatus, as previously described by Lakhkar et al. (2012).

2.2.2 X-ray diffraction analysis

X-ray diffraction analysis (XRD) was performed using a Bruker - D8 Advance Diffractometer (Bruker, Coventry, UK) in flat plate geometry using Ni filtered Cu Kα radiation. Data was collected at 2θ values ranging from 10° to 100° with a step size of 0.02° and a count time of 12s using a Lynx Eye detector (Bruker).

2.2.3 Differential thermal analysis

Differential thermal analysis (DTA) was carried out using a Setaram Differential Thermal Analyser (Setaram, Caluire, France) to determine the glass transition (T_g),

crystallization (T_c) and melting (T_m) temperatures. Powdered glass samples were heated from ambient up to 1000 °C at a heating rate of 20 °C min^{-1} under air purge. Readings were corrected against a blank run.

2.2.4 Fourier transform infrared spectroscopy

Fourier transform infrared spectroscopy was performed on glass powder samples using a Perkin Elmer System 2000 spectrometer (Perkin Elmer, USA) in the range 4000-400 cm^{-1}. Each spectrum was obtained by averaging 10 scans.

2.2.5 Dissolution study

To determine the degradation of the microspheres over time, 250 mg of microspheres were placed in 25ml of deionised water at pH 7. At 0, 1, 3, 7, 14 and 21 days, the solution was removed and stored for further analysis. The microspheres were oven dried and then reweighed and the weight loss was calculated as a percentage of the original weight. Triplicates of each sample were analysed for each time point.

2.2.6 Cobalt release

The release of cobalt ions from the glasses was studied using a Dionex ICS-2500 ion chromatography system (Dionex, UK), designed for determination of transition and lanthanide metals. Media harvested from the degradation study, containing the released cobalt ions from all the glass compositions, were eluted using an Ion Pac® CS5A cation ion exchange column with attached CG5A guard column. The MetPac® PDCA (Dionex, UK) was used as the eluant concentrate in which pyridine-2,6-dicarboxylic acid (PDCA) functions as a colorimetric complexing agent for divalent cations separation. Absorbance was detected at 530nm.The sample run time was set for 10min and each condition was analyzed in triplicate.

2.2.7 Cell culture

The human osteosarcoma cell line MG-63 (kind donation of Dr. Vehid Salih, Eastman Dental Institute, UCL) was used in this study. MG-63 cells were cultured in T-75 tissue culture flasks (Fisher Scientific, Loughborough, UK) with low glucose Dulbecco's Modified Eagle Medium (DMEM), supplemented with 10% fetal bovine serum (FBS) and 1% Antibiotic/Antimycotic (Anti/Anti), all supplied by Life Technologies (Inchinnan, Scotland). Cell cultures were maintained at 37°C/5% CO_2 and passaged every three days using trypsin-EDTA (Life Technologies) solution for 5min at 37°C. Cell number was determined using a Neubauer haemocytometer.

2.2.8 MG-63 expansion on microspheres under static and dynamic conditions

A monolayer of phosphate glass microspheres (5mg/well) was placed into low-adhesion 96-well plate (Corning Costar®, Appleton Woods, Birmingham, UK) in order to prevent cell attachment to the microwell surface. The microspheres were UV sterilized for 1h30min. MG-63 cells were seeded on the microspheres at a concentration of 1.5 x 10^4 cells per well and then placed in the incubator at 37°C/5% CO_2 for up to 14 days, with media replaced every two days.

The cell proliferation study was divided into three groups consisting of MG-63 cultures under static conditions and on an orbital shaker at two different speeds, 150 and 300rpm.
These speeds were selected based on an experimental fluid dynamic study on cylindrical, orbitally shaken bioreactors (Weheliye et al. 2013). According to this study, at low shaking frequencies, a two-phase system is observed within the cylindrical well, with a well-mixed area on top of the well (convection dominated) and a stagnant phase at the bottom (diffusion limited). As the shaking frequency increases, more mixing occurs, resulting in a reduction of the diffusion limited zone. They observed that for different systems, when a non-dimensional critical wave amplitude $\Delta h/h_c$ is reached, mixing extends to the bottom of the well, so that the entire vessel is convection limited. The critical speed N_c at which this transition occurs, can be calculated using the following equations, based on the calculation of the critical Froude number Fr_c, a dimensionless number representing the ratio between inertial and gravitational forces at which the transition phase occurs:

$$\frac{h}{di} = a_0 \frac{h}{\Delta h} Fr_c \quad (1)$$

$$N_c = \sqrt{\frac{g\ Fr}{2\ \pi^2 d_o}} \quad (2)$$

Where:

a_0=1.4 (constant of proportionality)

h=fluid height in the well

$(\Delta h/h)_c$=non dimensional critical wave amplitude

d_i=well inner diameter

d_o=shaker orbital diameter

Nc=transitional speed

Frc=critical Froude number

g=gravitational acceleration

As for our system, $h/d_i < (d_o/d_i)^{0.5}$, the critical wave amplitude can be calculated as $(\Delta h/h)_c = (d_o/d_i)^{0.5}$ and substituted in Eq. 1 to calculate the Fr_c. The critical speed N_c at which the transition occurs can the be determined from Eq. 2.

Table 2.2 summarizes the geometrical characteristics of the experimental system and the calculated Fr_c and N_c. As this model is very sensitive on the height of the fluid within the well, two different N_c were computed, based on upper and lower limit of fluid height used in the experimental setting. A range of critical speed between 340-350 RPM was calculated, for a volume within the well in the range of 150-160µl. Two speeds below N_c, 150 and 300 RPM, were then selected to investigate how enhanced mixing conditions would affect cell proliferation and metabolism, however keeping a diffusion limited zone where the cell-microspheres monolayer is located. A schematic representation of the fluid dynamic environment at both speed analyzed and at N_c is given in Figure 2.1.

Cells grown on the orbital shaker were allowed to attach to the microspheres for 24hrs statically before starting agitation.

		96 well plate	Unit
Well inner diameter	d_i	0.0064	m
Orbital diameter	d_o	0.01	m
Liquid volume (min)	Vl_{min}	0.00000015	m^3
Liquid volume (max)	Vl_{max}	0.00000016	m^3
Critical Froude number (min)	Fr_{cmin}	0.65	
Critical speed (min)	N_{cmin}	340	min^{-1}
Critical Froude number (max)	Fr_{cmax}	0.70	
Critical speed (max)	N_{cmax}	350	min^{-1}
Selected speed 1	N_1	150	min^{-1}
Selected speed 2	N_2	300	min^{-1}

Table 2.2: Summary of geometrical characteristics and calculated Fr_c and N_c (at minimum and maximum operating volume) for the experimental system. Speeds selected for the study are also reported.

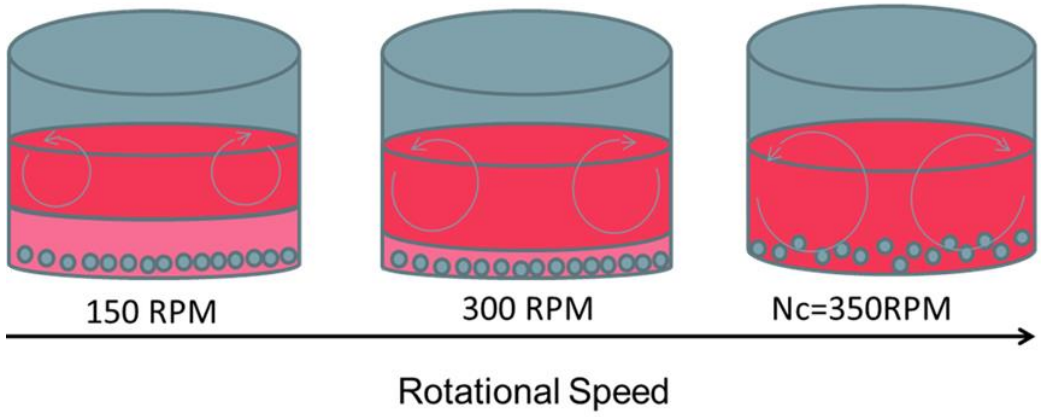

Figure 2.1: Schematic representation of mixing conditions in a 96 well plate at different shaking speed. At 150RPM, a distinction between the convective (top, red) and diffusive (bottom, pink) area is clearly observed. At 300 RPM, a reduction in size of the diffusion- dominated area is observed, with vortices increasing in size. At 350RPM, when the critical shaking frequency is reached, convection dominates the flow within the well.

2.2.9 Cell staining procedures

Cells were first fixed with 4% paraformaldehyde (PFA) for 10 minutes at room temperature and then washed twice with PBS (1 x 1 min and 1 x 5 min). For F-actin staining, cells were permeabilized with 0.5% Triton X-100 in PBS for 10 min at RT. Cells were stained with Alexa Fluor® 488 phalloidin (1:120 dilution in PBS, Life Technologies) for 20min at RT in the dark. Cells were washed twice with PBS (1 x 1 min and 1 x 5 min). Cells were counter-stained with propidium iodide (PI) (1μg/ml, Sigma, Poole, UK) for 10 min at RT in the dark. Images were obtained using a Radiance 2100 confocal microscope (BioRad, Loughborough, UK).

2.2.10 Cell proliferation assay

Cell proliferation was determined using the Cell Counting Kit-8 (CCK-8, Dojingo, Sigma). This test consists on a water-soluble tetrazolium salt, WST-8 that is reduced by dehydrogenase activities in cells to give a yellow-colour formazan dye, whose absorbance can be determined from the tissue culture media. The amount of the formazan dye, generated by the activities of dehydrogenases in cells, is directly proportional to the number of living cells.

For the assay, cells were seeded on monolayers of bioactive phosphate glasses (5mg/well) at a concentration of $1.5x10^4$ cells per well and incubated at 37°C/5%CO_2. At different time points, 10μl of CCK-8 reagent was added to each well in the plate and incubated for 2 hours. Supernatant from each well was then transferred to a new 96 well plate and OD readings were taken at 450nm in a multi-well SafireII plate reader (Tecan, Weymouth, UK). Cells cultured in 96-well plate tissue culture grade plates were used a control. Samples were analysed in triplicates and data presented as mean ± standard variation.

2.2.11 Metabolic profile assay

Glucose and lactate concentration in media collected from cells grown on monolayers of bioactive phosphate glass on low attachment 96-well plate were determined using YSI 2300 STAT Plus analyzer (YSI, Fleet, UK).

50μl of media were collected from each well, centrifuged at 13,000rpm for 30mins to remove any particulates and stored at 4°C until processed. Cells cultured in 96-well tissue culture grade plates were used a control. Triplicates of all conditions were analyzed and the mean ± standard variation was determined.

2.2.12 Human VEGF immunoassay

A human Quantikine® ELISA assay (R&D Systems, Bio-Techne, Abingdon, UK) was used to detect VEGF levels in cell culture supernatant. A monolayer of phosphate glass microspheres (30mg/well, corresponding to the surface area of one well of a 24 well plate) was placed into low-adhesion 24-well plates (Appleton Woods, UK) and then UV sterilized. MG-63

cells were seeded on the microspheres at a concentration of 9 x 10^4 cells per well and incubated at 37°C/5%CO_2. Cells grown on standard tissue culture 24-well plates were used as a control.

Medium was replaced every two days and cell culture supernatant was harvested at 24 and 72hrs post-seeding. Samples of cell culture supernatant were centrifuged at 13,000rpm for 20mins at 4°C and stored at -80°until processing. The ELISA assay was performed according to manufacturer instructions. The assay was repeated two times and each condition was analyzed in duplicate. Data are presented as mean ± standard variation.

2.2.13 Statistical analysis

All data are shown as mean ± standard deviation, if not differently stated.
Statistical signicance was assessed via a two-way ANOVA followed by Bonferroni's multiple comparison test (significance level ≤0.05), using GraphPad Prism software (GraphPad, USA), as reported per experiment.

2.3 Results

2.3.1 X-Ray Diffraction Analysis

The XRD spectra are shown in Figure 2.2. No crystalline phases were detected and a broad peak was observed at values of 2θ between 20-40°for all compositions, confirming the glassy nature of the samples.

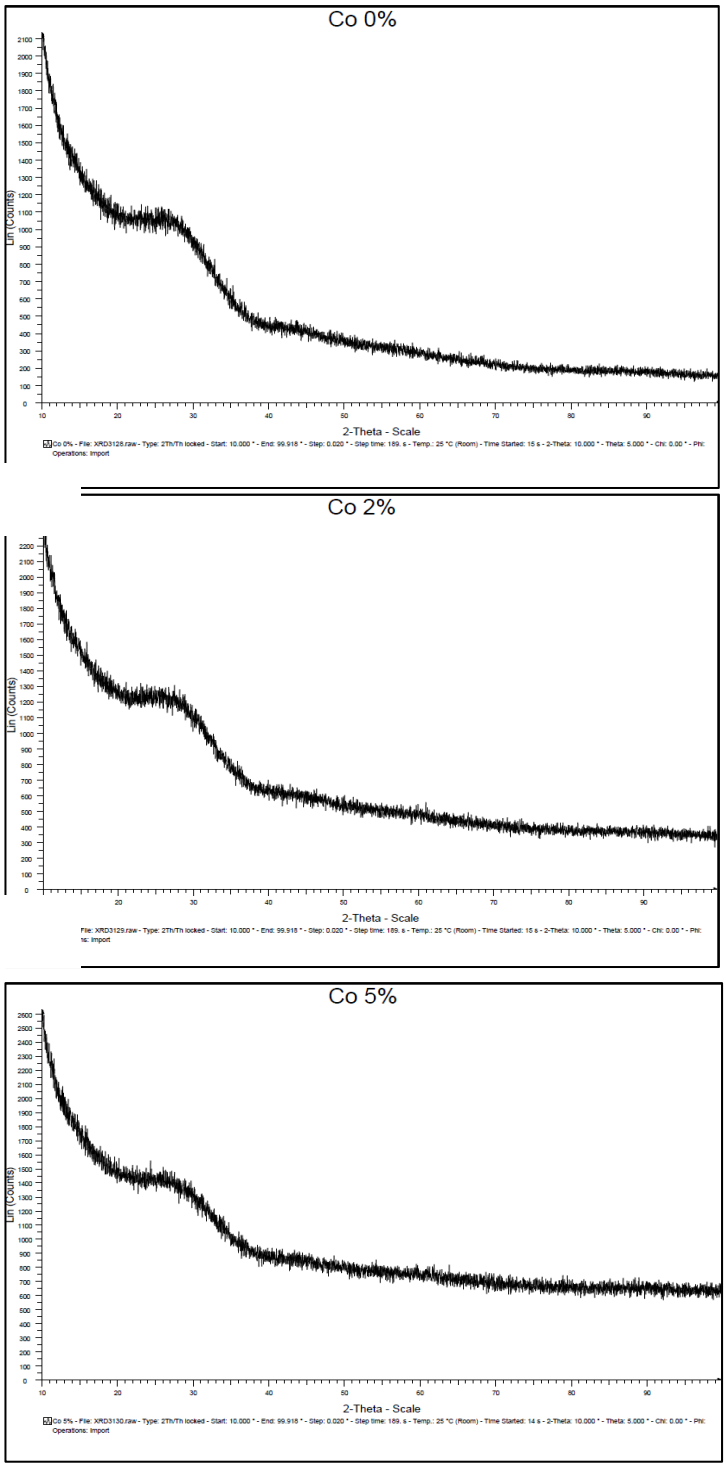

Figure 2.2: X-ray diffraction spectra for phosphate glass containing 0%, 2% and 5% mol CoO.

2.3.2 Fourier transform infrared spectroscopy

FTIR was used to determine any changes in chemical groups present in the glass structure, due to doping with metal oxides. In particular, the effect of increasing molar concentration of Co^{2+} on PO^{2-}, PO_3^{2-} and P-O-P groups was analysed (Figure 2.3).

In accordance to previous studies (Ensanya A. Abou Neel et al. 2009; I.-H. Lee et al. 2013; Lakhkar 2014), peaks in the spectra were assigned as follows:

- the absorption bands at 1260-1270 cm^{-1} correspond to asymmetric stretching of PO^{2-};
- the absorption bands at 1100 and 1000 cm^{-1} are assigned to the asymmetric and symmetric stretching of PO_3^{2-} respectively;
- the absorption bands at 890 and 730 cm^{-1} correspond to the asymmetric and symmetric P-O-P respectively.

Similar to what previously shown by Lee et al. (2013), there was a reduction in intensity of the bands with increasing Co^{2+} content. Furthermore, a shift towards higher energy is observed in correspondence of the PO^{2-} band, with increasing Co^{2+} content.

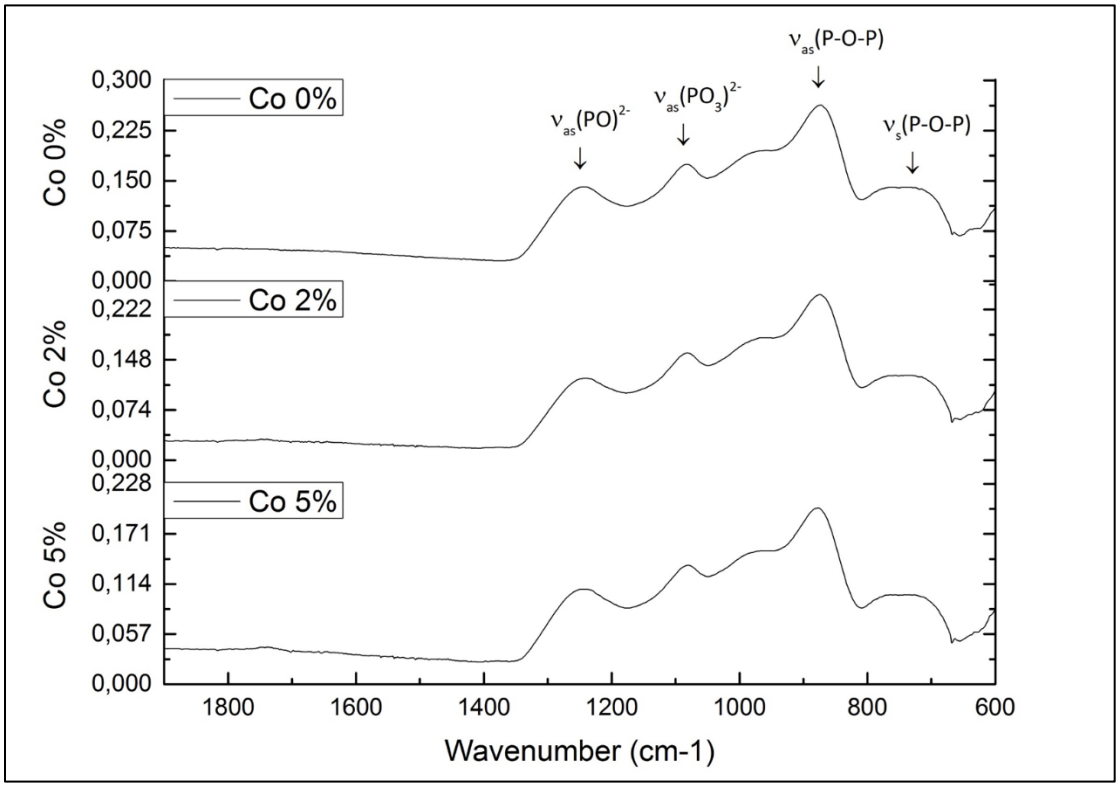

Figure 2.3: FTIR spectra for phosphate glass containing 0%, 2% and 5% mol CoO.

2.3.3 Differential thermal analysis

DTA was used to determine the glass transition (T_g), crystallization (T_c) and melting temperatures (T_m) (figure 2.4).

T_g, T_c and T_m are summarized in table 2.3. No significant changes in T_g and T_c were noticed between the three glass compositions. Two crystallization peaks were noticed for all glasses, together with a reduction in size in the T_m peak with increasing Co^{2+} content, confirming results previously seen by Lee et al. (2013). Furthermore, T_m was found to be inversely proportional to the Co^{2+} content.

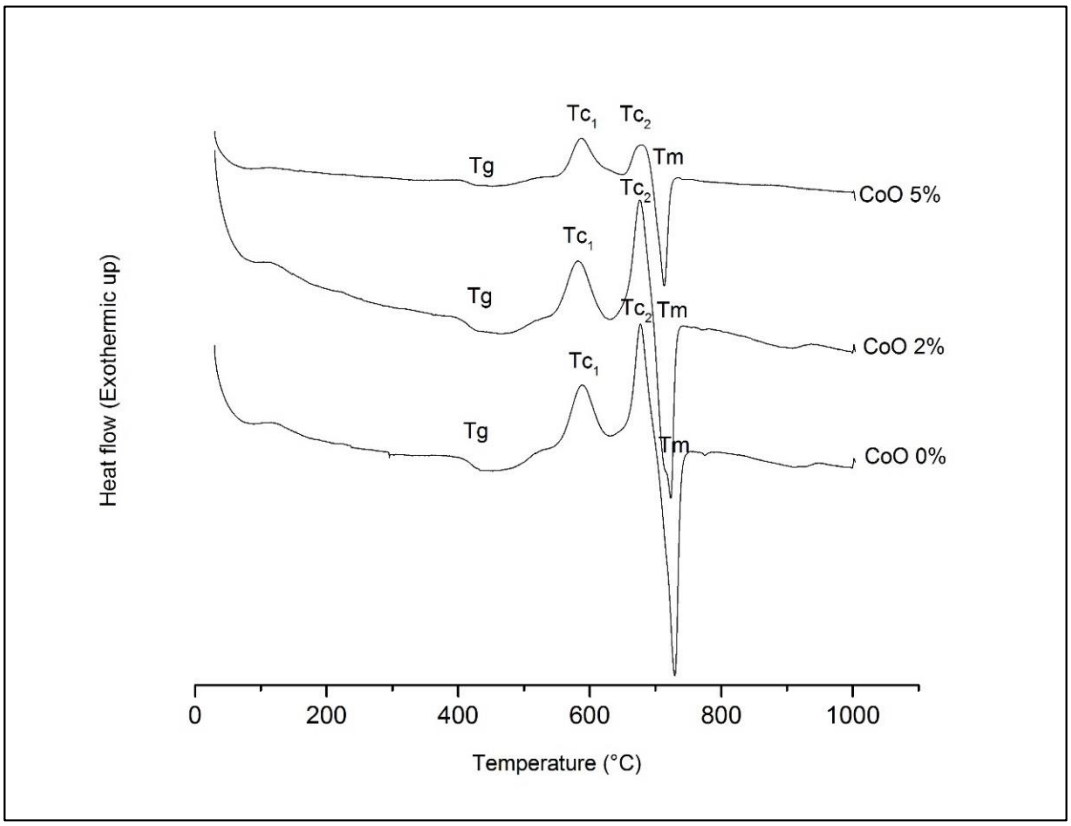

Figure 2.4: Differential thermal analysis spectra for phosphate glass containing 0%, 2% and 5% mol CoO.

	T_g (°C)	T_{c1} (°C)	T_{c2} (°C)	T_m (°C)
CoO 0%	415.4	588.3	677.0	729.3
CoO 2%	415.8	581.8	676.2	723.2
CoO 5%	416.2	586.2	678.5	713.2

Table 2.3: Summary of glass transition temperature (T_g), crystallization temperatures (T_{c1} and T_{c2}) and melting temperature (T_m) for phosphate glass containing 0%, 2% and 5% mol CoO.

2.3.4 Dissolution study

In the dissolution study, weight loss of the glass samples was assessed as a function of time (Figure 2.5). The dissolution rate clearly decreased with increasing cobalt content within the glass composition. Dissolution of cobalt-free glass was considerably faster than the other two compositions, showing a 24.5% (± 2.0%) weight loss at 21 days, compared to 18.7% (± 0.6%) and 17.5% (± 1.6%) of CoO 2% and 5% respectively. Dissolution rates are shown (figure 2.5) and were calculated as the slope of the regression line plotted for each composition. The statistical difference between the slopes of the regression lines was calculated on GraphPad Prism and was found to be statistically significantly ($p<0.0001$).

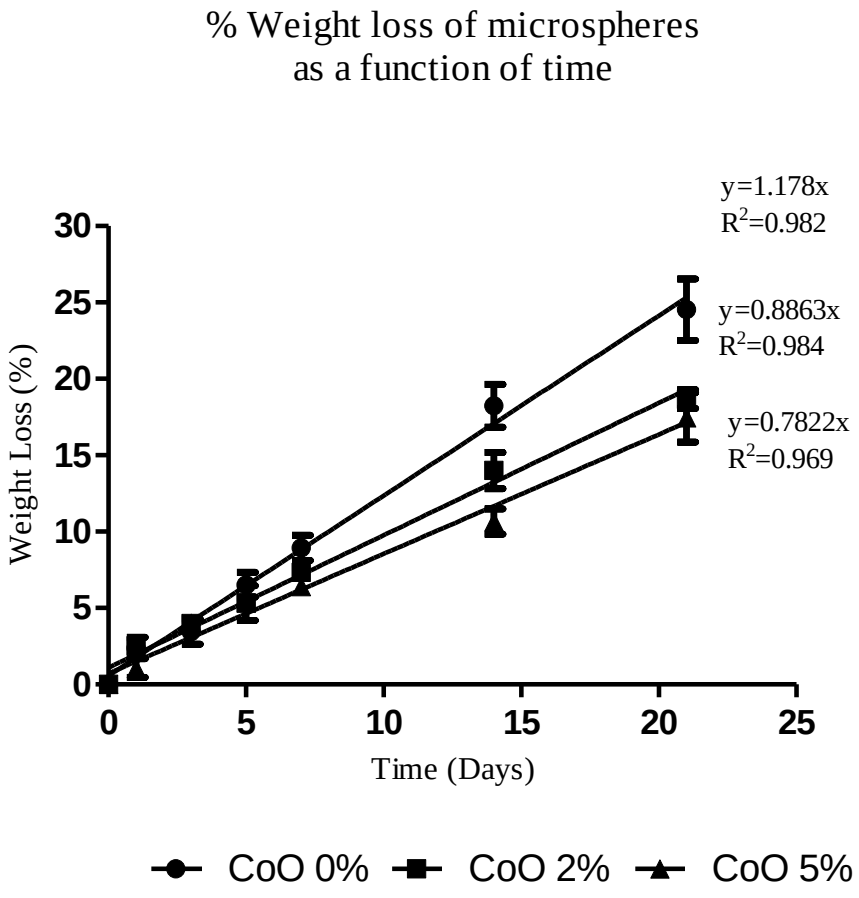

Figure 2.5: Dissolution profile for all three phosphate glass compositions, represented as percent cumulative weight loss as a function of time. Measurements were performed in triplicates at each time point and data are shown as mean ± standard deviation.

2.3.5 Cobalt release

Cumulative cobalt ions release from all three glass compositions over a period of 21 days was determined (Figure 2.6). Co^{2+} ions release from CoO 5% microspheres was consistently higher than CoO 2% throughout the period analysed. At day 3, the concentration of Co^{2+} ions released by CoO 5% (8.68 ±0.20 ppm, 147µM) was approximately three-fold higher than that of CoO 2% (3.27 ±0.17 ppm, 55µM).

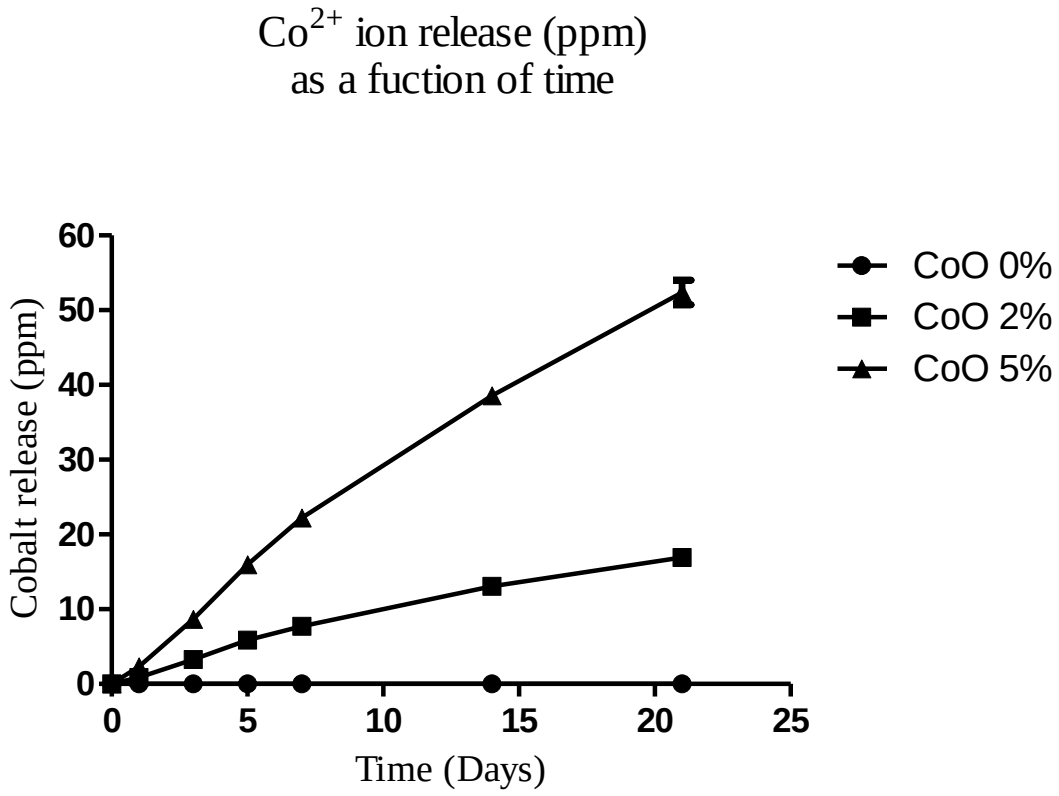

Figure 2.6: Cumulative Co^{2+} ion release presented as ppm g^{-1} as a function of time under static condition. Measurements were performed in triplicates at each time point and data are shown as mean ± standard deviation.

2.3.6 MG-63 culture on bioactive glass microspheres

The MG-63 cell line was successfully cultured on a layer of phosphate bioactive glass microspheres over a period of 13 days. Cell attachment and growth were observed on all three glass compositions, Co0%, Co2% and Co5%. Cell attachment to the microspheres was evident from the first day of culture (figure 2.7). After one week of culture, bridging of microspheres by cells became evident and the formation of clusters occurred. By the end of the two week culturing period, the formation of a single network of microspheres was observed.

The formation of 3D clusters was also shown through confocal microscopy (figure 2.8). Actin filaments in the cytoskeleton were stained using Alexa fluor® 488 phalloidin. Nuclei were stained in red using propidium iodide. Single or multi-layers of cells wrapped around the microspheres were clearly observed.

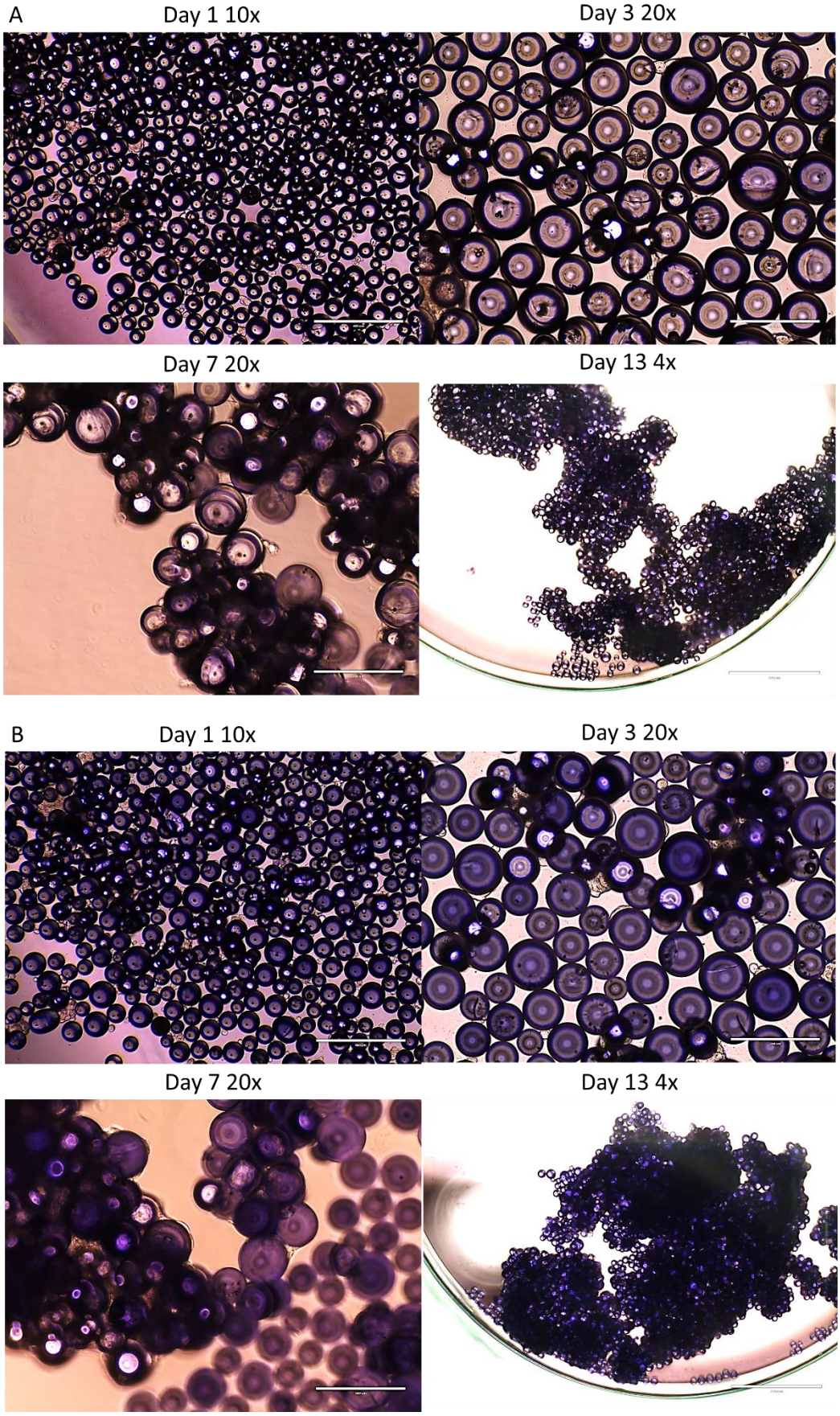

Figure 2.7: Phase-contrast microscopy images showing MG-63 culture on microspheres and cluster formation as a function of time on CoO 2% (A) and CoO 5% (B) microspheres. Scale bar 10x 400µm, 20x 200 µm, 4x 1000µm.

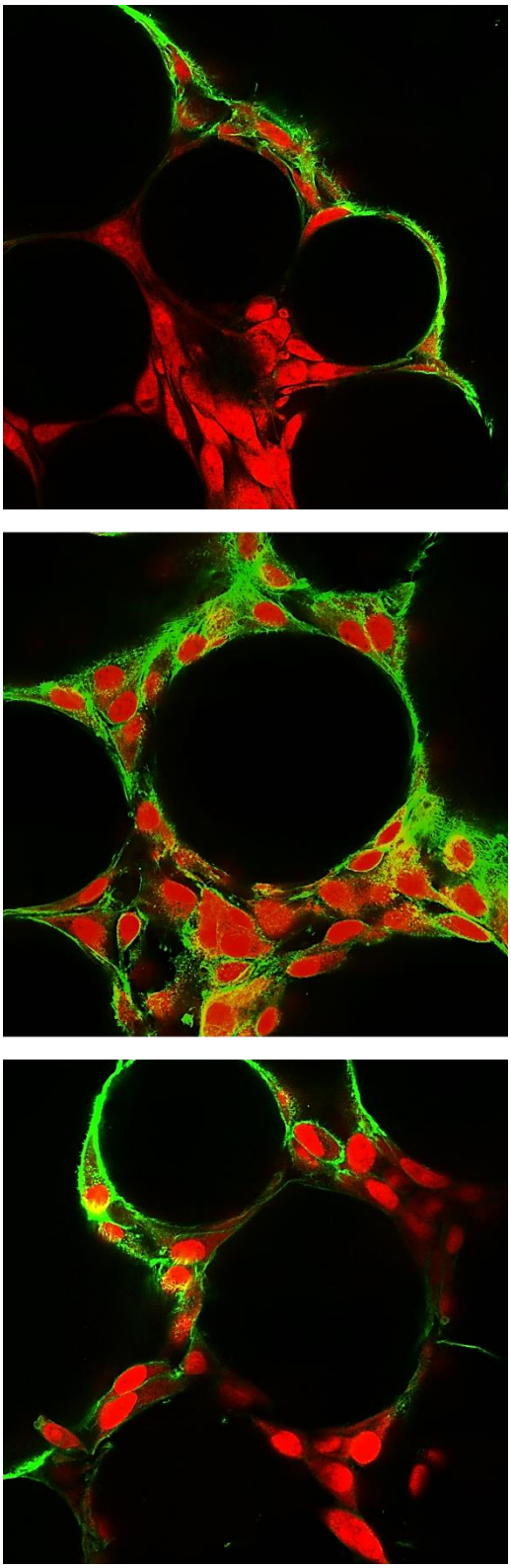

Figure 2.8: Confocal microscopy images of MG-63 cultured on phosphate glass microspheres. Nuclei are shown in red and the cytoskeleton in green. Images were obtained at 20x magnification.

2.3.7 Cells proliferation and metabolic profile

Growth curves for MG-63 cells cultured on monolayers of phosphate glass microspheres were generated for all three different glass compositions (figure 2.9) and for static and dynamic (150 rpm and 300 rpm) conditions (figure 2.10). The concentration of cobalt tested did not have any adverse effect on cells proliferation and comparable levels of expansion were obtained for all three substrates (~4.0 x 10^4 cells after two weeks of culture, $p>0.05$). On the other hand, the dynamic environment was found to have a significant impact on cell proliferation. For all glass compositions, cells cultured under static conditions or on the rotary shaker at 150rpm exhibited similar behaviour. Similarly, glucose consumption and lactate production profiles were comparable under both conditions (figure 2.11). Furthermore, in both conditions, nearly all microspheres were colonized by cells by the end of the two weeks culturing period and the formation of a single cluster was observed at day 13, as shown in figure 2.12. However, a small percentage of cell-free microspheres was observed at 150rpm, thus suggesting higher cell expansion per surface area than in static conditions.

On the other hand, at 300rpm, the formation of aggregates of carriers was less evident, and at day 13, a large surface area was still populated by cell-free microspheres. This was reflected in the growth curve data, showing inhibited cell growth throughout the timeframe analysed, independently of the glass composition (figure 2.10). A detrimental reduction in cell number occurred 48 hours from the start of agitation and the number of cells seem to plateau from day 5 to the end of the culture. Furthermore, for all glass compositions, glucose consumption and lactate production were significantly lower at 300rpm compared to static ($p<0.05$, starting from day 5 for all glass compositions), thus confirming limited growth under this condition (figure 2.11).

Next, the yield of lactate produced from glucose consumed ($Y_{lactate/glucose}$) (which indicates the rate of glycolysis) was characterized for all three compositions and for the tissue culture plastic control, in both static and 150 rpm conditions. As expected, $Y_{lactate/glucose}$ for the control stabilized at a value of ~2 from day 3 of culture. Cells grown on CoO 0% and 2% microspheres presented a higher ratio up to day 3 under static conditions that corresponded to the limited growth observed during early days of culture. From day 5, overlapping between the curves corresponding to the cells grown on the microspheres and the control was observed ($p>0.05$). For the CoO 5% microspheres, overlapping was observed starting from day 7. At 150 rpm, no significant differences between culture on the phosphate glass (PG) microspheres and the control was observed starting from day 3 ($p>0.05$).

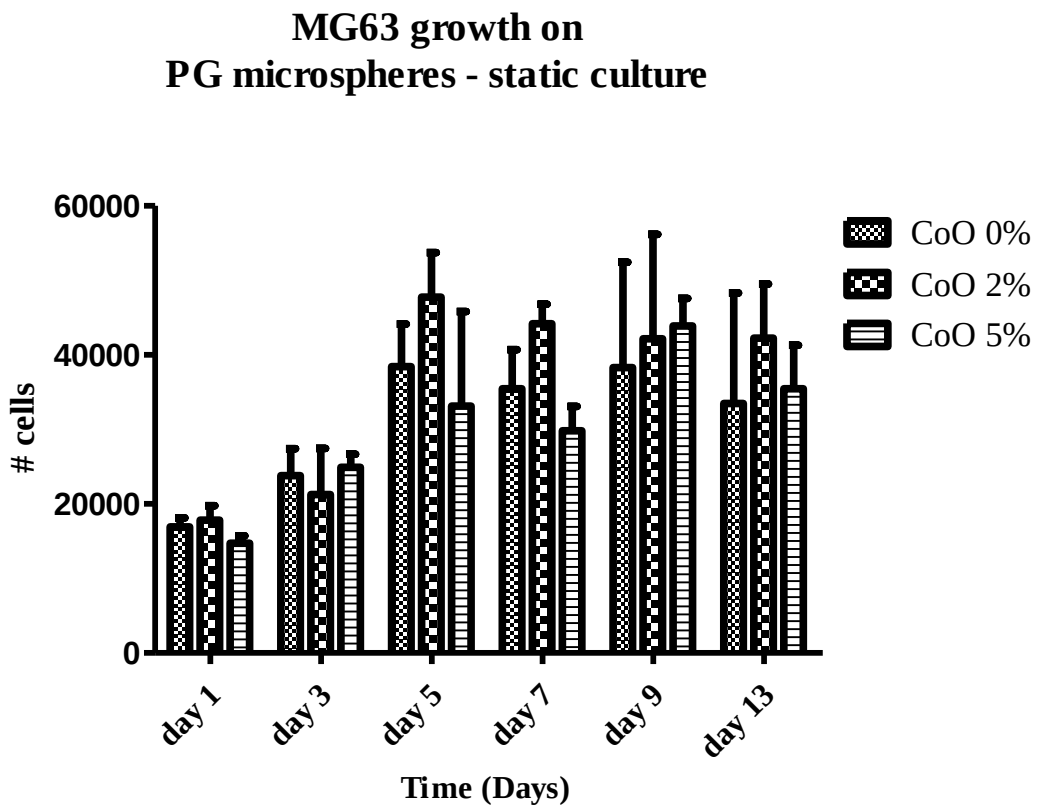

Figure 2.9: Growth curve of MG-63 cultured on PG microspheres over 13 days of static culture. Growth occurred on all PG compositions and cobalt doping did not have an effect on cell expansion at the concentrations tested. Each condition was repeated in triplicates and data are presented as mean ± standard deviation. Statistical significance was assessed using a 2-way ANOVA following Bonferroni post test, $p>0.05$ at all time points.

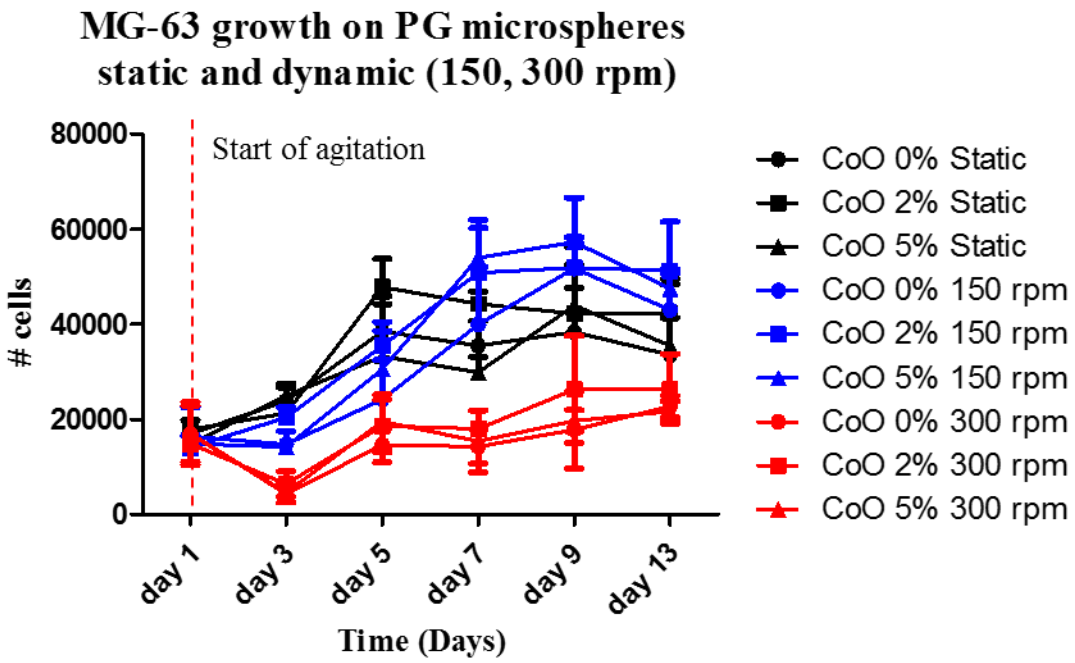

Figure 2.10: Growth curves for all three phosphate glass microspheres compositions (○ CoO 0%, □ CoO 2% and Δ CoO 5%) and culture conditions. Overlapping between growth curves of cells cultured on different microspheres, under the same dynamic environment, clearly shows the significant effect of mixing on cell growth. Overlapping between static culture (black curves) and 150 RPM (blue curves) is observed over time No significant differences between these two conditions were observed ($p>0.05$ at all time points). At 300 RPM (red curves), a significant decrease in cell number is observed after the start of the agitation regime and impaired cell growth is observed throughout the two weeks of culture. Significant differences in cell number ($p<0.05$) were observed starting from day 5 between 300rpm and the static control for all conditions. Each condition was repeated in triplicates and data are presented as mean ± standard deviation. Statistical significance was assessed using a 2-way ANOVA following Bonferroni post test.

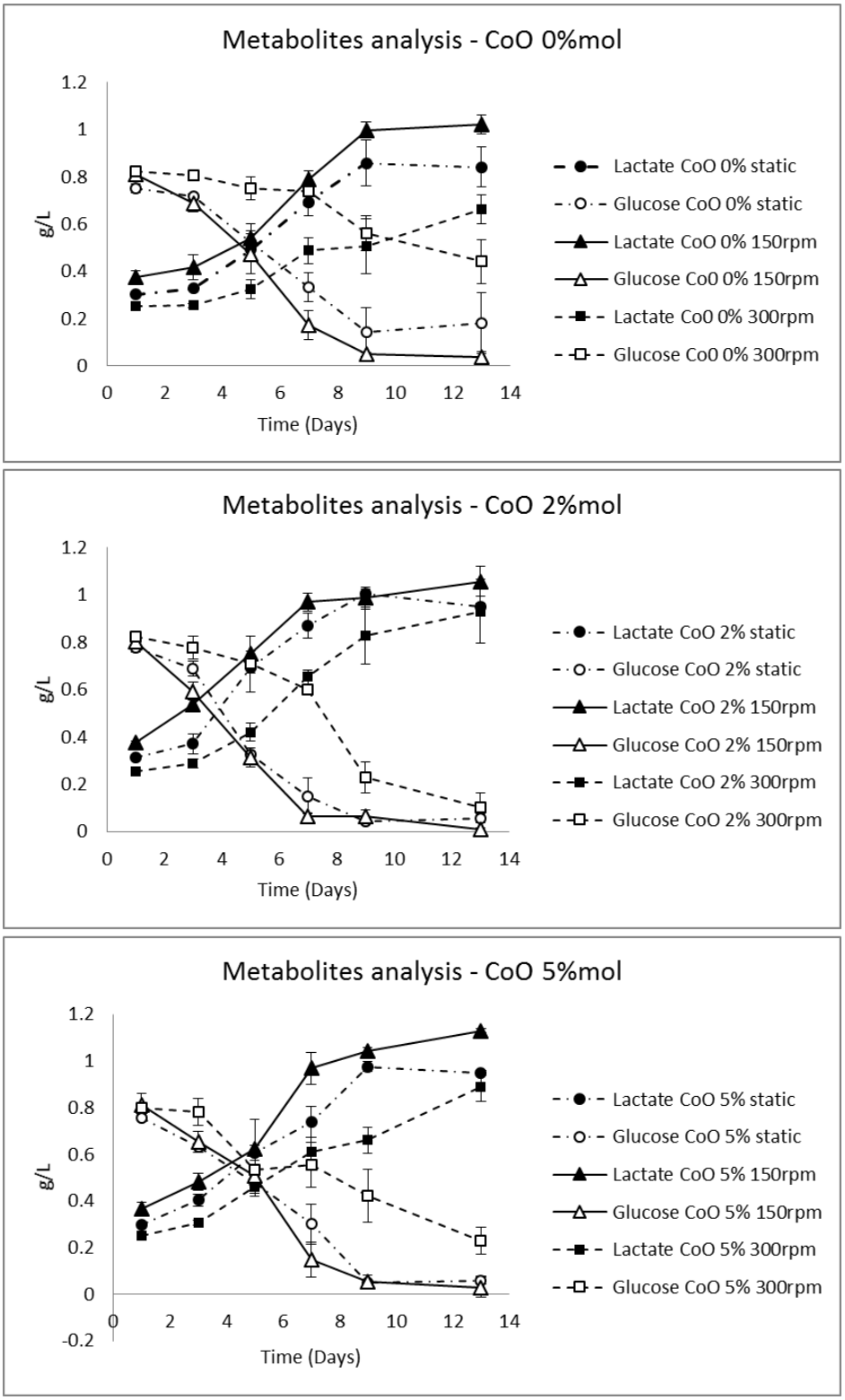

Figure 2.11: Lactate production and glucose consumption as a function of time of MG-63 cultured on phosphate glass microspheres statically or at different agitation regimes (150 and 300RPM). Overlapping between glucose consumption and lactate production curves are observed for all microsphere compositions in static culture and at 150 RPM ($p>0.05$). Significantly reduced glucose consumption and lactate production is observed for all compositions at 300RPM compared to static culture, matching the limited growth observed starting from day 5 ($p<0.05$). Each condition was analysed in triplicates and data are presented as the mean ± standard deviation. Statistical significance was determined using a two-way ANOVA followed by Bonferroni post-test.

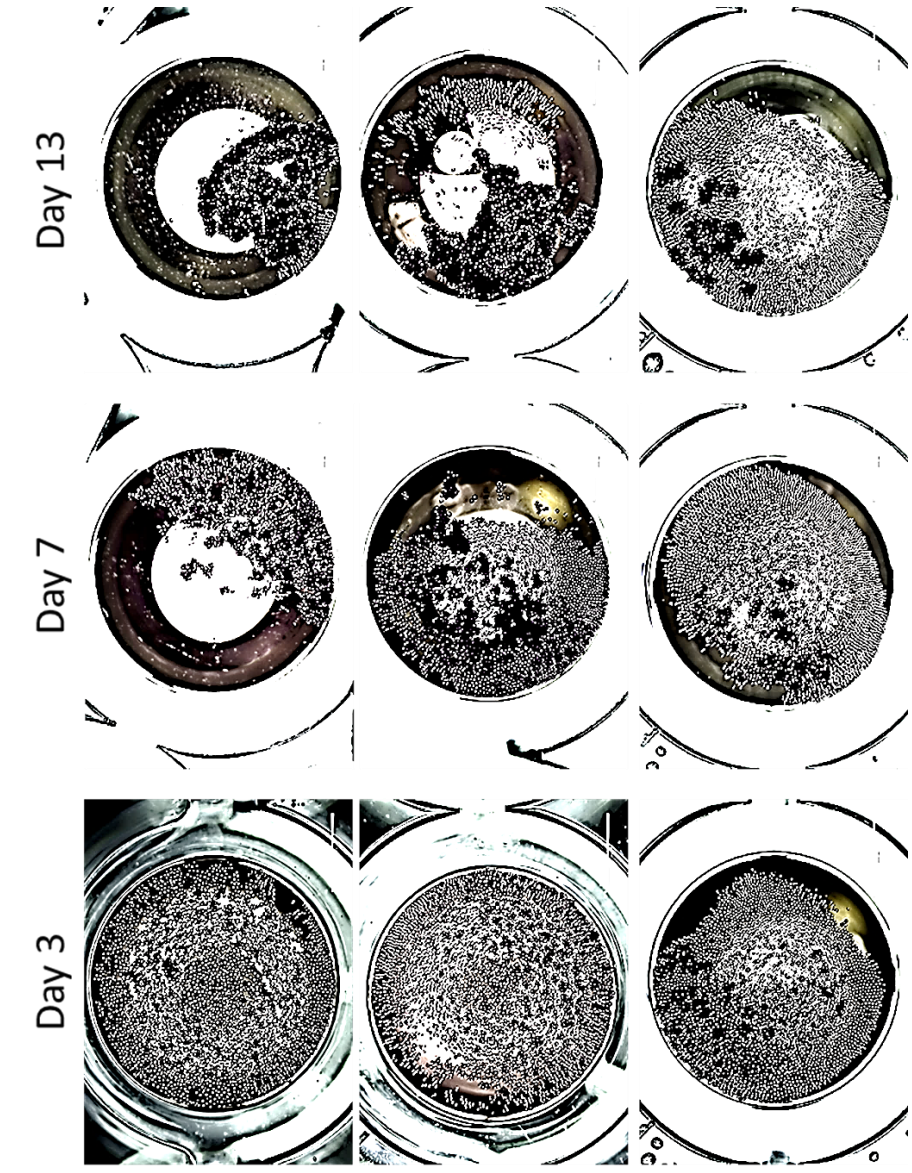

Figure 2.12: Effect of different dynamic conditions on cell clustering over a two week culturing period. At day 3, a monolayer of microspheres can be observed in all three conditions. After one week in culture, the formation of cell-microsphere clusters is evident and in static culture and at 150 RPM, only half of the surface of the well is occupied by the microspheres. A similar trend is observed at the end of the culturing period in both conditions. However, at 150 RPM, the presence of a small percentage of cell-free microspheres is noticed. At 300 RPM, no changes are observed between day 3 and day 13, with microspheres being still arranged in a monolayer and presenting limited clustering. Scale bar 2000µm.

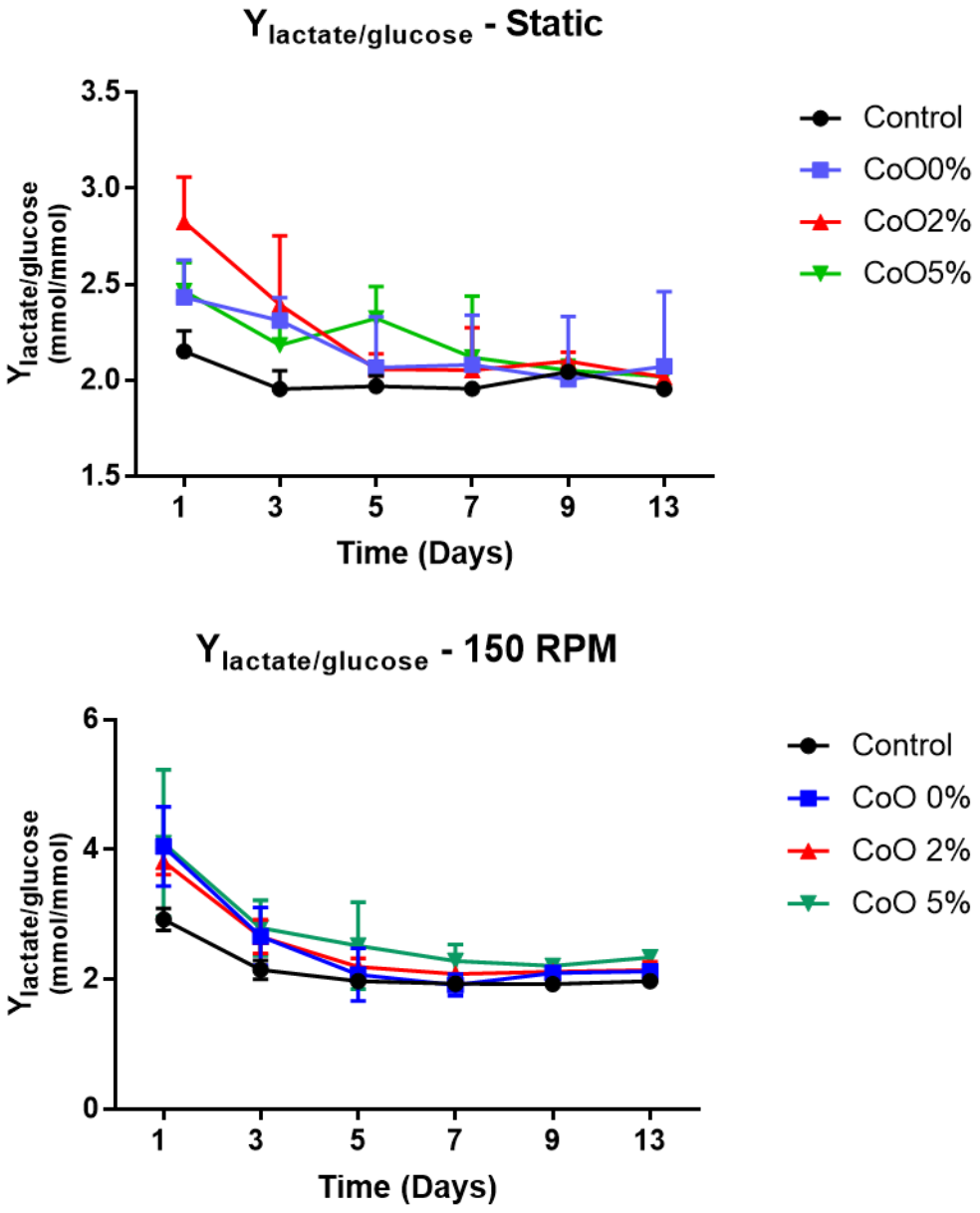

Figure 2.13: Lactate (mmol/L/cells) to glucose (mmol/L/cells) ratio of MG-63 cultured on phosphate glass microspheres under static condition or at 150RPM. Cells grown on standard tissue culture plastic were used as a control. Under static conditions, $Y_{lac/gluc}$ was found to be higher than the control at day 1 and 3 for all PG microspheres ($p<0.05$) and at day 5 for CoO 5% ($p<0.001$). However, no significant differences were observed after these time points ($p>0.05$). At 150 rpm, statistical significance between the PG microspheres and the control was reported only at day 1 ($p<0.01$). Data are shown as Mean ±StDev. Statistical significance was determined using a two-way ANOVA followed by Bonferroni's multiple comparison post-test.

2.3.8 Human VEGF immunoassay

The concentration of VEGF (mg/ml/cell) in supernatant, secreted by MG-63 cells under static conditions for all three glass compositions was measured (Figure 2.14). Cells grown in planar standard tissue culture plastic were used as a negative control. In all conditions, VEGF expression was found to increase with time, with higher concentrations observed after three days of culture. Significant higher levels of expression were observed for cells cultured on the cobalt-doped microspheres at both time points. At day 1, however, Co-induced VEGF secretion was not found to be significantly higher than the control conditions ($p>0.05$). At day 3, VEGF secretion on both Co-doped microspheres was found to be significantly higher than in CoO 0% and the plastic control. Highest expression was observed on CoO 2% after 72 hours of culture (0.045±0.026 pg/ml/cell). Interestingly, VEGF expression by cells cultured CoO 5% microspheres was significantly lower than CoO 2% ($p<0.05$). The cobalt free glass and plastic control displayed a similar behaviour, with minimal VEGF expression at both time points.

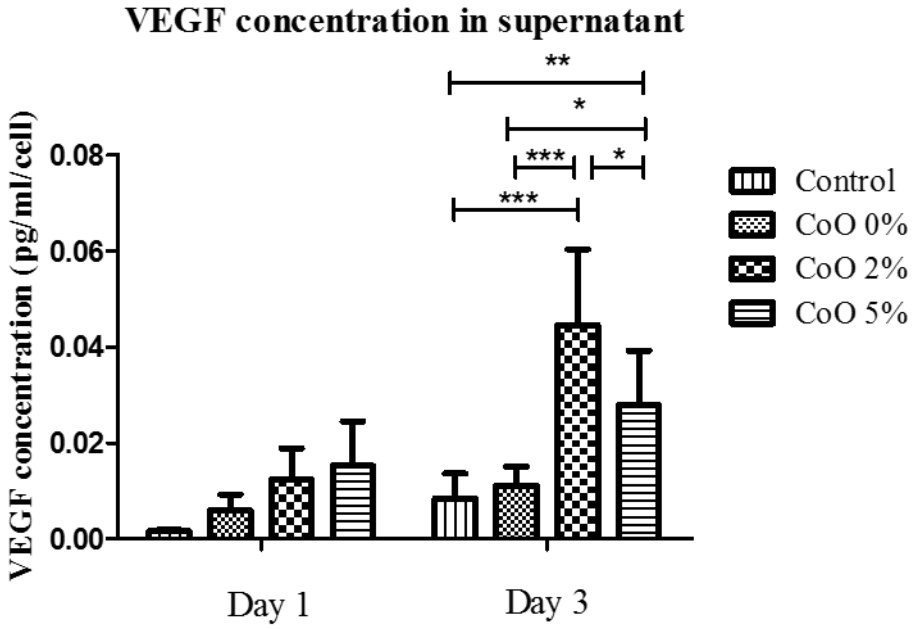

Figure 2.14: VEGF expression of MG-63 grown on phosphate glass microspheres. VEGF concentration in the supernatant was normalized per cell number. Cells grown on tissue culture plastic were used as a control. Pooled data from two repeated experiments are presented and data are shown as mean± standard deviation, n=4. Statistical significance was determined using a 2-way ANOVA followed by Bonferroni's multiple comparison test, *p>0.05, ** p<0.01, *** p<0.001.

2.4 Discussion

Phosphate glasses have been identified as a suitable biomaterial for bone tissue engineering applications (Knowles 2003; Brauer 2012). Key features of these materials are their capacity to being fully resorbed and the versatility of their structure to incorporate therapeutic ions (Lakhkar et al. 2013). Thanks to these characteristics, phosphate bioactive glasses can be classified as a "third generation biomaterial", meaning that the implant is not only temporary, but plays an active role in the regeneration of the damaged tissue (Knowles 2003). Doping with titanium has been identified as a way to improve glass stability and decrease the degradation rate. In particular, incorporation of 5% mol TiO_2 has been found to be biocompatible and to promote osteogenic responses (Abou Neel et al. 2007; E. a. Abou Neel & Knowles 2008; Kiani et al. 2012). As *in vivo* vascularization represents a key issue in tissue engineering, metal ions mimicking hypoxia like cobalt have been investigated as strategies to induce angiogenic responses (Wu et al. 2012; I.-H. Lee et al. 2013; Quinlan et al. 2015).

In this study, Co-doped phosphate glass microspheres presenting 5% mol TiO_2 and increasing molar concentration of CoO (0, 2 and 5% mol) were developed and the effect of the different compositions on the physical properties and biocompatibility of the glasses was tested.

2.4.1 Cobalt doping – effect on physical properties of phosphate glass

Glass presenting increasing concentration of cobalt were made by lowering the calcium content, while keeping the molar concentration of phosphate, sodium and titanium constant. The XRD analysis performed confirmed the amorphous nature of all the glass compositions tested. Substituting CaO with CoO resulted in small variations in the FITR spectra, in terms of a reduction in intensity and a shift to higher wavenumbers of the asymmetric P-O-P bond, similarly to what previously observed by (I.-H. Lee et al. 2013). Increasing CoO content resulted in a decrease of the melting temperature and broader crystallization peaks. This has been previously reported as the result of a more disordered state in the presence of higher CoO content (I.-H. Lee et al. 2013).

Binary doping with cobalt and titanium had a significant effect on microsphere dissolution. In CoO 0%, 25% weight loss occurred in a period of three weeks, while this was reduced to approximately 20% for compositions containing cobalt. Dissolution followed a linear trend during the three week period analyzed. The solubility experiments were performed in deionized water, however it has been shown that phosphate glass dissolution in acellular simulated body fluid (SBF) (Navarro et al. 2003) or in cell culture medium (Patel & Knowles 2006) occurs at a slower rate. Phosphate-glass microsphere degradation in the presence of cells should then be investigated and the degradation time compared to the suggested range of 3 to 6 months for scaffolds for cranio-maxillofacial applications (Bose, Roy, et al. 2013).

In terms of cobalt ions release this was found to be proportional to the original cobalt content in the glass composition, however it did not follow a linear trend. Interestingly, Co^{2+} ions released by the CoO 2% glass composition were found to be in the biologically active range of 3-12 ppm identified by Quinlan et al. (2015), within the first two weeks of analysis. Co^{2+} ions within this range were found to induce angiogenic responses, without altering cell viability. However, as for the degradation rate, the actual Co^{2+} concentration in cell culture media is potentially lower than that measured in deionized water.

2.4.2 Effect of cobalt on MG-63 cell culture

Biocompatibility studies were performed using the osteosarcoma cell line MG-63. All three glass compositions were found to be biocompatible and to support cell attachment and proliferation, independently of cobalt content. Adhesion to the microspheres was successfully shown by microscopy (Figure 2.7). Cells were found to attach to the glass surface from within the first hours of culture. Rearrangement of the cytoskeleton by spreading and flattening of the cells around the microspheres also occurred within the first 24 hours. This was particularly evident through labelling of the cytoskeleton, through which it was possible to observe cells wrapping around the microspheres (Figure 2.8).

The formation of a 3D network, by bridging together of adjacent cells, was also observed. However, not all the cells directly attached to the surface of the microspheres; instead cell-to-cell attachment also occurred. Since the microspheres were not treated to enhance cell adhesion in this study, surface coating could represent a potential strategy to increase cell attachment to the microspheres and to promote growth. Indeed, modifications in surface chemistry (Mitra et al. 2013), topography (Brett et al. 2004; Wall et al. 2009) and tethering of fusion proteins (J. H. Lee et al. 2013) have all been identified as successful strategies to improve adhesion properties of biomaterials.

Clusters of increasing size, consisting of groups of microspheres surrounded by cells, formed during the two weeks of culture, until all carriers aggregated to form a single macroscopic structure of approximately 3mm in diameter. Confocal microscopy was used to visualize the 3D nature of the network and nuclei staining showed the presence of mono or multi-layers of cells around the surface of the carriers (Figure 2.8). The formation of these aggregates of cells and carriers potentially lends itself to a bottom-up approach, in which micro-units of tissue are created separately and are then fused together to produce large, custom-shaped pieces of tissue at the point of delivery, rather than a traditional approach that defines the scaffold shape prior to seeding cells.

The different concentrations of cobalt tested did not have a negative effect on cell expansion capacity. This result was particularly relevant, as cobalt induced toxicity has been reported from wear, corrosion and leaching of CoCr implants (Bose, Fielding, et al. 2013), due

to oxidative damage to cells by reactive oxygen species (ROS), causing DNA strand breaks and oxidation of bases (Simonsen et al. 2012). In this work, Co^{2+} ions released in deionised water by CoO 5% microspheres over three days (the interval used for media exchange was of two days) corresponds to approximately 150μM. However, as previously stated, the actual concentration sensed by cells is lower than that detected in deionised water, thus explaining the lack of cytotoxicity observed even at the highest cobalt concentration.

The capacity of cobalt to enhance VEGF expression was also confirmed, supporting other's observations that Co^{2+} ions can induce hypoxia-like responses in cells (Wu et al. 2012; Azevedo et al. 2014; Quinlan et al. 2015) by stabilization of the α-subunits of the HIF transcription factors (Yuan et al. 2003). In this study, the concentration of VEGF in culture was higher in cells grown on microspheres containing cobalt than in the Co-free microspheres. Despite the cobalt ions release curve (figure 2.6) shows that at day 3, the amount of cobalt being released from CoO 5% is almost three times higher than that being produced by the CoO 2% microspheres, this did not correspond to a relative increase in VEGF production, but in a reduction in expression compared to CoO 2%. This was in line with previous observations (I.-H. Lee et al. 2013) showing no direct correlations between increasing Co^{2+} molar concentration and VEGF secretion. Wu et al. (2012) showed enhanced VEGF gene expression and HIF-1α expression by bone marrow MSCs cultured on mesoporous bioactive glass scaffold doped with 5% mol CoO in comparison to 2% mol scaffold, however, even in their study, this did not translate into enhanced VEGF secretion in the media. In this study, cobalt-free microspheres performed similarly to the plastic control showing minimal level of VEGF secretion.

2.4.3 Effect of agitation on cell culture

As part of this study, the effect of mixing conditions on cell proliferation and cluster formation was also investigated, to test whether hydrodynamic culture conditions could improve cell growth on phosphate glass microspheres. Due to the high density of the microspheres proposed in this study, carriers complete suspension could not be achieved, however mixing was introduced in the system to promote mass transfer within the cell culture environment and to limit gradient formation in terms of dissolved oxygen, nutrients, pH (Lara et al. 2006) and in this specific case, ionic species released by the glass.

Weheliye et al. (2013) previously showed how to characterize flow and mixing dynamics in a cylindrical shaken bioreactor. They observed a mixing pattern characterized by the formation of two counter-rotating toroidal vortices. At low shaking frequency, the formation of two distinct zones within the reactor was observed. A first zone, close to the free surface, was dominated by convection, while a second zone, close to the bottom of the plate, below the vortical structures, was dominated by diffusion. As the shaking frequency *N* was increased, the size and magnitude of the vortices increased, until extending over the entire height of the

cylinder, thus dominating the flow conditions within the reactor. At higher rotational speed the flow pattern changed, with the vortices rotating in opposite direction compared to the movement of the system. This "out of phase" phenomenon was found to start at a specific critical shaking frequency, *Nc*. For this system, *Nc* was found to be equal to 350rpm. Two rotational speeds, both of which were lower than *Nc* where then selected and investigated. Specifically, cell proliferation was studied at 150rpm and 300rpm shaking frequency and compared to static culture.

Mild agitation at 150rpm promoted cell proliferation, with cells reaching approximately a four fold increase in number after approximately nine days in culture, before plateauing. Compared to static culture, agitation at 150rpm performed better towards the second half of the culturing period (although this effect was not found to be statistically significant). When the culture plates were shaken at the higher agitation rate of 300rpm, a detrimental effect on cell growth was observed. The formation of clusters was inhibited and by the end of the culturing period, a large majority of carriers was not colonized by cells. The growth curves showed a drop in cell number after 48 hours from the start of the agitation regime. After that point, the number of cells slightly increased again, but then remained constant over the next days of culture (Figure 2.9). The presence of limited number of small, round shaped aggregates was noticeable. However, cells were not able to spread and attach to the free microspheres. On the other hand, colonization of the totality of carriers by cells occurred under static conditions. At 150rpm, despite the highest cell yield, a small percentage of cell-free microspheres was present, thus suggesting that a higher cell/surface ratio was obtained at this dynamic condition.
Further investigations will be required to identify an optimal speed (or agitation regime) within the range analysed, to improve proliferation on the microspheres substrate and to support the formation of clusters of controlled size.

Metabolic data showing lactate production and glucose in the supernatant correlate with trends observed in the growth curves. Higher lactate production and glucose uptake was observed at 150rpm, followed by static culture and with minimum glucose consumption observed at 300rpm, correlating to the limited growth observed. Enhanced mixing conditions with more homogenous distribution of nutrients and oxygen within the well could be responsible for the general improvement in cell proliferation observed at 150rpm.

The metabolic analysis was particularly relevant to understand whether cobalt-induced hypoxia or 3D culture could have an effect on cell metabolism, as post-translational stabilization of the hypoxia-inducible transcription factor HIF-1 has been reported to upregulate the rate of glycolysis (Lum et al. 2007). In particular, $CoCl_2$ (100μM) induced hypoxia has been reported to cause a metabolic switch in hMSCs, in terms of increased lactate release and impaired oxygen consumption rate (Hsu et al., 2013). Furthermore, this was found to inhibit the capacity of hMSCs to osteodifferentiate. For this experiment, cells grown on tissue culture

plastic in 2D monolayer were used a control. The theoretical lactate to glucose $Y_{lactate/glucose}$ ratio (which expresses the level of glycolysis) is ~ 2 (Wagner 1997; Higuera et al. 2012), with higher values usually associated with anaerobic metabolism. From figure 2.12, it was found that $Y_{lactate/glucose}$ stabilized at a value of ~2 after 72 hours of culture for the control. An initial higher ratio was observed on all phosphate glass microspheres. However, the $Y_{lactate/glucose}$ eventually stabilized around 2 from the day 5 for CoO 0% and 2% and starting from day 7 for CoO 5%, under static culture. Under dynamic conditions, no significant differences between the control and all PG microspheres were observed starting from day 3. Thus, cobalt-doping at the concentrations tested did not have a significant impact on altering cellular metabolism.

2.5 Conclusion

Phosphate bioactive glass microspheres doped with titanium and cobalt were shown to be a biocompatible substrate. Cobalt was found not to be cytotoxic at the concentration tested and successful growth of a model human osteoblastic cell line was obtained on all glass compositions.

The importance of dynamic culture conditions was clearly shown. A suitable reactor system, in which cells can be exposed to optimal mixing conditions and at the same time be kept packed to favour the formation of clusters of controlled size and the colonization of cell-free carriers, should be investigated. Future studies should focus on the analysis of new rotational speeds within the range investigated, as well as new seeding density in terms of both carriers and cells, as these variables have been shown to play a key role on microcarriers aggregation (Mei et al., 2010).

Compared to commercially available microspheres, those analysed in this study present the advantage of being fully resorbable, thus simplifying the bioprocessing sequence, as a harvesting step is not required after expansion. Furthermore, the combined properties of titanium and cobalt are particularly promising for bone regeneration. From this preliminary study, cobalt doping did not have a negative effect on cell growth and comparable proliferation was noticed on all compositions. In terms of VEGF production, the increase in cobalt concentration did not translate in more VEGF being secreted, similarly to what observed in previous studies (Wu et al. 2012; I.-H. Lee et al. 2013). CoO 2% was identified as the composition inducing highest VEGF secretion. Thus, keeping the cobalt content to a minimum value of 2% is sufficient to simulate a hypoxic state and to promote angiogenic responses. However, it is essential to determine whether this translates into functional outputs such as promoting endothelial cells proliferation and vessel formation, *in vitro* and *in vivo* and to test the effect of binary doping on osteodifferentiation.

In addition to these studies, the activation of osteogenic markers is a key element to be taken into account when evaluating the suitability of this material for bone regeneration purposes. Thus, further studies will enable us to have a broader view of the effect of Ti/Co-doped phosphate bioactive glass on osteoblastic cells.

The dynamic data suggest that a bioreactor configuration, able to provide the required mixing environment and to promote cells clustering, should be identified and investigated. For example, a perfusion bioreactor, where microspheres and cells can be packed together and exposed to continuous perfusion, offers an ideal set-up for this particular system.

Furthermore, it must be taken into account, that all experiments were performed using an osteosarcoma cell line. Although this line was chosen since it provides a good human model for cells of osteoblastic origin, the suitability of biomaterials for tissue engineering approaches must ultimately be confirmed using a clinical relevant cell type, such as MSCs.

Chapter 3. Ti/Co-doped phosphate glass microspheres: effect on MSC expansion, osteodifferentiation and angiogenic responses

The work described in this chapter was in part carried out at the Tissue Engineering and Microfluidics Laboratory (TEaM), University of Queensland, Brisbane, Australia, under the supervision of Professor Justin Cooper-White.

3.1 Introduction

As previously stated, MSCs are particularly suitable for bone tissue engineering applications, due to their dual capacity to self-renew and to differentiate towards an osteogenic phenotype (Granero-Molto et al. 2008). Due to the high numbers of cells required for the treatment of individual patients, microcarriers have been widely investigated as a substrate to rapidly expand MSCs in suspension within stirred bioreactors (Chen et al. 2013). For example, Hervy et al. (2014), reported a >10,000 fold expansion of bone marrow derived hMSCs on synthetic microcarriers in spinner flasks over a 40 day culturing period. They then represent a cost-effective solution to maximize cell growth compared to traditional 2D culture. Most commercially available microcarriers are made of either hard material such as plastic or glass, or soft particles such as dextran or gelatine and they can be chemically functionalized or coated to improve attachment (Hervy et al., 2014).

However, compared to most commercial microcarriers, the phosphate glass (PG) microspheres investigated in this study release ionic species that can actively promote biological responses of cells and are fully soluble. Apart from metal dopants, all main components of phosphate glasses (i.e. phosphorus and calcium) are found in the inorganic phase of bone and can modulate biological responses on bone cells. In particular, calcium and inorganic phosphate in the extracellular fluid are required for ECM calcification. Calcium is involved in several signalling mechanisms regulating proliferation and differentiation of both mesenchymal precursors (Riddle et al. 2006; Viti et al. 2016) and osteoblasts (Maeno et al. 2005). Similarly, inorganic phosphate plays a role in osteoblast differentiation through activation of the ERK1/2 signalling pathway (Beck 2003) and is a main component of osteodifferentiation media in the form of beta-glycerolphosphate. Spontaneous differentiation of MSCs towards an osteogenic phenotype in response to Ca^{2+} and PO_4^{3-} supplementation in the media or released from Ca/P scaffolds has been shown even in the absence of dexamethasone and ascorbic acid (Barrère et al. 2006; Müller et al. 2008; Chai et al. 2014; Shih et al. 2014; Viti et al. 2016).

The work in this chapter sought to determine whether similar levels of cell expansion could be obtained when growing human bone marrow MSCs on phosphate glass microspheres (which are implantable) compared to control particles made of plastic (which are not). The control particles used in this study were Synthemax II (Corning), which are microcarriers made of polystyrene and coated to maximize cell attachment. Furthermore, the capacity of phosphate glass microspheres to induce spontaneous differentiation of hMSCs in the absence of osteogenic media was tested. In particular, while the role of titanium doped phosphate glass in inducing osteodifferentiation has been extensively reported (Abou Neel et al. 2007; Abou Neel et al. 2014), the effect of cobalt on MSC differentiation is less well elucidated.

Due to the close relationship between matrix secretion and cell maturation in osteoblast development, the composition of the ECM being secreted by hMSCs in response to culture on the PG microspheres was analysed. Also, as 3D culture of MSCs has been reported to induce spontaneous osteodifferentiation (Tseng et al. 2012), experiments were divided into two main groups:

1) conditioned media experiment: the effect of soluble species released by PG microspheres on MSCs cultured in 2D in tissue culture plastic (TCP) was studied and the response compared to that of MSCs grown in standard culture media (negative control) and osteogenic media (positive control);
2) 3D culture experiment: MSCs were grown on microspheres in standard growth media and their expression profile was compared to that of MSCs grown on Synthemax II microcarriers.

Finally, as cobalt doping was chosen to provide a hypoxic environment that would stimulate angiogenesis, he capacity of CoO 2% microspheres to promote direct or cell-mediated functional vascular responses was tested *in vitro* and *ex vivo*, in comparison to other experimental conditions. As previously stated, the CoO 5% composition was excluded from further studies, as an increase in cobalt content did not translate into enhanced VEGF secretion. For the *in vitro* characterization, the capacity of human umbilical cord endothelial cells (HUVECs) to form tubular structures on a Matrigel substrate under different conditions was investigated. In particular, the effect of soluble species released by the PG microspheres and that of conditioned media released by MSCs cultured on PG microspheres was tested. Finally, a CAM assay was used to test the vascularization capacity of cell-free or MSCs seeded microspheres *ex vivo*.

3.2 Methods

3.2.1 Cell culture

Human bone marrow derived MSCs (Lonza, Verviers, Belgium) were obtained from supplier at P2. Cells were seeded at a density of 4,000 cells/cm^2 according to manufacturer instructions in T-175 tissue culture flask with DMEM low glucose (1g/L) plus Glutamax ™ (Gibco™, Life Techologies, Paisley, UK), supplemented with 10%FBS (Gibco™, Life Techologies, UK) and 1%A/A (Gibco™, Life Techologies, UK).

Cell cultures were maintained at 37°C/5% CO_2 and passaged upon reaching confluency using trypsin-EDTA (Gibco™, Life Techologies, UK) solution for 5min at 37°C. Cell number was determined using a Neubauer haemocytometer.

Five different donors were used in this study. Number of donors used in each assay is reported individually. All experiments were performed with cells at passage P4-P5.

3.2.2 2D experimental setting: MSCs culture for microcarriers conditioned media experiment

MSCs were seeded on 96 well plate tissue culture plastic at a seeding density of 4,000 cells/cm^2 for the control group and of 10,000 cells/cm^2 for the conditioned media and osteodifferentiation groups. MSCs were allowed to attach for 24 hours in standard growth media (DMEM low glucose 1g/L plus Glutamax ™, supplemented with 10%FBS and 1%A/A), before media was changed for each experimental condition.

The following media composition were then applied to each group:

1) Control group: standard growth media;
2) Osteodifferentiation: osteoblast differentiation media prepared by supplementing standard growth media with 50µM ascorbic acid-2 phosphate, 10mM β-glycerolphosphate and 100nM dexamethasone;
3) Microspheres conditioned media group: 30mg of CoO 0% and 2% PG microspheres were weighed and placed in 24 well plates. Following 1h 30min UV sterilization the microspheres were soaked in 900µl of standard growth media and incubated at 37°C/5% CO_2. After 24 hours, the conditioned media were aspirated and 0.22µm filtered. Media were replaced every three days for each condition.

3.2.3 3D experimental setting: MSCs expansion on microcarriers and cell quantification

A monolayer of CoO 0% and 2% PG and Synthemax II (Corning) microspheres were placed into low-adhesion 96-well plate (Costar®) in order to prevent cell attachment to the

microwell surface. As the microspheres presented a different size distribution, surface area available for cell attachment was kept constant between the different microcarriers by adding different quantity of each composition. The microspheres were UV sterilized for 1h30min.
MSCs were seeded on the microcarriers monolayer at a seeding density of 5,000 cells/well and then placed in the incubator at 37°C/5%CO_2 for up to 14 days, with media replaced every two days.

Cell number was assessed at six different time points using a Quant-iT™ Picogreen ® dsDNA kit (Invitrogen- P7589). At each time point, triplicates of each condition were washed with 0.2M carbonate buffer and lysed with 150µl 0.1% Triton-X in 0.2M carbonate buffer. Lysates were stored at -80°C until processing. On the day of the experiment, lysate samples were thawed at 37°C and pipetted up and down to fully lyse the cells. 50µl of sample were transferred to a 96 well plate. A standard solution of Lambda DNA was prepared and 50µl of each dilution was transferred in triplicates to the 96 well plate. A working solution of the PicoGreen reagent was prepared by making a 1:50 dilution in TE buffer. The working solution was kept in foil and 50µl of the working solution were added to each sample/standard. The plate was shaken and incubated in the dark for five minutes at RT. The plate was read at 485nm emission and 538nm emission using a fluorescent plate reader (Synergy HT, BioTek, USA). Two independent experiments were performed using two different donors, six replicates per condition.

Cell metabolic activity was assessed at six different time points using the Cell Counting Kit-8 (CCK-8, Dojindo, Japan), as previously described. The experiment was performed in static condition and on a rotatory shaker at two different speeds, 70 and 150RPM, to test the impact of dynamic conditions on MSCs proliferation on micropheres. Two independent experiments were performed using one donor, in triplicates.
For RT-PCr, a monolayer of CoO 0%, 2% and Synthemax II microspheres was placed in 24 ultra-low attachment plates (Costar®) and UV sterilized for 1h30min. MSCs were seeded at a density of 30,000 cells/well. The following time point were analyzed: day 4, 7 and 14. Three independent experiments were performed using three different MSCs donors.

3.2.4 Immunocytochemistry

Samples from the 2D (conditioned media) and 3D (microspheres) experimental groups were tested for ECM protein expression through immunocytochemistry.
Samples from the 2D group were fixed at day 7 and 10 post seeding.
Samples from the 3D group were fixed at day 7 and 14 post seeding.
In both experimental groups, cells were fixed in 4% PFA (in PBS) for 20 mins, rinsed with PBS (3x) and blocked in 3% BSA for 1 hour at RT.

Samples were then incubated with the following staining solution (in 3% BSA): 1/200 type I collagen (Abcam), 1/200 fibronectin, 1/100 osteopontin (Abcam) and 1/100 osteocalcin (BD Bioscience). Primary antibody incubation was performed overnight at 4°C. After PBS rinsing (3x), secondary antibody incubation was performed for 1 hour at RT in the dark using the following staining solution (in 3% BSA): 1/300 Alexa Fluor 488 (Life Technologies) and 1/300 Alexa Fluor 594 (Life Technologies). This was followed by nuclear staining with 1/1000 Hoechst 33342 (Life Technologies) for 5 min at RT. Wells were then rinsed and stored in PBS until imaging.

Alizarin Red (AR) staining was performed to stain for calcium. Samples were fixed in 4% PFA (in PBS) for 20 mins at RT and rinsed with deionised water (x 3). Staining with 40mM AR (in dH_2O, pH 4.2) was performed for 1hr. Samples were then rinsed with deionised water to remove excess stain.

HIF-1α nuclear staining was performed only on the 2D group at day 7. Cells were fixed in 4% PFA in PBS and permeabilized with 0.2% Triton™ X-100 (Sigma) and 10% goat serum (Vector Labs) in phosphate-buffered saline (Lonza) for 1 h. This was followed by blocking with 10% goat serum for 1hr. The primary antibody anti-human HIF-1α (BD Biosciences, BD610958) was applied in PBS with 0.2% Triton X-100 and 10% goat serum, and kept at 4°C overnight. Cells were washed three-times in PBS, and secondary antibody 488-Alexa Fluor was applied for 1 h at room temperature in the dark, followed by Hoechst staining.
All fluorescent samples were analysed using a LSM Zeiss 710 confocal microscope and an Evos Fluorescent Cell Imaging System (Thermo Scientific) with 5x, 10x and 20x objectives.

3.2.5 Alkaline phosphatase activity

The ALP activity of MSCs grown on CoO 0%, 2% and Synth II microspheres was measured at 1, 4, 7 and 14 days of culture using a colorimetric method based on the conversion of p-nitrophenyl phosphate (pNPP) into p-nitrophenol in the presence of ALP. Briefly, 50 µL of each defrosted samples described in Section 2.2.3 was mixed with 50 µL of 0.33 mg/ml pNPP solution in ALP assay buffer and incubated in the dark at 37°C for one hour. The absorbance of the resulting yellow samples containing p-nitrophenol (i.e., the reaction product) was measured at a wavelength of 405 nm using the microplate reader (Synergy HT, BioTek, USA) and then compared with a standard curve constructed with a range of known concentrations of p-nitrophenol. The ALP activity was normalized by the DNA content and incubation time and thus expressed as µmol of p-nitrophenol produced per hour per microgram of DNA. Two independent experiments were performed using two different donors, six replicates per condition.

3.2.6 RNA isolation and cDNA synthesis

RNA isolation and cDNA synthesis Total RNA was isolated using an RNeasy Mini Kit with on-column DNase treatment (QIAGEN VWR, Stockholm, Sweden) according to the protocol given by the manufacturer. The concentration and purity of RNA was determined by using a NanoDrop spectrophotometer (NanoDrop Technologies, Inc., Rockland, DE). cDNA was synthesised from 100 ng of RNA using SuperScript III First-Strand Synthesis SuperMix (Invitrogen, Life Technologies) in a total volume of 21 μL, as per manufacturer's instructions. An equivalent volume of DNase and RNase-free water (Sigma) was used in place of RT Enzyme Mix for no-RT controls.

3.2.7 Quantitative real-time polymerase chain reaction (qPCR)

qPCR reactions were set up in triplicates with each reaction having a total volume of 10 μL containing 1X Platinum SYBR Green qPCR SuperMix-UGD (Invitrogen), 0.2 μM forward and reverse primers and 1 μL cDNA. A CFX Connect™ Real-Time PCR Detection System (Bio-rad, USA) was used at standard cycling parameters of 50 °C for 2 min, 95 °C for 2 min and then 95 °C for 15 s and 60 °C for 30 s for a total of 40 cycles. qPCR data were analysed using the delta delta method (ΔΔCt) using GAPDH as the reference gene and expression in the Synthemax II microcarriers as control.

3.2.8 Human VEGF immunoassay

A Quantikine® ELISA assay (R&D Systems) was used to detect VEGF level in cell culture supernatant. Cell culture supernatant was harvested at day 1 and 7 from MSCs cultured on CoO 0%, 2% and Synthemax II microspheres in low attachment 96 well plates. Cell culture supernatant was collected from two separate experiments, performed using two different donors. Samples of cell culture supernatant were centrifuged at 13000rpm for 20mins at 4°C and stored at -80°until processing. The ELISA assay was performed according to manufacturer instructions and normalized per DNA content, as quantified by Picogreen ®.

3.2.9 *In vitro* vascularization assay

Human umbilical vein endothelial cells (HUVECs) (kind donation from Dr Enca Martin-Rendon's lab at the University of Oxford) were used in this study.

HUVECs were maintained in EGM™-2 (Lonza) consisting of EBM™-2 supplemented with Bulletkit™ (Lonza) at 37°C and 5%CO2. HUVECs were used within passage P4-P6. The day before the start of the vascularization assay, EGM™-2 was removed and replaces with EBM™-2, in the absence of growth factors.

For the in vitro vascularization assay, a Growth Factor Reduced (GFR) Matrigel® (Corning) was used as a substrate for endothelial cells attachment. Matrigel® is a solubilized basement membrane preparation extracted from the Engelbreth-Holm-Swarm (EHS) mouse sarcoma, a tumor rich in extracellular matrix proteins. The GFR Matrigel® presents a reduced level of growth factors and a more characterized compositions, compared to standard Matrigel®. For this study, 55µl of Matrigel solution was added to wells of a precooled 96 well plate and incubated at 37°C for 1 hour. HUVECs were seeded at a density of 15,000 cells/well in 75µl of EBM (Lonza). Conditioned media from PG microspheres were obtained as previously described. The effect of conditioned media from the microspheres was tested in three independent experiments, with four replicates per condition.

The effect of conditioned media from MSC seeded microspheres was tested in two independent experiments, using two different donors, with five replicates per condition.

Figure 3.1 summarizes all experimental conditions tested and give a graphical representation of the experimental procedure.For each experimental condition, 75µl of conditioned or control media was added per well. Images were taken at 18hrs from seeding.

Exp. Group 1) Microspheres Conditioned Media
CoO 0% in EGM-2 (7 days incubation @ 37°C)
CoO 2% in EGM-2 (7 days incubation @ 37°C)
+ve control EGM-2
Exp Group 2) Microspheres + MSCs Conditioned Media
CoO 0% + MSCs in DMEM LG/10% FBS/1%A/A (harvested at day 7)
CoO 2% + MSCs in DMEM LG/10% FBS/1%A/A (harvested at day 7)
+ve control EGM-2 / -ve control DMEM

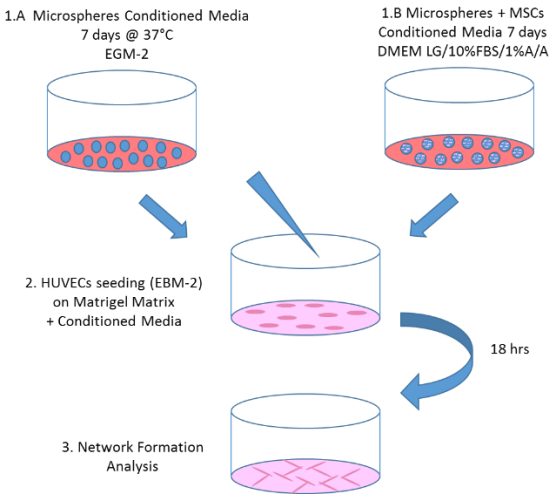

Figure 3.1: Graphical representation of Matrigel in vitro vascularization assay.

3.2.10 *Ex vivo* CAM assay

Fertilized White Leghorn chicken eggs were incubated at 37 °C in a humidified atmosphere (at >60 % relative humidity). After three days incubation, 2 to 3 ml of albumin was withdrawn, using a 21 gauge needle, through a small opening at the large blunt edge of the egg to minimize adhesion of the shell membrane with CAM. A square window of 1 cm^2 was opened in the egg shell and sealed with transparent adhesive tape to prevent dehydration. The eggs were returned for further incubation.

On embryonic day 8, the following implants were placed on top of the CAM:

1) clusters of equivalent size of MSCs cultured on CoO 0% and 2% microspheres for seven days.
2) equivalent volumes of CoO 0%, CoO 2% and Synth II microspheres embedded in 35µl type I collagen gel (BD, Bioscience), produced according to manufacturer instruction.

After implantation, eggs window where sealed with transparent adhesive tape and returned to the incubator. Images were taken seven days post implantation and samples of CAM containing the implant material were harvested and fixed in 4% PFA for 1hr at RT.

3.2.11 Statistical analysis

All data are shown as mean ± standard deviation, if not differently stated. Statistical signicance was assessed via one-way ANOVA, followed by Tukey's multiple comparison test (significance level ≤ 0.05) or two-way ANOVA followed by Bonferroni's multiple comparison test (significance level ≤ 0.05), using GraphPad Prism software (GraphPad, USA), as reported per experiment.

3.3 Results

3.3.1 MSC culture on bioactive glass microspheres

MSCs seeded on microspheres were found to attach to the phosphate glass surface. MSCs proliferation on phosphate glass microcarriers was monitored over a two week culturing period, with cells grown on Synthemax II microcarriers used as a positive control.

Similarly to MG-63 cells, the formation of clusters by phosphate bioactive glass microspheres containing MSCs started from the 5th day of culture and all five donors analysed followed similar trends (data not shown). For MSCs grown on Synthemax II microcarriers, clustering started only from the second week in culture.

The Picogreen ® assay was used to measure DNA content at each time point. Compared to other tests used to quantify cell number based on metabolic activity, this assay enables quantification of DNA content within cell lysate. It was then possible to accurately measure DNA content in clusters made of cells and microcarriers. Combined results obtained from two different donors are shown in figure 3.2. During the first five days of culture, a similar DNA content is observed between the phosphate glass and control microcarriers, thus suggesting similar cell attachment and proliferation between the conditions. It is interesting to note that, even in the absence of glass surface modification to enhance cell attachment, there was no difference in cell number at day 1 between the glass microspheres and the Synthemax II microcarriers. Although figure 3.2 shows a lower cell number on CoO 2% microspheres at day 1, suggesting impaired attachment to this composition, this was not found to be significant. However, at day 7, DNA content was found to be almost double in the Synthemax II control than in the phosphate microcarriers. After two weeks in culture, almost a 3-fold difference is observed between the experimental conditions and the control.

As shown in the previous chapter, dynamic culture seemed to have a major impact on MG-63 growth on phosphate glass microcarriers. For this reason, a preliminary study was performed with MSCs in order to investigate an optimal speed range that would enhance cell proliferation. As 150 RPM was identified as the optimum for MG-63 expansion, the same speed was applied to MSCs. However, this speed was found to be detrimental to MSC expansion compared with the static control in all conditions. Microscopy analysis (figure 3.3) showed that at 150RPM cluster formation was inhibited and several microcarriers were found to be cell-free. However, different from what was observed with the osteoblastic cell line when cultured at 300RPM, a decrease in cell number was not noticed after the start of the agitation regime, as shown in figure 3.4. The number of cells was similar to the control up to the fifth day in culture, after which it started dropping on all microcarrier composition.

It was hypothesised that as MSCs are immature, they will be more susceptible to the effect of flow-induced shear stress than MG-63 cells and therefore a lower agitation speed will be optimal for MSCs. Therefore, in a second experiment, agitation speed was reduced to 70RPM. At this speed, level of expansion was comparable to the static control in all three conditions (figure 3.4). Figure 3.3 shows that clusters of similar size were formed under static condition and at 70RPM; however, a higher number of cell-free microcarriers was found at 70RPM suggesting higher cell/surface ratio under this condition.

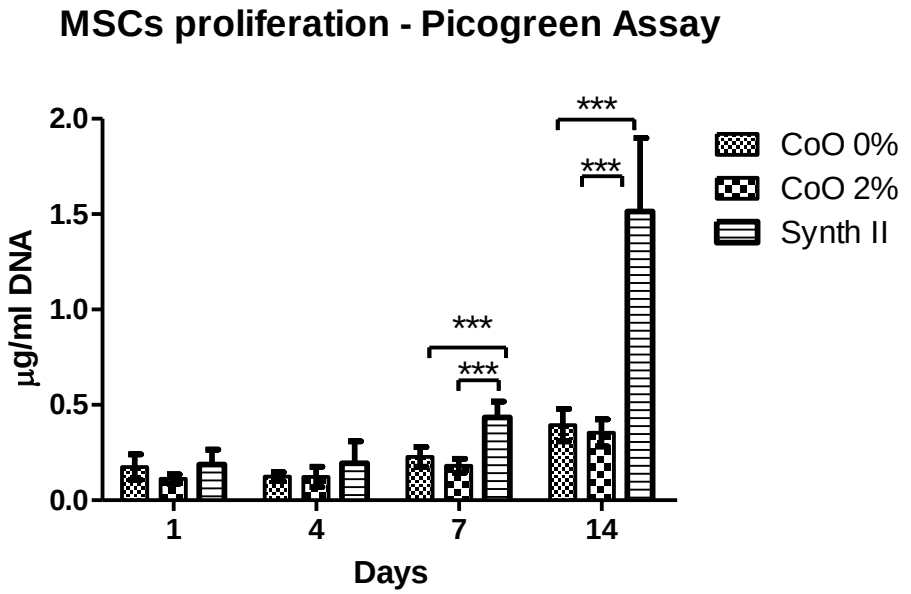

Figure 3.2: MSC proliferation on CoO 0%, 2% and Synthemax II microspheres over two weeks. Data at day 1 show similar number of cells between all experimental conditions, suggesting similar level of attachment to all microspheres. Starting from day 7 from seeding, DNA content on Synthemax II was found to be significantly higher than in the PG microspheres. Data show pooled results obtained from two different donors, n=6/donor. Data are shown as Mean ± SD, statistically compared by a two-way ANOVA followed by Bonferroni post test,*p<0.01.**

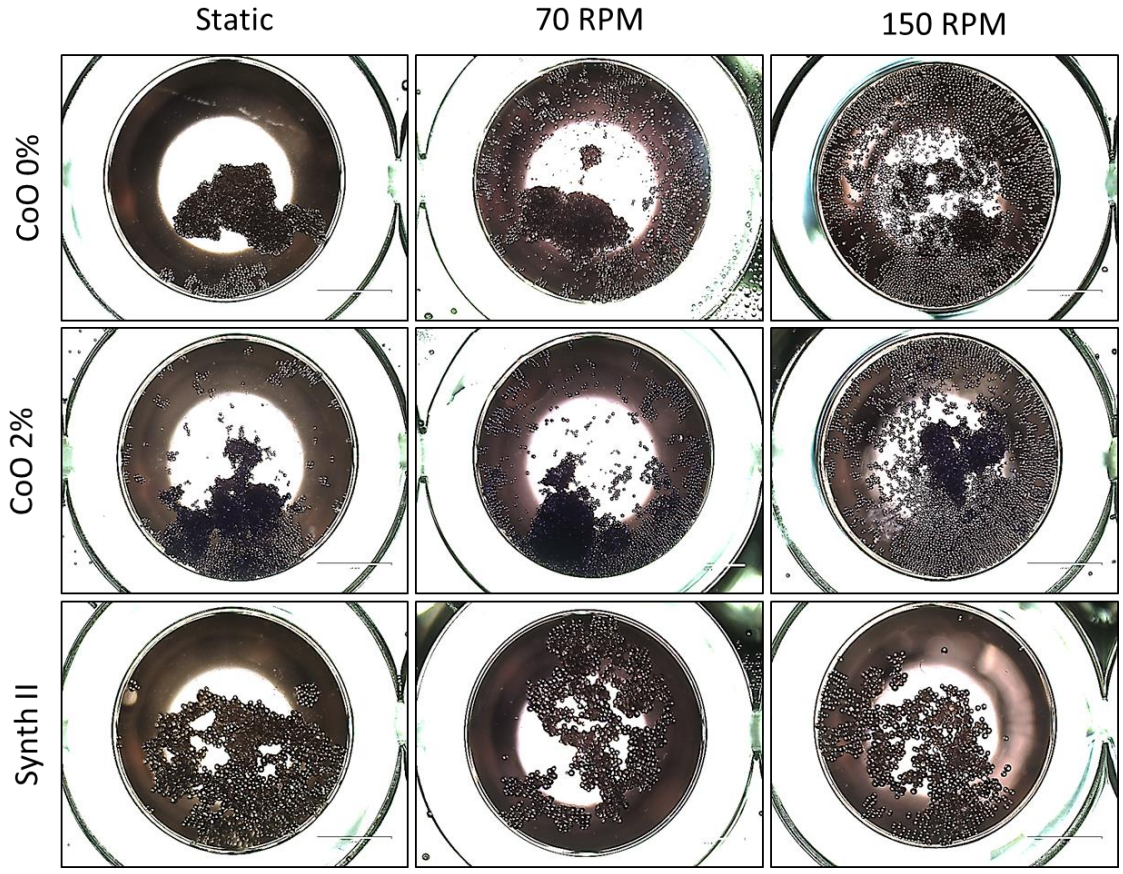

Figure 3.3: Phase contrast microscopy images showing MSC cultured on CoO 0%, 2% and Synthemax II microspheres at 2 weeks from seeding, under static or dynamic culture at 70 and 150RPM. The formation of aggregates of microspheres can be noticed on CoO 0% and 2% under static and 70 RPM culture. At 150 RPM, smaller clusters formed and most microcarriers were found to be cell-free. At 70 RPM some cell-free microspheres were observed at the edge of the well. Synthemax II microcarriers were bridged together by cells in a flat, spread construct under static and 70 RPM culture. Similarly to the PG microspheres, at 150 RPM aggregates of smaller size were observed.

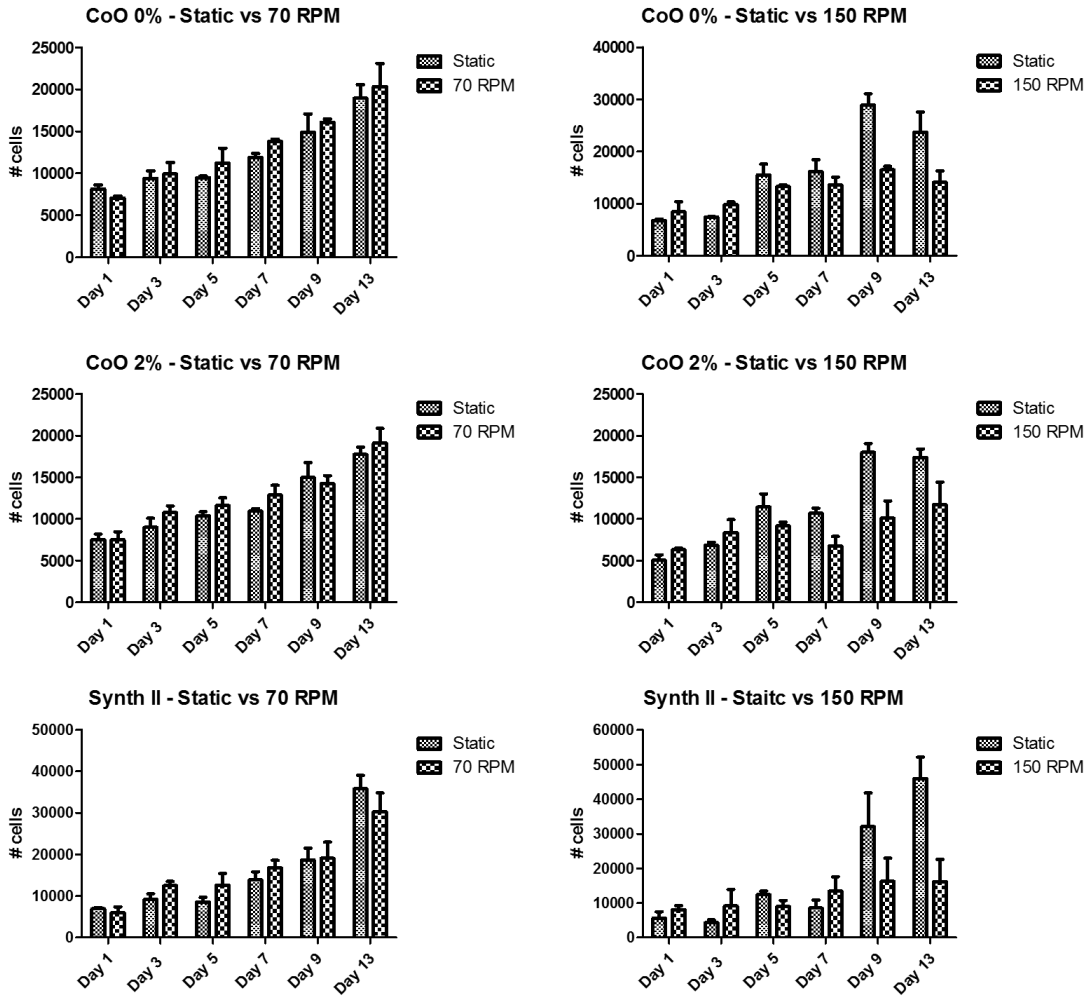

Figure 3.4: Cell number quantification of MSCs cultured on CoO 0%, 2% and Synthemax II microspheres over two weeks, under static or dynamic culture at 70 and 150RPM. In all conditions, the number of cells decreased when cultured at 150RPM, while not significant differences in cell number were noticed between culture at 70RPM and the static control. Each condition was reported in triplicates and data are shown as mean ± standard deviation.

3.3.2 Osteodifferentiation and ECM characterization

3.3.2.1 Conditioned media from phosphate glass microspheres induced osteodifferentiation and ECM expression

The expression of extracellular type I collagen and fibronectin was assessed because increased matrix deposition (and subsequent calcification) is known to be an early event in osteogenic differentiation (Lian & Stein 1995). Among the donors analysed, there was not a consistent pattern with respect to collagen type I and fibronectin expression at day 7 by MSCs cultured with conditioned media from CoO 0% and 2% microspheres. In two out of the three independent donors analysed (figure 3.5, top panel) upregulation of collagen I was evident in the cobalt free group, presenting similar level of expression of the osteodifferentiated group. CoO 2% treated cells showed limited collagen I expression. An opposite trend was noticed for fibronectin (figure 3.5, lower panel), whose secretion was upregulated in the presence of CoO 2% CM in the form of thicker fibers. The third donor analysed, however, presented a different trend (figure 3.6). Both collagen I and fibronectin were upregulated independently of the microspheres composition. It is interesting to note that this donor presented higher level of collagen I and fibronectin expression even in the undifferentiated control and it is possible that this is the reason for the different response in the treated groups.

Osteopontin and osteocalcin expression were also tested in MSCs treated with phosphate glass CM after 10 days in culture. Two donors were tested and found to have a similar response, with osteocalcin being expressed in the presence of CoO 0% CM, while being downregulated in the CoO 2% group (figure 3.7, lower panel). The expression of osteopontin, on the other hand, was not particularly enhanced by the phosphate glass, independently of the composition and was found to be similar to that of the undifferentiated control, as shown in figure 3.7 (top panel).

Next, expression of alizarin red at day 10 of culture (figure 3.8). Calcium staining was found to be higher in the CoO 0% treated group than the CoO 2%, although being lower than the osteodifferentiated group. In particular, the alizarin red staining shows the presence of calcium deposits in the CoO 0% group that are not detectable in the CoO 2% and the undifferentiated group.

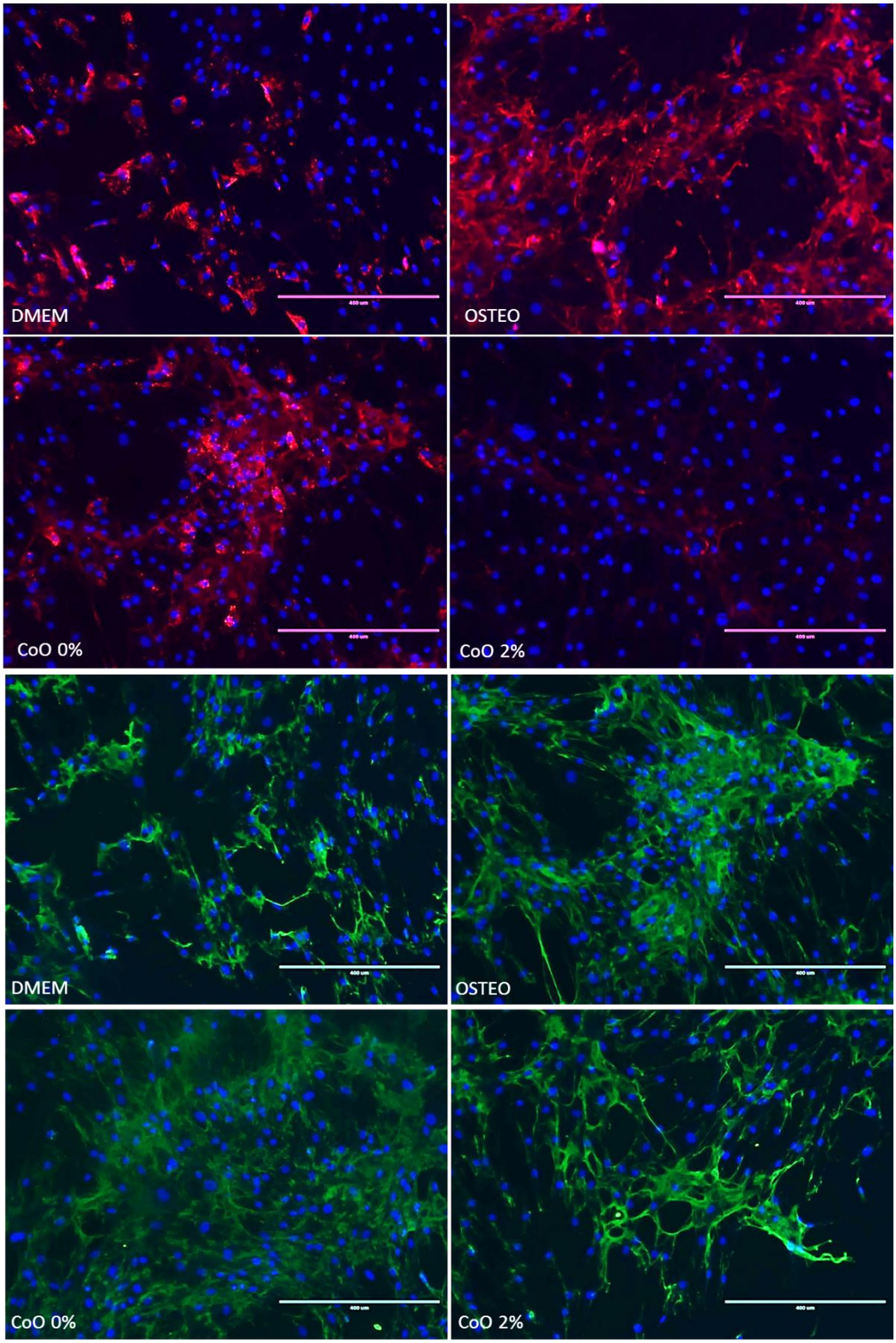

Figure 3.5: Microscopy analysis of extracellular expression of Collagen I (Red) and Fibronectin (Green), Nuclei (Blue) of MSCs grown with conditioned media from PG microspheres at day 7. Type I collagen upregulation was noticed on osteodifferentiated cells and on cells grown with CoO 0% CM. Cytoplasmic expression of Type I collagen is observed on the negative control, while limited expression was seen in the CoO 2% treated group. Fibronectin extracellular expression in the form of thick fibers was observed in the CoO 2% group, while being less structurally developed under treatment with CoO 0% CM. Images are representative of the trend in expression observed in two independent experiments performed using different MSCs donors. Scale bar 400µm.

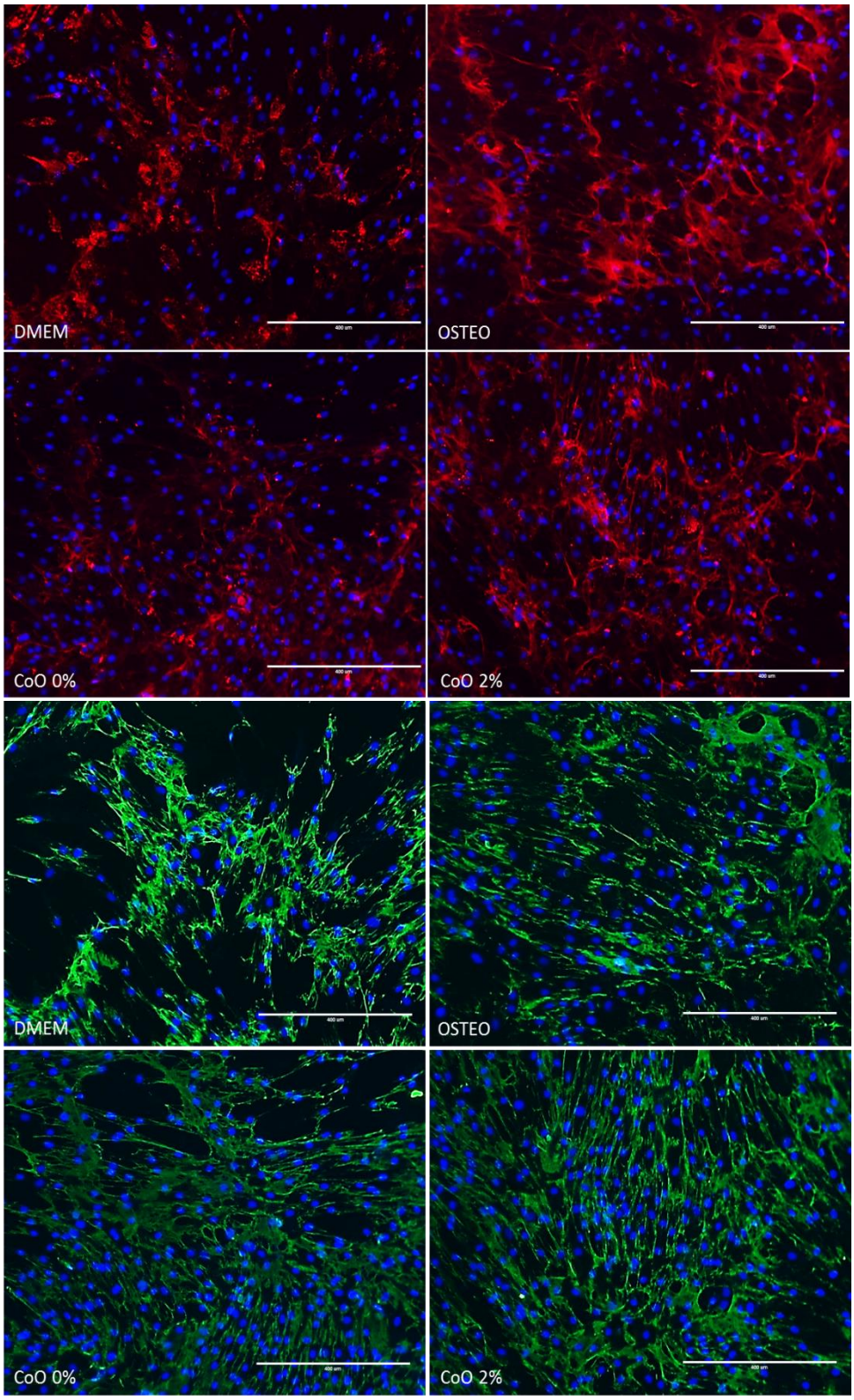

Figure 3.6: Microscopy analysis of extracellular expression of Collagen I (Red) and Fibronectin (Green), Nuclei (Blue) of MSCs grown with conditioned media from PG microspheres at day 7. Type I collagen upregulation was noticed on osteodifferentiated cells and on cells grown with CoO 0% and CoO 2% CM. Secreted Type I collagen was found to be expressed also in the negative control, however to a lower extent than the osteodifferentiated and CM samples. Similarly, fibronectin was found to be expressed in both CoO 0% and CoO 2% treated MSCs. However, also in this case, a more structured distribution of fibronectin fibers is observed in the CoO 2% group. Scale bar 400µm.

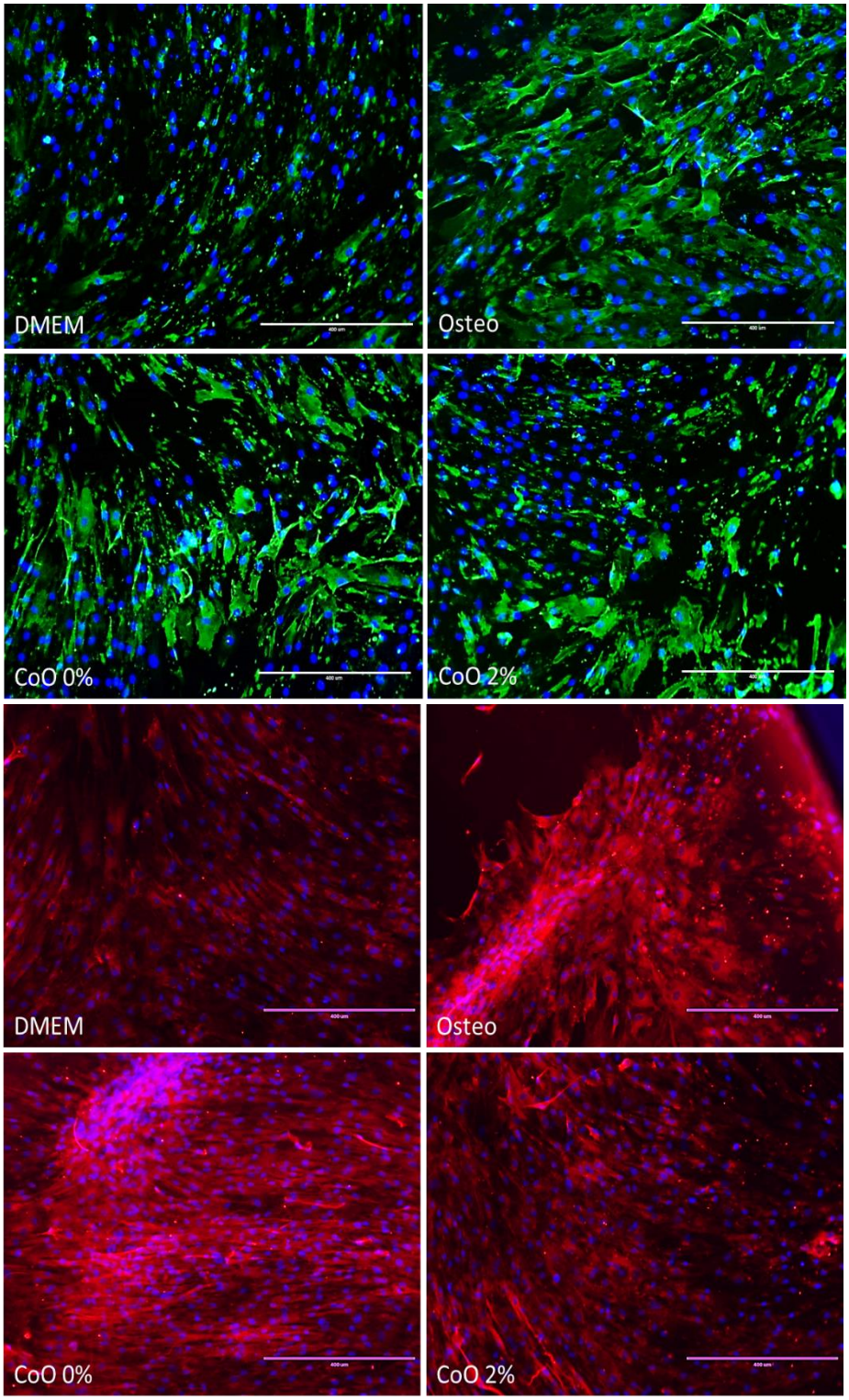

Figure 3.7: Microscopy analysis of extracellular expression of Osteopontin (Green) and Osteocalcin (Red), Nuclei (Blue) of MSCs grown with conditioned media from PG microspheres at day 10. As expected both proteins were upregulated in the osteodifferentiated group. Osteopontin secretion was not found to be uniform in samples treated with CM from PG microspheres, independently of the presence of cobalt. Osteocalcin expression similar in intensity to the positive osteodifferentiated control, were observed in the CoO 0% group. Images are representative of the trend in expression observed in two independent experiments performed using different MSCs donors. Scale bar 400µm.

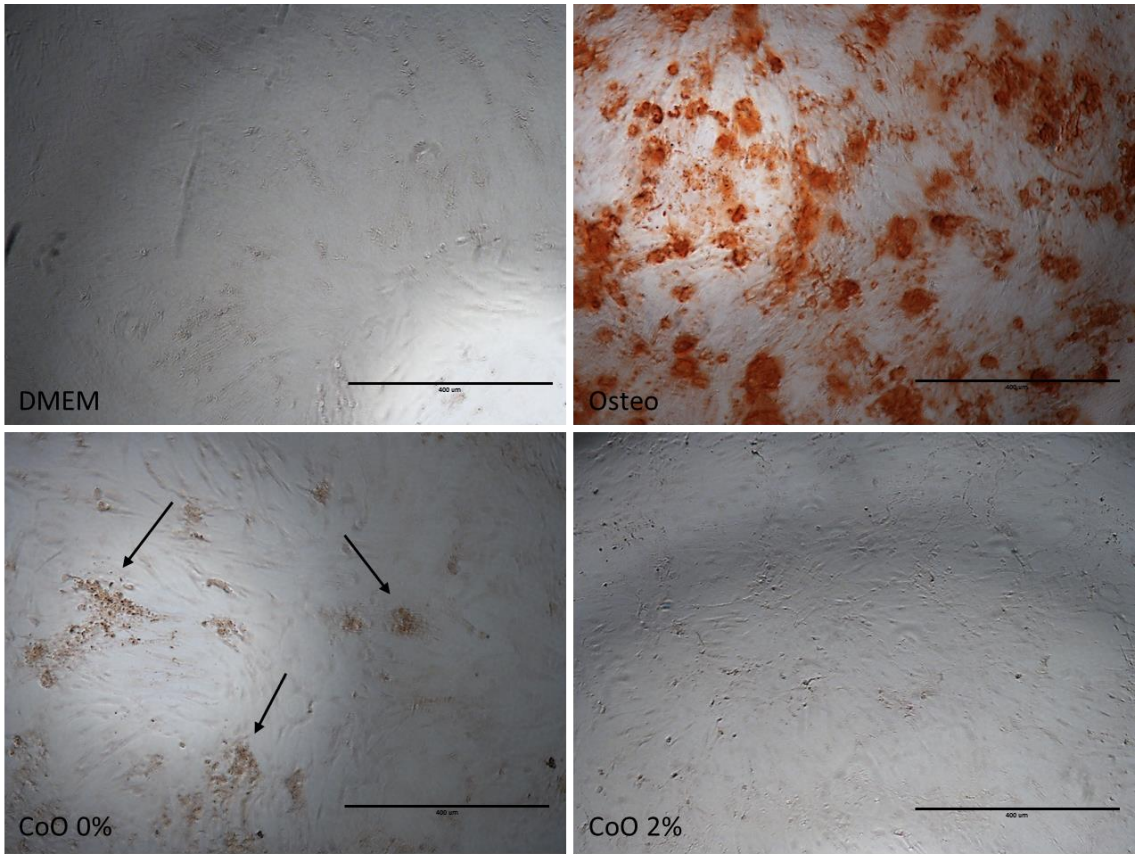

Figure 3.8: Alizarin Red staining of MSCs grown with conditioned media from PG microspheres at day 10. Calcium deposits are clearly stained in red in the osteodifferentiated group, while no staining is visible in the negative DMEM control. Calcium deposits were also noticed (arrows) on MSCs treated with CoO 0% CM. No clear presence of calcium deposits is noticed on the CoO 2% group. Images are representative of the trend in expression observed in two independent experiments performed using different MSCs donors. Scale bar 400µm.

3.3.2.2 ECM characterization and osteogenic markers expression

MSCs grown on phosphate glass microspheres were assessed for expression of collagen I, fibronectin, osteopontin and osteocalcin by immunohistochemistry.

Type I collagen and fibronectin expression followed a similar trend to the CM experiment, with type I collagen being upregulated on CoO 0% microspheres, while fibronectin was highly expressed on CoO 2% after one week in culture. Synthemax II microcarriers used as a negative control were found to induce minimal deposition of ECM proteins (figure 3.9a).

After two weeks in culture, all phosphate glass microspheres and MSCs were clustered in a single dense aggregate, embedded in an ECM network. When staining the ECM network to identify its components, it was found that both type I collagen and fibronectin were equally expressed on the CoO 0% microspheres. Both proteins were also expressed on the CoO 2% microcarriers, however they were distributed less uniformly throughout the construct and Type I collagen was lower than on CoO 0% microspheres (figure 3.9b).

When looking at osteopontin and osteocalcin expression (figure 3.10), generally the first was found to be more homogeneously expressed in the ECM in MSCs grown on CoO 0% microspheres. Expression of osteocalcin was less evident in the 3D culture and generally, a higher level of expression was detected after two weeks of culture. Lower proteins expression was detected in the presence of cobalt and on the Synthemax II microcarriers.

Furthermore, positive Alizarin Red staining was clearly visible on cells grown on phosphate glass microspheres, independently of the compositions, while it was not clearly expressed on the control microcarriers (figure 3.11).

ALP activity was also measured in all conditions at four time points (figure 3.12). ALP activity was upregulated on all three conditions up to day 4 and was found to decline over time. In particular, while activity on PG microspheres, remained constant from day 1 to 4, a decrease in expression was noticed on Synthemax II during this time interval. At day 4 and 7, ALP activity was found to be significantly higher on both PG microspheres, independently of the composition, compared to the control microcarriers. From day 7, a decline in expression was noticed also on the PG microspheres and no significant differences in expression were observed among the experimental conditions at day 14.

Osteogenic gene expression was also assessed by qPCR by looking at the expression of collagen I, osteopontin, runt-related transcription factor 2 (RUNX2) and distal-less homeobox 5 (DLX-5). Gene expression was normalized using the ΔΔCt, using GAPDH as the reference gene and expression on Synthemax II microcarriers as the control. Pooled data from three different donors (two technical repeats per donor) are shown in figure 3.13. A similar trend to that previously analysed by ICC was shown for collagen I and osteopontin, with the markers being upregulated in CoO 0% microspheres.

Differences in gene expression were mainly noticeable after one week in culture between the experimental conditions, while similar level of expression are achieved towards the end of the culturing period. Similarly, RUNXII and DLX-5 were found to be upregulated at day 7 on the CoO 0% microspheres, while being similar to the Synthemax II control at day 14.

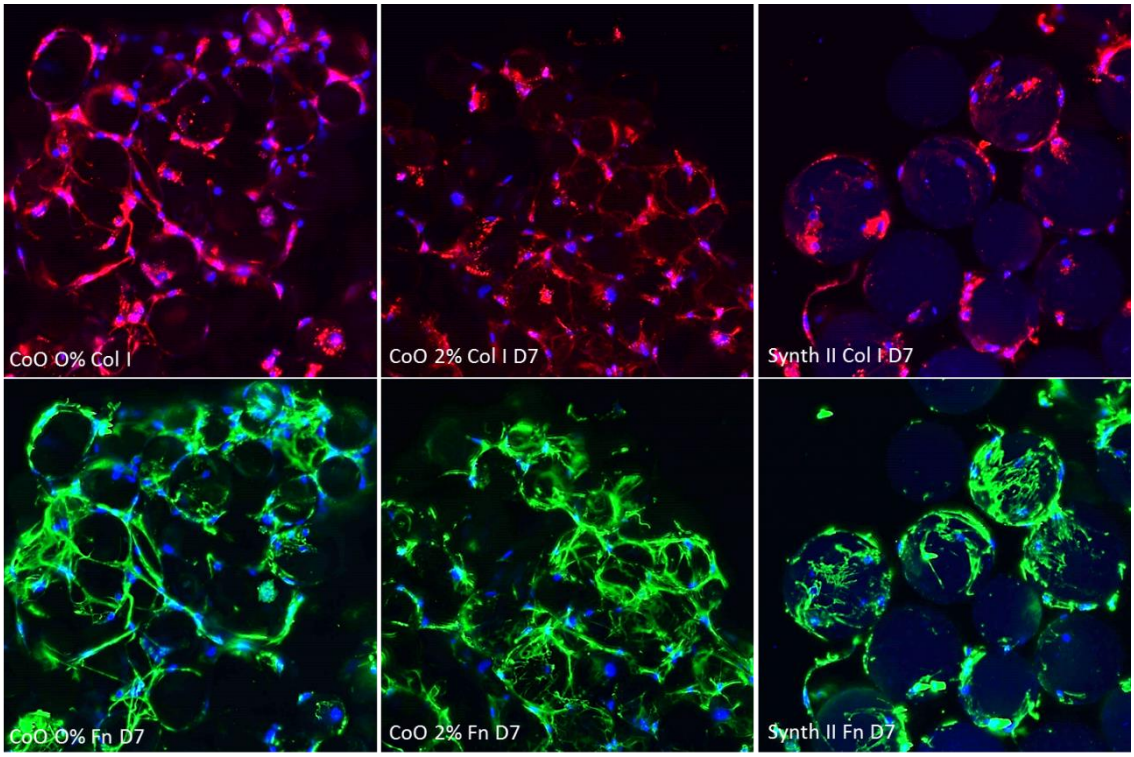

Figure 3.9 a: Confocal microscopy analysis of extracellular expression of type I collagen (Red) and fibronectin (Green), nuclei (Blue) of MSCs grown on CoO 0%, 2% and Synthemax II microspheres at day 7. Similar to the CM experiment, at day 7, type I collagen upregulation was observed on MSCs grown on CoO 0% microspheres, while fibronectin was upregulated on CoO 2%. Minimal protein expression in the ECM was noted on the Synth II microspheres at day 7. Images are representative of the trend in expression observed in three independent experiments performed using different donors. Images were obtained with x10 objective.

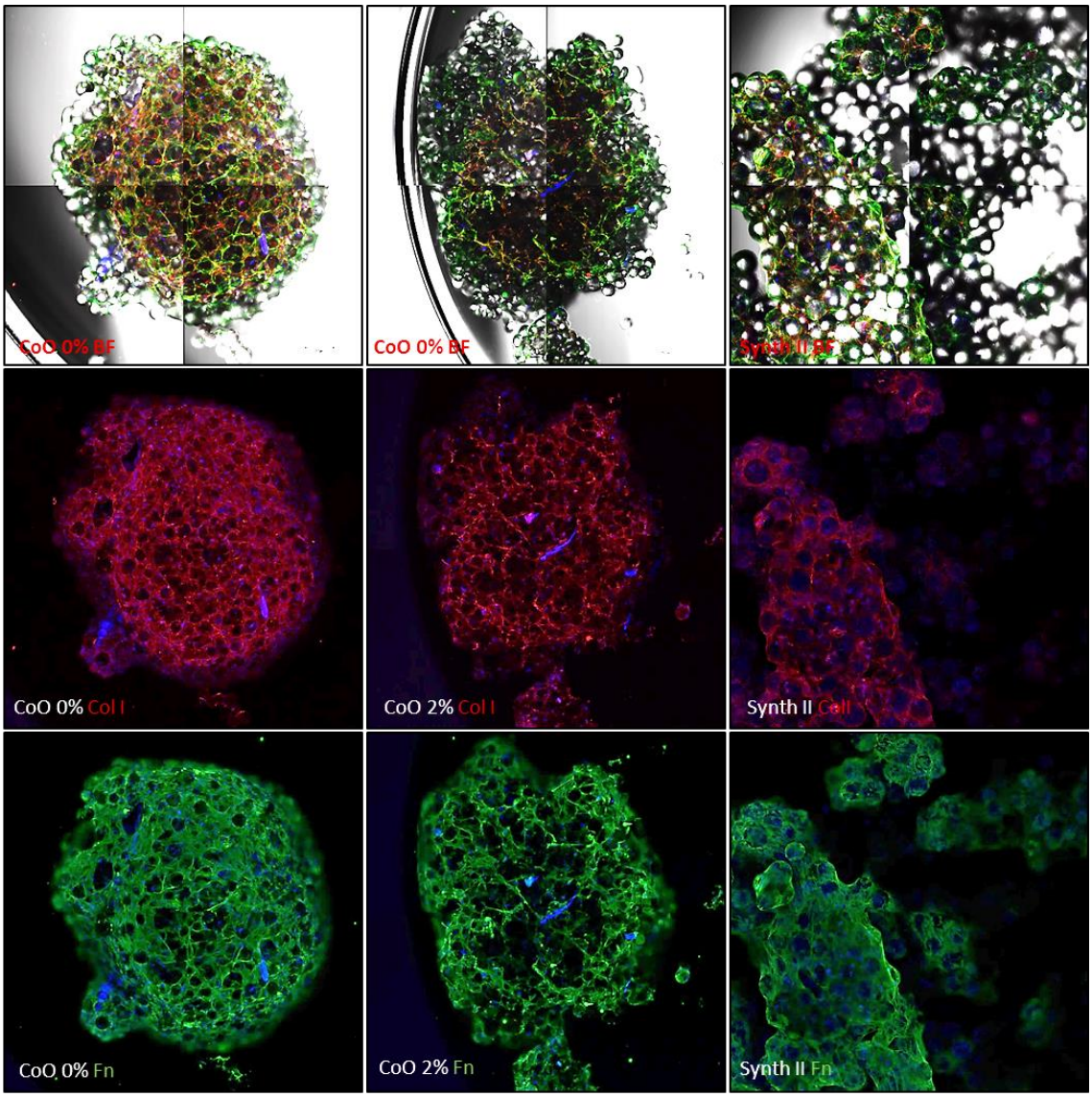

Figure 3.9 b: Confocal microscopy analysis of extracellular expression of type I collagen (Red) and fibronectin (Green), nuclei (Blue) of MSCs grown on CoO 0%, 2% and Synthemax II microspheres at day 14. Brightfield images are shown in the top panel. After 2 weeks in culture, both type I collagen and fibronectin were equally secreted and distributed on the CoO 0% scaffold. Both proteins were also expressed on the CoO 2% microspheres, however their secretion was found to be less uniformly distributed throughout the construct. Extracellular expression of type I collagen and fibronectin were also clearly visible on the Synthemax II microspheres. Images are representative of the trend in expression observed in three independent experiments performed using different donors. Images were obtained with x4 objective.

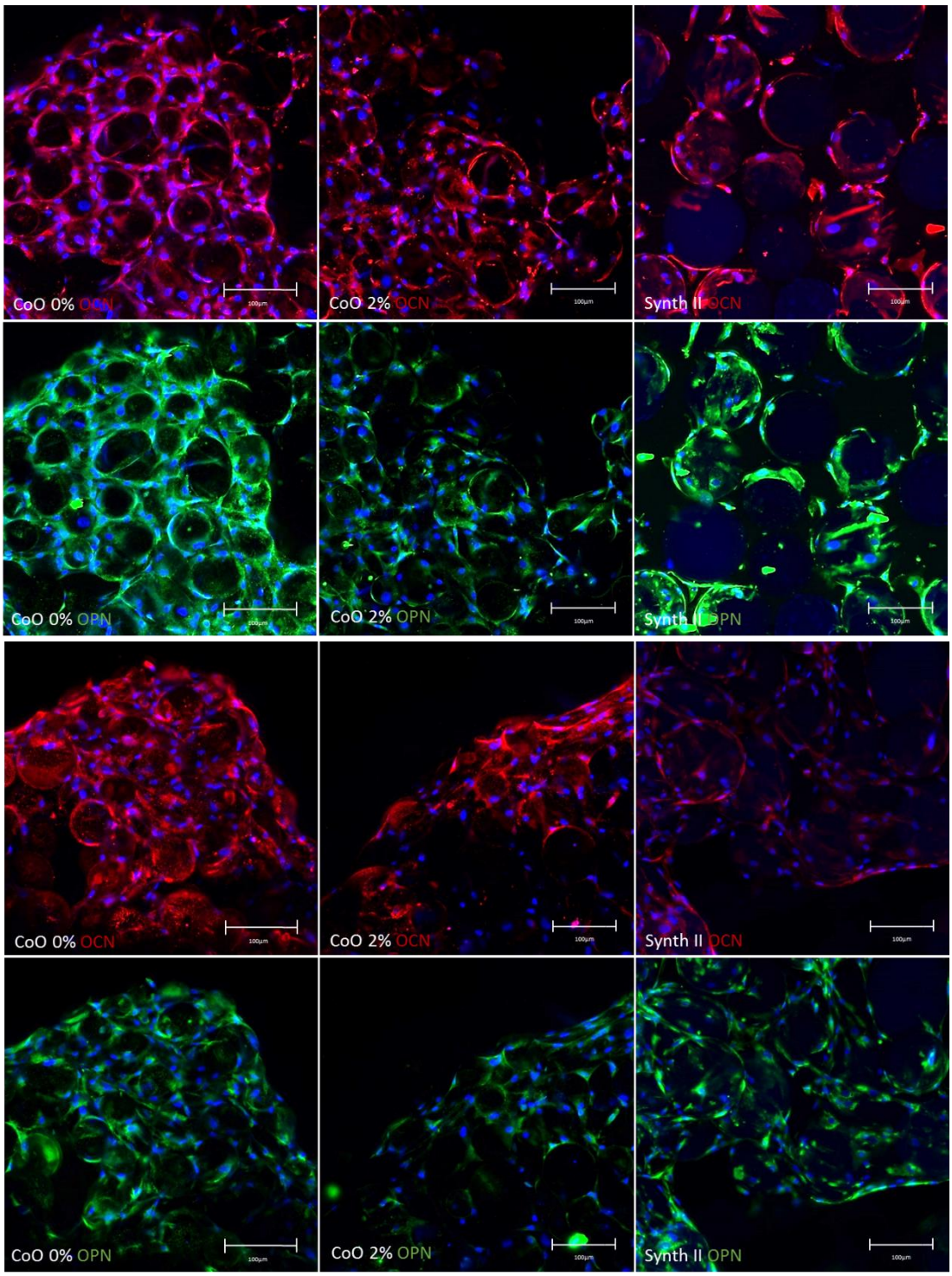

Figure 3.10: Confocal microscopy analysis of extracellular expression of osteocalcin (Red) and osteopontin (Green), nuclei (Blue) of MSCs grown on CoO 0%, 2% and Synthemax II microspheres at day 7 (i) and 14 (ii). Osteopontin and osteocalcin upregulation was observed on MSCs grown on CoO 0% microspheres compared to the other conditions at both time points. Images are representative of the trend in expression observed in two independent experiments performed using two different donors. Scale bar 100µm.

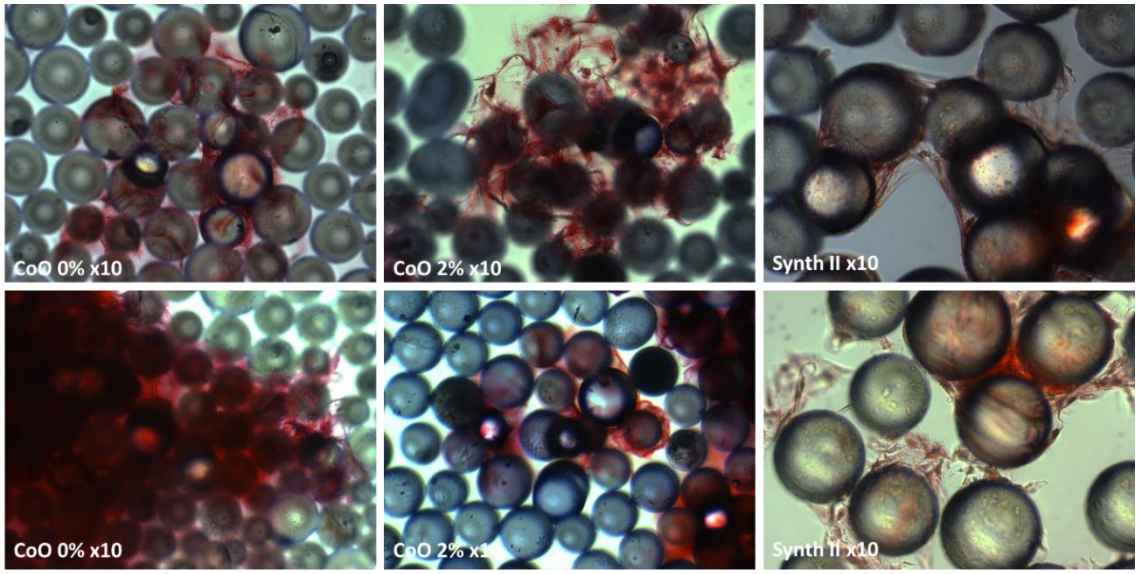

Figure 3.11: Alizarin Red staining of MSCs grown on CoO 0%, 2% and Synth II microspheres at day 10. Calcified matrix is observed on cells grown on both phosphate glass compositions. No clear alizarin red staining is noticed on Synth II group. Images are representative of the trend in expression observed in two independent experiments performed using two different MSCs donors. Images were obtained with x4 objective at day 14.

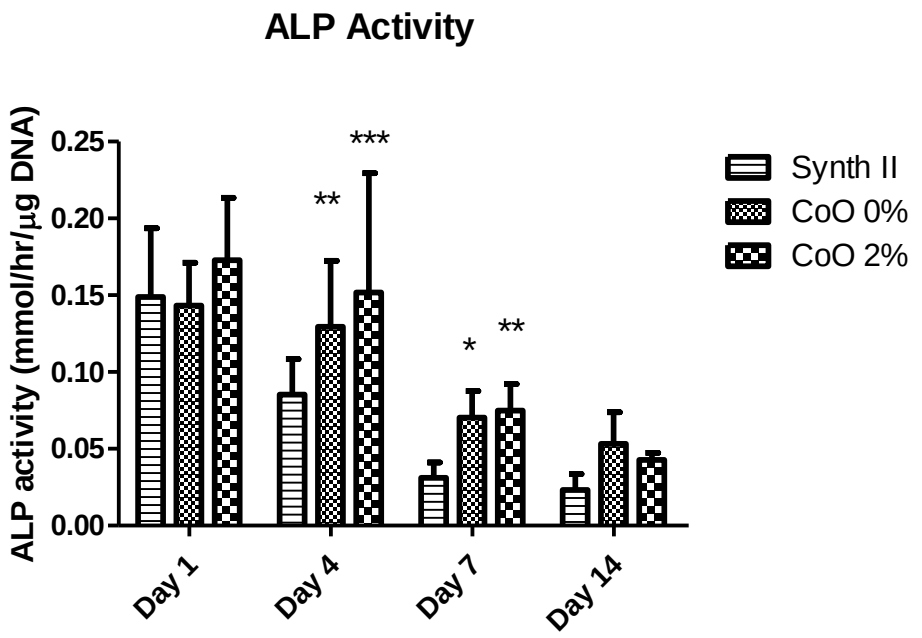

Figure 3.12: ALP activity of MSCs grown on CoO 0%, 2% and Synthemax II microspheres at day 1,4,7 and 14. ALP activity was found to be upregulated at day 1 and day 4 on the PG microspheres, with decrease in activity starting from day 7. On Synthemax II microspheres, the decline in expression started at day 4. At both day and 7, ALP activity was significantly higher on the PG microspheres than Synthemax II control. However, at day 14, a drop in activity was noticed in all conditions, with no significant differences in expression. Data shown combine results obtained from two different donors, with each condition being tested in triplicates. Data are shown as Mean ± SD, statistically compared by a two-way ANOVA followed by Bonferroni's post test, using Synth II as a control *p<0.05, **p<0.01, ***p<0.001.

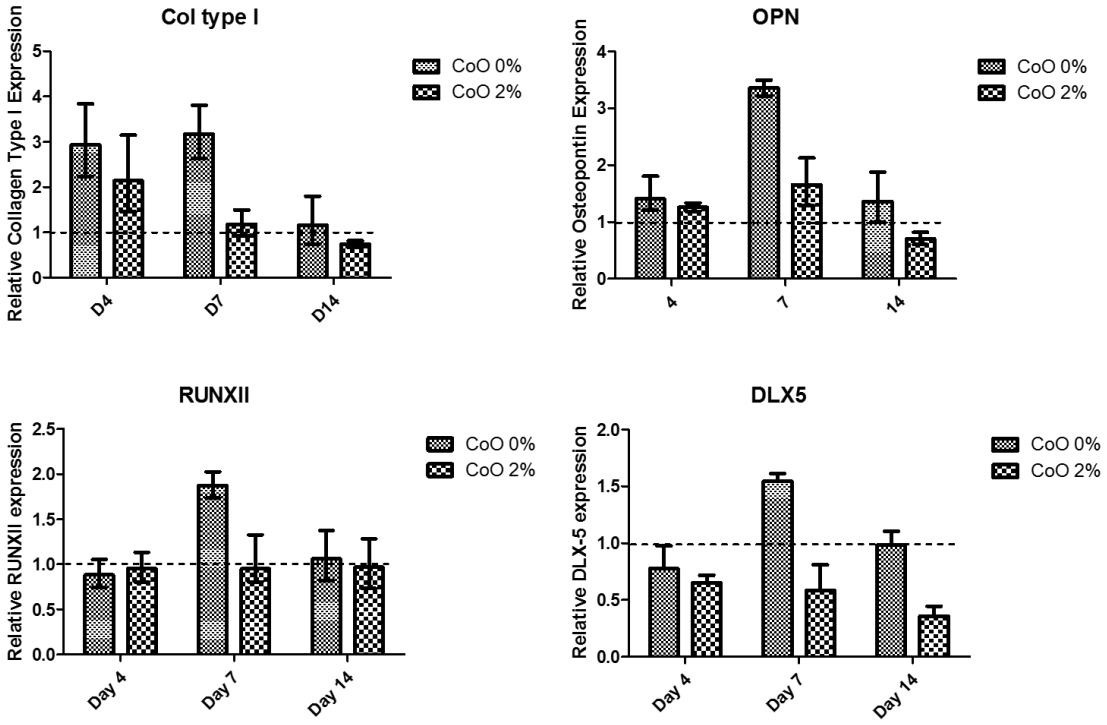

Figure 3.13: Gene expression quantification by qPCR of MSCs grown on CoO 0%, 2% and Synth II microspheres at day 4,7 and 14. Gene expression was normalized against GAPDH expression (reference gene) and using expression on Synthemax II as a baseline (dotted line on the graph). Upregulation of all four genes occurred on CoO 0% microspheres at day 7, while gene expression on CoO 2% was found to be comparable to the Synthemax II control at all time points. The graph shows pooled data from three independent experiments performed using different donors, with two technical replicates per experimental condition. Data are shown as Mean ± SEM.

3.3.3 Angiogenesis

3.3.3.1 VEGF Expression

VEGF concentration in supernatant taken from MSCs cultured with different microspheres (normalized by DNA content) is shown in figure 3.14.

After 24 hours from seeding, VEGF secretion was found to be significantly higher in cells grown on CoO 2% microcarriers compared to the Synthemax II control ($p<0.01$). However, no significant differences in VEGF secretion were observed between cobalt-free and CoO 2% microspheres ($p>0.05$). After seven days in culture, there was an increase in VEGF expression on both phosphate microspheres. No significant changes are observed in the control group over time. CoO 2% clearly induced enhanced VEGF secretion compared to the cobalt free composition ($p<0.05$) and the control ($p<0.001$). Significantly higher VEGF expression was also observed on cobalt-free phosphate glass microspheres, compared to Synth II ($p<0.001$).

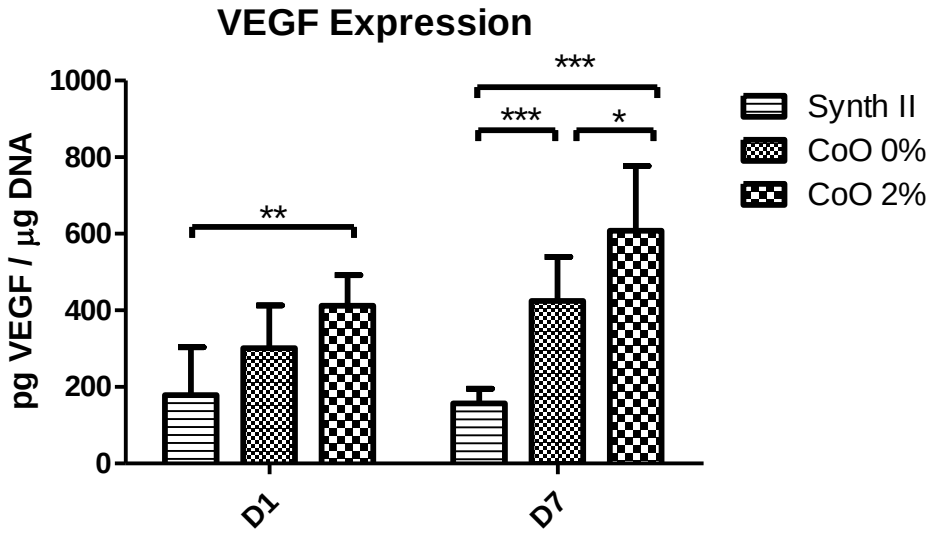

Figure 3.14: VEGF expression in cell culture supernatant by MSCs grown on CoO 0%, CoO 2% and Synthemax II microspheres at day 1 and day 7 from seeding. Upregulation of VEGF secretion on the CoO 2% microspheres compared to the control was observed since the first day in culture. Not significant differences are observed between the two PG microspheres at this time point. After seven days on culture, significant higher VEGF expression was observed between CoO 2% and all other experimental conditions. Expression on CoO 0% was also significantly higher than the Synthemax II control. The graph shows data combined from two independent experiments, performed using different donors, in triplicates. Data are shown as Mean ± St Dev, statistically compared using a two-way ANOVA followed by Bonferroni's post test, *p<0.05, **P<0.01, ***p<0.001.

3.3.3.2 HIF-1α expression

Expression of HIF-1α by MSCs cultured with media conditioned with ionic species released by microcarriers is shown in figure 3.15. A clear HIF-1α nuclear expression was observed in almost all of the cells grown with the CoO 2% conditioned media. Culture with CoO 0% conditioned media induced a smaller percentage of HIF-1α positive cells. The control group did not express the hypoxic marker.

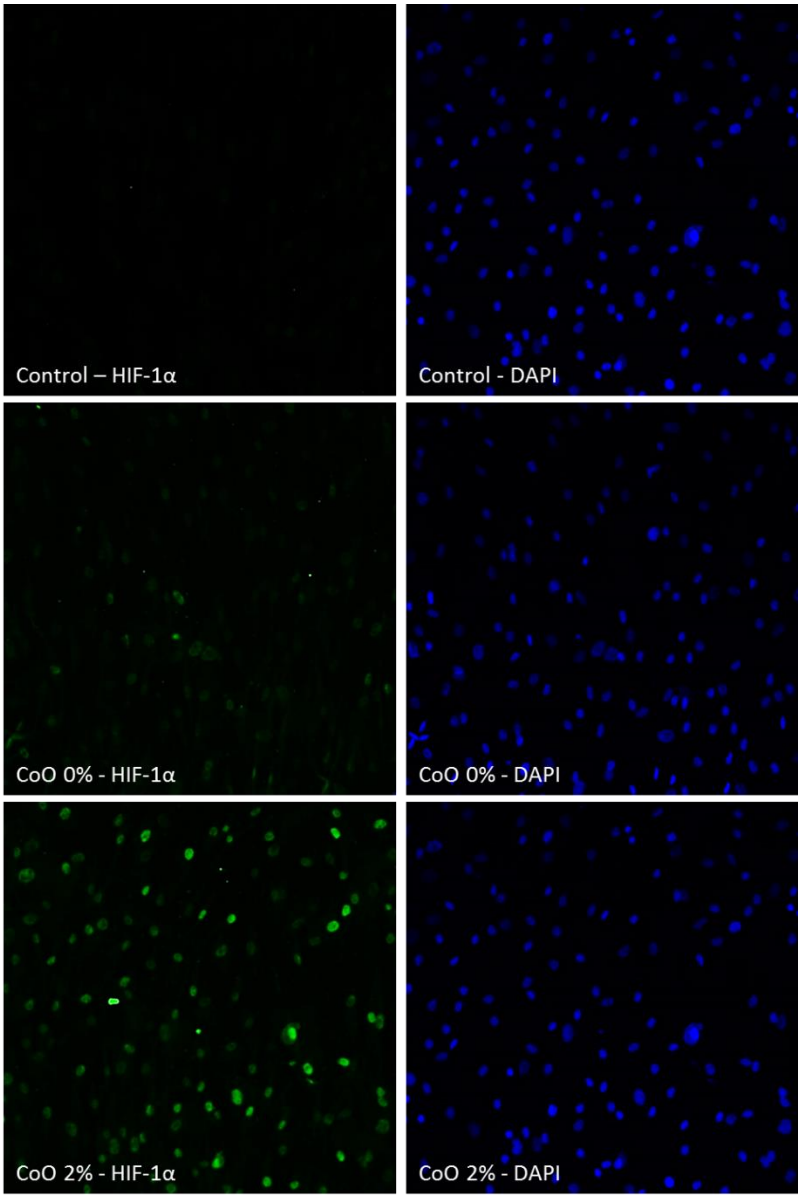

Figure 3.15: Microscopy analysis of nuclear expression of HIF-1α (green) in MSCs treated with CM from CoO 0% and 2% microspheres. MSCs grown in standard culture media were used as a negative control. Cell nuclei were stained with Hoechst (blue). Nuclear expression of HIF-1α is clearly evident on MSCs exposed to CoO 2% CM, indicating activation of the hypoxic pathway. Some positive stained cells were observed in CoO 0%, while no positive staining was observed in the negative control. Images are representative of the trend in expression observed in two independent experiments performed using different MSCs donors.

3.3.3.3 In vitro vascularization

The effect of ionic species released by phosphate glass microspheres on tubule formation is reported in figure 3.16. A significantly higher number of junction points and meshes were detected under the effect of CoO 0% conditioned media ($p<0.05$; $p<0.01$). Interestingly, the presence of cobalt did not have a direct effect on the capacity of HUVECs to form tubular structures. Despite the similar number of branching points between the CoO 2% and the positive control, sprouting structures appear less robust and developed in the presence of cobalt.

Tubular formation by HUVECs was also assessed in the presence of conditioned media from MSCs grown on microspheres. Two different donors were analysed as shown in figure 3.17. The response was found to be donor dependent. Results from one donor show no significant difference in tubule formation between the three different experimental conditions. All conditions resulted in a lower number of junction points and meshes compared to the positive control (C,E,G). A different trend was observed for the second donor, where CoO 2% conditioned media enhanced tubule formation significantly compared to the other conditions and the negative control (D,F,H). Not significant differences between the CoO 2% and the positive control were observed.

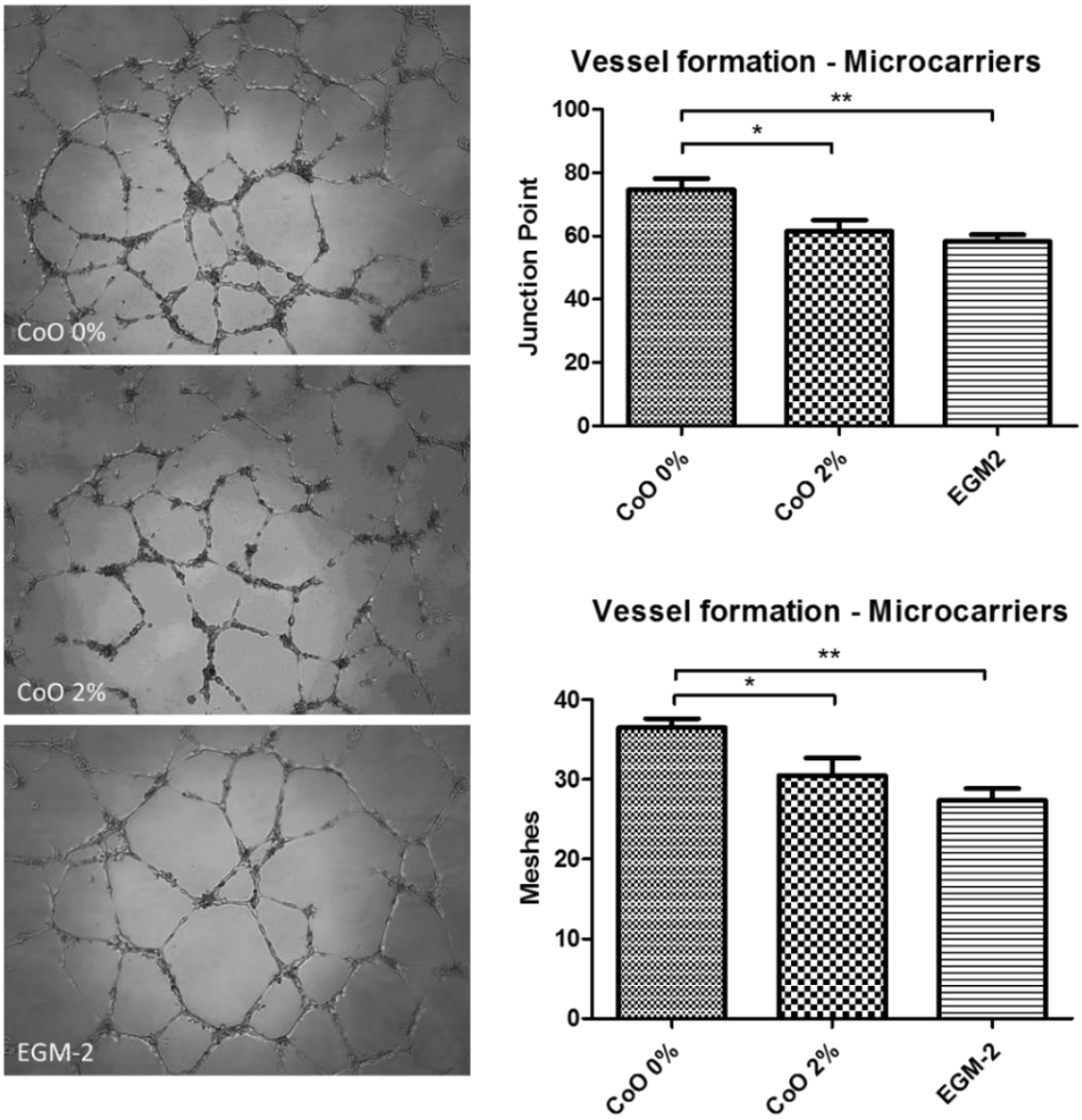

Figure 3.16: Matrigel assay testing the effect of CM from CoO 0% and 2% microspheres on endothelial cells tubule formation. Images were taken 18hrs from HUVECs seeding on Matrigel matrix and cells incubated with growth factors enriched endothelial media (EGM-2) were used as a positive control. Images show an increase in tubule formation when HUVECs were grown with CoO 0% CM, resulting in enhanced junction point and meshes formation. CoO 2% performed similarly to the positive control in terms of junction points number. However, from a visual analysis, tubule formed appear less developed and robust in the presence of cobalt ions. Data were obtained from three independent experiments (n=4/experiment) and are shown as Mean ± StDev, and statistically compared by a one-way ANOVA followed by Tukey's multiple comparable test *p<0.05, **p<0.01, ***p<0.001.

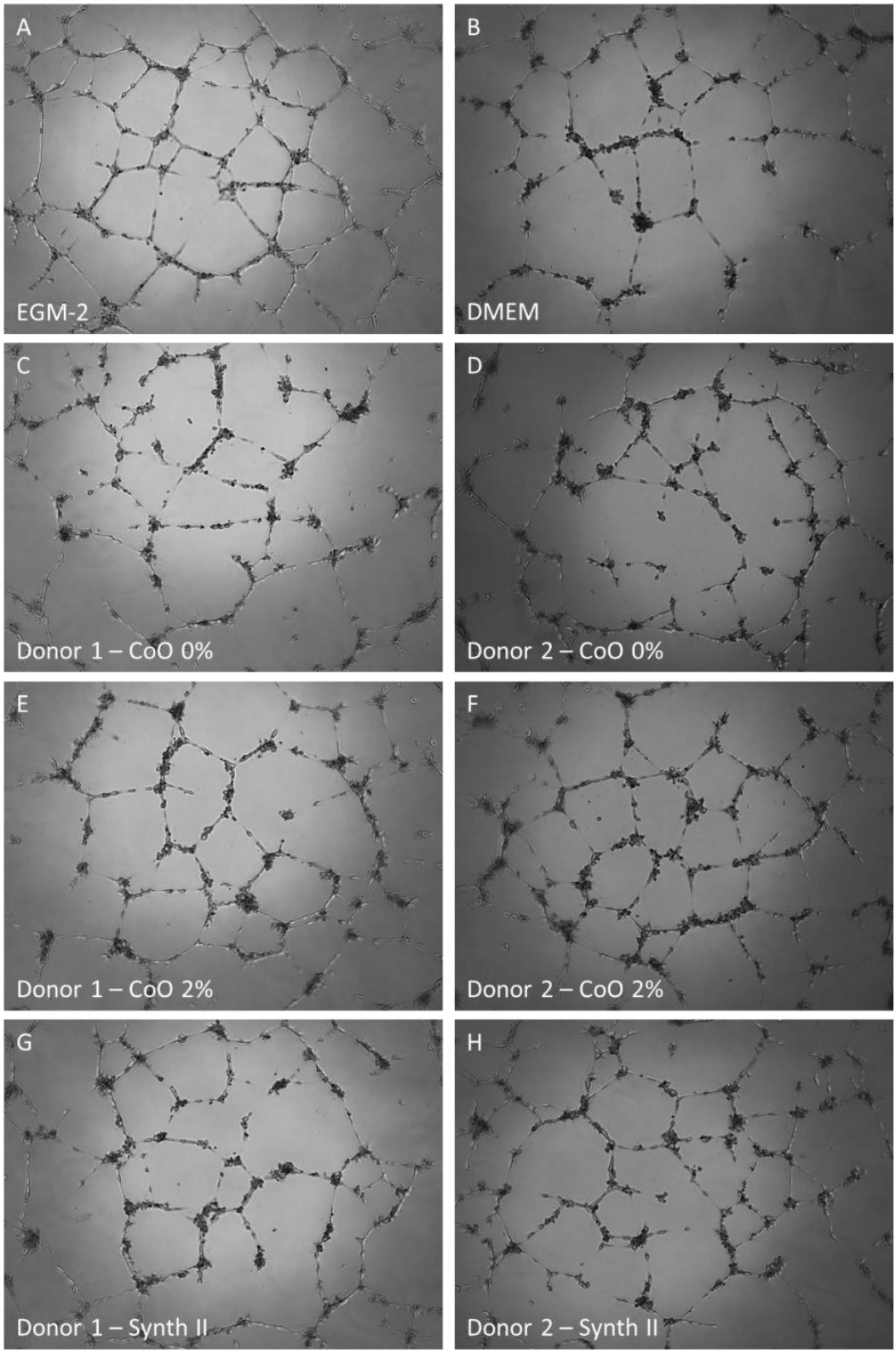

Figure 3.17 a: Microscopy images of Matrigel assay testing the effect of CM from MSCs grown on CoO 0%, 2% and Synthemax II microspheres for 7 days on endothelial cells tubule formation. The experiment was performed using two different donors and HUVECs incubated with EGM-2 on the Matrigel matrix, were used as a positive control, while those incubated in DMEM as a negative control.

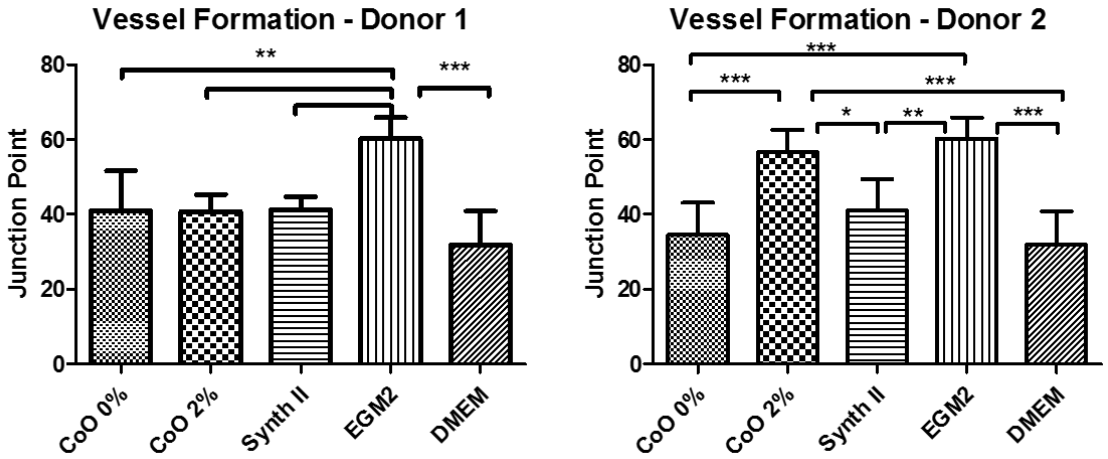

Figure 3.17 b: Quantification of junction points in Matrigel assay. For the first donor, not significant differences between the three CM analysed were observed and the positive control was found to perform better than any other experimental condition. However, for the second donor, CM from MSCs cultured on CoO 2% microspheres was found to have an effect comparable to that of the positive control. In both donors, no differences were observed between CoO 0% and Synthemax II. Data are presented as Mean ± StDev, n=5 and statistically compared by a one-way ANOVA followed by Tukey's multiple comparable test *p<0.05, **p<0.01, ***p<0.001.

3.3.3.4 Ex vivo vascularization

A chicken chorio-allantoic membrane (CAM) assay was used to test the angiogenic potential of the phosphate glass microcarriers *ex vivo*. Two experimental groups were analyzed. In the first group, MSCs were grown on CoO 0% and CoO 2% microspheres for seven days. The cell-seeded microspheres were then harvested and implanted in the CAM, at day 8 from embryo fertilization. The second group consisted of equal volumes of CoO 0%, 2% and Synthemax II microspheres embedded in collagen gel. Collagen gel without particles was used as a negative control. The cell-free gel-microsphere constructs were implanted in the CAM, at day 8 from embryo fertilization. Both experimental groups were harvested seven days post implantation.

High embryo survival rate was obtained in all groups (data not shown) and in all conditions tested vascularization of the implant was noticed (figure 3.18). New formed vessels branching out from the scaffolds were evident in all constructs. Branching vessels were then quantified (Figure 3.19). Cell-seeded scaffolds generally scored less than cell-free implant and despite the higher VEGF expression of MSCs grown on CoO 2% microcarriers, no significant differences between the CoO 0% and Co2% with cells groups were noticed.

The number of newly formed vessels between the cell-free CoO 0% and CoO 2% microspheres was also comparable. Generally, a lower number of branches was found on the cell-free Synthemax II microcarriers, however this trend was not found to be significant ($p>0.05$). No evident vessel ingrowth towards the microspheres-free collagen gel was observed (3.18 I L).

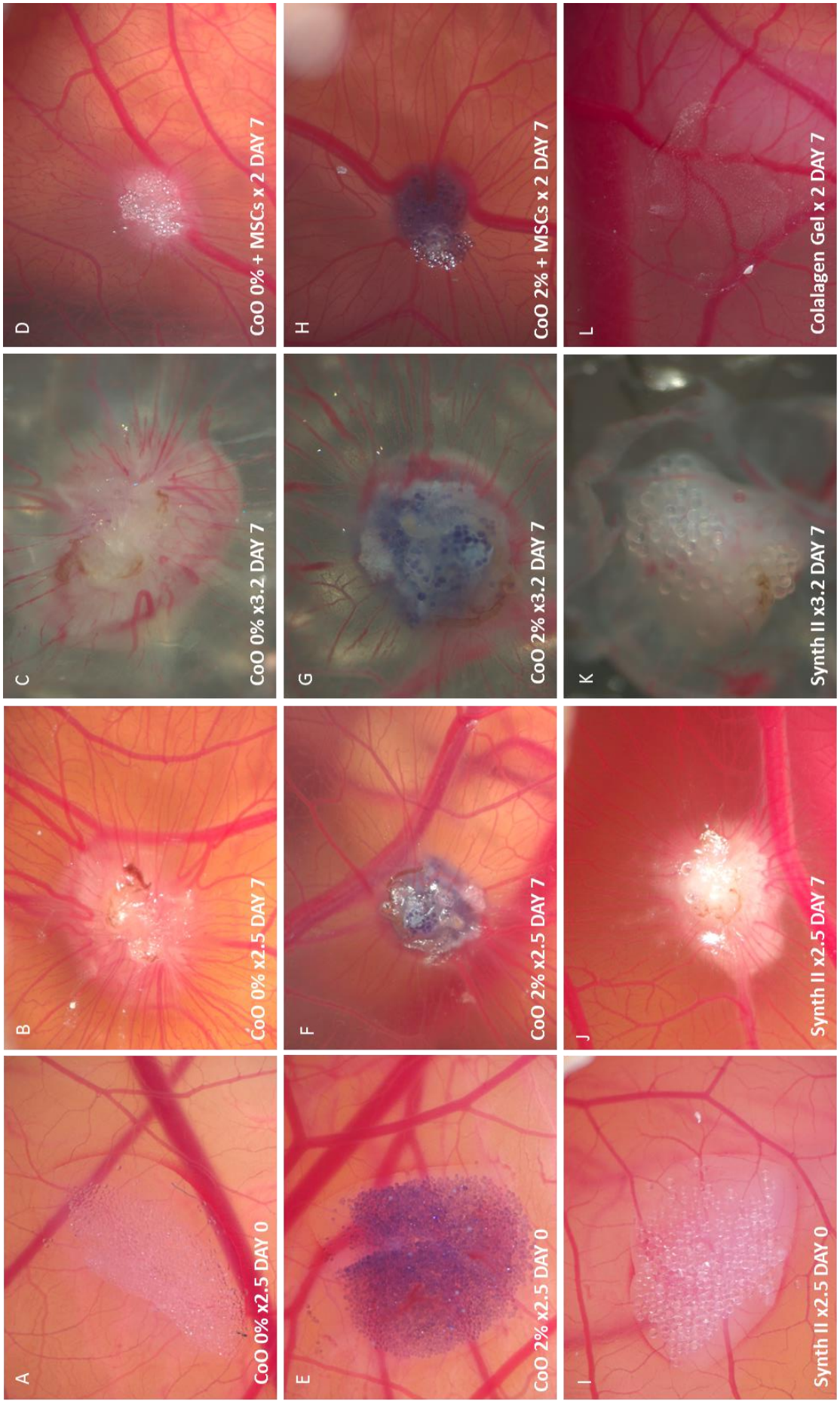
A
CoO 0% x2.5 DAY 0
B
CoO 0% x2.5 DAY 7
C
CoO 0% x3.2 DAY 7
D
CoO 0% + MSCs x 2 DAY 7
E
CoO 2% x2.5 DAY 0
F
CoO 2% x2.5 DAY 7
G
CoO 2% x3.2 DAY 7
H
CoO 2% + MSCs x 2 DAY 7
I
Synth II x2.5 DAY 0
J
Synth II x2.5 DAY 7
K
Synth II x3.2 DAY 7
L
Colalagen Gel x 2 DAY 7

Figure 3.18: Ex vivo vascularization in the CAM assay testing the effect of cell loaded and cell-free microspheres on new vessels formation. MSCs were cultured on PG microspheres for seven days before implantation in the CAM. Cell-free microspheres were embedded in a type I collagen gel before implantation. All implants were harvested after seven days from the day of implantation. As shown in the images (A,E,I), cell-free microcarriers appear as a monolayer on the CAM surface at the day of implantation. On the harvesting day, all type of microspheres were found to be clustered together in a single mass, with evident vessels ingrowth (B,F,J). Patches of collagen gel (L), without microcarriers, were also implanted as a negative control and found to present minimal level of vascularization. Clusters of cells and microcarriers were also implanted and found to be successfully vascularized at the end of the incubation time (D,H).

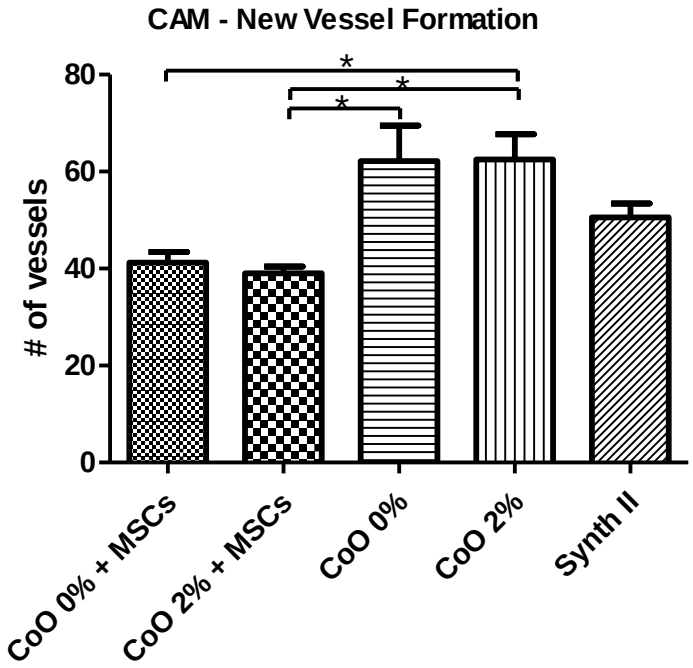

Figure 3.19: Quantification of vessel ingrowth formation in the CAM assay for all conditions tested. Cell-loaded microcarriers were found to be less vascularized than the cell-free scaffold. Highest number of new formed vessels was observed on cell-free CoO 0% and 2% microspheres, although this was not found to be significant compared to the Synthemax II. Data are presented as Mean ± StDev, n=4 – 8, and statistically compared by a one-way ANOVA followed by Tukey's multiple comparison test, *p<0.05.

3.4 Discussion

3.4.1 MSCs culture on bioactive glass microspheres

It has been estimated that 40-100 x 10^6 MSCs/patient are required for the treatment of non-union bone defect (Chen et al. 2013). Due to the high cell doses required per treatment, microcarrier technology has been introduced as a potential solution to overcome the technical limitations of traditional 2D culture (Chen et al. 2013). Microcarriers allow rapid cell expansion in a bioreactor system, growth of cells in a 3D environment (Martin et al. 2011) and can also be used as a scaffold for *in vivo* implantation, if made of a biodegradable and biocompatible material (Chen et al. 2013).

As in Chapter 2 it was shown that osteoblastic cells can be cultured on Ti/Co-doped phosphate glass microspheres, here the response of hBM-MSCs to these materials was investigated. The polystyrene Synthemax II microcarriers were used as a positive control. These microcarriers are commercially available and have been optimized for MSC culture, as their surface is treated to enhance cell attachment, maximizing yield and viability.

The growth of MSCs on CoO 0%, CoO 2% and Synthemax II microcarriers was tested for a total period of 2 weeks and the number of cells at each time point was tested by measuring the DNA content. Even though the PG microspheres were not coated to enhance cells adhesion, cell numbers at day 1 were similar between all three conditions, showing comparable levels of attachment and viability. As expected, in terms of long term expansion, Synthemax II performed better than the PG microspheres and significantly higher numbers of cells were achieved at day 7 and day 14. Similar to MG-63, MSCs started clustering on the PG microspheres from the fifth day on culture and aggregates of increasing size where formed during the culturing period, until almost all microspheres were embedded in a single construct. However, even in static culture, this was not the case for the Synthemax II microcarriers, where aggregation started occurring only towards the end of the culturing period.

Even if at a slower rate compared to the positive control, the number of cells on the PG microspheres kept increasing throughout the two weeks of culture. Cells viability was also confirmed by their capacity to secrete matrix and to keep modifying the culturing environment by microspheres aggregation. As all cultures were performed in non-osteogenic media, it was hypothesised that ionic species released by PG microspheres could be a potential cause of the slower growth rate shown towards the second half of the culturing period. However, even though cell yield was lower than the optimised polystyrene matrix, from a tissue engineering perspective, is more desirable to produce an implantable construct presenting the correct phenotype and that mimics the physiological microenvironment, rather than higher yield of immature cells.

Preliminary experiments were also performed to test the effect of dynamic conditions on MSCs cultured on microspheres. According to results previously obtained with the osteoblastic cell line, 150RPM was selected as a potential shaking speed to enhance cell proliferation. However, this speed was found to be detrimental on all microspheres cultures, including the Synthemax II. It was originally hypothesised this effect being the result of MSCs being more sensitive to shear than more mature osteoblastic cells, thus leading to a significant reduction in cell number since the start of the dynamic regime. However, no difference in cell number was noticed at day 3, which corresponds to 48 hours after the start of the agitation regime. Similar cell number was observed up to day 5, after which a drop in cell number was observed on the dynamic regime. Microscopy suggested that clustering was inhibited and that most microspheres were found to be cell-free at the end of the culturing period. Whether the incapacity to form clusters due to the agitation regime or the impact on high levels of shear within the well on the cells, caused the drop in cell number remains to be determined.

The shaking speed was then reduced to test whether mild agitation could improve cell growth by reducing the agitation to within the bounds of permissive. Compared with the 150RPM agitation speed, 70RPM led to improved cell yield that was similar to the static control. However, no significant improvements over the static control were seen for all three conditions. A visual analysis by microscopy shows the presence of more cell-free microspheres at 70RPM, suggesting higher cell numbers per surface area than the static control. Future works will aim at testing new shaking speeds, within the range of the values analysed, in order to determine whether a significant improvement in cell culture could be achieved within this setting or whether new ways to introduce mixing (i.e. perfusion) should be investigated.

3.4.2 ECM characterization

Extracellular matrix proteins have a key role not only as a physical support for MSC attachment, but also as a source of biochemical stimuli that can regulate cell physiology and phenotype (Hidalgo-Bastida & Cartmell 2010). Lian & Stein (1995) identified three fundamental phases in osteoblast maturation. A first phase corresponding to osteoblast proliferation and ECM-secretion, with upregulation of type I collagen and fibronectin. Accumulation of type I collagen was found to lead to a second phase characterised by limited cell proliferation, together with upregulation of genes associated with a bone phenotype and maturation of the ECM. This was followed by a mineralization phase, where another set of genes was upregulated such as bone sialoprotein, osteonectin and osteocalcin. Therefore, due to the close interplay between the ECM and osteoblast maturation, it is crucial to develop orthopaedic biomaterials that should either present or induce ECM secretion in order to simulate cellular microenvironment (Brighton & Albelda 1992).

As it has been previously reported that phosphate glass biomaterials induce type I collagen upregulation (Abou Neel et al. 2014), the effect of titanium and cobalt on inducing ECM secretion by hMSCs was investigated. In order to distinguish between the effect of the ionic components released by the glass and that of the 3D support of the microspheres on ECM secretion, two experimental groups were analysed. The first group consisted on hMSCs grown on 2D TCP and cultured with conditioned medium obtained by soaking phosphate glass microspheres in MSCs growth media for 24 hours. The second experimental group consisted in culturing MSCs directly on the phosphate glass microspheres.

For the 2D culture, it was noted that while type I collagen was mainly upregulated on MSCs cultured with ionic species released by CoO 0% microspheres, fibronectin was mainly secreted in the presence of CoO 2%. Negative control cells cultured with control media showed minimum levels of extracellular collagen and fibronectin after one week in culture, while both proteins were upregulated by osteodifferentiated MSCs.

A similar trend was also observed on cells cultured directly on the microspheres. After one week in culture, deposition of the ECM was noticed on all donors grown on phosphate glass microspheres, thus causing the formation of aggregates. On the other hand, ECM secretion by cells grown on polystyrene microcarriers was not observed during the first week in culture and protein expression was mainly detected intracellularly. Type I collagen and fibronectin were co-expressed on phosphate glass microspheres, however the first protein was found to dominate the ECM in the absence of cobalt, while thicker fibronectin fibers were found in response to CoO 2%. A similar trend was observed by Grayson et al. (2006) when growing hMSCs on 3D PET constructs under hypoxic conditions. Considerably higher levels of fibronectin expression were detected for hMSCs cultured on 3D scaffolds under hypoxic conditions, while collagen was upregulated in normoxic culture. As losses of fibronectin expression have been correlated to differentiation, the author identified hypoxia as a promoter of the undifferentiated state of hMSCs. Similarly, the hypoxic state induced by cobalt ions could be responsible for the different trends in type I collagen and fibronectin deposition observed. However, while hypoxia has been reported to promote hMSC proliferation, there were not significant differences in cell growth in the presence of cobalt.

Expression of the non-collagenous proteins osteopontin and osteocalcin was then studied, as these proteins are expressed during the ECM mineralization phase (Barrère et al. 2006). Similar to type I collagen, in 3D culture, osteopontin was found to be more expressed on CoO 0% microspheres than CoO 2% and to decrease over time from day 7 to 14. Osteocalcin followed a similar trend, although generally being less expressed than osteopontin.

Finally, the effect of phosphate glass conditioned media on early mineralization, by AR staining, was studied. Early evidence of calcium deposition could be observed on MSCs in response to conditioned medium from CoO 0% microspheres, although significantly less

pronounced than cells on full osteogenic media. Similarly to results observed in previous studies (Osathanon et al. 2015; Birgani, Gharraee, et al. 2016), no evidence of calcium deposits was found in the presence of cobalt ions. When performing AR staining on MSCs cultured on the microspheres, positive staining was observed on phosphate glass independently of cobalt and this was found to be more intense than on plastic microcarriers.

3.4.3 Osteogenic markers expression

As differences in ECM deposition by MSCs were observed in the presence of cobalt-doped microspheres, suggesting inhibition of osteodifferentiation, the role of cobalt in osteogenesis was further investigated. While most studies agree on the capacity of cobalt of inducing hypoxia and have focused on its role on angiogenesis, the effect of cobalt on osteogenesis is less well understood. Here, the effect of Co^{2+} released by PG microspheres on hMSCs osteodifferentiation was tested *in vitro*, in the absence of osteogenic supplements.

As part of this study, ALP activity, an early osteogenic marker, was measured. A peak in activity for all three conditions was noticed at day 1 in culture. ALP activity was found to be stable up to day 4 on both PG microspheres while a decline was observed from day 7 to 14. Declining expression started as early as day 4 on Synthemax II microspheres. Significantly higher ALP activity compared to the control was noted on both PG compositions at day 4 and 7, while at day 14 ALP was downregulated on all conditions.

Inhibition of alkaline phosphatase activity has been reported on cells exposed to inorganic phosphates in culture medium, without however compromising the mineralization capacity of osteoblasts. It has been hypothesised that in scaffolds releasing Ca and P species, alkaline phosphatase activity might be altered compared to other substrates (Barrère et al. 2006). For example, Sadat-Shojai et al. (2013) investigated ALP activity by the osteoblastic cell line MC3T3-E1, when grown in the presence of hydroxyapatite (HA) nanocomposite in standard growth media. They reported maximum ALP activity at day 1 on all conditions tested, with higher activity observed on compositions presenting the higher proliferation rate between day 1 and 4. However, despite the peak in ALP activity being found to occur earlier than what is usually reported in literature, mineral deposition occurred starting from day 7, as assessed by AR staining. No AR staining was observed in the negative control that however showed a similar trend in ALP activity to the HA filled composite. Similarly, in this study, positive AR staining was observed on cells grown on PG microspheres. However, even if a similar trend in ALP expression was noted between all three compositions, this did not translate into enhanced AR expression in MSCs cultured on Synthemax II microspheres. As it is known that orthophosphate species are released by PG microspheres (Lakhkar et al. 2013), their accumulation in cell culture medium and consequent inhibition of ALP activity could be a possible cause of the trend observed.

In order to quantify qualitative trend observed by ICC staining, RT-PCR was then performed on MSCs grown on the microspheres to quantify the expression of four osteogenic markers: type I collagen, osteopontin, RUNX-II and DLX-5. Markers expression by MSCs grown on CoO 0% and CoO 2% microspheres was normalized against expression on Synthemax II. Type I collagen and osteopontin expression followed a similar trend to that shown by the staining. All four markers were upregulated in CoO 0% microspheres at day 7, while difference in expression with CoO 2% and Synthemax II was less evident after two weeks in culture. As it has been shown than 3D culture on microcarriers in the absence of osteogenic media can lead to spontaneous osteodifferentiation of MSCs through altered cytoskeletal tension (Tseng et al. 2012), this can possibly explain upregulation of osteogenic markers even on the Synthemax II microcarriers over 2 weeks in culture.

It is interesting to note that almost the totality of osteogenic markers at all time points analysed in this study were suppressed in the presence of cobalt ions. The RT-PCR profile together with ECM expression of osteogenic proteins suggest a detrimental role of cobalt ions on MSCs osteodifferentiation and altered matrix secretion. This is in line with previous observations from Osathanon et al. (2015) that reported upregulation of stem cell markers (i.e. REX1 and Oct-4) and downregulation of ostegenic markers (i.e. AR, ALP, RUNXII and osteocalcin) on human periodontal ligament cells treated with cobalt chloride. However, an opposite trend was reported by Ignjatović et al. (2015) that showed enhanced bone matrix formation *in vivo* when hydroxyapatite nanoparticles with the highest cobalt concentration were implanted in an osteoporotic bone defect. Due to the heterogeneous responses reported in literature, it would be interesting to test the effect of Ti/Co doped phosphate glass microspheres *in vivo* and to verify whether the reduced expression of osteogenic markers *in vitro* does translate to impaired osteoregeneration.

3.4.3 Effect of Co-doped PG microspheres on angiogenic responses

3.4.3.1 HIF-1a expression and VEGF secretion

The capacity of cobalt to mimic hypoxic conditions has been widely investigated. The mechanism of action of the Co^{2+} cations have not yet been fully elucidated, however studies suggest activation of the hypoxia pathway, through inhibition of HIF-1α proteolytic inhibition (Yuan et al. 2003). Upregulation of HIF-1α and VEGF expression in response to cobalt ions have been proved in several studies (Wu et al. 2012; Azevedo et al. 2014; Quinlan et al. 2015) .

In this study, the activation of the HIF pathway of cells cultured in monolayers in the presence of cobalt releasing PG microspheres was studied by HIF-1α immuno-labelling and quantification of VEGF release in the supernatant. MSCs grown with CoO 2% conditioned media clearly showed nuclear expression of HIF-1α after one week in culture. A small percentage of HIF-1α positive cells was also observed in response to CoO 0% conditioned

media, while no positive staining was detected on the control group. Similarly, hMSCs grown on CoO 2% microspheres were found to significantly upregulate VEGF secretion in the supernatant as early as at 24 hours from seeding. At day 1, similar level of VEGF in the supernatant were found between CoO 0% and CoO 2%, with concentration being significantly higher than the control group. After one week in culture, both PG microspheres were found to promote VEGF expression compared to the plastic microspheres, with the highest level of secretion achieved in the presence of cobalt.

3.4.3.2 Matrigel assay – endothelial tube formation

Once this was established, the functional effect of cobalt doped PG microspheres was tested, by testing their capacity to stimulate formation of tubular structures by endothelial cells. In a first set of experiment, the microspheres were soaked in endothelial cell media for one week. A Matrigel tubule formation assay was then performed, culturing endothelial cells with the microsphere conditioned media for 18 hours. The number of branch points and meshes formed was then quantified. Interestingly, the cobalt free microcarriers were found to stimulate tubule formation more than the CoO 2% composition and the positive control. Similarly, Peters et al. (2005) showed that even though expression of HIF-1α was enhanced by endothelial cells exposed to different Co^{2+} concentrations, this did not translate in enhanced *in vitro* angiogenesis and actually resulted in impaired vessel formation, even at low cobalt exposure. An opposite trend, however, was observed by Quinlan et al. (2015). They reported the formation of more mature and longer tubules on endothelial cells cultured on Matrigel in the presence of cobalt releasing bioactive glass scaffold. However, this effect was found to be time-dependent and to significant only at 4 and 12 hrs from seeding, while no differences were observed after 24 hrs. As the concentration of Co^{2+} ions in their study was similar to that tested in this experiment, one possible cause of discrepancy can be the different time points analysed. In this study tubule formation at 18hrs from seeding was evaluated; it would then be interesting to investigate whether Co^{2+} could promote vessel formation at earlier time points. Also, as Co^{2+} free microspheres performed better than the positive control, it would be interesting to elucidate mechanisms underlying this result. A possible reason could be the effect of higher concentration of ionic species such as calcium in conditioned media from Co^{2+} free microspheres on endothelial cells proliferation.

A second study was performed to test the effect of hMSC conditioned media on EC tubule formation. hMSCs were grown on CoO 0%, CoO 2% and Synthemax II microspheres for seven days and their media was then collected and used for the experiment. In this case, the response was found to be donor-dependent. While one donor showed no significant differences between groups treated with conditioned media from all three microspheres, in the second donor, Co^{2+} doped microspheres scored better than the other groups and was found to perform

similarly to the positive control. As the conditioned media from the microspheres did not contain any additional supplements, different concentration of VEGF or other growth factors released by the different donors could be responsible for the differential response.

3.4.3.3. CAM assay

Finally, the effect of PG on *ex vivo* vascularization was investigated using the chorioallantoic membrane assay. The chick embryo chorioallantoic membrane (CAM) is an extraembryonic membrane which serves as a gas exchange surface and presents a dense capillary network (Ribatti 2012). The CAM is a powerful assay used to investigate the angiogenic and antiangiogenic activity of different molecules and compounds *in ovo*. It has also been used to test the angiogenic potential of different cell-free or cell-loaded scaffolds. Cell implants in particular allows the continuous delivery of growth factors thus simulating a more "physiological" interaction with the CAM vasculature (Ribatti 2012). Key advantages of this method are the high embryo survival rate, the relatively easy methodology, the low cost, reproducibility and reliability of experiments that do not need to be performed in sterile conditions (Ribatti 2012). However, the CAM assay can be difficult to monitor and newly-formed vessels can be hard to distinguish from the pre-existing vessels. Furthermore, nonspecific inflammatory reactions can result from grafting and might lead to vessel formation that can hardly be distinguished from implant induced angiogenic activity (Ribatti 2012).

In this study, two experimental groups were tested: cell-microsphere (CoO 0% and 2%) constructs and cell-free microspheres (CoO 0%, 2% and Synthemax II) embedded in collagen gel. All implants were harvested after one week incubation and were found to be successfully vascularized and new formed vessels growing towards the constructs were clearly visible.
Quantification showed a lower number of vessels being formed in cell-loaded scaffold, compared to the cell-free. A possible explanation might be in the different structure of the two experimental groups: while cell-loaded scaffold appears as a solid cluster embedded in a thick ECM, cell-free microspheres implanted in the collagen gel appear like a monolayer on the CAM surface. Gaps in between the microcarriers and the soft collagen gel probably facilitated vessel ingrowth and, after seven days' incubation, shrinking of the cell-free constructs was noticed, with vessels growing in between the particles.

This is particularly interesting from a tissue engineering perspective, suggesting that control of construct size, shape and length of pre-implantation cell culture need to be carefully determined and controlled during *in vitro* modular tissue assembly. Furthermore, as MSCs have been found to induce immunomodulation, lower unspecific vessel formation due to reduced inflammatory responses could have occurred in the presence of the cellularised scaffold.

A trend showing more vessels growing towards the PG microspheres, compared to the Synthemax II microspheres was observed, although it was not found to be significant. The

collagen gels (microspheres-free) used as a negative control were hard to identify at the end of the incubation period and no newly formed vessels towards the scaffold could be observed.

Interestingly, cobalt doping did not have any effect on enhancing vessel formation and no differences were found between PG microspheres in both experimental settings. Similarly to the Matrigel assay, the presence of cobalt, despite the enhanced VEGF secretion and HIF-1α nuclear translocation observed *in vitro*, did not translate into a functional outcome *ex vivo*.

3.5 Conclusion

From this study, the compatibility of CoO 0% and CoO 2% microspheres for hMSCs culture was determined. MSCs growth and viability was reported over the culture period analysed. However, in terms of expansion, polystyrene microcarriers performed significantly better and enabled significantly higher cell doublings compared to the phosphate glass material, even under static conditions. However, simple cell expansion alone is not sufficient to gauge success, as high yield of cells that do not possess the correct characteristics do not have a therapeutic potential in bone regeneration.

It was then hypothesised that ionic species released by the phosphate glass material could be responsible for MSCs differentiation, thus leading to an arrest in self-renewal. Extracellular ICC staining of the ECM, together with osteogenic gene expression by qPCR, showed an early expression of osteogenic markers on Ti-doped phosphate glass microspheres in the absence of osteogenic supplements. This was evident both on cells cultured with media enriched with soluble species released by the microspheres and on cells grown directly on their surfaces. Doping with titanium and cobalt simultaneously, however, lead to downregulation or delayed expression of these markers. It would then be interesting to study whether cobalt itself has a role in preventing osteodifferentiation or whether the trend observed is a result of a slower release of ionic species (Ca, P, Na and Ti), due to the lower degradation rate of this composition, thus leading to a delay in cell response.

The capacity of cobalt to induce angiogenic responses both *in vitro* and *ex vivo* was investigated. VEGF upregulation on cells cultured on cobalt-doped microspheres and HIF-1α nuclear translocation on cells grown with cobalt-enriched media, proved the capacity of activating the hypoxic pathway. However, functional assays performed *in vitro* and *ex vivo* did not show an evident capacity of cobalt of improving Ti-doped phosphate glass vascularization potential.

In vivo testing of both phosphate glass compositions in a bone defect could probably help in understanding whether the responses observed *in vitro* and in the CAM assay, translate into comparable functional outcomes in an animal model.

Chapter 4. Design, fabrication and validation of a multiplex perfusion microbioreactor for optimizing process conditions for 3D bone tissue production

The work described in this chapter was in part carried out at the Tissue Engineering and Microfluidics Laboratory (TEaM), University of Queensland, Brisbane, Australia, under the supervision of Professor Justin Cooper-White.

4.1 Introduction

The importance of reproducing the complex, three-dimensional, dynamic environment *in vitro* that cells naturally experience *in vivo*, has been widely discussed in the literature (Bouet et al. 2015; Antoni et al. 2015; Huh et al. 2011; Gottwald et al. 2007). Therefore, the development of a platform that could mimic defined physiological microenvironments or niches has been the focus of many research groups (Drew M. Titmarsh et al. 2013; Peerani & Zandstra 2010; Wagers 2012). Microfluidic technologies are powerful tools to study 3D cell culture and perform cell-based assays, as they provide a platform in which complex and dynamic microenvironments can be closely reproduced, controlled and optimized (Li et al. 2012).

Microfluidics is defined as the manipulation of fluids at the micron scale, through the fabrication of devices presenting three-dimensional microstructured geometries (Titmarsh et al. 2014). These geometric configurations at this length scale, allow tight control over most physical variables, thus resulting in a highly defined local microenvironment (Titmarsh et al. 2014).

Soft lithography usually represents the technique of choice when producing Lab-on-a-Chip technology and involves generating a soft polymeric mould such as a polydimethylsiloxane (PDMS) replica from an original hard master, produced by lithography (Kim et al. 2008). Apart from PDMS, other materials of choice are thermoplastic (polystyrene, polycarbonate, polypropylene) and glass or mixtures of these substrates (Titmarsh et al. 2014). The devices can be integrated with valves and pumps to control fluid flow and can be placed in incubators to enable cell culture or fitted with continuous monitoring equipment.

Microfluidic technologies have been developed for a variety of biotechnology applications as they allow to reduce the scale and cost of experiments, as well as to tightly manipulate fluids, thus enabling a spatiotemporal control of the microenvironment (Bettinger & Borenstein 2010).

In this chapter, a multiplex perfusion microbioreactor was developed to culture cells on microspheres under perfusion and to screen the effect of multiple variables on bone tissue formation within a well defined microenvironment using minimum quantities of reagent. This reduces significantly the cost of process development and reduces the risk of failure when moving processes to larger scale bioreactors that consume large amounts of material. Preliminary experiments were performed to assess potential applications of the device in terms of identifying optimal combination of flow rate, microspheres and media composition that promote mesenchymal stem cell proliferation, expression of osteogenic markers and support vascular cells attachment.

The device was developed as part of a collaboration with the Tissue Engineering and Microfluidics Laboratory (TEaM) at the University of Queensland (Brisbane, Australia), under

the supervision of Professor Justin Cooper-White. The design of the microfluidic bioreactor was based on an existing device for 2D planar cell culture previously developed in Prof. Cooper-White's research group (Titmarsh et al. 2013). The original design was modified to introduce new features such as to incorporate microcarriers or 3D scaffolds, for process transfer applications, as described in the following paragraphs.

4.2 Microfluidic bioreactor design and fabrication

4.2.1 Technical specifications

A microfluidic bioreactor was developed to culture cells on microspheres under perfusion culture in a controlled microenvironment.

The device was designed and fabricated in order to include and meet the following design criteria and technical specifications:

1) Provide a 3D environment for cell growth;
2) Enable testing of multiple materials in parallel in a single device;
3) Create a perfused culture environment that could potentially provide mechanical stimulation, favour metabolic activity and enhance the cell differentiation process;
4) Minimize the quantity of reagents (cells, scaffold biomaterial, cell culture media) used per experiment;
5) Enable testing of cell-material interactions;
6) Control microspheres aggregation and tissue formation;
7) Simplify imaging and data collection and quantification from 3D scaffolds.

The device consists of two layers of PDMS, a bottom layer presenting the cell culture chambers and a top layer with the microfluidic channels. The bottom layer presents 24 chambers, aligned in series of six, across four parallel rows. Chamber size and spacing was based on the dimension a 384 well plate, so that the device could be read and analysed using a conventional plate reader. The height of the chamber was set to 180µm, in order to accommodate a wide range of microspheres. Microspheres (or other type of scaffolds) can be loaded from the top of the chambers manually. The top layer presents four parallel channels, connected by flow partition unit at the inlet and outlet. The channels are aligned on top of the four series of chambers upon plasma bonding, following microspheres loading. Dimensions of the device are reported in Table 4.1. The internal volume of the device is ~131µl and the bioreactor fits on a 25 x 75 mm microscope cover slip. Working volume is then significantly reduced, meaning that cells and reagents required per experiment are minimized.

In order to reduce the formation of clusters and to control the diameter of the aggregates, chambers were equipped with an array of pillars, spaced equally throughout the well. The pillars counteract the capacity of cells to pull microspheres together and prevent the formation of a single macro-aggregate. Furthermore, as the total eight of the culturing area (chamber + channel) is approximately 300µm, this prevent the formation of aggregates presenting more than two or three layers of microspheres. Through these physical constraints,

aggregates of controlled size can be obtained and monitoring, image acquisition and analysis through microscopy is drastically simplified.

	Chamber	Channel
Diameter/Width (cm)	0.365	0.4
Height (cm)	0.018	0.015
Length (cm)	-	3
Total Volume	131µl	

Table 4.1: Microfluidic bioreactor dimensions.

4.2.2 Microbioreactor fabrication and assembly

The 2-layer layout was drawn using the software Layout Editor and printed onto HY2 glass plates (Konica Minolta) using a photoplotter (MIVA Xenon Photoplotter, MIVA Technologies, Germany). Devices features were formed by SU-8 2100 (Microchem, Cambridge, MA, USA) photolithography. Feature height and integrity were confirmed by optical surface profilometry (Veeco NT1100, Plainview, NY, USA). SU-8 device masters were silanized with chlorotrimethylsilane (CTMS) to facilitate easy removal of the moulded device. Devices were then formed with standard soft lithography techniques with poly(dimethylsiloxane) (PDMS; Sylgard 184, Dow Corning, Midland, MI, USA), using a 10:1 mixture of silicon elastomer and curing agent. The mixture was then degassed under vacuum and poured onto the master and cured at 65°C for 1-2 hrs. After cutting, chambers in the bottom layer were then filled with microspheres. Input and output ports were obtained on the top layer (channel) through a 0.5mm biopsy puncher. Device layers were bonded with O_2 plasma (Harrick Plasma, 20 s, 10 W, 380 mTorr O2), with the channel PDMS layer aligned on top of the bottom layer.

The device was then left overnight at 95°C. The device was then submerged in 70% ethanol under vacuum, in order to be gradually filled with liquid, preventing bubble trapping within the device, as described by Monahan et al. (2001). The device was then perfused by connecting the inlet to a syringe pump, through external connections made of tygon tubing and stainless steel couplers (Linton Intrumentations, Diss, UK).

Equal distribution of microspheres throughout the device was tested by analysing images of each chambers via ImageJ (figure 4.2). The number of microspheres was found to be ~1450 per chamber, corresponding to ~35,000 per reactor that is equivalent to the number of carriers necessary to cover the area of a well in a 24 wells plate.

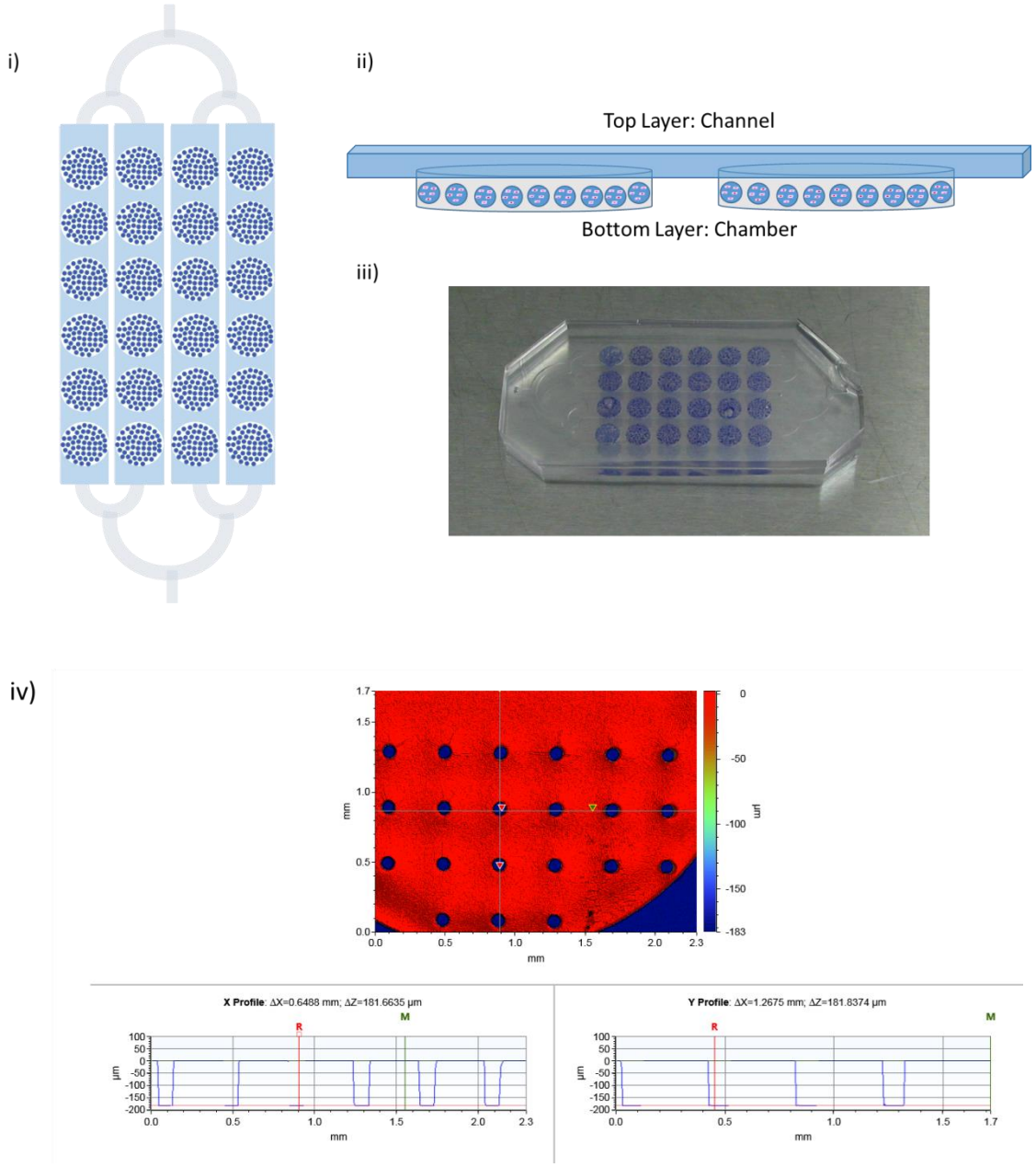

Figure 4.1: Microfluidic bioreactor schematic and optical surface profilometry. i) Top view of the microfluidic bioreactor, consisting of a bottom layer presenting chambers to accommodate microspheres and perfusion channels on the top layer; ii) Side view of two chambers filled with microspheres, interconnected by a perfusion channel; iii) A microfluidic bioreactor made of PDMS using soft-lithography techniques and filled with phosphate glass microspheres; iv) Optical surface profilometry of a chamber, showing the depth of the camber at two different points x and y; a depth of ~180 µm was confirmed and the presence of posts is shown in blue.

4.3 Methods and results

4.3.1 Microcarrier cell culture within the microfluidic platform

Human bone marrow MSCs (Lonza, Slough UK) at P4-P5 were used for all experiments. Upon reaching confluency, cells were detached using trypsin/EDTA as described in section 3.2.1 and resuspended at a density of $1x10^6$/ml in media. Cells were then injected using a 1ml syringe within the microfluidic device and allowed to settle within the chambers. The device was then washed with fresh media in order to remove cells from the channels. The device was then placed in an incubator at 37°C/5% CO2 overnight before starting perfusion, in order to allow the cells to attach to the microspheres. After washing with PBS, bioreactors were fixed in 4% PFA and Hoechst nuclear staining was applied for 5 min at RT. In order to test uniform cell distribution upon seeding, images of each chamber were taken after seeding and cells were counted using ImageJ. Cells were found to be equally distributed across the bioreactor (figure 4.2). As the area of the images analysed was 0.02 $cm^2$and that of the chamber is 0.1 cm^2, the seeding density was found to be equal to $10x10^3$ cells/cm^2, corresponding to approximately ~1000 cells per chamber.

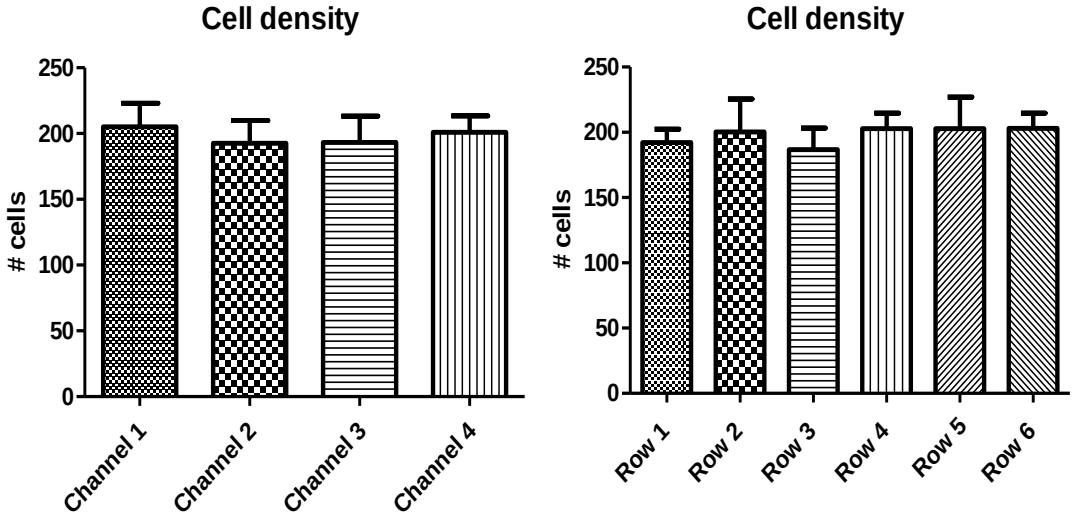

Figure 4.2: Cell number quantification across all chambers and rows after MSCs seeding on the bioreactors. Cell nuclei were labelled with Hoechst and images of one random field (x10) of each chamber were taken from three independent experiments. No variations in cell number was observed, thus uniform cell distribution across the reactor was achieved in all chambers. Image size: 0.02 cm^2. Number of cells was quantified using ImageJ. Data are presented as Mean ± StDev; n=6 for channels, n=4 for rows.

4.3.2 Establishment of minimum flow rate for cell culture

Reducing the scale at which cells are cultured has a dramatic effect on the physical characteristics of the microenvironment and as a consequence, on cell behaviour (i.e. cell proliferation, metabolites consumption, protein expression) (Paguirigan & Beebe 2009). A key characteristic of microscale cultures is the higher cell volume density compared to traditional macroscale cultures. As volume is significantly reduced, cells are exposed to an environment which presents a lower reservoir of nutrients and growth factors, coupled to a faster accumulation of waste (Paguirigan & Beebe 2009). Previous works have shown the impact of volume density and channel height on microfluidic cultures compared to macroscale cultures in terms of cell proliferation and cellular response to soluble factors (Yu et al. 2005; Yu et al. 2007).

Young and Beebe have introduced the effective culture time (ECT) -the time interval between medium changes- as a parameter to establish a way to determine appropriate perfusion rate to replenish media based on media exchange frequency at the macroscale.

Here, the flow rate necessary to replenish entirely media within the microfluidic bioreactor based on ECT in a 96 well plate was calculated. In a typical experiment performed in a 96 well plate (as described in section 3.2.3), $5x10^5$ cells/well are seeded, corresponding to a concentration of $1.56x10^4$ cells/cm^2. As 150μL of medium are added to each well, this corresponds to a fluid height of 4680 μm. Media is replenished every three days (72 hrs).

In the microfluidic bioreactor, the cell density is of $10x10^3$cells/ chamber, corresponding to a seeding density of $1.0x10^4$ cells/cm^2. The height of the chamber is 150 μm. In order to keep the ratio between height and seeding density constant between the macroscale and microscale culture, the following applies:

$$\frac{h1}{\sigma 1} = \frac{h2}{\sigma 2}$$

Where:

h_1=height in the 96 well plate

σ_1=cell density in the 96 well plate (cells/surface area)

h_2=calculated microfluidic chamber height

σ_2=cell density in the microfluidic chamber (cells/surface area)

However, from the calculation above the calculated chamber height h_2 is equal to 3000 μm, which is higher than the actual height of the microfluidic chamber (180 μm).

The time necessary to replenish media in the microfluidic chamber will then be equal to:

$$ECT_m = ECT \times \frac{hm}{h2}$$

Where:

ECT_m=ECT microfluidic chamber

ECT=ECT 96 well plate

h_m= microfluidic chamber height

	96 well plate	Microfluidic chamber
σ (cells/cm^2)	1.56x10^4	1.0x10^4
h (μm)	4680	180
ECT (hr)	72	4.3
V (μL)	150	1.6

Table 4.2: ECT comparison between 96 well plate and microfluidic chamber.

From the calculations above, the ECT of the microfluidic device is equal to 4.3 hrs, corresponding to a flow rate at the inlet of the device of ~30μL/hr (assuming that the total volume of the device is equal to 131μL).

However, previous experiments have shown that an ideal ECT for microfluidic cultures was found to be between 8 to 12 hrs, with more frequent media exchange resulting in lower cell proliferation (Young & Beebe 2010).

In this study, the aim was to identify a flow rate that would sustain cell growth and proliferation throughout all chambers, however enabling accumulation and diffusion of ionic species release by the scaffold, in order to test their effect on cell behaviour. For this reason, the ECT was set to 8 hrs, resulting in a flow rate of 17μL/hr. However, when performing the MSC-microsphere culture experiment at 17μl/hr, a significant decrease in cell number was noticed between the first chamber and the following five chambers, after 7 days culture ($p<0.001$). Decrease in viability was further supported by the decrease in clustering observed by microscopy analysis. Clustering was evident in the first chambers, with almost the totality of microspheres being colonized by cells. However, starting from the 4th chamber, most microspheres were found to be cell-free, thus occupying a wider surface area as shown in figure 4.3a This flow rate was then found to be detrimental to cell growth, probably due to not sufficient media exchange and progressive accumulation of waste towards the end of the device.

It was then decided to minimally increment the flow rate from 17 to 20μl/hr, reducing the ECT from 8hrs to 6.5 hrs, in order to keep the flow rate low enough to capture the effect of soluble factors throughout the chambers, but increasing media exchange to support cell proliferation. Interestingly, this minimum increase in flow rate was sufficient to ensure cell viability along the device, with cell number increasing from the first half to the second half of the reactor, however this was not found to be significant ($p>0.05$). Furthermore, even though

surface area occupied by clusters of microspheres was found to be constant along the bioreactor ($p>0.05$), an increase in clusters size is observed from chamber 1 to chamber 6 (figure 4.3b).

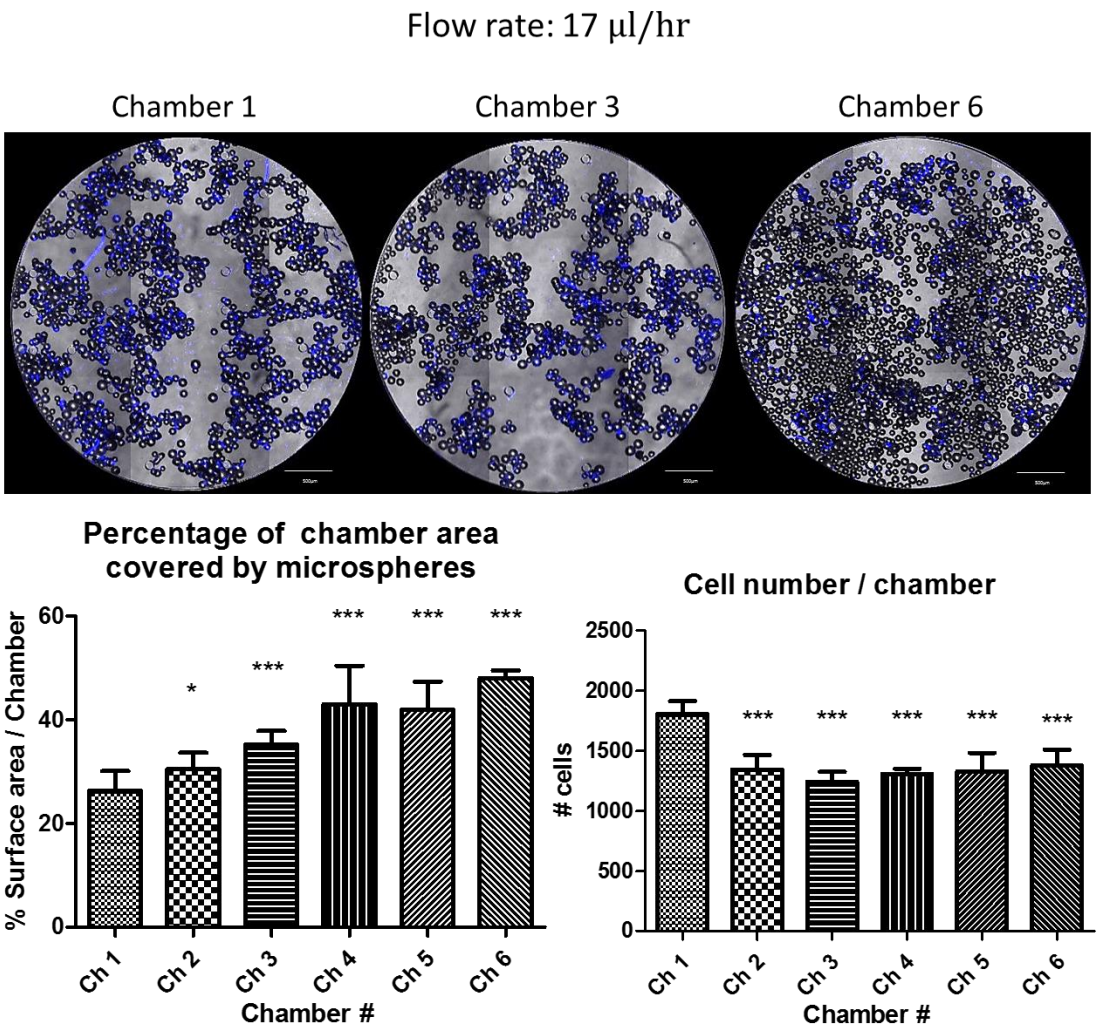

Figure 4.3 a: Effect of 17µL/hr flowrate on MSCs cell culture within the microfluidic bioreactor. At this flowrate was found to be detrimental for cell survival over a 7 days culture period and cell number dramatically decreased from the first row to the other chambers in the reactor ($p<0.001$). Furthermore, cell clustering, as shown by microscopy, was inhibited and the presence of cell-free microspheres is evident on the last row of chambers. Data were pooled from two independent bioreactors (using different MSCs donors) and are shown as Mean ± StDev, N=3-4. Representative images for each experiment are shown, scale 500µm. Statistical significance was assessed via a two-way ANOVA followed by Bonferroni post test, *$p<0.05$, ***$p<0.001$.

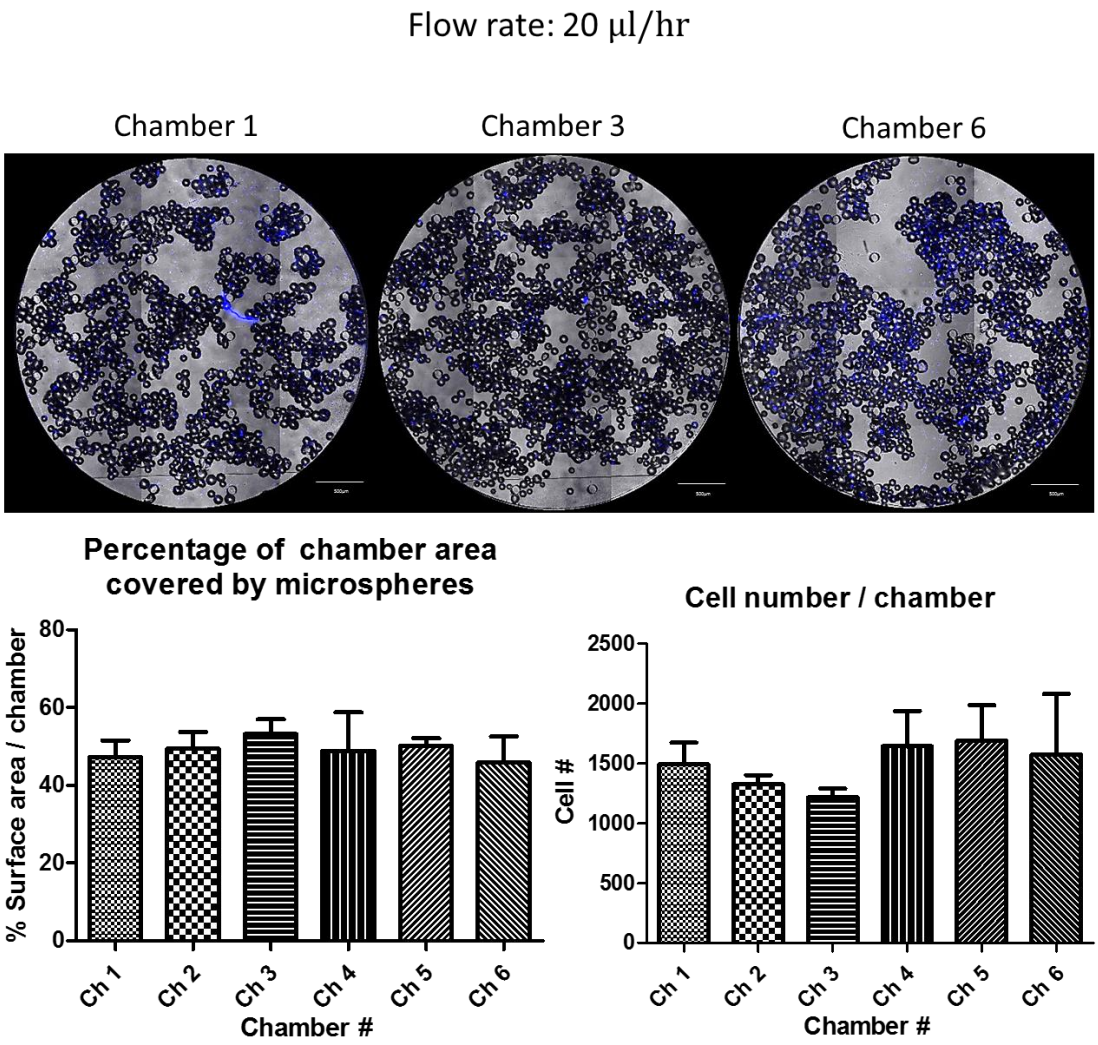

Figure 4.3 b: Effect of flow rate of 20µL/hr on MSCs cell culture within the microfluidic bioreactor. At this flowrate, cell number was found to increase in the second half of the bioreactor (however, this effect was not found to be significant, p>0.05). Similar level of clustering was observed in all chambers (p>0.05). Data were pooled from two independent bioreactors (using different MSCs donors) and are shown as Mean ± StDev, N=3-4. Representative images for each experiment are shown, scale 500µm. Statistical significance was assessed via a two-way ANOVA followed by Bonferroni post test.

4.3.3 Comparison between media compositions

A second experiment was performed to test the effect of different media composition on differentiation of MSCs cultured on CoO 0% and Synth II microspheres. Growth media (DMEM) and osteodifferentiation media (OSTEO) (as described in section 3.2.2) were tested in bioreactors loaded with CoO 0% and Synth II microspheres (two rows per composition).

Firstly, the effect of different media on cell clustering with CoO 0% microspheres was investigated. In the presence of osteodifferentiation media, clustering was enhanced, as measured by a reduction in the amount of bioreactor surface area covered by cell-microsphere material (figure 4.4). Microscopy revealed the difference between DMEM and osteogenic media (figure 4.5), with microspheres being arranged as a monolayer in the presence of DMEM, while being organized in denser aggregates in osteodifferentiation media. In the case of the polystyrene Systemax II microspheres, there was a striking difference, as no significant level of clustering was observed even in the presence of osteogenic media.

The final observation made in this experiment was type I collagen deposition. Increased extracellular deposition was noted on both Co 0% and Synthemax II in the presence of osteogenic media. However, CoO 0% microspheres displayed not only enhanced type I collagen production but also subsequent clustering and tissue-like aggregate formation compared to Systemax II microspheres, confirming results previously observed in static culture.

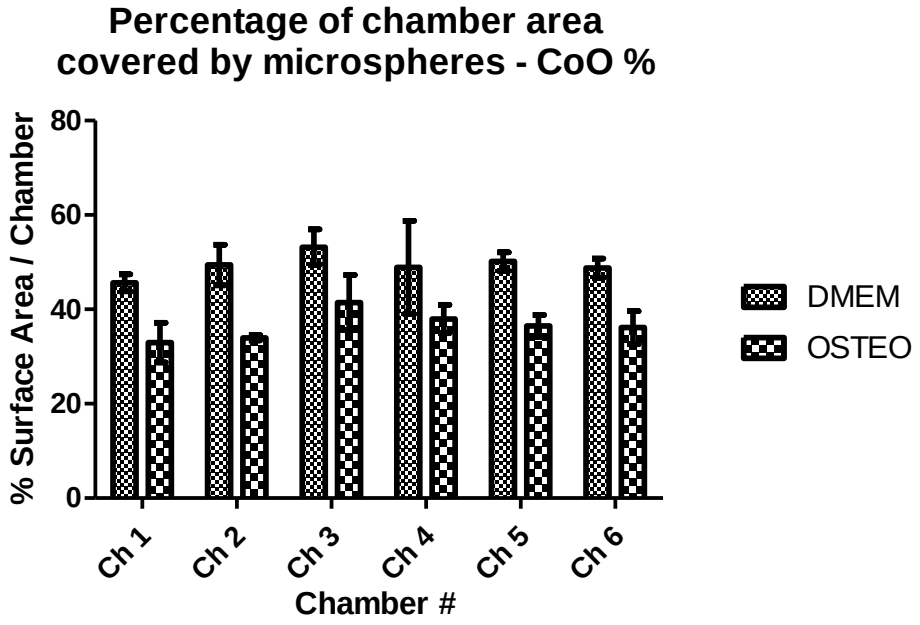

Figure 4.4: Effect of osteogenic media on MSCs clustering when cultured on CoO 0% microspheres. MSCs were grown on CoO 0% microspheres for seven days within the microfluidic bioreactor and perfused with growth media (DMEM-control group) and osteogenic media. Surface area occupied by microspheres was calculated using ImageJ. Osteogenic media was found to enhance clustering, thus decreasing the total area occupied by cell-microsphere aggregates, compared to the control. Per each condition, pooled data from two independent bioreactors (using different donors) are shown as Mean ± StDev, n=2.

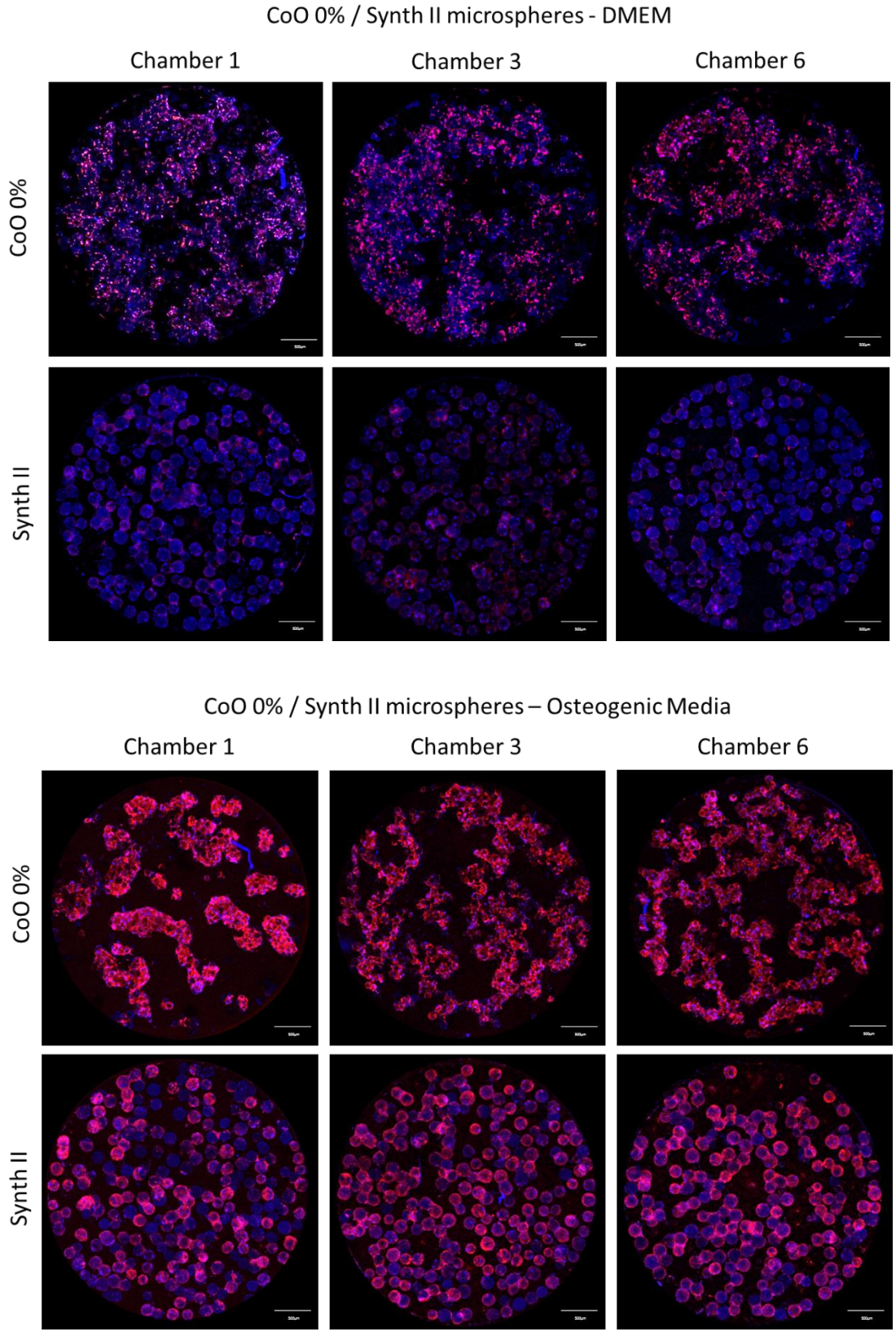

Figure 4.5: Effect of media composition on type I collagen (Red) expression of MSCs (Hoechst-Blue) cultured in the microfluidic bioreactor for 7 days on CoO 0% and Synth II microspheres. MSCs grown on CoO 0% were found to upregulate type I collagen expression in the control media (top panel), compared to those grown on Synth II microspheres. Furthermore, enhanced clustering is observed on the CoO 0% substrate. Osteogenic media significantly upregulated type I collagen expression in both microspheres composition (lower panel). However, even in this case, enhanced clustering and matrix expression was observed on the phosphate glass scaffold. The experiments

were performed using two different donors, showing a similar trend. Confocal images obtained with one representative MSC donor are shown in the figure, bar=500µm.

4.3.4 FN expression on CoO 0% and 2% microspheres and MSC/HUVECs co-culture

A co-culture experiment was performed to test the capacity of HUVECs to attach to MSCs cultured on CoO 0% and 2% microspheres. Bioreactors were filled with the two material compositions (two rows per composition) and MSCs were cultured for 7 days in standard growth media, at a perfusion rate of 20µl/hr as previously described.

A group of bioreactors were fixed at this stage and stained for extracellular fibronectin expression. Another group of bioreactors was left in culture. After MSC culture for 7 days, a monolayer of HUVECs (P5) was tagged with a fluorescent cell tracker (according to manufacturer instructions), trypsinized and resuspended at a density of $1x10^6$ cells/ml. The cell solution was perfused within the bioreactor. The bioreactor was then perfused with a 50:50 DMEM/EGM-2 media solution. After 24 hours, one group of reactors was fixed, after removal of unattached cells by perfusion with PBS. In a second experimental group, cells were left in co-culture for 48 hours, in 50:50 DMEM/EGM-2 media, at a perfusion rate of 20µl/hr.

All bioreactors were fixed in 4% PFA for 20 min at RT, blocked in 3% BSA for 1 hr at RT and labelling of extracellular fibronectin (1:200) was performed overnight at 4°C. Secondary antibody (1:300) was applied for 1 hr at RT and nuclei were stained using a Hoechst solution (1:1000) for 5 min at RT. Images were then obtained using a confocal microscope and mean fluorescent intensity was quantified using ImageJ. Fibronectin was downregulated on CoO 2% microspheres ($7.5 x10^7$ FU) compared to those cobalt-free ($10 x10^6$ FU) (figure 4.6), throughout the entire bioreactor.

In the experiment where HUVECs were subsequently added, the pattern of upregulated fibronectin production was conserved (figure 4.7). HUVECs attachment was found to be proportional to the fibronectin secreted and in particular to be enhanced on CoO 0% microspheres ion chambers 4 and 5, where higher levels of fibronectin secretion were observed (figure 4.8). HUVECs alignment in tubular-like structures, connecting adjacent clusters, was observed after 48-hours co-culture within the bioreactor (figure 4.9).

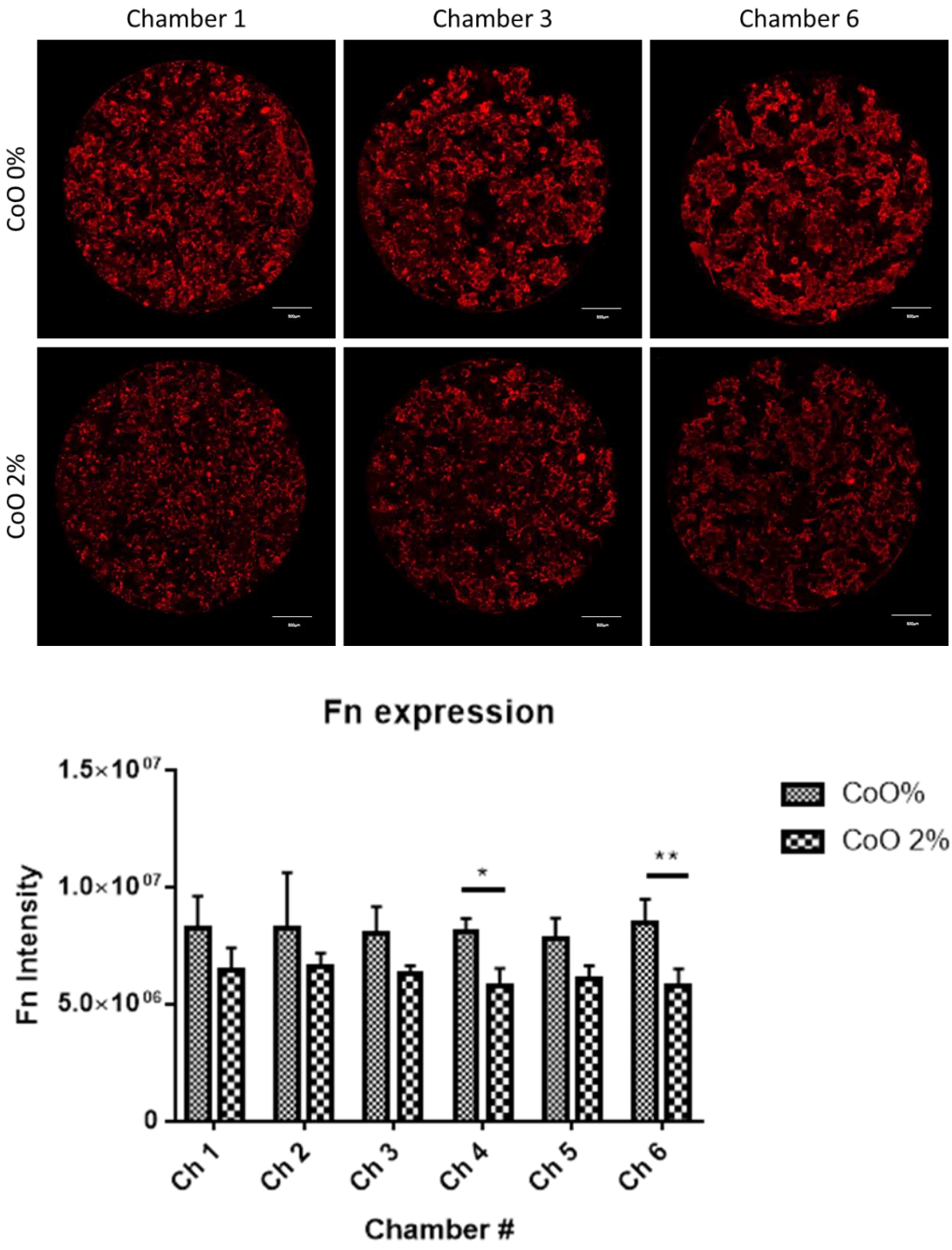

Figure 4.6: Extracellular fibronectin expression (red) of MSCs cultured within the microfluidic bioreactor for seven days on CoO 0% and 2% microspheres, in standard growth media. Enhibited fibronectin expression was shown by cells grown on CoO 2% microspheres, differently to what previously observed in static culture. The same trend was obversed on two different donors. Representative images (top panel) from one donor are shown. Bar=500µm. Average fibronectin intensity was measured using ImageJ and pooled data from two different donors are shown (lower panel) as Mean ± StDev,n=4. Statistical significance was assessed via a two-way ANOVA followed by Bonferroni post test, *p<0.05, **p<0.01.

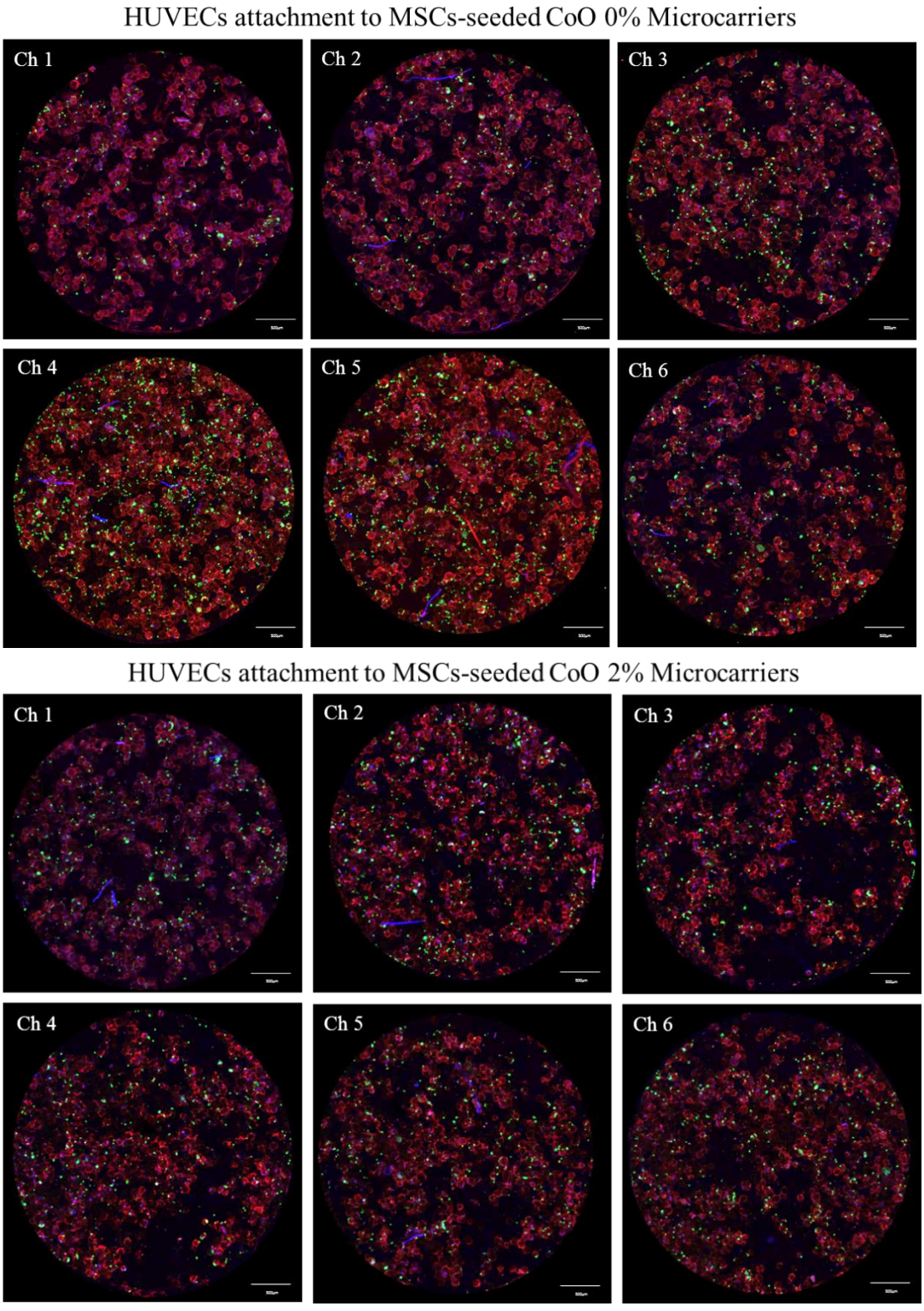

Figure 4.7: MSCs-HUVECs co-culture on CoO 0% and 2% microspheres. MSCs were cultured in DMEM for 7 days before HUVECs seeding. Fibronectin (red) secretion in the ECM is evident in all chambers, although being downregulated in CoO 2% microspheres. HUVECs (green) attachment to MSCs-microsphere clusters is evident in all conditions. The experiment was repeated twice and representative images are shown. Bar=500μm.

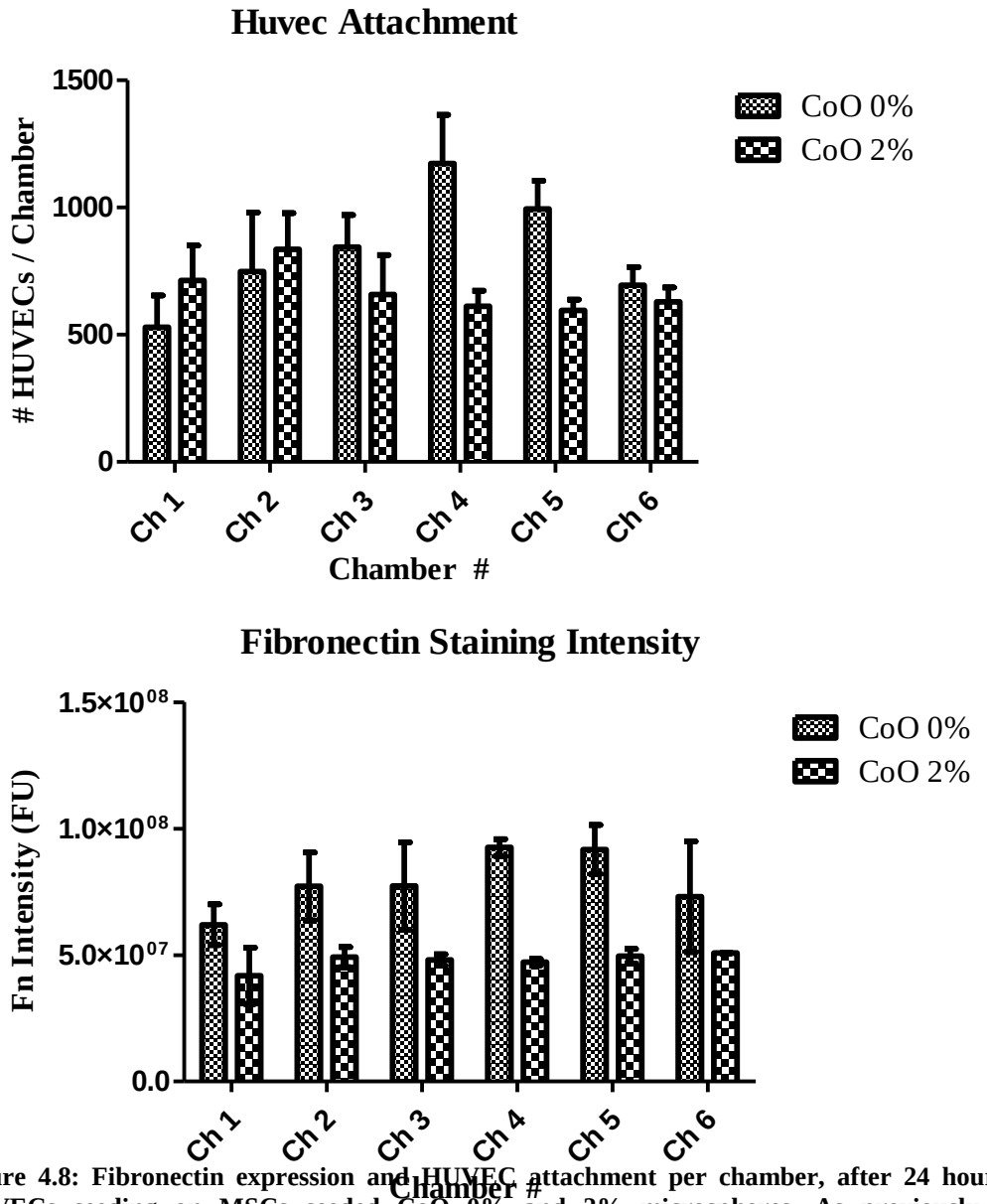

Figure 4.8: Fibronectin expression and HUVEC attachment per chamber, after 24 hours from HUVECs seeding on MSCs seeded CoO 0% and 2% microspheres. As previously shown, fibronectin expression was found to be downregulated on CoO 2% microspheres. HUVECs were found to attach to all chambers, independently of the glass compositions, however highest attachment was observed on CoO 0% microspheres in chamber 4 and 5. Pooled data from two independent experiments are shown as Mean ±StDev, n=2.

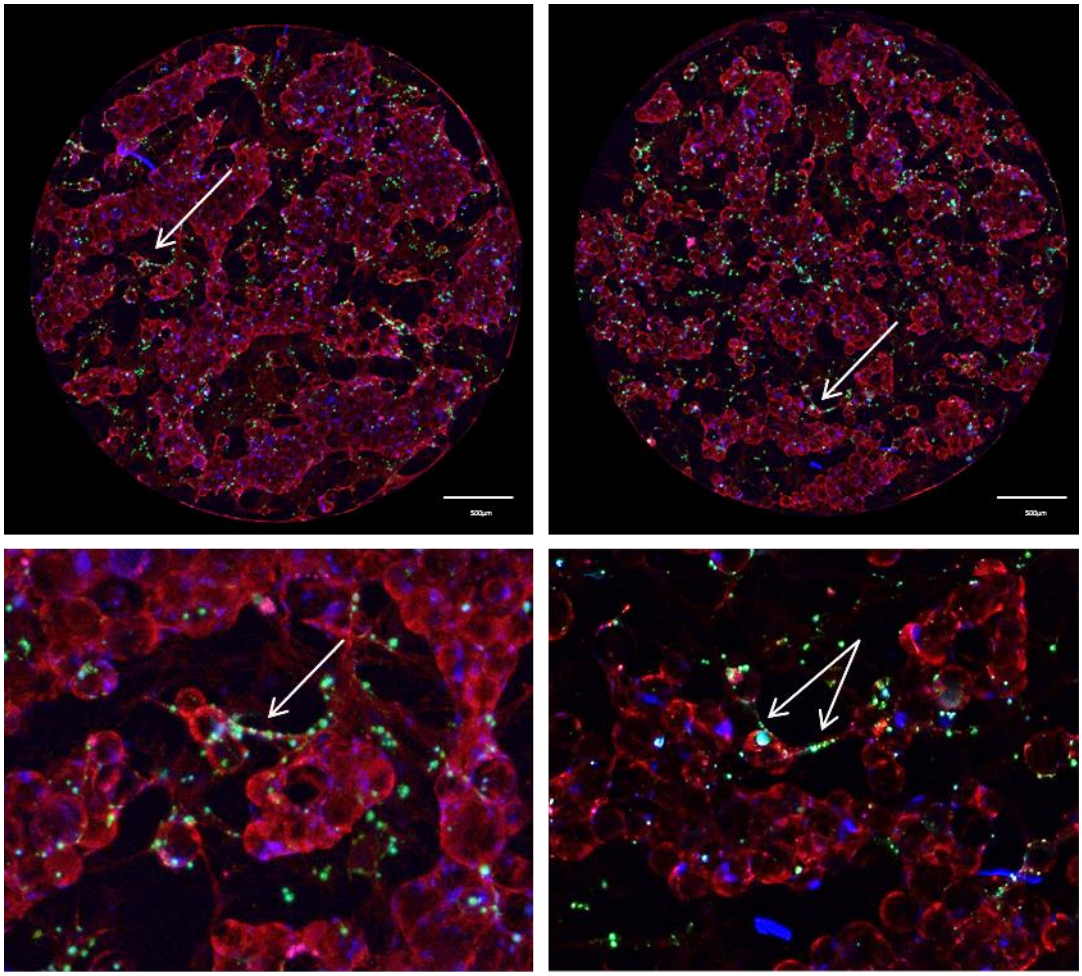

Figure 4.9: MSCs-HUVECs co-culture on CoO 0% and 2% microspheres. MSCs were cultured in DMEM for 7 days before HUVEC seeding. After 24 hours HUVEC attachment, perfusion was started and cells were co-cultured for 48 hours before fixing. Enhanced clustering and fibronectin (red) expression is evident and HUVECs (green) were found to attach to secreted matrix. The formation of tubule-like structures (as indicated by the arrows), connecting microspheres was observed in some chambers. Bar=500μm.

4.4 Discussion

Tissue engineering is the result of complex interactions between multiple variables. The type, source and donor of cells, the material, size and shape of the 3D scaffold, the growth media and its supplements, the flow rate, collectively represent a plethora of combinations of variables whose effect on tissue development is tremendously challenging to screen individually under conventional experimental conditions.

Perfusion bioreactors have been identified as the most efficient culture systems for tissue engineering, as they enhance homogenous mass transfer as well as cell distribution, growth, and differentiation on the scaffold (Bouet et al. 2015). Furthermore, they can be used to mechanically stimulate cell fate (Bouet et al. 2015). Several perfusion bioreactor configurations have been designed for bone tissue engineering applications and they are usually able to accommodate cell-scaffold constructs ranging from 0.04 to 2.7cm^3 (Rauh et al. 2011).

Microfluidics tools represent an advantageous alternative to conventional scale bioreactors, as they allow provision of a controlled spatiotemporal microenvironment at substantially reduced scale, thus allowing on one the one hand tight control of the experimental space, and on the other, significant reduction in the quantity of reagents, thus limiting the cost of high-throughput screening. It has then widely applied in the field of tissue engineering (Bhatia & Ingber 2014; Andersson & Berg 2004; Inamdar & Borenstein 2011).

Several examples are also found in the bone tissue engineering field. For example, the proliferation and differentiation of osteoblastic cells (MC3T3-E1) was measured inside microdevices made of 150 μm repetitive channels and 300 μm chambers under static and dynamic conditions. The results obtained were then compared with conventional cultures on PDMS–coated Petri dishes (Leclerc et al. 2006). Several flow rates, 0,5, and 35μL/min were investigated, corresponding to different level of shear stress. High viability (85%) was observed at 5μl/min, while a significant reduction in viable cells (10%) occurred at 35μL/min. Interestingly, higher ALP expression was observed in the microfluidic device both under static and dynamic (5μL/min), compared to PDMS-coated Petri dish. The device was used to identify optimal shear stress levels at which cells would proliferate and undergo enhanced differentiation (assessed by ALP activity) compared to the 2D static control.

Lee et al. (2011) created a multi-channel microfluidic device that would enable real-time observation of the development of mineralized 3D tissue-like structures by osteoblasts. In addition, the device was used to visualize the complex interactions between osteoblasts with bacteria and antibiotics, and to perform reproducible co-culture experiments free from cross-contamination whilste using a very small amount of the culture medium.

In a second study, they inkjet-printed micropatterns containing antibiotic and biphasic calcium phosphate (BCP) nanoparticles dispersed in a poly(D,L-lactic-co-glycolic) acid matrix

within a microfluidic device containing eight chambers (Lee et al. 2012). The device enabled data generation with significantly reduction in the number of biomaterial samples and culture experiments required. Moreover, the platform enabled *in situ* monitoring of the dynamic interactions of biomaterials with bacteria as well as with tissue cells simultaneously.

Another microfluidic platform filled with hydroxyapatite was used as a mineralized bone tissue model to investigate bone angiogenesis (Jusoh et al. 2015). The platform was designed to integrate fibrin ECM with the synthetic bone mineral HA to provide *in vivo*-like microenvironments for bone vessel sprouting and could be used as a drug screening platform or as a bone disease model.

In previous studies in this thesis, it was demonstrated how dissolution products from phosphate glass microspheres could induce biological responses on mesenchymal stem cells, even in the absence of exogenous factors. These studies were limited to two glass compositions and to one type of media. However, it would be more valuable to design an experimental platform that allows the testing of a larger number of new conditions. To meet this challenge, a perfused microfluidic bioreactor was then developed, based on an existing design for 2D planar cell culture (Titmarsh et al. 2013), to screen multiple combinations of biomaterials and media feed in parallel, through miniaturized culture chambers. Using microfluidics, only small quantities of cell-seeded microspheres were needed and could be captured and cultured under perfusion conditions. Similarly to the device previously developed by Titmarsh et al. (Titmarsh et al. 2013), the microbioreactor potentially enables testing of simultaneously exogenous (in our case both media composition and scaffold) and paracrine signalling (serial chamber arrangement) on proliferation, osteogenic differentiation and angiogenic responses of mesenchymal stem cells.

Firstly, the capacity of the device to support cell attachment to the microspheres was tested, followed by cell growth and proliferation over time. Homogenous cell distribution across the device upon seeding was firstly established. Approximately 1000 cells/chambers were counted, thus significantly reducing the number of cells required per experiment. This is of particular relevance when dealing with autologous cell sources, where only limited cell numbers might be available for *in vitro* testing. Cells were found to be viable and to successfully attach to the microspheres.

Initially, a flow rate of 17µL/hr was tested, corresponding to a complete media change of the device occurring in 8hrs. However, this flowrate was found to be detrimental to cell viability on CoO 0% microspheres after seven days in culture. Only cells growing in the first half of the device were found to be viable at the end of the seven days culturing period. Cell viability was assessed by measuring the surface area occupied by microspheres: viable and proliferating cells were able to cluster microspheres together, thus occupying a smaller surface area, while limited cell growth correlated with microspheres remaining as a monolayer,

minimally colonised by cells. Furthermore, when analysing cell number, it was interesting to note a drastic reduction from the first to the second chamber of the device. Reduced cell viability can be due to insufficient media exchange at the selected flow rate coupled to accumulation of wastes within the chambers. The flowrate was then minimally increased to 20µl, reducing the time to completely exchange media to 6.5hrs. This flowrate was found to promote cell clustering throughout the device and we observed an increase in cell number from the first half of the reactor to the second half. An increase in aggregates size was noted between the first and last chamber, corresponding to a relative increase in cell number.

This flowrate was then used for further experiments, as it provided sufficient media exchange to ensure cell viability and proliferation and could provide, potentially, accumulation and diffusion of ionic species released by the microspheres. This was of particular interest as this would enable to elucidate interactions between cell and material.

It is interesting to note that compared to static cell culture (as shown in figure 2.12 and 3.3, in Chapter 2 and 3 respectively), a more homogenous distribution of aggregates was obtained within the bioreactor, due to the combined effect of the physical constraints of the chambers and that of perfusion. Thus, compared to the rotational mixing investigated in previous chapters, perfusion was shown to provide a better bioprocessing environment for this particular system.

As in previous experiments, the capacity of phosphate glass microspheres to induce osteogenic responses in the absence of osteogenic media was tested, in this work the device was used to test different media compositions. Bioreactors filled with CoO 0% and Synth II microspheres (two rows per composition) were made and the effect of standard growth media (DMEM) and osteogenic media on cell clustering and type I collagen secretion was investigated. Osteogenic media was found to induce clustering and matrix secretion on CoO 0% microspheres. This response was consistent among different donors and osteogenic media could represent an alternative to accelerate the differentiation process during micro-tissue development and assembly *in vitro*. A preliminary experiment was also performed to assess the effect of growth media supplemented with dexamethasone only on cells grown on CoO 0% microspheres (data not shown). Enhanced clustering and matrix production was noted also in this case, thus suggesting that individual supplements can enhance the osteogenic potential of the raw material. Further experiments should be performed to identify an optimum media composition that could further stimulate *in vitro* osteogenesis.

When looking at Synth II microspheres, limited clustering was observed under both media compositions and the microspheres appear as a monolayer even after seven days in culture. Type I collagen expression was also limited on the plastic microspheres and was partially enhanced during culture with osteogenic supplements.

It was previously shown in Chapter 3, the capacity of phosphate glass microspheres doped with cobalt to enhance fibronectin secretion. The same effect was investigated in the bioreactor to determine whether a similar behaviour would be observed under dynamic conditions. A bioreactor was filled with CoO 0% and 2% microspheres (two rows per composition) and stained for extracellular fibronectin expression after seven days in culture. It was interesting to note an opposite trend compared to the static control, with a downregulation in fibronectin expression in the presence of cobalt, compared to the cobalt-free composition. This gives an interesting insight into different responses of MSCs grown on the phosphate glass microspheres under perfusion, compared to static culture. Mechanisms triggered by the accumulation of cobalt ions in static culture might not be activated under perfusion. Continuous removal of ionic species might be responsible for the different protein expression and these altered responses need to be taken into consideration when translating from static culture to a dynamic environment, such as a bioreactor.

To test the hypothesis that enhanced fibronectin deposition would favour endothelial cells attachment, MSCs and HUVECs were co-cultured within the bioreactor. Firstly, MSCs were cultured for seven days within the device. Fluorescent tagged HUVECs were then injected within the reactor and their capacity to attach to the matrix secreted by MSCs grown on CoO 0% and 2% microspheres was monitored. As previously shown, fibronectin expression was downregulated on CoO 2% microspheres and enhanced HUVEC attachment to the CoO 0% microspheres was observed. A control experiment was performed in 96 well plates. However, the size and thickness of the aggregates formed under static culture prevented the acquisition of clear images that could be easily quantified. Physical constraints imposed by the dimensions of the bioreactor enabled a fast, multi-scan acquisition of the entire well and to easily quantify the number of cells attaching under each condition.

In another experiment, after seeding HUVECs within the bioreactor and allowing them to attach for 24 hours, a co-culture of both cell types was performed for 48 hours. This was the longest MSCs culture within the device for a total of ten days and lead to the formation of aggregates of MSCs and microspheres, with HUVECs successfully anchored to the ECM. Furthermore, the presence of some endothelial cells linearly arranged in the form of a tubular vessel and bridging together adjacent clusters were also observed.

Experiments performed in the device confirmed some of the results previously observed in 96 well plates, such as type I collagen upregulation in CoO 0% compared to Synth II microspheres. However, through the device it was possible to visualize the importance of clustering on MSCs osteodifferentiation and to rapidly screen different media feeds. Loss of viability through the arrayed chambers at reduced flow rate also helped elucidate potential cytotoxic effects of the biomaterial at this microscale.

Furthermore, some of the effects observed under static conditions such as fibronectin upregulation in the presence of cobalt were not confirmed under perfusion and an opposite trend was actually noted. Through the capacity to grow cells in a dynamic perfused environment, it is possible to predict cell behaviour in larger perfused bioreactors more closely. The geometry of the platform enabled rapid image acquisition and analysis, thus improving the quantity and quality of data that can be obtained by microscopy. Furthermore, the geometry of the chambers induced a more uniform formation of clusters compared to what observed in static culture in 96 well plate.

The preliminary experiments described present only some of the possible applications of the microfluidic platform in analysing mechanisms underlying bone tissue formation on 3D scaffolds *in vitro*. The experiments here described mainly focused on phosphate glass microspheres, but the device can easily accommodate other types and shapes of scaffolds. The reduced scale of the system allows us to perform multiple tests using minimum quantities of reagents, in terms of biomaterial, cells and media/growth factors. As the bioreactor is perfused, the effect of mechanical stimulation could be also studied by testing different flow rates or adjusting the height of the channel layer. This would modify the shear stress acting on the cells.

The studies performed mainly relied on microscopy and immunocytochemistry to measure cell behaviour within the device. However, spent media can be harvested and collected separately from the four rows and used for other types of biochemical analysis (i.e. metabolites analysis, ELISA, etc.). Cells could also be harvested from the device by trypsinization and then gene expression quantified by qPCR analysis.

Furthermore, the same platform could be potentially used to screen the formation of other tissue types and due to its versatility, further elements of complexity can be integrated to the system to test new parameters (e.g. by incorporating a combinatorial mixing unit to test different concentrations of growth factors on cell responses, or by using biosensors for online measurement).

4.5 Conclusion

Standardisation of protocols for cell isolation, expansion, scaffold seeding and culture pre-implantation will represent a key driver in the transition of bone tissue engineering therapies from the lab to the clinics (Ma et al. 2014). In particular, the development of appropriate bioreactor systems will enable standardized and scalable manufacturing protocol. However, due to the complexity and large set of variables that influence artificial tissue formation *ex vivo*, screening of multiple conditions is required to identify an optimal combination of culture parameters. Therefore, an adaptation of a novel multiplex miniaturized perfusion bioreactor was developed to screen multiple different scaffold compositions (i.e. microspheres), media compositions and media flow rates to ultimately produce micro units of engineered bone tissue within the device.

Microbioreactors enable the relationship between process parameters such as channel size, flow rate, shear stress and cell responses (i.e. proliferation, differentiation) to be mapped simultaneously (Coutinho et al. 2011). The key advantage is that multiple different microsphere substrates and nutrient feeds can be screened in parallel in microliter quantities. Therefore, they enable the study of tissue formation within a well-defined microenvironment using minimum quantities of reagents. This reduces significantly the cost of process development and reduces the risk of failure when of moving processes to larger scale bioreactors that consume large and costly amounts of material.

The device consists of 24 perfused chambers that enable parallel screening of multiple scaffold biomaterials for bone tissue engineering applications, under different fluid flow conditions. Four parallel rows of serial chains (6 wells per chain) enable downstream effects of secreted paracrine factors to be assessed, along with effect of accumulated scaffold degradation products. The device was used to test the effect of different microspheres and bioprocess conditions (i.e. flowrate, media feed) on cell proliferation, along with osteogenic (i.e. bone formation) and angiogenic (i.e. vessel formation) responses. Results obtained with the bioreactor confirmed the capacity of Ti-doped phosphate glass microspheres to spontaneously induce ECM secretion by MSCs and this effect was further enhanced in combination with osteogenic media. Furthermore, the physical constraints of the device in combination with perfusion enabled a more uniform aggregation of cells and microspheres, thus offering a potential strategy to control the clustering effect observed in static culture.

As perfusion bioreactor are particularly suitable for modular tissue engineering applications, information obtained at the small scale using this system could be potentially translated to larger scale set-up, thus enabling the production of larger unit of tissue, using a controlled, standardized manufacturing process.

Chapter 5. Discussion and future work

5.1 Discussion

The present research focused on the development and characterization of a novel tissue engineering approach based on the use of phosphate bioactive glass microspheres as a scaffold to deliver mesenchymal stem cells for the treatment of bone defects. Despite presenting a less well documented clinical history compared to other ceramics, phosphate glasses have been widely investigated *in vitro* and *in vivo*, with promising results in promoting osteogenic responses and good level of osseointegration (Ensanya Ali Abou Neel & Knowles 2008). Being fully degradable in non-toxic species, they could potentially overcome any concerns related to long-term implantation side-effects. Moreover, they present a versatile structure that can be easily modified by integration of metal dopants. This approach has been widely reported not only to control their degradation profile, but also to induce specific biological functions (Lakhkar et al. 2013). Here, it was investigated the effect of a combinatorial doping with titanium and cobalt to promote osteogenic differentiation and angiogenesis, as a potential cost-effective alternative to the use of growth factors.

As most commercially successful bioactive glass bone substitutes have been manufactured in the form of granules or particulates to facilitate filling of bone defects of different sizes and shapes (Jones 2015), in this study the glass was processed in the form of microspheres. Compared to other geometries, microspheres present several advantages: they present a large surface area for cells attachment and that promote faster degradation rate and ion release, they can be manufactured to present regular size and shape (Hossain et al. 2014) and the spherical shape could facilitate filling of irregular shaped defects (Perez et al. 2014). In particular, in this study, a modular approach was proposed, where microspheres coupled to cells are used as building blocks to create micro units of tissue that could then be implanted in the bone defect. The network formed between cells and microspheres provide an interconnected structure that could promote and support new bone formation and a matrix to induce vessel ingrowth (Mei, Luo, Tang, Ye, Zhou & W.-S. Tan 2010).

Three compositions of phosphate glass microspheres were investigated, containing 5% mol TiO_2 and different concentrations of CoO (0, 2 and 5% mol). Substituting CaO with CoO resulted in small variations in the physical properties, as shown by XRD, FTIR and differential thermal analysis. However, in terms of microspheres degradation, compositions presenting binary doping with cobalt and titanium presented a significantly slower degradation rate than the cobalt-free control.

Similarly, cobalt ion release was monitored over time. As expected, the CoO 5% glass presented significantly higher release of cobalt ions compared to CoO 2% composition. The latter, however, showed cumulative cobalt ions release in the biologically active range of 3-12 ppm (Quinlan et al. 2015) within the first two weeks analysed. Cobalt ion concentration within

this range has been found to promote angiogenesis *in vitro* and *in vivo*, without showing adverse cytotoxic effects.

Biocompatibility of the glass microspheres was tested by growing the osteosarcoma cell line MG-63 on the microspheres. Cell attachment and growth was observed in all glass compositions and the concentrations of cobalt tested were not found to be cytotoxic. The spontaneous formation of aggregates of cells and microspheres was also observed. In terms of metabolism, cobalt-induced hypoxia was not found to significantly affect the rate of glycolysis at all concentration tested, differently to what observed in previous studies (Hsu et al. 2013).

To test the capacity of cobalt to induce angiogenesis through activation of the HIF-1α pathway, the concentration of VEGF secreted in the media by cells cultured on the three different glass compositions and on culture tissue plastic, was tested. Similarly to what previously shown in other studies (Steinbrech et al. 2000; Quinlan et al. 2015), in this work cobalt capacity to induce VEGF expression was found to be dose dependent and significant effects were observed only within narrow dose and time ranges. The CoO 2% composition was successfully identified as being able to promote VEGF secretion, without affecting cell proliferation and viability.

As dynamic culture presents several advantages over static cultures and has been found to have significant positive effects on cell viability, proliferation, metabolism, aggregation and differentiation (Kinney et al. 2011), preliminary experiments were performed to test the effect of hydrodynamic conditions on MG-63-microspheres interactions, by using a plate shaker to introduce mixing. Even though an optimal shaking speed was not identified in this study, the key role of mixing on this particular system was clearly proved. Low rotational speed favored cell proliferation and enhanced metabolic activity, as well as promoting cell-microspheres aggregation. However, compared to static culture, no significant increase in cell proliferation was observed. Experiments performed at higher speed resulted in inhibition of cell growth coupled to reduced number and size of aggregates, indicating that a critical threshold in mixing rate (and consequently fluid shear stress) exists after which cell viability diminishes. Future studies will aim at identifying an optimal speed within the range analysed that support enhanced proliferation as well as enabling a better control of aggregate formation.

The preliminary biocompatibility characterization was followed by a more extensive investigation of the effects of the microspheres on hBM-MSCs, a clinically relevant cell source for tissue engineering applications. Similar to MG-63, biocompatibility, cell proliferation over time and formation of clusters were confirmed also with MSCs grown on PG microspheres. Polystyrene microcarriers (Synthemax II) were used as a control in this study. The surface of these microcarriers has been specifically treated to promote MSC attachment and long term expansion (Hervy et al. 2014). As expected, significantly higher expansion was obtained on the control microspheres.

Apart from better attachment of MSCs to the treated plastic surfaces rather than glass, it was hypothesised that spontaneous differentiation induced by ionic species released by the PG microspheres could be a further reason leading to the arrest in self-renewal. In particular, together with metal ions, calcium and phosphate species are released during phosphate glass dissolution and osteodifferentiation induced by these ions either as media supplements or from scaffold release has been widely reported (Barrère et al. 2006; An et al. 2015; Chai et al. 2014; Müller et al. 2008). In this study, spontaneous matrix secretion in response to the PG substrate occurred, in the absence of osteogenic media supplements. In particular, the production of extracellular type-I collagen and fibronectin over time was observed and this was of particular relevance as it represent a preliminary step in osteoblast maturation (Lian & Stein 1995).

Glass-induced osteogenesis was confirmed by both ICC staining and qPCR, that showed upregulation of osteogenic markers when MSCs were grown on Ti-doped microspheres, compared to the plastic control, in the absence of osteogenic supplements. Furthermore, even when MSCs were cultured in monolayers with media supplemented with eluate from the Ti-doped microspheres, a similar response was observed. Interestingly, upregulation of osteogenic markers did not occur in the presence of binary doping with cobalt, thus suggesting an inhibitory role of cobalt on osteodifferentiation.

While titanium has been widely reported in the literature as a promoter of osteogenic responses (Barrias et al. 2005; Abou Neel et al. 2014; Lakhkar et al. 2015), the effect of cobalt on MSCs is less well understood and several studies showing heterogeneous responses have been published (Wu et al. 2012; Ignjatović et al. 2013; Quinlan et al. 2015; Ignjatovic et al. 2015; Birgani, Fennema, et al. 2016). The *in vitro* experiments shown in this thesis clearly suggest a downregulation of osteogenic responses. However, whether this is due to an inhibitory effect of cobalt-induced hypoxia or to the slower degradation rate of the binary-doped glass, thus leading to a slower release of known pro-osteogenic ions, could not be determined. The use of small molecules to mimic hypoxia through activation of the HIF pathway has been identified as a powerful strategy to enhance bone vascularization and regeneration in vivo (Drager et al. 2015), due to the close interplay of this signaling pathway on coupling angiogenesis to osteogenesis (Schipani et al. 2009). However, previous studies have identified the potential of hypoxia conditioning in maintaining cells in an undifferentiated state thus inhibiting osteodifferentiation (Grayson et al. 2006; Yang et al. 2011; Osathanon et al. 2015).

More clearly documented is the effect of cobalt on angiogenesis, through stabilization and activation of the HIF pathway. Cobalt mediated angiogenic responses have been reported *in vitro* (Azevedo et al. 2010; Wu et al. 2012; Quinlan et al. 2015) and *in vivo* (Buttyan et al. 2003; Fan et al. 2010; Birgani, Fennema, et al. 2016). In this work, the capacity of cobalt of inducing a hypoxic-like state was shown by upregulation of HIF-1α and VEGF secretion by MSCs grown on CoO 2% PG microspheres. However, this did not translate into enhanced functional

response, both in terms of *in vitro* vascularization of endothelial cells in a Matrigel assay and in a CAM model of vascularization. This is in line with a previous study from Peters et al. (2005) that showed that even though endothelial cells over-expressed HIF-1α in response to Co^{2+} exposure, their capacity to form vessels was impaired. Other studies (Zhang et al. 2012; Quinlan et al. 2015) have showed improvement of endothelial tubule formation in response to cobalt ions released by bioglasses, however this was found to be time dependent and to occur at earlier time point compared to that analysed in this study.

Taken together, the results obtained, suggest that cobalt doping does not improve the functionality of titanium-doped phosphate bioactive glass, neither in terms of osteogenic or angiogenic induction. On the other hand, titanium doping alone was found to induce both responses and to support cell proliferation of MSCs over time. Future studies should then be addressed to further investigate this glass composition in combination with MSCs in a bone defect model. Due to the close relationship between osteoblasts and endothelial cells *in vivo*, it is possible that titanium-doped PG microspheres by inducing MSCs to undergo osteogenic differentiation could also promote vascular responses, whereas cobalt, by inhibiting osteogenic induction, also suppresses accompanying angiogenic support.

Due to the complexity of the field and the necessity to screen the interplay between numerous factors for bone tissue culture ex vivo, emerging technologies like microfluidic bioreactors represent a powerful tool to perform high-throughput investigations, minimizing experimental timing and cost (Titmarsh et al. 2014) and providing better control of environmental parameters (Li et al. 2012). In this work, a novel microfluidic bioreactor was designed for multiple screening of bioprocess variables in 3-D perfused cell culture, with the ultimate goal of identifying optimal conditions for bone tissue generation.

The microfluidic bioreactor was developed from an existing device for 2D planar cell culture previously developed in Prof. Cooper-White's research group (Titmarsh et al. 2013), whose design was modified to accommodate microspheres or other types of scaffold. Channels placed above the chambers enables cell loading and continuous media perfusion along the chambers. Preliminary experiments were performed to test the potential use of the device to investigate the effect of different substrates and media feed on cell behaviour, under perfusion culture.

MSCs were successfully cultured within the device for up to one week and cell proliferation, as well as cluster formation was observed over time. Due to chamber dimension constraints, clusters of controlled height were formed, thus facilitating image acquisition and quantification of extracellular matrix protein expression. For example, type I collagen secretion by cells cultured on phosphate glass microspheres and polystyrene microcarriers was compared, when cultured with growth media or media supplemented with osteogenic factors. Similarly to what was observed under static conditions, enhanced matrix secretion occurred on the

phosphate microspheres and this effect was further enhanced in the presence of osteogenic media. On the other hand, limited collagen secretion and cluster formation was observed on the plastic microspheres, even in presence of osteogenic supplements.

The device also enabled to test the effect of perfusion on cell-phosphate glass interaction. For example, while fibronectin secretion was found to be upregulated when cells were grown on cobalt-doped microspheres under static conditions, this response was not observed under perfusion. Continuous removal of ionic species is a possible explanation for the different behaviour observed.

These preliminary studies confirmed the potential use of the device to screen multiple conditions in parallel and to identify optimal cell culture parameters using minimum quantities of reagents, in an engineered microenvironment that provides more experimental control than a traditional 96 well plate. Furthermore, they proved the suitability of perfused cell culture in this particular cell-scaffold system.

5.2 Future work

One main limitation observed in this study was the reduced proliferation of both MG-63 and BM-MSCs on PG microspheres compared to tissue culture plastic, in line with results previously observed in similar studies (Guedes et al. 2013; I.-H. Lee et al. 2013). Furthermore, microscopy showed cell-cell attachment as well as growth in interstitial spaces between the microspheres, thus suggesting limited cell adhesion affinity to the PG substrate. Future studies aim at improving cell attachment to phosphate glass are required. Surface functionalization with cell-adhesive proteins for example has been reported as a potential strategy to improve initial cell anchorage (Perez et al. 2015) and to direct cellular responses, such as differentiation (J. H. Lee et al. 2013; Lee et al. 2014) and could been potentially applied to this system.

Scaling up of the system will be required to produce enough material for *in vivo* applications. In this study, some preliminary investigations were performed to test the effect of mixing on cell culture. However, the solid filled nature of the microspheres, together with their high density, imposed significant limitations. If on one side this enables to have all cells on the surface of the microspheres, thus minimizing the risk of not uniform nutrients distribution and the formation of necrotic areas within the pores, on the other hand it makes the spheres not buoyant (Park et al. 2013). For example, stirred tank bioreactors are not suitable for this system, as the impeller speed required to keep the bulk microspheres in suspension would be detrimental for cell growth. As examples of hollow or macroporous glass microspheres exist in the literature (Hossain et al. 2014), it would be interesting to test these configurations within a bioreactor setting as they have decreased density and increased buoyancy. Furthermore, porosity plays as a key role in osteogenesis as it enables migration and proliferation of osteoblasts and

mesenchymal cells, as well as endothelial cells for vascularization (Karageorgiou & Kaplan 2005).

Together with microspheres surface porosity, in this particular system void spaces between particles also needs to be taken into consideration. Void volume between the spheres can be controlled by altering the size of the particles. The size range of the PG microspheres was kept constant due to technical limitations of the spheroidization protocol that limit the particle size distribution to 63-106μm (Lakhkar et al. 2012). However, larger microspheres would correspond to increased interstitial porosity. As shown by the CAM experiment in Chapter 3, lower vascularization occurred on the cells-seeded microspheres compared to the cell-free scaffold, probably due to interstitial spaces saturated with ECM and MSCs, thus impairing endothelial cells penetration and attachment. Thus, further studies should be performed to identify optimum cell culture time on microspheres and optimal clusters size and porosity to promote *in vivo* engraftment.

Furthermore, this work mainly focused on testing the osteodifferentiation potential of phosphate glass using BM-MSCs and their vascularization capacity using endothelial cells. Together with testing other potential sources of MSCs (i.e. adipose derived, umbilical cord), it would of great interest to test the response of osteoclasts to the material. In particular, *in vitro* experiments could be performed to test the capacity of osteoclasts to form resorption pits on the scaffold and to remodel calcified matrix. Osteoclast-mediated glass resorption, as opposed to solution-mediated should also be monitored over time. This would be of particular relevance as hypoxia has been widely reported to induce osteoclastogenesis and bone resorption (Arnett et al., 2003). These studies will provide a more complete picture of the biological activity of the material.

Moreover, in all experiments, Synthemax II microcarriers were used as a control, as they enable to grow cells on an inert substrate in a 3D spherical arrangement. However, in future experiments, a more extensive screening of bioactive microspheres should be performed in order to test the osteogenic potential of titanium-doped phosphate glass in comparison to that of other potential candidate biomaterials for bone regeneration. Furthermore, most experiments were performed in the absence of osteogenic media. However, preliminary studies performed in the microfluidic bioreactor showed the capacity of phosphate glass microspheres in combination with osteogenic media to upregulate type I collagen expression. Thus, the combined effect of microspheres and osteogenic supplements should be further investigated.

In vivo studies would be required to clearly understand which phosphate glass compositions favours regeneration, whether titanium doping alone or in combination with cobalt. Clinical translation of this system would require transition to a GMP manufacturing set-up. All experiments were performed using research-graded consumables that would not be adequate for a clinical setting. For example, media supplemented with FBS was used in all

experiments. The clinical use of FBS has been questioned due to its undefined compositions, lot to lot variability and the possibility of containing harmful contaminants or pathogens (Panchalingam et al. 2015). Transition to a serum free or chemically defined media are potential alternative options.

As in this case, the drug product consists of cells combined with a biomaterial scaffold, extensive testing will be required of the two individual components before and after product assembly (Lee et al. 2010). In particular, quality and potency assays need to be developed to test viability, self renewal, death and differentiation while cells are being cultured on the scaffold. Most of the *in vitro* studies performed have looked at population wide, qualitative responses, however more detailed product characterization is required, to investigate the presence of subpopulations at different differentiation stages and to identify thresholds of potency markers expression as indicators of clinical efficacy. Furthermore, formation of aggregates of controlled size will need to be achieved, to ensure standardization of the final construct.

Cryopreservation of the tissue-engineered construct is another key step requiring investigations, as it would greatly enhance flexibility in patient treatment. While cryopreservation of cells is an established procedure, cryopreservation of tissue-engineered constructs is still at its infancy. Current studies are focusing on the development of a process that would allow consistent cell recovery and viability, as well as retention of the extracellular matrix and scaffold architecture post thawing (Kofron et al. 2003; Costa et al. 2012; Bissoyi et al. 2014). However, compared to cell suspension, the extracellular matrix secreted by cells makes the cryopreservation process more difficult, as gradients in cryoprotectant diffusion may occur (Kofron et al. 2003). Together with conventional slow cooling cryopreservation, vitrification has been proposed as an alternative technique for banking of bone tissue-engineered constructs (Kuleshova et al. 2007). The establishment of effective cryopreservation protocol need to be followed by a parallel development of controlled strategies for thawing of the tissue-engineered construct.

In terms of the microfluidic bioreactor, experiments performed so far have mainly be limited to end of point image analysis. However, the device offers the potential of performing a wider range of techniques, as cells can be easily harvested from the system, as well as spent culture media. Currently cells can be harvested via trypzination and collection at the outlet of the device. Cells belonging to the same row can then be pooled together and screened for PCR analysis or other molecular biology techniques. Modifying the structure of the device by addition of a removable lid, could facilitate cells harvesting from individual chambers, in order to test the potential effect of paracrine signalling across the six chambers. Furthermore, the recent development of sensors designed for microfluidic applications could significantly improve the type and quantity of online information that could be collected continuously from the device (Grist et al. 2010; Wu & Gu 2011). As successful cell culture was obtained within the

bioreactor and better control of cell-microspheres aggregation was achieved compared to static culture, this system could also potentially be scaled-up for larger tissue production. In particular, as previously stated, due to the physical characteristics of the microspheres, a perfusion system is particularly suitable, as it allows to provide homogenous mass transfer through the cell-sphere clusters.

5..3 Conclusions

In conclusion, a novel potential bottom up tissue engineering approach for the treatment of bone defects based on phosphate glass microspheres was investigated. Compared to scaffold of predefined dimension, the modular system here described present a potential flexible solution to address osseous defects of different size and shape. Among the compositions studied, titanium-doped phosphate glass microspheres emerged as the most promising candidate, as it was found to induce the activation of osteogenic differentiation pathway on MSCs and to promote vessel formation by endothelial cells. The positive outcome observed *in vitro* suggest a clinical potential of the tissue engineered approach developed as part of this work and future experiments need to be designed to prove the efficacy of the system *in vivo*. Future studies will then be aimed at characterizing this approach in an animal model and to translate the current manufacturing process to a clinical setting.

Finally, the microfluidic bioreactor described enabled to successfully culture MSCs on microspheres under perfusion and to investigate the effect of several culture parameters on this particular system. Identifying optimal culture conditions by limiting the number of experiments and consumables required allows to significantly accelerating the transition to a larger scale manufacturing process. As perfusion bioreactors are particularly suitable for modular tissue-engineering applications, information obtained with the microfluidic bioreactor could be potentially translated to a scaled-up system for the manufacturing of larger quantity of bone tissue *ex vivo*.

Appendix 1. Commercial evaluation of a multiplex perfusion microbioreactor for process optimization in cell therapy manufacturing

UCL Advances PhD Enterprise Scholarship

Carlotta Peticone, Dept. Biochemical Engineering, UCL

Supervisor: Dr Ivan Wall, Dept. Biochemical Engineering, UCL

A.1.1 Aim

The key output from my PhD research was the development and testing of a microfluidic device to be used as a high-throughput screening platform for the development of new manufacturing processes and products in the regenerative medicine field. The device was originally designed and tested to screen multiple variables in bone tissue engineering, the area of focus of my PhD project. However, as the use of the platform can be translated to a broader range of applications in cell therapy manufacturing, this technology presents a potential commercial value.

In this chapter, a commercial evaluation of the platform is provided. Advantages and limits of the proposed technology with respect to competitor products are reviewed, together with strategies to overcome current limitations to commercial translation.

A.1.2 Introduction

A.1.2.1 Process development in cell therapy and tissue engineering manufacturing

Regenerative medicine is an emerging interdisciplinary area of research focusing on replacing or generating human cells, tissue or organs, to restore or establish normal function (Mason & Dunnill 2011). Over the next 20 years, this emerging industry is expected to change healthcare provision by delivering stem cell-derived products that will benefit aging populations globally.

However, the widespread application of stem cell therapies is currently limited due to difficulties in reproducibly manufacturing large enough quantities of functional products that meet clinical demand and are economically feasible. While in the case of protein based drugs and vaccines the product is separated from the cells that are simply used as a manufacturing vehicle, in regenerative medicine manufacturing the cells are the product and the whole bioprocess is critical to determine their integrity and phenotype (Mason & Hoare 2007).

For example, in cell therapy, a selected cell population is firstly isolated and selected, then expanded by sub-culturing until the required cell-dose number is reached and then harvested and formulated to be administered to the patient (Bartel 2014). In tissue engineering, cells are usually first expanded and then seeded onto a scaffold that provides a 3D support and guides the growth, proliferation and differentiation of new cells (Williams & Sebastine 2005); the so-obtained tissue-construct can then be implanted to the patient.

Both cell therapies and engineered tissues can either be autologous, where the cells used for the treatment are derived from the same patient receiving the therapy, or allogeneic, where cells derived from a universal donor are used to treat multiple patients. Whether the product is autologous or allogeneic will cause significant changes to the bioprocess in terms of scalability,

economic feasibility, cGMP burden, level of automation, lot variation and risk of contamination and cross-contamination (Ratcliffe et al. 2011).

As most cell therapy therapies have been originally developed in academic settings using planar culture in T-flasks and well plates (Rowley 2010; Bartel 2014), there is a need to move to automated or semi-automated manufacturing as preliminary studies move to early clinical application and then to widespread commercial use. Traditional planar technologies are labour intensive, thus leading to high risks of contamination and variation between batches. They typically require a high footprint, as large surface areas are required to meet the high cell dose required for some therapies. Furthermore, these technologies mainly impose a static mode of culture, thus creating a heterogeneous environment that can negatively affect the quality of the final product.

Bioreactors offer several advantages compared to traditional technologies, not only in terms of improved cell yield and scalability, but also in process control and reproducibility (Liu et al. 2014). As bioreactors provide a dynamic environment, effective mass transfer and oxygen supply can be achieved and this is of crucial importance for high cell-density culture (Liu et al. 2014) or for cells cultured on 3D scaffolds (Korossis et al. 2005). Furthermore key variables such as pH, dissolved oxygen, nutrients levels, waste product concentrations and shear forces resulting from fluid flow, can be controlled through the use of sensors and probes (Liu et al. 2014). As most stem cells are adherent, microcarriers are often used within bioreactors, in order to provide a surface to which cells can adhere to, while being agitated or perfused in the reactor.

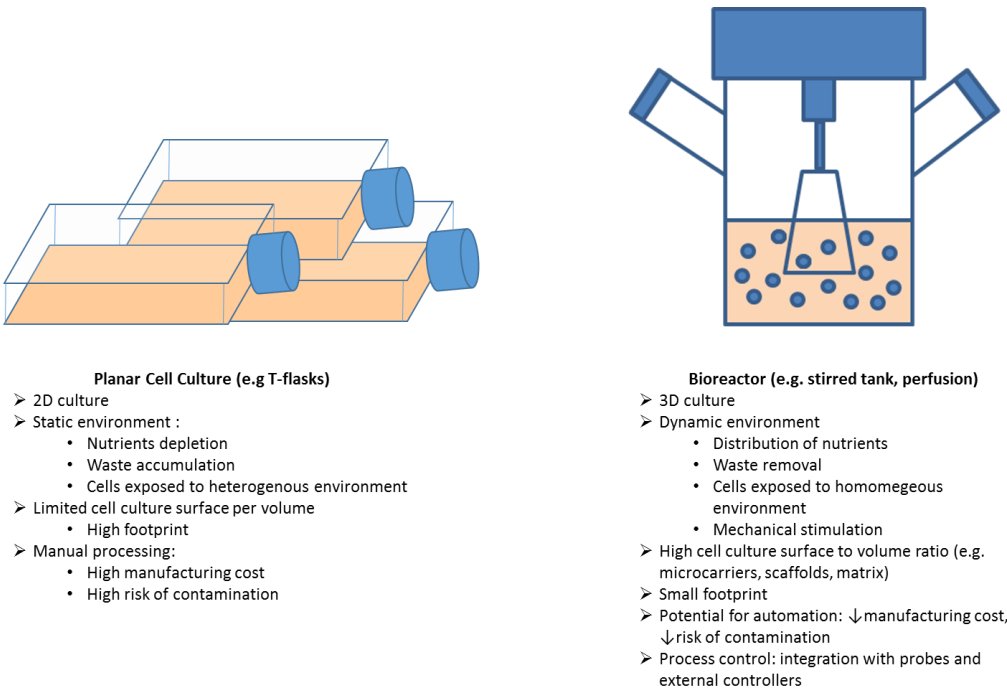

Figure A.1: Comparison between planar and bioreactor technologies for cell culture

In tissue engineering, the bioreactor is a powerful system that enables homogenous cell seeding through the scaffold and while facilitating uniform biochemical and biomechanical stimuli that can support appropriate tissue development (Korossis et al. 2005).

As the bioprocessing environment is the combined effect of multiple parameters that can affect the cell product, key critical input variables must be identified and controlled to maintain final product specifications. However, this can be an extremely challenging task in cell-based therapy due to the intrinsically complexity of the input variables (Ratcliffe et al. 2011). Uncontrolled process variation is highly undesirable for manufacturing and good manufacturing practise (cGMP) processes and represents a regulatory and practical barrier to successful manufacture of cell-based products (Ratcliffe et al. 2011).

Apart from the starting cell material, all the chemical, biophysical and mechanical cues to which the cells are exposed, along with frequency and intensity of exposure, need to be investigated and optimised, as they play a key role in determining the characteristics of the final product (Wall & Brindley 2013). For example, variables such as media composition, cytokines and media exchange rate need to be optimized for each culture system. Furthermore, because numerous cell culture substrates (including biomaterial scaffolds and microcarriers) with different properties, have been developed from different environments (commercial manufacturing facilities to academic labs) there is a need to screen and compare multiple candidates to determine best cell culture substrate for different cell types.

Using a "One factor At a Time" (OFAT) approach is not an adequate strategy in process development, as it would not take into consideration interactions between variables. Hence, a multivariate design should be used to test multiple variables in parallel (Thomas et al. 2008). As performing multiple tests at full scale is not economically feasible, microscale processing techniques represent a powerful tool to investigate multiple process variables to speed up translation to manufacturing scale (Micheletti & Lye 2006) and to optimize each step of the bioprocessing sequence, from cell isolation to post-implantation monitoring (Titmarsh et al. 2014). In the last decade, microfluidic technologies have become very popular in the biological sector as they provide a cost-effective solution to perform high-throughput analysis.

A.1.2.2 Microfluidic technologies in process development

Microfluidic devices are able to handle and manipulate fluids at the micrometer scale (Duncombe et al. 2015). At these length scales, it is possible to predict with high precision mass and energy transfer, and devices can be designed with controlled environmental conditions such as temperature, pH, dissolved gas concentration, shear stress, and medium exchange rates (Titmarsh et al. 2014). This is of particular relevance for biological applications, as these technologies offer the capacity to mimic and control complex cellular microenvironments *ex vivo*. Often referred to as Lab on a Chip (LOC) or µTAS (micro total analysis systems), these

technologies enable the high-throughput screening of multiple samples, at reduced sample volume and cost (Ho et al. 2015). Several microfluidic devices have been developed for a wide range of applications from cellular analysis, from point of care (POC) diagnostics to the development of "organs on chips" (Ho et al. 2015) to study tissue *ex vivo*.

The versatility of fabrication techniques enables the design of complex three-dimensional microstructures to address specific biological questions. Combinations of chambers, channels, valves and membranes can be reproduced into soft elastomers such as poly(dymethilsiloxane) (PDMS), thermoplastic materials (polystyrene, polycarbonate) or glass (Titmarsh et al. 2014). PDMS, in particular, is the gold standard material for microfluidic applications, as fabrication on polymers is easier and less expensive, thus making it suitable for rapid design prototyping (Tang & Whitesides 2010). Furthermore, PDMS presents physical properties that make it ideal for biological applications, like being transparent, gas permeable, not toxic and presenting a tuneable Young's modulus (Tang & Whitesides 2010).

Due to their capacity to provide a precise control of the cellular microenvironment, microfluidic technologies can be applied in several areas of cell-processing research, from addressing fundamental biological questions to bioprocess development (Titmarsh et al. 2014).

From a process development point of view, microfluidic technologies are particularly helpful for screening combinatorial effects of different variables on cell phenotype, minimizing reagents and experimental time and cost. Microfluidic bioreactors, for example, can be designed to identify optimal conditions for cell culture at larger scale. Compared to traditional in vitro assays using static multiple well plate, these technologies allow to study cell behaviour in a dynamic 3D environment, thus facilitating transition from planar culture to full scale bioreactors. Media composition, feeding rate or substrate for cells attachment are some of the variables that could be potentially screened at the microscale.

Another potential area of application in process development is that of quality control assays, as multiple tests need to be performed for regulatory purposes to characterize cellular material derived from different donors, batches or at different stage of the manufacturing process (Titmarsh et al. 2014). Microfluidic technologies could represent a cost effective solution to minimize the number of cells required, being particularly relevant in characterization of autologous therapies.

A.1.2.3 Commercialization of microfluidic technologies: perspectives and current challenges

In 2013, the global microfluidic market was valued at $1.59 billion and it is projected to reach $8.64 billion by 2023 (Yetisen & Volpatti 2014). FluidicMEMS report a list of 273 microfluidics/lab-on-a-chip companies in 2015 spread across the globe (FluidicMEMs 2015).

Despite the promising figures, the number of microfluidic technologies that have been successfully commercialized are only a small percentage of the devices that have been created in academic laboratories (Blow 2009). This represents a significant opportunity, yet one faced with either physical or perceived barriers to commercialisation.

Lack of standardization and of integration with existing workflows have been identified as key hurdles in their widespread adoption at the commercial level (Volpatti & Yetisen 2014). In terms of standardization, a key issue is represented by academic articles in the microfluidic field failing to report reproducibility statistics or to quantify chip-to-chip variability (Volpatti & Yetisen 2014).

Furthermore, although PDMS is the most widely used material in the field at laboratory scale research, it cannot be easy translated to a commercial set-up due to its high cost compared to standard low-cost polymers used by the industry such as poly (methyl methacrylate) (PMMA) and polycarbonate (Volpatti & Yetisen 2014). Leaching of uncured oligomers from PDMS into microchannels and absorption of hydrophobic molecules from serum-containing media into the polymer bulk have been reported and can alter the environment in which cells are cultured (Regehr et al. 2009). Also, from a biologic perspective, and as polystyrene is the gold-standard in tissue culture plasticware, microfluidic devices would be more attractive if made of a thermoplastic material (Berthier et al. 2012). Thus, shifting from soft-lithography to PS microfabrication when feasible or making PDMS manufacturing easily scalable are two possible strategies to overcome current limitations (Berthier et al. 2012; Volpatti & Yetisen 2014).

Lack of integration of microfluidic chips with standard lab equipment is another limitation to their potential commercial application (Volpatti & Yetisen 2014). Most systems require external pumps or software for data analysis (Volpatti & Yetisen 2014) and in many applications off-chip sample preparation is required (Nge et al. 2013). This increases the complexity of using the platform. As the operator might not be familiar with microfluidics handling, making user-friendly chips, from which the user can easily obtain data, is another key requirement for their widespread adoption (Blow 2007).

Another key issue to take into consideration is comparison with existing technology. In order to market the technology, the performance and cost-effectiveness of the microfluidic product need to be significantly better than the full scale existing alternatives (Volpatti & Yetisen 2014). uFluidix, a Canadian contract manufacturing company that specializes in scalable production of customised micro devices made of PDMS or thermoplastic materials, reports how microfluidics ventures often underestimate the competition through existing technologies (Sofla 2013). In particular, they report that for microfluidic devices whose aim is to miniaturize, integrate or automate existing processes, rather than offering a technology that cannot be replicated at larger scale, is more difficult to find a commercial application, due to the macro-scale counterpart often being as efficient and less expensive. For example, they show that

100 single layer chips can be produced in two weeks for $40/chip. This manufacturing cost can often be prohibitive from a customer perspective for a single-use chip.

Finally, the lack of a "killer application" that can perform better than existing technologies and that can be widely adopted by the scientific community is what is still preventing microfluidics technologies from reaching their full commercial potential (Blow 2007).

A.1.3 Design, fabrication and validation of a multiplex perfusion microbioreactor for optimizing process conditions for 3D tissue production

A.1.3.1Platform description and technical specifications

As part of my PhD, I developed a microfluidic perfusion bioreactor for multiple parallel screening of bioprocess variables in 3D cell culture. The microfluidic platform was developed as part of a collaboration between the Department of Biochemical Engineering at UCL and the Tissue Engineering and Microfluidics (TEaM) lab lead by Professor Justin Cooper-White at the Australian Institute of Bioengineering and Nanotechnology (AIBN), University of Queensland, Australia. I spent nine months at AIBN designing and developing the platform and performing preliminary validation experiments. The device was then brought back to UCL, where further validation was undertaken.

The bioreactor design is based on a platform previously developed in the TEaM lab presenting 270 culture chambers for arrayed 2D cell culture (Titmarsh et al. 2012).
The bioreactor consists of 24 chambers arranged across four parallel rows of serial chains (6 wells per chain). Each chamber was designed to accommodate microcarriers or scaffolds for 3D cell culture. As the microbioreactor was fabricated using PDMS soft-lithography, the platform is disposable and can be economically and rapidly fabricated for multiple, reproducible experiments.

The device consists of two layers: a bottom layer that accommodates the chambers for cell culture and a top layer incorporating the overlying fluidic channels. Scaffold/microcarrier loading into the device was performed manually before bonding the two layers. Each row can accommodate a different substrate, thus enabling the screen of multiple conditions in a single device. After bonding of the two layers, cells can be loaded using the inlet port and equally distributed across all chambers. By connecting the device to a syringe pump, it is possible to perfuse the internal chambers with the desired media. The system can then be incubated for long term cell culture. The flow rate can be adjusted to monitor the effect of frequency of media exchange or shear stress on cell culture.

The device fits within a standard microscope coverslip, thus making it suitable for cell imaging using standard inverted microscopes. Chamber dimensions and spacing are that of a

standard 384 well plate, thus making the system compatible with conventional plate readers. The entire internal volume of the device is ~130µl, thus minimizing the number of cells and reagents used per experiment. Spent media is collected through the outlet ports.

The device was originally developed and used to test the effect of different microcarriers and media conditions on mesenchymal stem cell proliferation, along with osteogenic (i.e. bone formation) and angiogenic (i.e. vessel formation) responses. One example of data acquisition within the reactor is provided in figure A.2. Experiments have been performed to validate homogenous cell distribution across the reactor, long-term cell culture within the device, co-culture of two different cell types and suitability for high-quality image acquisition and analysis. Furthermore, data obtained with the platform have been compared to results observed in conventional static culture.

The same platform could be potentially used to screen the formation of other tissue types and due to its versatility, and further elements of complexity can be integrated to the system to test new parameters (i.e. a combinatorial mixing unit to test a gradient of growth factor concentrations on cell response or incorporation of biosensors for online measurement).

There is significant potential to use this type of platform in the emerging cell and gene therapy industry to optimise culture media and feeding regime, to identify optimal differentiation protocols and to screen the effect of multiple parameters in a high-throughput fashion. Indeed, our collaborators and inventor of the baseline technology at the University of Queensland, have recently set up Scaled Biolabs, a company that specializes in the development of microfluidic platform for cell therapy manufacturing optimization, biologics production and immuno-oncology applications (Scaled Biolabs 2017). By incorporating advanced mixing capabilities Scaled Biolabs can perform cell cultures using potentially thousands of discrete cell cultures in a system that can pinpoint optimal media composition to control cell fate.

There are potentially numerous applications for the modified device that can house 3D structures such as microcarriers. One example is presented in the following paragraph.

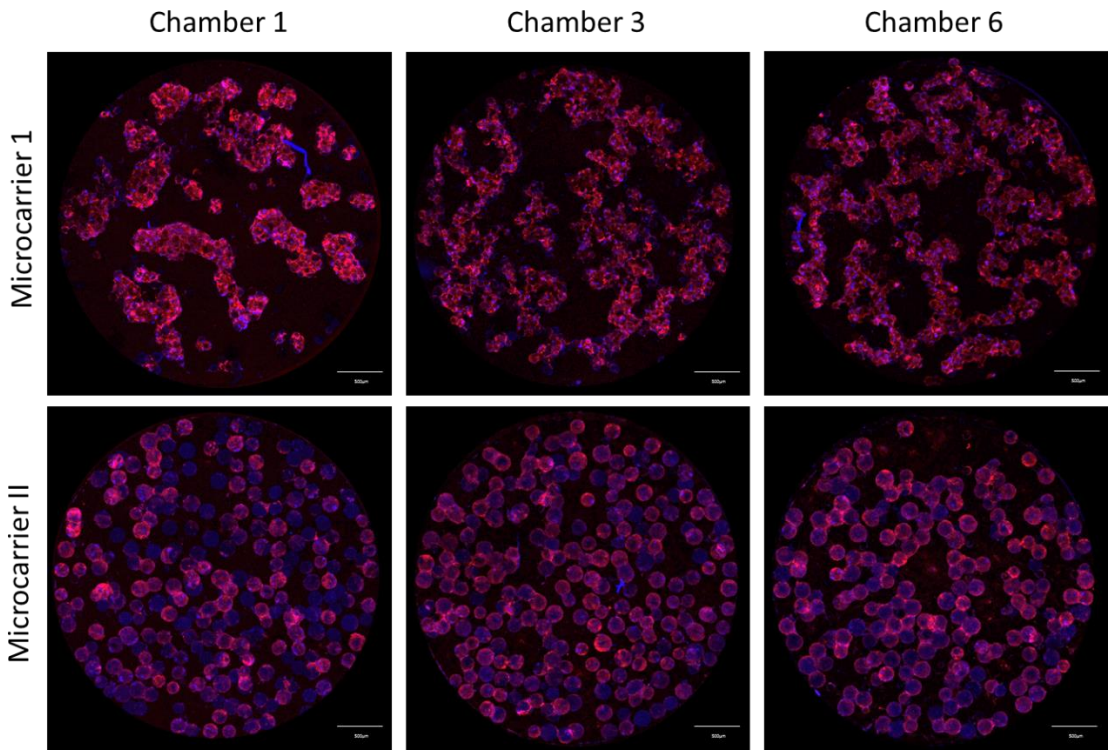

Figure A.2: Differential response on type I collagen (red) secretion (i.e. osteogenic marker) of stem cells when grown on different microcarriers within the microbioreactor. When grown on microcarrier type I, upregulation of type I collagen along the chambers is evident, as the result of a substrate-modulated response. On cells grown on microcarrier type 2, limited collagen secretion is noticed, thus indicating lower capacity of the material to induce osteogenesis.

A.1.3.2. Potential application: High-throughput microfluidic processing to predict large scale stem cell culture

Scale up of the manufacturing process is one of the main challenges currently faced by the cell therapy industry to meet the requirement of treating large numbers of patients during clinical trials and the commercialization phase. Together with high yield, the cellular product needs to present the correct phenotype. Compared to traditional 2D culture, microcarriers represent a valuable solution as they offer a support for adherent cell expansion within a bioreactor set-up.

Microcarriers made of different materials or presenting different surface coatings are available in the market. However, surface coating as well as mechanical properties (i.e. stiffness) have been shown to impact stem cell fate and to drive their differentiation towards different phenotypes (Sart et al. 2013; Merten 2015). Furthermore, as many existing manufacturing processes have been validated in 2D, there is a need to undertake robust process development to identify the optimal culture conditions when switching to 3D culture (i.e. type of microcarrier, media composition and media exchange rate).

The goal of future development work could be to develop a screening strategy based on the microfluidic platform here described, to study the effects of different microcarrier coatings on the expansion and differentiation capacity of different adherent cells. This type of study will allow the microfluidic platform's use to be expanded to a larger number of cell types and microcarrier compositions, thus testing its performance in a wider set of applications. It will increase understanding of which cell-microcarrier combinations are compatible, not only from a cell yield perspective but also in terms of cell phenotype markers, hence reducing risk of failure when transitioning to large scale bioreactors.

Once fully established, the screening platform will provide the industry with a cost-effective solutions to test a wide range of microcarriers and feeding regimes, thus minimizing the time and costs currently required to transition from 2D to 3D culture.

A.1.4 Comparison with existing technologies

Several companies have pursued the development of miniaturized bioreactors that enable to grow cells under perfusion and/or in a 3D environment.

For example, Kirkstall Ltd commercializes the Quasi-Vivo technology, a series of modular components that can be connected in different configurations to create physiologically relevant conditions for *in vitro* cell culture and allows flow perfusion and media recirculation. The chambers are of the size of a 24 well plate, thus presenting an intermediate size between large scale and microfluidics. They present two main format: the QV500 and the QV900.

The QV500 consists of modular silicone chambers that can be arranged in different configurations and that can accommodate 3D scaffolds (Kirkstall 2016a). The starter kit consists of 3 QV500 chambers, a reservoir bottle, tubing and luers, 3 loading trays, coverslips and a user guide and it is sold for £863, while a pack of five chambers costs £975. The chambers can be autoclaved up to three times. The QV900 consists of 6 wells of the size of a 24 well plate in the footprint of a standard well plate (Kirkstall 2016b). Tubings connecting the six chambers can be arranged in different ways and in-situ imaging of cells can be performed. The system is disposable, with the starter kit including 3 QV900 Trays, 2 reservoir bottles, loading trays, tubing & luers & a user guide being sold for £979. For further experiments, 12 trays can be bought for £3300.

Reinnervate has developed a perfusion plate, consisting of a six well plate made of non-tissue culture treated PS (Reinnervate 2016). The plate presents four serially connected chambers for cell culture and two wells used for sampling, at the inlet and outlet respectively. One single condition can then be screened per plate. Media can be recirculated if required and scaffolds can be accommodated in the culture chambers. The cost of two plates and luer locks (tubings excluded) is €131 or €359 for ten plates.

Another commercial platform is the CellAsic ONIX produced by Millipore. It is a single use system that has the footprint of a conventional 96 well plate and presents four chambers for cell culture (D=2mm, H=1.4mm) (Millipore 2016). Four different solutions can be perfused through each chamber and there are two wells for waste accumulation at the outlet. The system is run through a control system that enables control of flow rates through the chambers. This platform requires a microscope equipped with a culture chamber. Alternatively, gravity-driven perfusion can be also performed. This does not require the control system, however it is not possible to switch between different media solutions and to control the flowrate. The cost of five plates is £338.

Similarly, Fluxion Bioscience presents Bioflux, a standard 48 well plate equipped with microfluidic channels at the bottom of the plate (Fluxion 2016). Each flow channel connect an input well to an output well, with an observation area placed in between the wells. This limits access to the culture area, thus making the system not ideal for loading and screening 3D scaffolds. The control instrument applies controlled pneumatic pressure to ensure the desired level of flow rate and corresponding shear stress. The minimum volume required per sample is 20µl per well. The plates are disposable and 48 well plates (enable to screen 24 conditions in parallel) are sold for $190/plate. The Bioflux controller and software need to be purchased to operate the plates.

The systems above present the advantages of being assembled in a standard well plate format, thus being compatible with conventional plate readers and inverted microscopes and to be made of standard or medical graded material for tissue culture. The main limitation associated with most of these systems, however, is the prohibitive cost of the plates, considering that most units are disposable. Furthermore, the need to use a specific controller unit on the one hand enables better (via automated) control of the system, but this comes at the expense of significant capital investment. Finally, apart from the Bioflux and CellAsic Onix, the other systems are still relatively big, requiring large amount of reagents for their operation and thus not being ideal for high throughput screening. Table A.1 summarizes the characteristics of each system described and of the newly developed microfluidic bioreactor.

	Quasi Vivo	Reinnervate	CellAsic Onix	BioFlux	Prototype
Chamber size	24 well plate	6 well plate	D=2mm x H=1.4 mm	W=0.35mm H=0.07mm	384 well plate
Max. number experimental conditions	6	1	4	24	4
Serial Chamber Arrangement	Y	Y	N	N	Y
Perfusion	Y	Y	Y	Y	Y
External Equipment	Pump	Pump	Control System	Control System	Pump
3D scaffold	Y	Y	N	N	Y
Disposable	Y	Y	Y	Y	Y
Unit price	£275/plate (pk of 12 plates, kit not included)	€35.9/plate (pk of 10 plates + luer locks, tubings and pump not included)	£67.6/plate (pk of five plates, controller not included)	$190/plate (controller not included)	N/A

Table A.1: Technical specifications of the prototype platform in comparison to commercially available technologies.

A.1.5 Platform development

As previously described, the versatility of the proposed microfluidic platform can be applied to a wide range of different applications. Furthermore, modifications of the original layout could be easily performed and the device could be further customized to meet the requirement of the client. However, to maximize the number of collaborations and to potentially commercialize the device, some improvements need to be implemented and are currently being investigated.

Firstly, there is a need to increase the range of experiments that could be performed on the platform. The device has mainly been used for end of point analysis, as data acquisition was performed using a confocal microscope, that required several hours to scan the entire platform. Online microscopy could be performed using a microscope equipped with a culturing chamber unit. However, the development of new generation plate readers, that enable rapid 3D scanning of multiple well plate, could represent a valid alternative to acquire data at several time points, minimizing the time outside of the incubator. As the size and spacing of the chambers is based

on a 384 well plate, the platform can be easily integrated and analysed by standard plate reader or fitted in a conventional slide holder for microscopy. Systems such as the InCell 6000 Image Analyser (GE Healthcare) offer enormous scope for high content image analysis if integrated with the platform and can accommodate devices in multiwell plate or microscope slide formats.

Furthermore, fluorescent dye could be used to detect online signalling such as protein secretion or metabolic influx. Other type of measurements such as metabolites analysis and protein secretion could also be performed on collected spent media. The device could also be easily fitted with oxygen sensors that could enable online monitoring of cell growth with continuous data acquisition from the outside of the reactor. Furthermore, making the cell culture chambers accessible by adding a removable lid to the current device, could enable cell harvesting at the end of the culture for PCR or flow cytometry analysis.

As previously stated, transition from PDMS to PS could also favour acceptance from a wider scientific community, it would simplify comparison with standard tissue culture platform and protocols and would enable a more cost-effective mass production (Halldorsson et al. 2015). Fabrication using PMMA and PS as substitute materials and subsequent comparative studies could be performed to test any differences in device operation and cell responses in devices fabricated from alternative materials. Also, as we found a percentage of devices failing during the experiments, with ineffective bonding being the main cause of failure, transitions to PMMA and PS could solve this issue, thus improving reproducibility for device robustness.

A.1.6 Conclusion and future work

Currently, despite the commercial small-scale platforms available and the increasing number of prototypes produced in academic settings, there is still a need to produce a disposable perfused miniaturized bioreactor for 3D cell culture, that allows to easily culture cells on scaffolds and to perform high throughput screening of variables. Commercially available systems are either prohibitive in terms of cost for single-use or require external control system for being operated. The proposed technology could fill the gap in technology currently seen and could provide a useful tool for rapid screening of process variables.

The potential platform development strategy proposed above would address some of the key technical issues currently faced by microfluidic technologies. Future studies could focus on improving the current design and to extend the scope of the device to multiple applications.

As a CDA is in place between UCL and the University of Queensland, filing a patent application in collaboration between both parties, based on cell-material screening would represent the first step towards the commercialization of the platform.

As a starting point, the London Centre for Nanotechnology (LCN) based in the UCL campus could represent a potential partner for device fabrication in the UK, as they provide

access to their equipment to private users. A service provider business model could be adopted to optimise microcarriers and other process parameters to meet a customer's needs to reduce risk of failure when they address scale up of their cell culture processes.

A key driver in commercialization is the reduction of the unit cost of the device, by using material suitable for commercial scale production. Currently, two days are required for fabrication, as several overnight steps are required for PDMS curing and bonding, and the process is manual. Transition to PS will enable the use of conventional automated techniques used for multiple well plate production, significantly reducing the unit cost. Only by providing a unit price suitable for single-use experiments, it will be possible to maximize transition from conventional experimental settings to the platform, especially within academic labs.

In conclusion, the microfluidic bioreactor described offers a cost effective solution to identify optimum operating conditions in process development, thus de-risking transition from lab to manufacturing scale of cell-based therapies. Further studies aimed at testing the use of the platform for a broader range of applications within the cell therapy field and at optimizing the platform manufacturing process would make it more sustainable and robust from a commercialization perspective.

6. References

Abou Neel, E.A. et al., 2009. Bioactive functional materials: a perspective on phosphate-based glasses. *Journal of Materials Chemistry*, 19(6), pp.690–701.

Abou Neel, E.A. et al., 2007. In vitro bioactivity and gene expression by cells cultured on titanium dioxide doped phosphate-based glasses. *Biomaterials*, 28(19), pp.2967–77.

Abou Neel, E.A. et al., 2009. Structure and properties of strontium-doped phosphate-based glasses. *Journal of the Royal Society, Interface / the Royal Society*, 6(34), pp.435–446.

Abou Neel, E.A., Chrzanowski, W. & Knowles, J.C., 2014. Biological performance of titania containing phosphate-based glasses for bone tissue engineering applications. *Materials science & engineering. C, Materials for biological applications*, 35, pp.307–13.

Abou Neel, E.A. & Knowles, J.C., 2008. Biocompatibility and other properties of phosphate-based glasses for medical applications. In L. Di Silvio, ed. *Cellular Response to Biomaterials*. Woodhead Publishing Ltd, pp. 156–178.

Abou Neel, E.A. & Knowles, J.C., 2008. Physical and biocompatibility studies of novel titanium dioxide doped phosphate-based glasses for bone tissue engineering applications. *Journal of Materials Science: Materials in Medicine*, 19(1), pp.377–386.

Amini, A.R., Laurencin, C.T. & Nukavarapu, S.P., 2012. Bone tissue engineering: recent advances and challenges. *Critical reviews in biomedical engineering*, 40(5), pp.363–408.

An, S., Gao, Y. & Ling, J., 2015. Characterization of human periodontal ligament cells cultured on three-dimensional biphasic calcium phosphate scaffolds in the presence and absence of L-ascorbic acid, dexamethasone and beta-glycerophosphate . *Experimental and therapeutic medicine*, 10(4), pp.1387–1393.

Andersson, H. & Berg, A. Van Den, 2004. Microfabrication and microfluidics for tissue engineering : state of the art and future opportunities. *Lab Chip*, 4, pp.98–103.

Andrews, R.E. et al., 2011. Effects of cobalt and chromium ions at clinically equivalent concentrations after metal-on-metal hip replacement on human osteoblasts and osteoclasts: Implications for skeletal health. *Bone*, 49(4), pp.717–723.

Antoni, D. et al., 2015. Three-Dimensional Cell Culture: A Breakthrough in Vivo. *International Journal of Molecular Sciences*, 16(3), pp.5517–5527.

Azevedo, M.M. et al., 2015. Hypoxia Inducible Factor-Stabilizing Bioactive Glasses for Directing Mesenchymal Stem Cell Behavior. *Tissue Engineering Part A*, 21(1-2), pp.382–389.

Azevedo, M.M. et al., 2010. Synthesis and characterization of hypoxia-mimicking bioactive glasses for skeletal regeneration. *Journal of Materials Chemistry*, 20(40), p.8854.

Bancroft, G.N. et al., 2002. Fluid flow increases mineralized matrix deposition in 3D perfusion culture of marrow stromal osteoblasts in a dose-dependent manner. *Proceedings of the National Academy of Sciences of the United States of America*, 99(20), pp.12600–5.

References

Banwart, J.C., Asher, M.A. & Hassanein, R.S., 1995. Iliac crest bone graft harvest donor site morbidity. A statistical evaluation. *Spine*, 20(9), pp.1055–60.

Barradas, A.M.C. et al., 2011. Osteoinductive biomaterials: current knowledge of properties, experimental models and biological mechanisms. *European cells & materials*, 21, pp.407–428.

Barrère, F., van Blitterswijk, C.A. & de Groot, K., 2006. Bone regeneration: Molecular and cellular interactions with calcium phosphate ceramics. *International Journal of Nanomedicine*, 1(3), pp.317–332.

Barrias, C.C. et al., 2005. Proliferation, activity, and osteogenic differentiation of bone marrow stromal cells cultured on calcium titanium phosphate microspheres. *Journal of Biomedical Materials Research - Part A*, 72(1), pp.57–66.

Bartel, R.L., 2014. Stem Cells and Cell Therapy: Autologous Cell Manufacturing. In A. Atala & J. Allickson, eds. *Translational Regenerative Medicine*. Elsevier Inc., pp. 107–112.

Beck, G.R., 2003. Inorganic phosphate as a signaling molecule in osteoblast differentiation. *Journal of Cellular Biochemistry*, 90(2), pp.234–243.

Berrey, B.H. et al., 1990. Fractures of allografts. Frequency, treatment, and end-results. *The Journal of bone and joint surgery. American volume*, 72(6), pp.825–833.

Berthier, E., Young, E.W.K. & Beebe, D., 2012. Engineers are from PDMS-land, Biologists are from Polystyrenia. *Lab on a Chip*, 12(7), pp.1224–1237.

Bettinger, C.J. & Borenstein, J.T., 2010. Biomaterials-based microfluidics for engineered tissue constructs. *Soft Matter*, 6(20), pp.4999–5015.

Bhatia, S.N. & Ingber, D.E., 2014. Microfluidic organs-on-chips. *Nature Biotechnology*, 32(8), pp.760–772.

Birgani, Z.T., Gharraee, N., et al., 2016. Combinatorial incorporation of fluoride and cobalt ions into calcium phosphates to stimulate osteogenesis and angiogenesis. *Biomedical Materials*, 11(1), p.015020.

Birgani, Z.T., Fennema, E., et al., 2016. Stimulatory effect of cobalt ions incorporated into calcium phosphate coatings on neovascularization in an in vivo intramuscular model in goats. *Acta Biomaterialia*, 36, pp.267–276.

Bissoyi, A. et al., 2014. Cryopreservation of hMSCs seeded silk nanofibers based tissue engineered constructs. *Cryobiology*, 68(3), pp.332–342.

Blow, N., 2007. Microfluidics: in search of a killer application. *Nature Methods*, 4(8), pp.665–670.

Blow, N., 2009. Microfluidics: the great divide. *Nature Methods*, 6(9), pp.683–686.

Boccaccini, A.R., Kneser, U. & Arkudas, A., 2012. Scaffolds for vascularized bone regeneration: advances and challenges. *Expert review of medical devices*, 9(5), pp.457–60.

Bose, S., Fielding, G., et al., 2013. Trace element doping in calcium phosphate ceramics to understand osteogenesis and angiogenesis. *Trends Biotechnol*, 18(9), pp.1199–1216.

References

Bose, S., Roy, M. & Bandyopadhyay, A., 2013. Recent Advances in Bone Tissue Engineering Scaffolds. *Trends Biotechnol*, 30(10), pp.546–554.

Botchwey, E.A. et al., 2001. Bone tissue engineering in a rotating bioreactor using a microcarrier matrix system. *Journal of Biomedical Materials Research*, 55(2), pp.242–253.

Bouet, G. et al., 2015. *In Vitro* Three-Dimensional Bone Tissue Models: From Cells to Controlled and Dynamic Environment. *Tissue Engineering Part B: Reviews*, 21(1), pp.133–156.

Boyde, a. et al., 1999. Osteoconduction in large macroporous hydroxyapatite ceramic implants: Evidence for a complementary integration and disintegration mechanism. *Bone*, 24(6), pp.579–589.

Brauer, D.S., 2012. Phosphate Glasses. In J. R. Jones & A. G. Clare, eds. *Bio-Glasses: An Introduction*. Chichester: John Wiley & Sons Ltd.

Brett, P.M. et al., 2004. Roughness response genes in osteoblasts. *Bone*, 35, pp.124–133.

Brighton, C.T. & Albelda, S.M., 1992. Identification of integrin cell-substratum adhesion receptors on cultured rat bone cells. *Journal of Orthopaedic Research*, 10(6), pp.766–73.

Brindley, D. et al., 2011. Bioprocess Forces and Their Impact on Cell Behavior: Implications for Bone Regeneration Therapy. *Journal of Tissue Engineering*, 2011(October), p.620247.

Bruder, S.P., Jaiswal, N. & Haynesworth, S.E., 1997. Growth kinetics, self-renewal, and the osteogenic potential of purified human mesenchymal stem cells during extensive subcultivation and following cryopreservation. *Journal of Cellular Biochemistry*, 64(2), pp.278–94.

Brydone, a S., Meek, D. & Maclaine, S., 2010. Bone grafting, orthopaedic biomaterials, and the clinical need for bone engineering. *Proceedings of the Institution of Mechanical Engineers. Part H, Journal of engineering in medicine*, 224(12), pp.1329–1343.

Buttyan, R. et al., 2003. Acute intravesical infusion of a cobalt solution stimulates a hypoxia response, growth and angiogenesis in the rat bladder. *The Journal of urology*, 169(6), pp.2402–2406.

Canadas, R.F.. et al., 2015. Cartilage and Bone Regeneration: How Close We Are to the Bedside? In L. J., B. P., & A. A., eds. *Translating Regenerative Medicine to the Clinic*. Academic Press, pp. 89–106.

Caplan, A., 1991. Mesenchymal stem cells. *Journal of orthopaedic research : official publication of the Orthopaedic Research Society*, 9(5), pp.641–50.

Catelas, I. et al., 2001. Cytotoxic and apoptotic effects of cobalt and chromium ions on J774 macrophages ± Implication of caspase-3 in the apoptotic pathway. *Journal of Materials Science : Materials in Medicine*, 12, pp.949–953.

Chai, Y.C. et al., 2014. In vivo ectopic bone formation by devitalized mineralized stem cell carriers produced under mineralizing culture condition. *BioResearch open access*, 3(6), pp.265–77.

References

Chamberlain, G. et al., 2007. Concise review: mesenchymal stem cells: their phenotype, differentiation capacity, immunological features, and potential for homing. *Stem cells (Dayton, Ohio)*, 25(11), pp.2739–49.

Chan, B.P. et al., 2010. Mesenchymal stem cell-encapsulated collagen microspheres for bone tissue engineering. *Tissue engineering. Part C, Methods*, 16(2), pp.225–235.

Chen, A.K.-L., Reuveny, S. & Oh, S.K.W., 2013. Application of human mesenchymal and pluripotent stem cell microcarrier cultures in cellular therapy: Achievements and future direction. *Biotechnology Advances*, 31(7), pp.1032–1046.

Chen, Q. & Thouas, G.A., 2015. Metallic implant biomaterials. *Materials Science and Engineering R: Reports*, 87, pp.1–57.

Clarke, B., 2008. Normal bone anatomy and physiology. *Clinical journal of the American Society of Nephrology : CJASN*, 3 Suppl 3, pp.S131–S139.

Clover, J. & Gowen, M., 1994. Are MG-63 and HOS TE85 human osteosarcoma cell lines representative models of the osteoblastic phenotype? *Bone*, 15(6), pp.585–591.

Cooke, A.M., 1955. Osteoporosis. *Lancet*, 265.

Costa, P.F. et al., 2012. Cryopreservation of cell/scaffold tissue-engineered constructs. *Tissue engineering. Part C, Methods*, 18(11), pp.852–8.

Coutinho, D. et al., 2011. Micro- and nano technology in tissue engineering. In P. Norbert & C. V. Suscheck, eds. *Tissue Engineering: from lab to clinic*. Springer Berlin Heidelberg, pp. 3–29.

Czekanska, E.M. et al., 2012. In search of an osteoblast cell model for in vitro research. *European Cells and Materials*, 24, pp.1–17.

David, B., Bemsidhoum, M. & Potier, E., 2007. Bone Tissue Engineering. In J. J. Mao et al., eds. *Translational Approaches in Tissue Engineering and Regenerative Medicine*. Artech House Publishers.

Davies, J.E., 1996. In vitro modeling of the bone/implant interface. *Anatomical Record*, 245(2), pp.426–445.

Declercq, H. et al., 2004. Isolation, proliferation and differentiation of osteoblastic cells to study cell/biomaterial interactions: Comparison of different isolation techniques and source. *Biomaterials*, 25(5), pp.757–768.

Delloye, C. et al., 2007. Bone allografts: What they can offer and what they cannot. *The Journal of bone and joint surgery. British volume*, 89(5), pp.574–579.

Digirolamo, C.M. et al., 1999. Propagation and senescence of human marrow stromal cells in culture: A simple colony-forming assay identifies samples with the greatest potential to propagate and differentiate. *British Journal of Haematology*, 107(2), pp.275–281.

Dimitriou, R. et al., 2011. Complications following autologous bone graft harvesting from the iliac crest and using the RIA: A systematic review. *Injury*, 42(SUPPL. 2), pp.S3–S15.

Discacciati, M. et al., 2013. Numerical simulation of orbitally shaken viscous fluids with free surface. *International Journal for Numerical Methods in Fluids*, 71(3), pp.294–315.

Dominici, M. et al., 2006. Minimal criteria for defining multipotent mesenchymal stromal cells. The International Society for Cellular Therapy position statement. *Cytotherapy*, 8(4), pp.315–7.

Drager, J., Harvey, E.J. & Barralet, J., 2015. Hypoxia signalling manipulation for bone regeneration. *Expert reviews in molecular medicine*, 17(e6), pp.1–16.

Duncombe, T. a., Tentori, A.M. & Herr, A.E., 2015. Microfluidics: reframing biological enquiry. *Nature Reviews Molecular Cell Biology*, 16(9), pp.554–567.

Dutt, K. et al., 2003. Three-dimensional model of angiogenesis: coculture of human retinal cells with bovine aortic endothelial cells in the NASA bioreactor. *Tissue engineering*, 9(5), pp.893–908.

Ebraheim, N. a, Elgafy, H. & Xu, R., 2001. Bone-graft harvesting from iliac and fibular donor sites: techniques and complications. *The Journal of the American Academy of Orthopaedic Surgeons*, 9(3), pp.210–218.

Epstein, N.E., 2011. Pros, cons, and costs of INFUSE in spinal surgery. *Surgical neurology international*, 2, p.10.

Fan, W., Crawford, R. & Xiao, Y., 2010. Enhancing in vivo vascularized bone formation by cobalt chloride-treated bone marrow stromal cells in a tissue engineered periosteum model. *Biomaterials*, 31(13), pp.3580–3589.

Fazzalari, N.L., 2011. Bone Fracture and bone fracture repair. *Osteoporosis International*, 22(6), pp.2003–2006.

Fleury, C. et al., 2006. Effect of cobalt and chromium ions on human MG-63 osteoblasts in vitro: Morphology, cytotoxicity, and oxidative stress. *Biomaterials*, 27(18), pp.3351–3360.

FluidicMEMs, 2015. FluidicMEMS - List of Microfluidics Companies. Available at: http://fluidicmems.com/list-of-microfluidics-lab-on-a-chip-and-biomems-companies/ [Accessed January 20, 2016].

Fluxion, 2016. BIOFLUX SYSTEMS: In-vivo Conditions for Live Cell Assays. Available at: http://fluxionbio.com/bioflux/[Accessed January 20, 2016].

Frauenschuh, S. et al., 2007. A microcarrier-based cultivation system for expansion of primary mesenchymal stem cells. *Biotechnology Progress*, 23(1), pp.187–193.

Friedenstein, A.J., Chailakhjan, R.K. & Lalykina, K.S., 1970. The development of fibroblast colonies in monolayer cultures of guinea-pig bone marrow and spleen cells. *Cell and tissue kinetics*, 3(4), pp.393–403.

Friedenstein, A.J., Gorskaja, J.F. & Kulagina, N.N., 1976. Fibroblast precursors in normal and irradiated mouse hematopoietic organs. *Experimental hematology*, 4(5), pp.267–74.

Gottwald, E. et al., 2007. A chip-based platform for the in vitro generation of tissues in three-dimensional organization. *Lab on a chip*, 7(6), pp.777–85.

Granero-Molto, F. et al., 2008. Role of mesenchymal stem cells in regenerative medicine: application to bone and cartilage repair. *Expert opinion on biological therapy*, 8(3), pp.255–268.

Grayson, W.L. et al., 2006. Effects of Hypoxia on Human Mesenchymal Stem Cell Expansion and Plasticity in 3D Constructs. *Journal of cellular physiology*, 207(1), pp.12–22.

Grayson, W.L. et al., 2008. Effects of initial seeding density and fluid perfusion rate on formation of tissue-engineered bone. *Tissue engineering. Part A*, 14(11), pp.1809–20.

Grayson, W.L. et al., 2015. Stromal cells and stem cells in clinical bone regeneration. *Nature Reviews Endocrinology*, 11(3), pp.140–150.

Greenwald, a S. et al., 2001. Bone-graft substitutes: facts, fictions, and applications. *The Journal of bone and joint surgery. American volume*, 83-A Suppl, pp.98–103.

Grist, S.M., Chrostowski, L. & Cheung, K.C., 2010. Optical oxygen sensors for applications in microfluidic cell culture. *Sensors (Basel)*, 10(10), pp.9286–9316.

Guedes, J.C. et al., 2013. TiO(2)-doped phosphate glass microcarriers: a stable bioactive substrate for expansion of adherent mammalian cells. *Journal of Biomaterials Applications*, 28(1), pp.3–11.

Guldberg, R.E., 2009. Spatiotemporal delivery strategies for promoting musculoskeletal tissue regeneration. *Journal of bone and mineral research : the official journal of the American Society for Bone and Mineral Research*, 24(9), pp.1507–11.

Guldberg, R.E., Boerckel, C.R. & Dosier, C.R., 2007. Translational Approaches for Engineering Bone Repair. In J. J. Mao et al., eds. *Translational Approaches in Tissue Engineering and Regenerative Medicine*. Artech House Publishers.

Hadjidakis, D.J. & Androulakis, I.I., 2006. Bone remodeling. In *Annals of the New York Academy of Sciences*. pp. 385–396.

El Haj, a J. & Cartmell, S.H., 2010. Bioreactors for bone tissue engineering. *Proceedings of the Institution of Mechanical Engineers. Part H, Journal of engineering in medicine*, 224(May), pp.1523–1532.

Halldorsson, S. et al., 2015. Advantages and challenges of microfluidic cell culture in polydimethylsiloxane devices. *Biosensors and Bioelectronics*, 63, pp.218–231.

Hambor, J.E., 2012. Bioreactor design and bioprocess controls for industrialized cell processing: Bioengineering strategies and platform technologies. *BioProcess International*, 10(6), pp.22–33.

Hass, R. et al., 2011. Different populations and sources of human mesenchymal stem cells (MSC): A comparison of adult and neonatal tissue-derived MSC. *Cell communication and signaling : CCS*, 9(1), p.12.

Hench, L.L., 2011. Bioactive materials for gene control. In L. L. Hench, J. R. Jones, & M. B. Fenn, eds. *New materials and technologies for healthcare*. Singapore World Scientific, pp. 25–48.

Hench, L.L., 2006. The story of Bioglass. *Journal of Materials Science: Materials in Medicine*, 17(11), pp.967–978.

Hench, L.L., Xynos, I.D. & Polak, J.M., 2004. Bioactive glasses for in situ tissue regeneration. *Journal of Biomaterials Science, Polymer Edition*, 15(4), pp.543–562.

Hernigou, P. et al., 2005. Percutaneous Autologous Bone-Marrow Grafting for Nonunions INFLUENCE OF THE NUMBER AND CONCENTRATION OF PROGENITOR CELLS. *The Journal of bone and joint surgery.*, pp.1430–1437.

Hervy, M. et al., 2014. Long term expansion of bone marrow-derived hMSCs on novel synthetic microcarriers in xeno-free, defined conditions. *PLoS ONE*, 9(3), pp.1–7.

Hewitt, C.J. et al., 2011. Expansion of human mesenchymal stem cells on microcarriers. *Biotechnology Letters*, 33(11), pp.2325–2335.

Hidalgo-Bastida, L.A. & Cartmell, S.H., 2010. Mesenchymal Stem Cells, Osteoblasts and Extracellular Matrix Proteins: Enhancing Cell Adhesion and Differentiation for Bone Tissue Engineering. , 16(4), pp.405–412.

Higuera, G. a et al., 2012. Patterns of amino acid metabolism by proliferating human mesenchymal stem cells. *Tissue engineering. Part A*, 18(5-6), pp.654–64.

Ho, C.M.B. et al., 2015. 3D printed microfluidics for biological applications. *Lab On A Chip*, 15(18), pp.3627–3637.

Hollister, S.J. & Murphy, W.L., 2011. Scaffold Translation: Barriers Between Concept and Clinic. *Tissue Engineering Part B: Reviews*, 17(6), pp.459–474.

Holtorf, H.L. et al., 2005. Flow perfusion culture of marrow stromal cells seeded on porous biphasic calcium phosphate ceramics. In *Annals of Biomedical Engineering*. pp. 1238–1248.

Hong, S.J., Yu, H.S. & Kim, H.W., 2009. Preparation of porous bioactive ceramic microspheres and in vitro osteoblastic culturing for tissue engineering application. *Acta Biomaterialia*, 5(5), pp.1725–1731.

Hoppe, A., Güldal, N.S. & Boccaccini, A.R., 2011. A review of the biological response to ionic dissolution products from bioactive glasses and glass-ceramics. *Biomaterials*, 32(11), pp.2757–74.

Hossain, K.M.Z., Patel, U. & Ahmed, I., 2014. Development of microspheres for biomedical applications: a review. *Progress in Biomaterials*, 4(1), pp.1–19.

Hsu, S.-H., Chen, C.-T. & Wei, Y.-H., 2013. Inhibitory effects of hypoxia on metabolic switch and osteogenic differentiation of human mesenchymal stem cells. *Stem cells (Dayton, Ohio)*, 31(12), pp.2779–88.

Huh, D., Hamilton, G. a. & Ingber, D.E., 2011. From 3D cell culture to organs-on-chips. *Trends in Cell Biology*, 21(12), pp.745–754.

Ignjatovic et al., 2015. Enhanced Osteogenesis of Nanosized Cobalt-substituted Hydroxyapatite. , 12, pp.604–612.

Ignjatović, N. et al., 2013. Nanoparticles of cobalt-substituted hydroxyapatite in regeneration of mandibular osteoporotic bones. *Journal of Materials Science: Materials in Medicine*, 24, pp.343–354.

Inamdar, N.K. & Borenstein, J.T., 2011. Microfluidic cell culture models for tissue engineering. *Current Opinion in Biotechnology*, 22(5), pp.681–689.

Jang, K. et al., 2008. Development of an osteoblast-based 3D continuous-perfusion microfluidic system for drug screening. *Analytical and Bioanalytical Chemistry*, 390(3), pp.825–832.

Jin, G.Z. et al., 2012. Performance of evacuated calcium phosphate microcarriers loaded with mesenchymal stem cells within a rat calvarium defect. *Journal of Materials Science: Materials in Medicine*, 23(7), pp.1739–1748.

Jones, J.R., 2015. Reprint of: Review of bioactive glass: From Hench to hybrids. *Acta Biomaterialia*, 23(S), pp.S53–S82.

Joshi, S., Gowda, A.S. & Joshi, C., 2013. Comparative evaluation of NovaMin desensitizer and Gluma desensitizer on dentinal tubule occlusion: A scanning electron microscopic study. *Journal of Periodontal and Implant Science*, 43(6), pp.269–275.

Jusoh, N. et al., 2015. Microfluidic vascularized bone tissue model with hydroxyapatite-incorporated extracellular matrix. *Lab Chip*, 15(20), pp.3984–3988.

Kadiyala, S., Jaiswal, N. & Bruder, S.P., 1997. Culture-Expanded, Bone Marrow-Derived Mesenchymal Stem Cells Can Regenerate a Critical-Sized Segmental Bone Defect. *Tissue Eng*, 3(2), pp.173–185.

Kaigler, D. et al., 2006. VEGF scaffolds enhance angiogenesis and bone regeneration in irradiated osseous defects. *Journal of bone and mineral research : the official journal of the American Society for Bone and Mineral Research*, 21(5), pp.735–744.

Karageorgiou, V. & Kaplan, D., 2005. Porosity of 3D biomaterial scaffolds and osteogenesis. *Biomaterials*, 26(27), pp.5474–5491.

Kasper, C. et al., 2007. A Newly Developed Rotating Bed Bioreactor for Bone Tissue Engineering. *Topics in Tissue Engineering*, 3, pp.1–15.

Kassem, M. et al., 1997. Demonstration of cellular aging and senescence in serially passaged long-term cultures of human trabecular osteoblasts. *Osteoporosis international*, 7(6), pp.514–24.

Keating, A., 2012. Mesenchymal stromal cells: New directions. *Cell Stem Cell*, 10(6), pp.709–716.

Kiani, A. et al., 2012. Titanium-containing bioactive phosphate glasses. *Philosophical Transactions of the Royal Society A: Mathematical, Physical and Engineering Sciences*, pp.1352–1375.

Kim, P. et al., 2008. Soft Lithography for Microfluidics : a Review. *Biochip Journal*, 2(1), pp.1–11.

Kinney, M.A., Sargent, C.Y. & McDevitt, T.C., 2011. The multiparametric effects of hydrodynamic environments on stem cell culture. *Tissue engineering. Part B, Reviews*, 17(4), pp.249–262.

Kirkstall, 2016a. QV500 Cell Culture Chamber. Available at: http://kirkstall.org/index.php/qv500-cell-culture-chamber/ [Accessed February 2, 2016].

Kirkstall, 2016b. QV900 Cell Culture 6-Chamber Tray. Available at: http://kirkstall.org/index.php/qv900-cell-culture-6-chamber-tray/ [Accessed February 2, 2016].

Kitoh, H. et al., 2009. Differential effects of culture-expanded bone marrow cells on the regeneration of bone between the femoral and the tibial lengthenings. *Journal of pediatric orthopedics*, 29(6), pp.643–649.

Klöckner, W. & Büchs, J., 2012. Advances in shaking technologies. *Trends in Biotechnology*, 30(6), pp.307–314.

Knowles, J.C., 2003. Phosphate based glasses for biomedical applications. *Journal of Materials Chemistry*, 13(10), p.2395.

Kofron, M.D. et al., 2003. Cryopreservation of tissue engineered constructs for bone. *Journal of Orthopaedic Research*, 21(6), pp.1005–1010.

Kon, E. et al., 2000. Autologous bone marrow stromal cells loaded onto porous hydroxyapatite ceramic accelerate bone repair in critical-size defects of sheep long bones. *Journal of Biomedical Materials Research*, 49(3), pp.328–337.

Korossis, A. et al., 2005. Bioreactors in Tissue Engineering. In N. Ashammakhi & R. L. Reis, eds. *Topics in Tissue Engineering, Volume II*.

Kou, D. et al., 2016. Centimeter-sized biomimetic bone constructs fabricated via CBD-BMP2-collagen microcarriers and BMSC-gelatin microspheres. *J. Mater. Chem. B*, 4(3), pp.461–470.

Kou, S. et al., 2011. A multishear microfluidic device for quantitative analysis of calcium dynamics in osteoblasts. *Biochemical and Biophysical Research Communications*, 408(2), pp.350–355.

Kuleshova, L.L., Gouk, S.S. & Hutmacher, D.W., 2007. Vitrification as a prospect for cryopreservation of tissue-engineered constructs. *Biomaterials*, 28(9), pp.1585–1596.

Kuznetsov, S.A. et al., 2001. Circulating skeletal stem cells. *Journal of Cell Biology*, 153(5), pp.1133–1139.

Lakhkar, N.J. et al., 2013. Bone formation controlled by biologically relevant inorganic ions: Role and controlled delivery from phosphate-based glasses. *Advanced drug delivery reviews*, 65(4), pp.405–20.

Lakhkar, N.J., 2014. *Phosphate Glass Microspheres as Cell Microcarrier Substrates for Bone Tissue Engineering Applications*. University College London.

Lakhkar, N.J. et al., 2015. Titanium phosphate glass microcarriers induce enhanced osteogenic cell proliferation and human mesenchymal stem cell protein expression. *Journal of tissue engineering*, 6, pp.1–14.

Lakhkar, N.J. et al., 2012. Titanium phosphate glass microspheres for bone tissue engineering. *Acta biomaterialia*, 8(11), pp.4181–90.

Langer, R. & Vacanti, J.P., 1993. Tissue Engineering. *Science*, 260, pp.920–926.

Lara, A.R. et al., 2006. Living with heterogeneities in bioreactors. *Molecular Biotechnology*, 34(3), pp.355–381.

Leclerc, E. et al., 2006. Study of osteoblastic cells in a microfluidic environment. *Biomaterials*, 27(4), pp.586–595.

Lee, I.-H. et al., 2013. Development, characterisation and biocompatibility testing of a cobalt-containing titanium phosphate-based glass for engineering of vascularized hard tissues. *Materials Science and Engineering: C*, 33(4), pp.2104–2112.

Lee, J.H. et al., 2014. Biointerface control of electrospun fiber scaffolds for bone regeneration: Engineered protein link to mineralized surface. *Acta Biomaterialia*, 10(6), pp.2750–2761.

Lee, J.H. et al., 2013. Tethering bi-functional protein onto mineralized polymer scaffolds to regulate mesenchymal stem cell behaviors for bone regeneration. *Journal of Materials Chemistry B*, 1(21), p.2731.

Lee, J.-H. et al., 2012. Microfluidic 3D bone tissue model for high-throughput evaluation of wound-healing and infection-preventing biomaterials. *Biomaterials*, 33(4), pp.999–1006.

Lee, J.-H. et al., 2011. Microfluidic Approach to Create Three-Dimensional Tissue Models for Biofilm-Related Infection of Orthopaedic Implants. *Tissue Engineering Part C: Methods*, 17(1), pp.39–48.

Lee, K. et al., 2009. Cell therapy for bone regeneration--bench to bedside. *Journal of biomedical materials research. Part B, Applied biomaterials*, 89(1), pp.252–263.

Lee, M.H. et al., 2010. Considerations for tissue-engineered and regenerative medicine product development prior to clinical trials in the United States. *Tissue engineering. Part B, Reviews*, 16(1), pp.41–54.

Li, L. & Xie, T., 2005. Stem cell niche: structure and function. *Annual review of cell and developmental biology*, 21(1), pp.605–631.

Li, X.J. et al., 2012. Microfluidic 3D cell culture: potential application for tissue-based bioassays. *Bioanalysis*, 4(12), pp.1509–25.

Lian, J.B. & Stein, G.S., 1995. Development of the osteoblast phenotype: molecular mechanisms mediating osteoblast growth and differentiation. *The Iowa orthopaedic journal*, 15, pp.118–40.

Lindner, U. et al., 2010. Mesenchymal Stem or Stromal Cells: Toward a Better Understanding of Their Biology? *Transfusion medicine and hemotherapy : offizielles Organ der Deutschen Gesellschaft fur Transfusionsmedizin und Immunhamatologie*, 37(2), pp.75–83.

Liu, J.S. & Gartner, Z.J., 2012. Directing the assembly of spatially organized multicomponent tissues from the bottom up. *Trends in Cell Biology*, 22(12), pp.683–691.

Liu, N. et al., 2014. Stem cell engineering in bioreactors for large-scale bioprocessing. *Engineering in Life Sciences*, 14(1), pp.4–15.

Liu, Y., Lim, J. & Teoh, S.H., 2013. Review: Development of clinically relevant scaffolds for vascularised bone tissue engineering. *Biotechnology Advances*, 31(5), pp.688–705.

Logeart-Avramoglou, D. et al., 2005. Engineering bone: challenges and obstacles. *Journal of cellular and molecular medicine*, 9(1), pp.72–84.

Lovett, M. et al., 2009. Vascularization strategies for tissue engineering. *Tissue engineering. Part B, Reviews*, 15(3), pp.353–70.

Lum, J.J. et al., 2007. The transcription factor HIF-1alpha plays a critical role in the growth factor-dependent regulation of both aerobic and anaerobic glycolysis. *Genes & development*, 21(9), pp.1037–1049.

Ma, J. et al., 2014. Concise review: cell-based strategies in bone tissue engineering and regenerative medicine. *Stem cells translational medicine*, 3(1), pp.98–107.

Maeno, S. et al., 2005. The effect of calcium ion concentration on osteoblast viability, proliferation and differentiation in monolayer and 3D culture. *Biomaterials*, 26(23), pp.4847–4855.

Malda, J. & Frondoza, C.G., 2006. Microcarriers in the engineering of cartilage and bone. *Trends in Biotechnology*, 24(7), pp.299–304.

Marcacci, M. et al., 2007. Stem cells associated with macroporous bioceramics for long bone repair: 6-to 7-year outcome of a pilot clinical study. *Tissue Engineering*, 13(5), pp.947–955.

Marolt, D. et al., 2006. Bone and cartilage tissue constructs grown using human bone marrow stromal cells, silk scaffolds and rotating bioreactors. *Biomaterials*, 27(36), pp.6138–6149.

Martin, J.Y. et al., 1995. Effect of Titanium Surface Roughness on Proliferation, Differentiation, and Protein Synthesis of Human Osteoblast-Like Cells (MG63). *J Biomed Mater Res*, 29(3), pp.389–401.

Martin, Y. et al., 2011. Microcarriers and their potential in tissue regeneration. *Tissue engineering. Part B, Reviews*, 17(1), pp.71–80.

Mason, C. & Dunnill, P., 2011. A brief definition of regenerative medicine. *Future Medicine*, 18(5), pp.243–245.

Mason, C. & Hoare, M., 2007. Regenerative medicine bioprocessing: building a conceptual framework based on early studies. *Tissue engineering*, 13(2), pp.301–311.

Mei, Y., Luo, H., Tang, Q., Ye, Z., Zhou, Y. & Tan, W.S., 2010. Modulating and modeling aggregation of cell-seeded microcarriers in stirred culture system for macrotissue engineering. *Journal of Biotechnology*, 150(3), pp.438–446.

Mei, Y., Luo, H., Tang, Q., Ye, Z., Zhou, Y. & Tan, W.-S., 2010. Modulating and modeling aggregation of cell-seeded microcarriers in stirred culture system for macrotissue engineering. *Journal of Biotechnology*, 150, pp.438–446.

Meijer, G.J. et al., 2008. Cell based bone tissue engineering in jaw defects. *Biomaterials*, 29(21), pp.3053–3061.

Merten, O.-W., 2015. Advances in cell culture: anchorage dependence. *Philosophical transactions of the Royal Society of London. Series B, Biological sciences*, 370(1661), p.20140040.

Micheletti, M. & Lye, G.J., 2006. Microscale bioprocess optimisation. *Current Opinion in Biotechnology*, 17(6), pp.611–618.

Millipore, M., 2016. CellASIC® ONIX Microfluidic Plates. Available at: https://www.merckmillipore.com/GB/en/life-science-research/cell-culture-systems/cellASIC-live-cell-analysis/microfluidic-plates/68eb.qB.wfkAAAFBWmVb3.sJ,nav?bd=1 [Accessed January 20, 2016].

Mitra, J. et al., 2013. Scaffolds for bone tissue engineering: role of surface patterning on osteoblast response. *RSC Advances*, 3(28), p.11073.

Monahan, J., Gewirth, a. a. & Nuzzo, R.G., 2001. A method for filling complex polymeric microfluidic devices and arrays. *Analytical Chemistry*, 73(13), pp.3193–3197.

Morishita, T. et al., 2006. Tissue engineering approach to the treatment of bone tumors: three cases of cultured bone grafts derived from patients' mesenchymal stem cells. *Artif Organs*, 30(2), pp.115–118.

Müller, P. et al., 2008. Calcium phosphate surfaces promote osteogenic differentiation of mesenchymal stem cells. *Journal of Cellular and Molecular Medicine*, 12(1), pp.281–291.

Narayan, R.J., 2010. The next generation of biomaterial development. *Philosophical Transactions of the Royal Society A: Mathematical, Physical and Engineering Sciences*.

Navarro, M. et al., 2003. Physicochemical Degradation of Titania-Stabilized Soluble Phosphate Glasses for Medical Applications. *Journal of the American Ceramic Society*, 86(8), pp.1345–1352.

Neuhaus, K.W. et al., 2013. Effectiveness of a calcium sodium phosphosilicate containing prophylaxis paste in reducing dentine hypersensitivity immediately and 4 weeks after a single application: A double-blind randomized controlled trial. *Journal of Clinical Periodontology*, 40(4), pp.349–357.

Nge, P.N., Rogers, C.I. & Woolley, A.T., 2013. Advances in microfluidic materials, functions, integration, and applications. *Chemical Reviews*, 113(4), pp.2550–2583.

Nichol, J.W. & Khademhosseini, A., 2010. Modular tissue engineering: engineering biological tissues from the bottom up. *Soft Matters*, 5(7), pp.1312–1319.

Novajra, G. et al., 2011. Effects of TiO2-containing phosphate glasses on solubility and in vitro biocompatibility. *Journal of Biomedical Materials Research - Part A*, 99 A(2), pp.295–306.

Osathanon, T. et al., 2015. Cobalt chloride supplementation induces stem-cell marker expression and inhibits osteoblastic differentiation in human periodontal ligament cells. *Archives of oral biology*, 60(1), pp.29–36.

Paguirigan, A.L. & Beebe, D.J., 2009. From the cellular perspective: exploring differences in the cellular baseline in macroscale and microfluidic cultures. *Integrative Biology*, 1(2), p.182.

Panchalingam, K.M. et al., 2015. Bioprocessing strategies for the large-scale production of human mesenchymal stem cells: a review. *Stem Cell Research & Therapy*, 6(1), p.225.

Park, J.-H. et al., 2013. Microcarriers designed for cell culture and tissue engineering of bone. *Tissue engineering. Part B, Reviews*, 19(2), pp.172–90.

Pasirayi, G. et al., 2011. Microfluidic Bioreactors for Cell Culturing: A Review. *Micro and Nanosystems*, 3, pp.137–160.

Patel, A. & Knowles, J.C., 2006. Investigation of silica-iron-phosphate glasses for tissue engineering. *Journal of Materials Science: Materials in Medicine*, 17(10), pp.937–944.

Patntirapong, S., Habibovic, P. & Hauschka, P. V., 2009. Effects of soluble cobalt and cobalt incorporated into calcium phosphate layers on osteoclast differentiation and activation. *Biomaterials*, 30(4), pp.548–555.

Peerani, R. & Zandstra, P.W., 2010. Review series Enabling stem cell therapies through synthetic stem cell – niche engineering. *Strategies*, 120(1), pp.60–70.

Perez, R.A. et al., 2014. Dynamic cell culture on calcium phosphate microcarriers for bone tissue engineering applications. *Journal of tissue engineering*, 5, pp.1–10.

Perez, R.A. et al., 2015. Therapeutically relevant aspects in bone repair and regeneration. *Materials Today*, 18(10), pp.573–589.

Peters, K. et al., 2005. Paradoxical effects of hypoxia-mimicking divalent cobalt ions in human endothelial cells in vitro. *Molecular and Cellular Biochemistry*, 270(1-2), pp.157–166.

Pipino, C. & Pandolfi, A., 2015. Osteogenic differentiation of amniotic fluid mesenchymal stromal cells and their bone regeneration potential. *World journal of stem cells*, 7(4), pp.681–90.

Price, N. et al., 1997. Human osteoblast-like cells (MG63) proliferate on a bioactive glass surface. *Journal of biomedical materials research*, 37(3), pp.394–400.

Qiu, Q. et al., 2007. Formation and Differentiation of Three-Dimensional Rat Marrow Stromal Cell Culture on Microcarriers in a Rotating-Wall Vessel. *Tissue Engineering*, 4(1), pp.19–34.

Quarto, R. et al., 2001. Repair of large bone defects with the use of autologous bone marrow stromal cells. *The New England Journal of Medicine*, pp.385–386.

Quinlan, E. et al., 2015. Hypoxia-mimicking bioactive glass/collagen glycosaminoglycan composite scaffolds to enhance angiogenesis and bone repair. *Biomaterials*, 52, pp.358–366.

Ratcliffe, E., Thomas, R.J. & Williams, D.J., 2011. Current understanding and challenges in bioprocessing of stem cell-based therapies for regenerative medicine. *British medical bulletin*, 100, pp.137–55.

Rauh, J. et al., 2011. Bioreactor systems for bone tissue engineering. *Tissue engineering. Part B, Reviews*, 17(4), pp.263–280.

Regehr, K.J. et al., 2009. Biological implications of polydimethylsiloxane-based microfluidic cell culture. *Lab Chip*, 9(15), pp.2132–2139.

Reinnervate, 2016. Reinnervate Perfusion Plate: Dynamic Circulation and Perfusion of Culture Medium Within a Multi-welled Plate. Available at: http://reinnervate.com/alvetex/science-portals/science-portal-perfused-3d-cell-culture/ [Accessed January 26, 2016].

Ribatti, D., 2012. Chicken chorioallantoic membrane angiogenesis model. *Methods in molecular biology*, 843, pp.47–57.

Riddle, R.C. et al., 2006. MAP kinase and calcium signaling mediate fluid flow-induced human mesenchymal stem cell proliferation. *American journal of physiology. Cell physiology*, 290(3), pp.C776–84.

Riehl, B.D. & Lim, J.Y., 2012. Macro and microfluidic flows for skeletal regenerative medicine. *Cells*, 1(4), pp.1225–1245.

Rodrigues, C.A. V et al., 2011. Stem cell cultivation in bioreactors. *Biotechnology Advances*, 29(6), pp.815–829.

Rowley, J.A., 2010. Developing Cell Therapy Biomanufacturing Processes. *Chemical Engineering Progress*, 106(11), pp.50–55.

Sadat-Shojai, M. et al., 2013. Nano-hydroxyapatite reinforced polyhydroxybutyrate composites: A comprehensive study on the structural and in vitro biological properties. *Materials Science and Engineering C*, 33(5), pp.2776–2787.

Salgado, A.J., Coutinho, O.P. & Reis, R.L., 2004. Bone tissue engineering: State of the art and future trends. *Macromol. Biosci.*, 4(8), pp.743–765.

Salter, E. et al., 2012. Bone Tissue Engineering Bioreactors: A Role in the Clinic? *Tissue Engineering Part B: Reviews*, 18(1), pp.62–75.

Sanzana, E.S. et al., 2008. Of the in vivo behavior of calcium phosphate cements and glasses as bone substitutes. *Acta Biomaterialia*, 4(6), pp.1924–1933.

Sart, S., Agathos, S.N. & Li, Y., 2013. Engineering stem cell fate with biochemical and biomechanical properties of microcarriers. *Biotechnology Progress*, 29(6), pp.1354–1366.

Scaled Biolabs, 2017. Scaled Biolabs: Accelarating Discovery. Available at: http://www.scaledbiolabs.com/ [Accessed January 4, 2017].

Schipani, E. et al., 2009. Regulation of osteogenesis-angiogenesis coupling by HIFs and VEGF. *Journal of Bone and Mineral Research*, 24(8), pp.1347–53.

Schliephake, H. et al., 2001. Use of cultivated osteoprogenitor cells to increase bone formation in segmental mandibular defects: an experimental pilot study in sheep. *International journal of oral and maxillofacial surgery*, 30(6), pp.531–537.

Shang, Q. et al., 2001. Tissue-engineered bone repair of sheep cranial defects with autologous bone marrow stromal cells. *The Journal of craniofacial surgery*, 12(6), pp.586–93; discussion 594–5.

Shi, S. & Gronthos, S., 2003. Perivascular niche of postnatal mesenchymal stem cells in human bone marrow and dental pulp. *J Bone Miner Res*, 18(4), pp.696–704.

Shih, Y.-R. V et al., 2014. Calcium phosphate-bearing matrices induce osteogenic differentiation of stem cells through adenosine signaling. *Proceedings of the National Academy of Sciences of the United States of America*, 111(3), pp.990–5.

Shrivats, A.R., McDermott, M.C. & Hollinger, J.O., 2014. Bone tissue engineering: State of the union. *Drug Discovery Today*, 19(6), pp.781–786.

Sikavitsas, V.I. et al., 2003. Mineralized matrix deposition by marrow stromal osteoblasts in 3D perfusion culture increases with increasing fluid shear forces. *Proceedings of the National Academy of Sciences of the United States of America*, 100(25), pp.14683–14688.

Simonsen, L.O., Harbak, H. & Bennekou, P., 2012. Cobalt metabolism and toxicology-A brief update. *Science of the Total Environment*, 432, pp.210–215.

Smith, B.D. & Grande, D. a, 2015. The current state of scaffolds for musculoskeletal regenerative applications. *Nat Rev Rheumatol*, 11(4), pp.213–222.

Sofla, A., 2013. A manufacturer's 2 cents on developing microfluidic products. Available at: http://ufluidix.com/2013/12/10/blogpost/ [Accessed January 10, 2016].

St John, T.A. et al., 2003. Physical and monetary costs associated with autogenous bone graft harvesting. *American journal of orthopedics (Belle Mead, N.J.)*, 32(1), pp.18–23.

Steinbrech, D.S. et al., 2000. VEGF expression in an osteoblast-like cell line is regulated by a hypoxia response mechanism. *American Journal of Physiology- Cell Physiology*, 278(4), pp.C853–60.

Tang, S. & Whitesides, G., 2010. Basic microfluidic and soft lithographic techniques. In Y. Fainman et al., eds. *Optofluidics: Fundamentals, Devices, and Applications*. McGraw-Hill Education, pp. 7–32.

Thomas, R.J., Hourd, P.C. & Williams, D.J., 2008. Application of process quality engineering techniques to improve the understanding of the in vitro processing of stem cells for therapeutic use. *Journal of Biotechnology*, 136(3-4), pp.148–155.

Titmarsh, D.M. et al., 2013. Arrayed cellular environments for stem cells and regenerative medicine. *Biotechnology Journal*, 8(2), pp.167–179.

Titmarsh, D.M. et al., 2014. Concise review: microfluidic technology platforms: poised to accelerate development and translation of stem cell-derived therapies. *Stem cells translational medicine*, 3(1), pp.81–90.

Titmarsh, D.M. et al., 2013. Full factorial screening of human embryonic stem cell maintenance with multiplexed microbioreactor arrays. *Biotechnology journal*, 8(7), pp.822–34.

Titmarsh, D.M. et al., 2012. Microbioreactor arrays for full factorial screening of exogenous and paracrine factors in human embryonic stem cell differentiation. *PloS one*, 7(12), p.e52405.

Tseng, P.-C. et al., 2012. Spontaneous osteogenesis of MSCs cultured on 3D microcarriers through alteration of cytoskeletal tension. *Biomaterials*, 33(2), pp.556–564.

Viti, F. et al., 2016. Osteogenic differentiation of MSC through calcium signaling activation: Transcriptomics and functional analysis. *PLoS ONE*, 11(2), pp.1–21.

Volpatti, L.R. & Yetisen, A.K., 2014. Commercialization of microfluidic devices. *Trends in Biotechnology*, 32(7), pp.347–350.

Wagers, A.J., 2012. The stem cell niche in regenerative medicine. *Cell Stem Cell*, 10(4), pp.362–369.

Wagner, R., 1997. Metabolic Control of Animal Cell Culture Processed. In H. Hauser & R. Wagner, eds. *Mammalian Cell Biotechnology in Protein Production*. Berlin: Walter de Gruiter.

Wall, I. et al., 2009. Modified titanium surfaces promote accelerated osteogenic differentiation of mesenchymal stromal cells in vitro. *Bone*, 45(1), pp.17–26.

Wall, I.B. & Brindley, D.A., 2013. Commercial Manufacture of Cell Therapies. In V. Salih, ed. *Standardisation in Cell and Tissue Engineering*. Woodhead Publishing Ltd, pp. 212–239.

Wang, Y. et al., 2007. The hypoxia-inducible factor-a pathway couples angiogenesis to osteogenesis during skeletal development. *Journal of Clinical Investigation*, 117(6), pp.1616–1626.

Weber, C. et al., 2010. Expansion of human mesenchymal stem cells in a fixed-bed bioreactor system based on non-porous glass carrier - Part A: Inoculation, cultivation, and cell harvest procedures. *International Journal of Artificial Organs*, 33(11), pp.782–795.

Weheliye, W., Yianneskis, M. & Ducci, A., 2013. On the fluid dynamics of shaken bioreactors-flow characterization and transition. *AIChE Journal*, 59(1), pp.334–344.

Williams, D. & Sebastine, I., 2005. Tissue engineering and regenerative medicine: manufacturing challenges. *IEEE proceedings of nanobiotechnology*, 152(6), pp.207–211.

Wu, C. et al., 2012. Hypoxia-mimicking mesoporous bioactive glass scaffolds with controllable cobalt ion release for bone tissue engineering. *Biomaterials*, 33(7), pp.2076–2085.

Wu, J. & Gu, M., 2011. Microfluidic sensing: state of the art fabrication and detection techniques. *Journal of biomedical optics*, 16(8), pp.080901–12.

Yagi, H. et al., 2010. Mesenchymal stem cells: Mechanisms of immunomodulation and homing. *Cell Transplantation*, 19(6-7), pp.667–679.

Yang, D.-C. et al., 2011. Hypoxia inhibits osteogenesis in human mesenchymal stem cells through direct regulation of RUNX2 by TWIST. *PloS one*, 6(9), pp.1–10.

Yang, Y., Rossi, F.M. V & Putnins, E.E., 2007. Ex vivo expansion of rat bone marrow mesenchymal stromal cells on microcarrier beads in spin culture. *Biomaterials*, 28(20), pp.3110–3120.

Yeatts, A.B. & Fisher, J.P., 2011. Tubular perfusion system for the long-term dynamic culture of human mesenchymal stem cells. *Tissue engineering. Part C, Methods*, 17(3), pp.337–48.

Yetisen, A.K. & Volpatti, L.R., 2014. Patent protection and licensing in microfluidics. *Lab on a chip*, 14(13), pp.2217–25.

Young, E.W.K. & Beebe, D.J., 2010. Fundamentals of microfluidic cell culture in controlled microenvironments. *Chemical Society reviews*, 39(3), pp.1036–1048.

Young, H.E. & Black Jr., A.C., 2004. Adult stem cells. *Anat Rec A Discov Mol Cell Evol Biol*, 276(1), pp.75–102.

Yourek, G. et al., 2010. Shear stress induces osteogenic differentiation of human mesenchymal stem cells. *Regenerative Medicine*, 5(5), pp.713–724.

Yu, H. et al., 2005. Diffusion dependent cell behavior in microenvironments. *Lab on a chip*, 5, pp.1089–1095.

Yu, H., Alexander, C.M. & Beebe, D.J., 2007. Understanding microchannel culture: parameters involved in soluble factor signaling. *Lab on a chip*, 7(6), pp.726–730.

Yuan, Y. et al., 2003. Cobalt inhibits the interaction between hypoxia-inducible factor- and von Hippel-Lindau protein by direct binding to hypoxia-inducible factor-a. *Journal of Biological Chemistry*, 278(18), pp.15911–15916.

Zhang, H. et al., 2005. Computational-fluid-dynamics (CFD) analysis of mixing and gas-liquid mass transfer in shake flasks. *Biotechnology and applied biochemistry*, 41(Pt 1), pp.1–8.

Zhang, H. et al., 2008. Engineering characterisation of a single well from 24-well and 96-well microtitre plates. *Biochemical Engineering Journal*, 40(1), pp.138–149.

Zhang, M. et al., 2012. Preparation, characterization and in vitro angiogenic capacity of cobalt substituted β-tricalcium phosphate ceramics. *Journal of Materials Chemistry*, 22, pp.21686–21694.

Zhang, X. et al., 2010. Use of orbital shaken disposable bioreactors for mammalian cell cultures from the milliliter-scale to the 1,000-liter scale. *Advances in Biochemical Engineering/Biotechnology*, 115, pp.33–53.

Zuk, P.A. et al., 2002. Human adipose tissue is a source of multipotent stem cells. *Mol Biol Cell*, 13(12), pp.4279–4295.